
# UNIVERSITÀ DEGLI STUDI DI PADOVA

**Dipartimento di Fisica e Astronomia "Galileo Galilei"**

**Master Degree in Physics**


**Final Dissertation**

# Schrödinger equation approach to the distribution of baryons in the Universe


**Thesis supervisor**

**Prof. Sabino Matarrese**

**Thesis co-supervisor**

**Dr. Daniele Bertacca**

**Candidate**

**Guido Occhipinti**



**Academic Year 2019/2020**

# Contents

# Chapter 1

# Introductory remarks

In this work we want to study how the Universe grew from be slightly inhomogeneous at early times to be largely inhomogeneous today also at scales of the order of hundreds of megaparsec, i.e. we want to study the evolution of structures of the Universe from small overdensities to big clusters of galaxies. We assume the Universe as flat and filled by non-relativistic matter and Dark Energy, i.e. we are neglecting relativistic particles and the curvature of the Universe in our study (in Sect.1.1 we present how to describe in full generality the Universe and why to restrict to this simpler scenario, see e.g. Fig.1.3). The matter component is divided in baryonic matter (the common non-relativistic matter of the Standard Model) and in dark matter, which is unknown kind of particles which interact only gravitationally [20]. This last matter component had to be non-relativist at the decoupling and so it takes the name of Cold Dark Matter (CDM) [20], in the following we will use simply the name DM but we always mean the cold form beside when explicitly said and in the Chapter 5 where we discuss another candidate for DM which is called fuzzy DM (FDM). We will restrict our study to large scales ($\gtrapprox$ 10Mpc) so that at early times and for a large part of its history the overdensity generated by the structure formation is small, such as perturbation theories can be used [20].
The generally accepted theory of structure formation is gravitational instability, which assumes the early Universe to be almost perfectly smooth with the exception of tiny deviations in density respect to the global cosmic background density and in velocity respect to the Hubble expansion [20]. The fluctuations in the temperature in the cosmic microwave background (CMB) reflects these density perturbations, thus from their observation we know that the primordial perturbations have been of the order of $10^{-5}$ [20].
Today the most accepted theory of the origin of these perturbations is that in the early Universe quantum perturbations were present and during the inflationary phase (a phase of accelerated and very rapid expansion of the Universe taken place before the radiation and matter dominated epochs) they expanded to macroscopic proportions [20]. Then the initial perturbations will grow under the effect of gravity perturbations. These can be explained in the following manner: nearby a region with an higher density the surplus of matter will exert an attractive gravitational force larger than the average, instead near low density regions the deficit of matter will lead to a weaker force. Thus the overdensity regions will expand less than the average, if pressure forces are not sufficient to counteract the gravitational pull more and more matter would be incorporated by accretion

until a collapse and the formation of a gravitational stable object, instead the regions with a density deficit will lead to the formation of voids. This interchange between structures and voids, usually called cosmic web, is shown magnificently in the simulation made by [70] and reported in Fig.1.1, where the DM density field is reported on various scales. On the largest no structure is discernible and the distribution appears homogeneous and isotropic; on smaller scales a filamentary structure appears, this is the so called cosmic web; on the smallest scale, taken in a region rich of galaxy clusters, we can observe several DM substructures which are gravitationally bound object orbiting within the cluster halo. These substructures are the remnants of dark matter halos that fell into the cluster at earlier times.

The early stage of the evolution of density perturbations can be described by linear theory and it is well know in literature [54, 56], it applies to the times just after the decoupling between radiation and matter at recombination and at large scales since small scale perturbations are the first to become non linear. Actually at any cosmic epoch we could define spatial scales such as the perturbations are still in the linear regime [20].
In this work we will present a model which try to describes the evolution of structures beyond the linear regime. In particular we will make an analogy between the matter distribution and a quantum matter distribution and study the latter with perturbation techniques. We will extend the results of previous studies (e.g. [67, 73, 77, 80]), which develop the model for a single-fluid composed of DM, to a two-fluid model composed by baryons and DM, i.e. the aim of this work is to study the evolution of baryons under the influence of DM gravitational potential field through a quantum-mechanical model. Hence we study the evolution of density perturbation to understand how the present distribution of matter in the Universe formed. We will follow the evolution of both ordinary (we will call it baryonic although it contains also electrons, but they will stick to ions due to Coulomb attraction) and dark matter in the presence of dark energy, which is modelled as a cosmological constant. We expect to be able to reproduce the distribution of the intergalactic medium (IGM), which is a plasma of baryonic matter (mostly ionized hydrogen) extending between galaxies. It has a filamentary form, as a web, and a very small density, e.g. $1 - 10$ particles for cubic meter. Thus it will be in a quasi-nonlinear stage and then it is well suited to a perturbation approach. The small residue of neutral hydrogen in the filamentary structures produces weak absorption lines which are seen in the spectra of distant quasars (the Ly$\alpha$ forest), these observations are an efficient probe of the high-redshift Universe [20].

The distribution of the IGM has already been studied quite successfully in the linear regime, with analytical models, and beyond through hydrodynamical codes. In [74] various models (which are a modification of the Zel'dovich approximation [79] and are based on obtaining the baryon distribution from the DM one imposing a filter) for the IGM distribution are confronted with an hydrodynamical simulation of DM. A representation of the matter distribution is given in Fig.1.2, where we show four panels, which are slices of thickness $\approx 0.1h^{-1}$ comoving Mpc at the same position along the z-axis at redshift $z = 3$, for the IGM and the DM distribution of the hydrodynamical simulations (top panels), the TZA field (bottom left panel) and the IGM field obtained with ZD method (bottom right). We can observe that the IGM distribution is more diffuse, this is an effect of the pressure, e.g. in underdense regions the gas pressure is pushing matter into the low-density voids [74]. Anyway it is clear that the IGM resembles the underlying DM

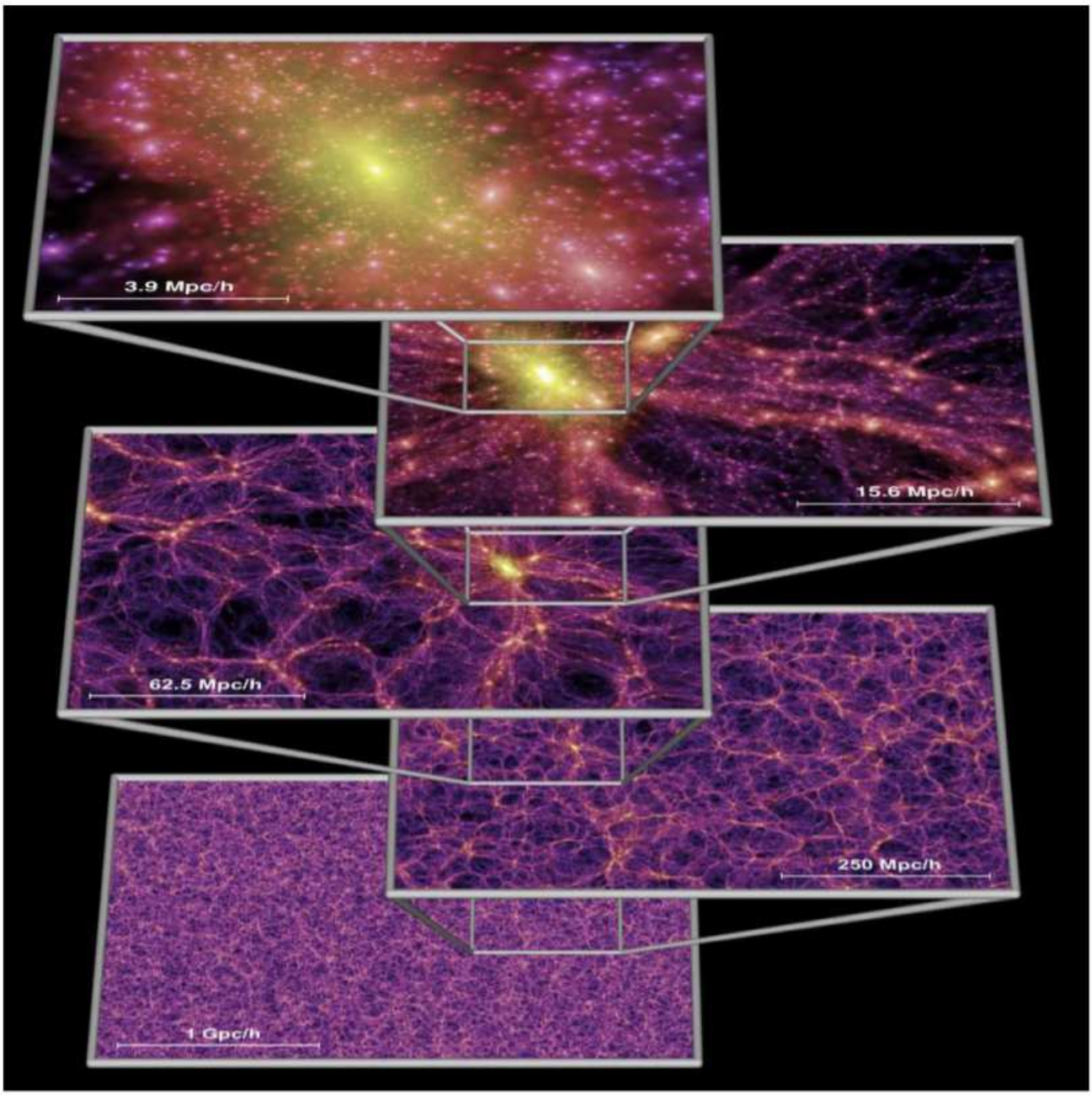


Figure 1.1: The dark matter density field on various scales. Each individual image shows the projected dark matter density field in a slab of thickness $15h^{-1}$Mpc (sliced from the periodic simulation volume at an angle chosen to avoid replicating structures in the lower two images), colour-coded by density and local dark matter velocity dispersion. The zoom sequence displays consecutive enlargements by factors of four, centred on one of the many galaxy cluster halos present in the simulation. This figure is provided by [70], for any further detail check the main text.

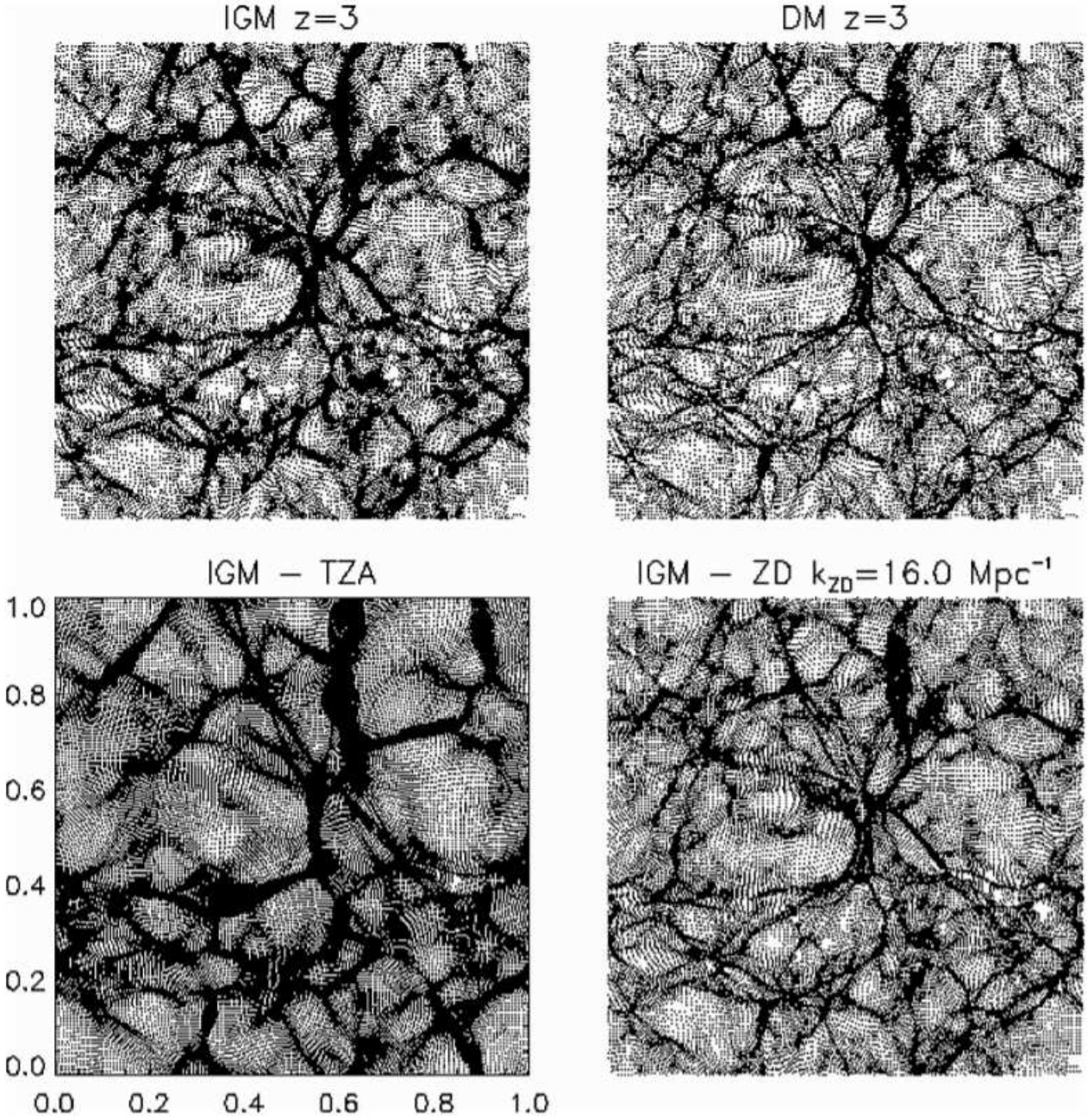


Figure 1.2: Slices along the z-axis of thickness $\approx 0.1h^{-1}$ comoving Mpc (coordinates in normalized units). Top panels: IGM distribution (left) and DM distribution (right), from the $z = 3$ output of the ΛCDM model. Bottom panels: Zel'dovich modelling of the IGM distribution from the initial conditions of hydrodynamical simulation (left-hand panel, TZA), Zel'dovich displacement added to DM particles to mimic baryonic pressure (right-hand panel, ZD). This figure is provided by [74], for any further detail check the main text.

distribution.
The work is organized as follows. In the following sections of this introductory chapter we will describes the basic aspects of cosmology and gravitational instability theory. In the second chapter we develop a quantum mechanical theory of the evolution of the large scale structure (LSS) based on the works [37, 67, 72, 77], which results we extend to the description of a collisional fluid (baryons) whose pressure is assumed barotropic (1.2.17). This quantum mechanical model has two possible interpretations. The first, which is the one we use, is that it describes through Schrödinger equations (coupled to a Poisson equation which describes the gravitational field) a classical matter field which evolves under the Vlaslov equation. In this case the Planck constant $\hbar$ and the particle mass $m$ are assumed to be free parameters of the model (they can be set arbitrarily) which are coupled in the single parameter $\nu = \hbar/m$. We use this model to describe the evolution of baryons under the DM gravitational field. The second interpretation is that the model describes a real quantum fluid and in this case $\hbar$ and $m$ assume their common value. This interpretation is interesting because it describes a new DM candidate which consists in ultra-light axion-like particles usually referred to as fuzzy DM (FDM) [30].
In the chapter 3 we solve the Schrödinger-Poisson system using quantum perturbation theory (QPT). We follow the work [67] which results we extend to an expanding background Universe and to the presence of baryons. In particular in this chapter we restrict to scales much larger than the Jeans scale such as the baryon pressure can be assumed as a perturbative correction to the dynamics (kinetic energy), due to Jeans instability theory [50]. This perturbative expansion provides semi-analytical results which if numerically solved can be computationally competitive with N-body simulations [67].
In chapter 4 we present a numerical code to solve the Schrödinger equations following the work [5] and extending its results to our cosmological problem. This code is interesting because it does not requires to restrict the study on very large scale (as the QPT of the chapter 3), hence through its use we could investigate a much broad range of scales. A similar code was already used by [80] to study a single-fluid composed by DM and it seems a promising numerical method since it is less computationally demanding than full N-body simulations [80].
In chapter 5 we depart a bit from the main argument of the work, i.e. the evolution of baryons under CDM potential. Here we use the Schrödinger model we depicted in chapter 2 to study a real quantum fluid, the FDM, and in particular the properties of quantum vortices following the work [30] (here we neglect the presence of baryons and we study a single-fluid of DM). This is interesting because the observation of these features in DM halos could be a probe for the FDM candidate [1, 30]. We extend the work of [30] to the possibility of a non negligible velocity dispersion for FDM, the velocity dispersion can be related to a pressure and an effective Jeans scale [15, 64]. We develop a simple model, describing it as the baryon pressure (1.2.17) and so using some of the results of the previous chapters, to show that the magnitude of the effects of the velocity dispersion over quantum vortices is selected by the effective Jeans scale. We conclude with chapter 6 where we present our results.

## 1.1 Robertson-Walker metric

We want to construct a model for the homogeneous and isotropic background Universe and since general relativity is closely related to geometry we have to use a geometrical model. Thus first of all we need to construct a metric, more specifically we can define the metric tensor $g_{ij}$ as

$$ds^2 = g_{ij}(\mathbf{x})x^i x^j \,, \tag{1.1.1}$$

where $ds^2$ represents the space-time interval between the points $x^i$ and $x^i + dx^i$.
If we suppose that we can describe the Universe as a continuous fluid and assign to each fluid element the spatial coordinates $x^\alpha (\alpha = 1, 2, 3)$ hence any point in space-time can be labelled by the coordinates $x^\alpha$, corresponding to the fluid element which is passing through the point, and by the proper time $t$ measured by a clock moving with the fluid element. The coordinates $x^\alpha$ are called comoving coordinates and we will make a large use of them later in this work. One can show only from geometrical considerations that the most general metric satisfying homogeneity and isotropy is called Robertson-Walker metric and is of the form [20]

$$ds^2 = (cdt)^2 - a(t)^2 \left[ \frac{d\varrho^2}{1 - K\varrho^2} + \varrho^2(d\theta^2 + \sin^2\theta d\varphi^2) \right] , \tag{1.1.2}$$

where we have used spherical polar coordinates: $\varrho$, $\theta$ and $\varphi$ are the comoving coordinates and $t$ the proper time; $a(t)$ is called scale factor and it encodes the expansion of the Universe. $K$ is called curvature parameter and is a constant which can be rescaled such as it can assume only the values $-1, 1$ and $0$ [20]. In the case $K = 0$ the space obeys to the Euclidean geometry and it is said to be flat; in the case $K = +1$ the geometry is like on an hypersphere so the space is closed, i.e its volume is finite, but it has no boundaries; in the case $K = -1$ the geometry is hyperboloidal, i.e. a curved space with negative Gaussian curvature, and the space is open [20]. If we write the metric as ($c = 1$) $ds^2 = dt^2 - dl^2$ we can parametrize respectively these three cases as

$$dl^2 = a^2(d\varrho^2 + \varrho^2 d\Omega^2) \,, \tag{1.1.3}$$

$$dl^2 = a^2(d\chi^2 + \sin^2\chi d\Omega^2) = a^2 \left( \frac{d\varrho^2}{1 - \varrho^2} + \varrho^2 d\Omega^2 \right) , \tag{1.1.4}$$

$$dl^2 = a^2(d\chi^2 + \sinh^2\chi d\Omega^2) = a^2 \left( \frac{d\varrho^2}{1 + \varrho^2} + \varrho^2 d\Omega^2 \right) , \tag{1.1.5}$$

where $d\Omega^2 = d\theta^2 + \sin^2\theta d\varphi^2$, $0 \leq \chi \leq \pi$ in (1.1.4) and $0 \leq \chi \leq \infty$ in (1.1.5).

### 1.1.1 The Friedmann equations

Now that we know the metric of our modelled Universe we can study the Einstein equation, which relate the geometry of the Universe to its energy content. They are

$$R_{ij} - \frac{1}{2} g_{ij} R = \frac{8\pi G}{c^4} T_{ij} \,, \tag{1.1.6}$$

where $R_{ij}$ and $R$ are the Ricci tensor and Ricci scalar, which can be derived from the metric. $T_{ij}$ is the energy-momentum tensor which for a perfect fluid, as we consider the

background Universe [20], can be written as (using from now the natural unit $c = 1$)

$$T_{ij} = (p + \rho)U_i U_j - p g_{ij} \,, \tag{1.1.7}$$

where $\rho$ is the energy density, $p$ the pressure and $U_k$ with $k = 1, .., 4$ the fluid 4-velocity. Using the RW metric the time-time component of the Einstein equations yelds [20]

$$\ddot{a} = -\frac{4\pi G}{3} (\rho + 3p)\, a \,. \tag{1.1.8}$$

The space-time components give just $0 = 0$. From the space-space components, using (1.1.8) for simplify the addends, we obtain

$$\dot{a}^2 + K = \frac{8\pi G}{3} \rho a^2 \,. \tag{1.1.9}$$

Actually these two equations are not independent, the second can be derived from the first if one assumes the expansion of the Universe to be adiabatic, as one should do because outside the Universe there is nothing with which exchange heat. The adiabaticity is described by the condition $dU + pdV = 0$, i.e.

$$d(\rho a^3) = -p da^3 \,, \tag{1.1.10}$$

which can be rewritten as

$$\dot{\rho} = -3\frac{\dot{a}}{a}(\rho + p) \,. \tag{1.1.11}$$

We define the Hubble parameter as $H = \dot{a}/a$ which describes the rate of expansion of the Universe, since the scale factor $a$ describes its expansion. Then we can rewrite equations (1.1.8), (1.1.9) and (1.1.11) in the common form

$$H^2 = \frac{8\pi G}{3} \rho - \frac{K}{a^2} \,, \tag{1.1.12}$$

$$\ddot{a} = -\frac{4\pi G}{3} a(\rho + 3p) \,, \tag{1.1.13}$$

$$\dot{\rho} = -3H(\rho + p) \,. \tag{1.1.14}$$

These are called Friedmann equations.
Since there are three variables ($a$, $\rho$, $p$) and we have only two independent equations to close the system we need an equation of state for the pressure. Another important observation is that the pressure entering in the Friedmann equations is a pure relativistic effect. This could be seen by a Newtonian derivation of these equations, which consist in derive them from just Newtonian dynamics and adiabaticity. It can be shown that the equation obtained with such a Newtonian fashion are identical to the Friedmann equations but the pressure term is missing in (1.1.13) [20].
From (1.1.12) we have to make other two important definitions. First we define the energy density needed to make the Universe flat, i.e. $K = 0$, this is called critical density and is given by

$$\rho_c(t) = \frac{3H^2(t)}{8\pi G} \,. \tag{1.1.15}$$

From it we can define the density parameter

$$\Omega(t) = \frac{\rho(t)}{\rho_c(t)}\,. \tag{1.1.16}$$

With these two new definitions we can rewrite (1.1.12) as

$$\frac{K}{a^2} = H^2(\Omega - 1)\,. \tag{1.1.17}$$

Hence it's clear that if $\Omega > 1$ ($\rho > \rho_c$) $K = +1$ and the Universe is closed, if $\Omega < 1$ $K = -1$ and the Universe is open and if $\Omega = 1$ $K = 0$ and the Universe is flat. In addiction note that since $K = const$ the Universe can never change from open to closed, flat or viceversa . Thus the observation of $\Omega$ is very important to understand in which case of geometry the Universe is, unfortunately for now the data are very near to $\Omega = 1$ and with an error too big to determine in which situation we are [20].

### 1.1.2 The Cosmological constant $\Lambda$

The cosmological constant $\Lambda$ is an adjunctive constant term of the Einstein equations. Historically Einstein added it to make possible to describe a static Universe but currently this term has proven helpful to model the accelerated expansion of the Universe. The modified Einstein equation are [20]

$$R_{ij} - \frac{1}{2}g_{ij}R - \Lambda g_{ij} = \frac{8\pi G}{c^4}T_{ij}\,. \tag{1.1.18}$$

Since today we use $\Lambda$ to model an "energy" [20] we prefer to put it on the right-hand side of the Einstein equation, redefining the energy-momentum tensor

$$R_{ij} - \frac{1}{2}g_{ij}R = \frac{8\pi G}{c^4}\tilde{T}_{ij}\,, \tag{1.1.19}$$

where

$$\tilde{T}_{ij} = T_{ij} + \frac{\Lambda}{8\pi G}g_{ij} = -\tilde{p}g_{ij} + (\tilde{p} + \tilde{\rho})U_iU_j\,, \tag{1.1.20}$$

where we defined an effective pressure $\tilde{p}$ and an effective density $\tilde{\rho}$ as

$$\tilde{p} = p - \frac{\Lambda}{8\pi G}\,, \qquad \tilde{\rho} = \rho + \frac{\Lambda}{8\pi G}\,. \tag{1.1.21}$$

With the redefinition of the Einstein equation (1.1.19) and through the use of the effective pressure and density we can immediately write the Friedmann equations as

$$H^2 = \frac{8\pi G}{3}\left(\rho + \frac{\Lambda}{8\pi G}\right) + \frac{K}{a^2}\,, \tag{1.1.22}$$

$$\ddot{a} = -\frac{4\pi G}{3}a\left(\rho + 3p - \frac{\Lambda}{4\pi G}\right)\,, \tag{1.1.23}$$

$$\dot{\rho} = -3H(\rho + p)\,. \tag{1.1.24}$$

From (1.1.23) it's clear that for an Universe filled only by the cosmological constant its expansion is accelerating. This is due the fact that the fluid modelled by $\Lambda$ has a negative pressure. We call this fluid Dark Energy and today we actually see the expansion of the Universe accelerate, hence we have a confirmation of the presence of this "fluid" because ordinary fluids cannot have negative pressure.
It's important to note from the Friedmann equations that in an Universe filled only by $\Lambda$ its density and $H$ are constant, then the scale factor has the simple expression

$$a \propto e^{Ht} \propto e^{(\Lambda/3)^{1/2}t} \,. \tag{1.1.25}$$

We can also define the critical "density" for an Universe filled by $\Lambda$ and the curvature such as

$$\Lambda_c = 3H^2 \tag{1.1.26}$$

and then the density parameter associate to Dark Energy

$$\Omega_\Lambda = \frac{\Lambda}{3H^2} \,. \tag{1.1.27}$$

Observations set the value of $\Omega_\Lambda$ today to $\Omega_{0\Lambda} \approx 0.7$ thus we expect it to be the largest component in the present Universe, while in the past it was smaller than the matter or radiation contributions [20]. We report the evolution of the density of the various components of the Universe in Fig.1.3 taken from [33], where is made use of the barotropic equation of state $w = P(\rho)/\rho$. Here in particular it was allowed to Dark Energy density to vary slightly with time, i.e. $w$ varies with time, and this is modelled by $w(z) = w_0 + w_a z/(1+z)$ where $w_0$ is the present value of $w$ and $w_a$ is a small coefficient to the time evolution of $w$. This model fits, besides the cosmological constant, many scalar field and some modified gravity expansion histories [33].

## 1.2 Gravitational instability fundamentals

In this section we review the basic aspects of gravitational instability theory which are relevant for the following part of this work (see e.g. [56] and [20]).
The matter content of the Universe can be described as a fluid, collisional in the case of baryons and collisionless in the case of dark matter. In particular to be possible to describe DM like a fluid, since it is very lightly interacting matter and so have a large free mean path, we need to assume the velocity dispersion of DM negligible. This can be demonstrated from the Boltzmann equations, as we report in section 1.3.
Since we are studying only non-relativistic particles another important assumption we do is to limit ourselves to a Newtonian description of gravity, this will be a good approximation as long as we treat only small perturbations, such as the gravitational potential is small, and scales smaller than the Hubble horizon, such as the interactions are instantaneous.
The first definition we need is the one of comoving coordinates $\mathbf{x}$, which are coordinates which follow the Universe expansion. We can define them from the proper coordinates $\mathbf{r}$ as

$$\mathbf{r} = a\mathbf{x} \,. \tag{1.2.1}$$

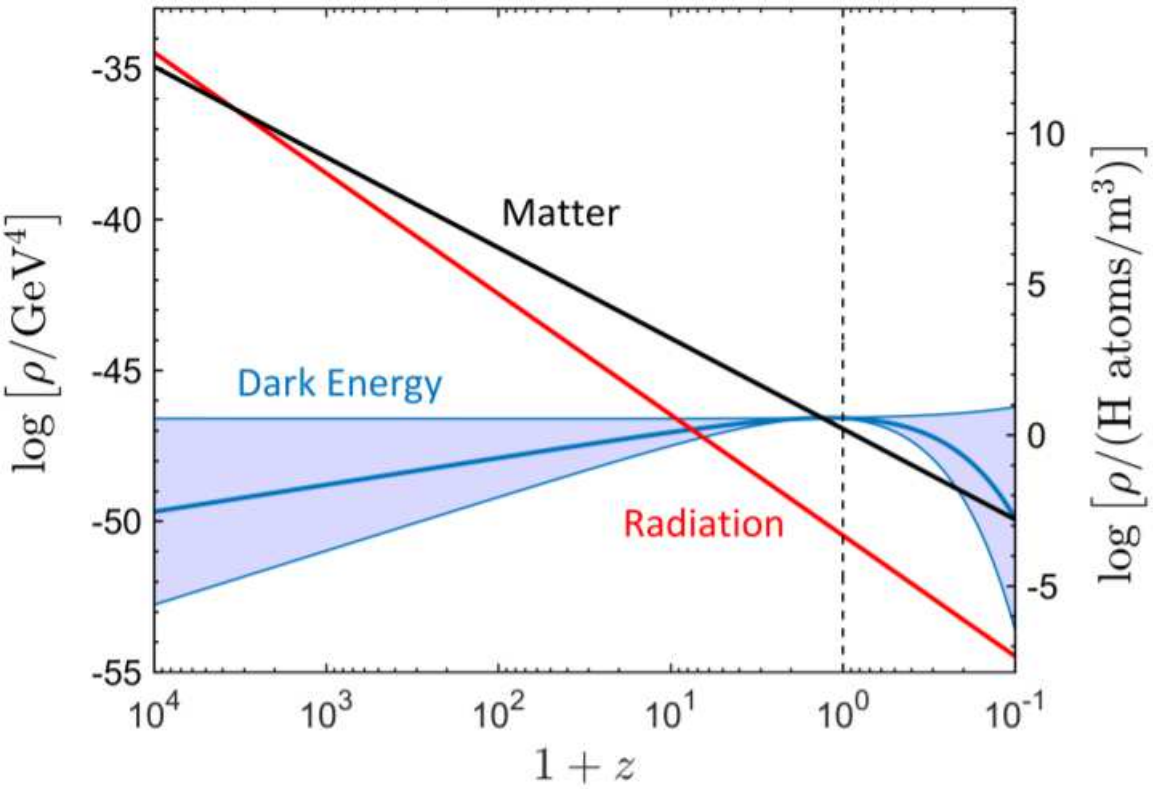


Figure 1.3: Energy density of species in the universe as a function of $(1+z)$, where $z$ is the redshift. The dashed vertical line indicates the present time ($z = 0$), with the past to the left and future to the right. Note that matter ($\propto (1+z)^3$ ) and radiation ($\propto (1+z)^4$) energy densities scale much faster with the expanding universe than the dark energy density, which is exactly constant for a cosmological constant $\Lambda$. The shaded region for dark energy indicates the energy densities allowed at $1\sigma$ (68.3% confidence) by combined constraints from current data assuming the equation of state is allowed to vary as $w(z) = w_0 + w_a z/(1+z)$. This figure is provided by [33], for any further detail check the main text.

Note that in this coordinates the velocity is made by two components if the Universe is not homogeneous, i.e. particles can move differently to just follow the space expansion and so $\mathbf{x}$ is not constant.

$$\dot{\mathbf{r}}(\mathbf{x},t) = H(t)\mathbf{r} + a\dot{\mathbf{x}} \tag{1.2.2}$$

Thus the second term can be considered as a perturbation over the homogeneous background and is called peculiar velocity $\mathbf{v} = a\dot{\mathbf{x}}$.
We will work in the comoving space so every length has to be rescaled accordingly, including derivatives, also the time one. For a general function f we have

$$\begin{aligned}
\frac{Df}{Dt}(\mathbf{r},t) &= \frac{Df}{Dt}(\mathbf{x},t) \\
\frac{\partial f}{\partial t}|_{\mathbf{r}} + \dot{\mathbf{r}}\cdot\nabla_{\mathbf{r}} f &= \frac{\partial f}{\partial t}|_{\mathbf{x}} + \dot{\mathbf{x}}\cdot\nabla_{\mathbf{x}} f \\
\frac{\partial f}{\partial t}|_{\mathbf{r}} + (H\mathbf{r} + a\dot{\mathbf{x}})\cdot\frac{1}{a}\nabla_{\mathbf{x}} f &= \frac{\partial f}{\partial t}|_{\mathbf{x}} + \dot{\mathbf{x}}\cdot\nabla_{\mathbf{x}} f \\
\frac{\partial f}{\partial t}|_{\mathbf{r}} &= \frac{\partial f}{\partial t}|_{\mathbf{x}} - H(\mathbf{x}\cdot\nabla_{\mathbf{x}})f\,,
\end{aligned} \tag{1.2.3}$$

where

$$\frac{D}{Dt}|_{\mathbf{x}} = \frac{\partial}{\partial t} + \dot{\mathbf{x}}\cdot\nabla \tag{1.2.4}$$

is the convective or Lagrangian derivative, which describes the rate of change of some physical quantities of a particle equipped with a space and time dependent velocity field. In the proper space the fluid equations, assuming constant entropy (i.e. adiabatic perturbations) are respectively the continuity and the Euler equations [56]

$$\dot{\rho} + \nabla_{\mathbf{r}}\cdot(\rho\dot{\mathbf{r}}) = 0\,, \tag{1.2.5}$$

$$\ddot{\mathbf{r}} + (\dot{\mathbf{r}}\cdot\nabla_{\mathbf{r}})\dot{\mathbf{r}} = -\frac{1}{\rho}\nabla_{\mathbf{r}} P - \nabla_{\mathbf{r}}\Phi_{tot}\,, \tag{1.2.6}$$

where $\rho(\mathbf{x},t)$ is the density, $P$ the pressure and $\Phi_{tot}(\mathbf{x},t)$ is the gravitational potential, which evolution is described by the Poisson equation

$$\nabla^2_{\mathbf{r}}\Phi_{tot} = 4\pi G\rho\,. \tag{1.2.7}$$

Since we want to describe the evolution of the Universe on large scales, which we expect to be slightly inhomogeneous, we have to introduce perturbations over the homogeneous background. We can define them as

$$\rho(\mathbf{x},t) = \bar{\rho}(t) + \bar{\rho}(t)\delta(\mathbf{x},t,) \quad \dot{\mathbf{r}}(\mathbf{x},t) = H(t)\mathbf{x} + a\dot{\mathbf{x}}, \quad \Phi_{tot}(\mathbf{x},t) = \bar{\Phi}(t) + \Phi(\mathbf{x},t)\,. \tag{1.2.8}$$

These satisfy the following equations in the comoving space [56]

$$\dot{\rho} + 3H\rho + \frac{1}{a}\nabla\cdot(\rho\mathbf{v}) = 0\,, \tag{1.2.9}$$

$$\frac{\partial\mathbf{v}_b}{\partial t} + H\mathbf{v}_b + \frac{1}{a}(\mathbf{v}\cdot\nabla)\mathbf{v} = -\frac{1}{a}\nabla\Phi - \frac{1}{a\rho}\nabla P\,. \tag{1.2.10}$$

In the background Universe $\mathbf{v} = 0$ hence the continuity equation for the background density is

$$\dot{\bar{\rho}} + 3H\bar{\rho} = 0\,, \tag{1.2.11}$$

which, since $H = \dot{a}/a$, gives the common decay of matter density in an expanding homogeneous Universe $\bar{\rho} \propto a^{-3}$. If we subtract this solution to the full continuity equation we obtain an equation for the fluctuation $\delta$, then we can write explicitly the fluid equations for the perturbations of baryons and DM.

- Continuity

$$\dot{\delta}_b + \frac{1}{a}\nabla \cdot ((1+\delta_b)\mathbf{v}_b) = 0 \tag{1.2.12}$$

$$\dot{\delta}_{DM} + \frac{1}{a}\nabla \cdot ((1+\delta_{DM})\mathbf{v}_{DM}) = 0 \tag{1.2.13}$$

- Euler

$$\frac{\partial \mathbf{v}_b}{\partial t} + H\mathbf{v}_b + \frac{1}{a}(\mathbf{v}_b \cdot \nabla)\mathbf{v}_b = -\frac{1}{a}\nabla\Phi - \frac{1}{a\rho_b}\nabla P_b \tag{1.2.14}$$

$$\frac{\partial \mathbf{v}_{DM}}{\partial t} + H\mathbf{v}_{DM} + \frac{1}{a}(\mathbf{v}_{DM} \cdot \nabla)\mathbf{v}_{DM} = -\frac{1}{a}\nabla\Phi \tag{1.2.15}$$

where $\mathbf{v} = a\frac{d\mathbf{x}}{dt}$ and $\Phi$ is the peculiar gravitational potential. We have to couple to these equations the perturbed Poisson equation, which in principle should account for both DM and baryons

$$\begin{aligned}\nabla^2\Phi = 4\pi G a^2 \delta\rho_m = 4\pi G a^2 \bar{\rho}_m \delta_m \approx 4\pi G a^2 \bar{\rho}_{DM}\delta_{DM} \approx \\ \approx 4\pi G a^2 \Omega_{DM}\rho_c \delta_{DM} \approx \frac{3}{2}H^2 a^2 \Omega_{DM}\delta_{DM}\,,\end{aligned} \tag{1.2.16}$$

where $\delta_m = (\bar{\rho}_b/\bar{\rho}_m)\delta_b + (\bar{\rho}_{DM}/\bar{\rho}_m)\delta_{DM}$ contains both baryons and DM, but since the mean mass fraction of baryons is much smaller than the one of DM $\bar{\rho}_b/\bar{\rho}_m << \bar{\rho}_{DM}/\bar{\rho}_m$ [56] we can neglect the baryons self gravity. And $\rho_c$ is the critical dentity defined as the density for which the Universe is flat, i.e. $\rho_c = 3H^2/(4\pi G)$ [56].
To close the system of equations we need also an equation of state for the baryons, i.e. a law for their pressure. For low to moderate baryon overdensity ($\delta_b < 10$) we can write $T = T_0(z)(1+\delta_b)^{\gamma-1}$, where $T_0$ is the Intergalactic Medium (IGM) temperature at mean density and at redshift $z$ [48]. Thus

$$P_b = \frac{\rho_b k_b T}{\mu m_p} = \frac{\bar{\rho}_b k_b T_0(z)}{\mu m_p}(1+\delta_b)^\gamma = \frac{k_b T_0}{\mu m_p \bar{\rho}_b^{\gamma-1}}\rho_b^\gamma\,. \tag{1.2.17}$$

Then we can compute also the pressure gradient in terms of the baryon density

$$\frac{\nabla P_b}{\rho_b} = \frac{\gamma}{\gamma-1}A\nabla\rho_b^{\gamma-1}\,, \qquad A = \frac{k_b T_0}{\mu m_p \bar{\rho}_b^{\gamma-1}}\,. \tag{1.2.18}$$

Another fundamental relation was noted by Zel'dovich [79] and is very useful to bind the density perturbations to the equation of motion. We call the comoving Lagrangian coordinates $\mathbf{q}$, which describe the initial particle distribution. Instead we define the comoving Eulerian coordinates as the usual comoving coordinates $\mathbf{x}$ describing the Universe through its evolution. Since mass is conserved there would be the same amount of mass

in an infinitesimal volume at the point $\mathbf{x}$ and at the point $\mathbf{q}$. If we call $\eta = \rho/\bar{\rho} = 1 + \delta$ we can write this conservation as

$$\begin{aligned} \eta(\mathbf{x}, D)d^3x &= \eta(\mathbf{q}, D_i)d^3q \\ (1 + \delta(\mathbf{x}, D))d^3x &= (1 + \delta(\mathbf{q}, D_i))d^3q = d^3q \end{aligned} \tag{1.2.19}$$

where we assumed the initial density perturbations to be null. Hence we can relate the density perturbations to the Jacobian $\mathcal{J}$ of the map of the change of coordinates between the Eulerian and Lagrangian ones.

$$\delta(\mathbf{x}, D)) = \mathcal{J}^{-1}(\mathbf{x}, D) - 1 \tag{1.2.20}$$

Note that if the coordinate map is singular the density diverges, this event is called a caustic and describes the structure formation due to shell-crossing, i.e. the clash of two or more particles, arriving from different points $\mathbf{q}$, in the point $\mathbf{x}$ at time $D$. We will define in a more clever way the density perturbations in the next chapter through a wave-mechanical study which overcome the caustic problem.

## 1.3 Fluid approximation

We show now that we can actually treat DM as a fluid, as we stated before. Since external forces cannot act on CDM, due to its weakly interacting nature, the gravitational forces must bind DM in a fluid. To demonstrate the fluid validity we need to derive the collisionless Boltzmann equation for the DM distribution.
From the Newtonian dynamics follow

$$\ddot{\mathbf{r}} = -\nabla_{\mathbf{r}}\Phi^{tot}_{DM}\,, \tag{1.3.1}$$

where $\Phi^{tot}_{DM}$ is the gravitational potential generated by DM, which follows the Poisson equation

$$\nabla^2\Phi^{tot}_{DM} = 4\pi G a^2 \rho_{DM},. \tag{1.3.2}$$

Then we write the Lagrangian for a DM particle, we will call it $\mathcal{L}'$ because later we have to "renormalize" it and for simplicity of notation we will set the mass $m = 1$.

$$\mathcal{L}' = \frac{1}{2}\dot{\mathbf{r}}^2 - \Phi^{tot}_{DM} = \frac{1}{2}\left(a\dot{\mathbf{x}} + \dot{a}\mathbf{x}\right)^2 - \Phi^{tot}_{DM} \tag{1.3.3}$$

We make a canonical transformation to eliminate the terms involving both $\mathbf{x}$ and $\dot{\mathbf{x}}$ or quadratic in $\mathbf{x}$. We can collect them in derivative of a quantity, which we call $\epsilon$.

$$a\dot{a}\mathbf{x}\dot{\mathbf{x}} + \frac{1}{2}\dot{a}^2\mathbf{x}^2 + \frac{1}{2}a\ddot{a}x^2 = \frac{d}{dt}\left(\frac{1}{2}a\dot{a}\mathbf{x}^2\right) = \frac{d}{dt}\epsilon \tag{1.3.4}$$

If we make the canonical transformation we obtain

$$\mathcal{L} = \mathcal{L}' - \frac{d\epsilon}{dt} = \frac{1}{2}a^2\dot{\mathbf{x}}^2 - \frac{1}{2}a\ddot{a}\mathbf{x}^2 - \Phi^{tot}_{DM}\,. \tag{1.3.5}$$

Then from the Friedmann equation (1.1.13) we can obtain the background density

$$\bar{\rho}_{DM} = -\frac{3a\ddot{a}}{4\pi G} \tag{1.3.6}$$

and thus, since this density is independent from the position, from the Poisson equation we obtain an expression for the background gravitational potential

$$\bar{\Phi}_{DM} = \frac{2}{3}\pi G\bar{\rho}_{DM}r^2 = -\frac{1}{2}a\ddot{a}x^2\,. \tag{1.3.7}$$

Hence in the Lagrangian remains just the perturbed potential $\Phi_{DM}$

$$\mathcal{L} = \frac{1}{2}a^2\dot{x}^2 - \Phi_{DM}\,. \tag{1.3.8}$$

Since the Boltzmann equation are derived from an Hamiltonian description we have to make a Legendre transformation.
First we have to compute the conjugate momentum

$$\mathbf{p} = \frac{\partial\mathcal{L}}{\partial\dot{\mathbf{x}}} = a\mathbf{v}\,. \tag{1.3.9}$$

Then we apply the Legendre transformation and find the Hamiltonian

$$H(\mathbf{x},\mathbf{p},t) = \mathbf{p}\cdot\mathbf{x} - \mathcal{L}(\mathbf{x},\dot{\mathbf{x}},t) = \frac{p^2}{2a^2} + \Phi_{DM} \tag{1.3.10}$$

and obtain the Hamilton equations

$$\dot{\mathbf{x}} = \frac{\partial H}{\partial\mathbf{p}} = \frac{\mathbf{p}}{a^2}\,, \tag{1.3.11}$$

$$\dot{\mathbf{p}} = -\frac{\partial H}{\partial\dot{\mathbf{x}}} = -\nabla\Phi_{DM}\,. \tag{1.3.12}$$

Finally we can write the collisionless Boltzmann equations and use the Hamilton ones to simplify it.

$$\begin{aligned}\frac{df}{dt} &= \frac{\partial f}{\partial t} + \dot{\mathbf{x}}\cdot\nabla_{\mathbf{x}}f + \dot{\mathbf{p}}\cdot\nabla_{\mathbf{p}}f = 0\\ \frac{df}{dt} &= \frac{\partial f}{\partial t} + \frac{\mathbf{p}}{a^2}\cdot\nabla_{\mathbf{x}}f - \nabla_{\mathbf{x}}\Phi_{DM}\cdot\nabla_{\mathbf{p}}f = 0\end{aligned} \tag{1.3.13}$$

We define now the first moments of the DM distribution. The zero-th order momentum is the mean density

$$\rho(\mathbf{x},t) = \frac{1}{a^3}\int d^3p f(\mathbf{x},\mathbf{p},t)\,, \tag{1.3.14}$$

where the factor $a^{-3}$ is due to the fact we are considering a comoving volume, usually $\rho \approx mnf$ and since we are considering an unitary mass $a^{-3}$ is actually the number density $n$.
The first order momentum is the mean velocity, which we keep calling $\mathbf{v}$ with an abuse of notation.

$$\mathbf{v}(\mathbf{x},t) = \frac{1}{Na}\int d^3p\mathbf{v}f(\mathbf{x},\mathbf{p},t) = \frac{1}{Na}\int d^3p\mathbf{p}f(\mathbf{x},\mathbf{p},t)\,, \tag{1.3.15}$$

where

$$N = \int d^3p f(\mathbf{x},\mathbf{p},t) \tag{1.3.16}$$

is the normalization factor.
If we integrate in $d^3p$ the Boltzmann equation (1.3.13) we obtain

$$(\dot{a^3\rho}) + a^{-2}\nabla_{\mathbf{x}} \cdot \int d^3p \mathbf{p} f - \nabla_{\mathbf{x}}\Phi_{DM} \cdot \int d^3p \nabla_{\mathbf{p}} f = 0 \tag{1.3.17}$$

and, since the last term is a surface term it gives 0 contribution, we find the continuity equation

$$\dot{\rho} + 3H\rho + \frac{1}{a}\nabla_{\mathbf{x}} \cdot (\rho \mathbf{v}) = 0\,. \tag{1.3.18}$$

To find the Euler equation we have to multiply the Boltzmann equation by $\mathbf{p}$ and integrate in $d^3p$. With a couple of easy steps we obtain

$$a^4\rho\dot{v^i} + a^4 H\rho v^i - a^3 v^i v^j \partial_j \rho - a^3 \rho v^i \partial_j v^j + a^3 \rho \partial_i \Phi_{DM} + a^{-2} \int d^3p p^i p^j \partial_j f = 0\,, \tag{1.3.19}$$

where $\partial_i = \frac{\partial}{\partial x^i}$ and we used the Einstein convention on repeated indexes. To understand the meaning of the last term we need to define the velocity dispersion tensor, which describes how much the velocity of a particle is far away from the mean value [20].

$$\Pi^{ij} = \frac{\langle p^i p^j \rangle}{a^2} - v^i v^j = \frac{1}{a}\left[ \frac{\int d^3p p^i p^j f}{\int d^3p f} - \frac{\int d^3p p^i f \int d^3p p^j f}{\left(\int d^3p f\right)^2} \right]. \tag{1.3.20}$$

Thus we can rewrite the last term of (1.3.19) as

$$\int d^3p p^i p^j \partial_j f = a\rho\partial_j \langle p^i p^j \rangle + a\langle p^i p^j \rangle \partial_j \rho \tag{1.3.21}$$

and dividing (1.3.19) by $a^4\rho$ we finally obtain

$$\dot{v^i} + Hv^i + \frac{1}{a}v^j\partial_j v^i = -\frac{1}{a}\partial_i \Phi_{DM} - \frac{1}{a\rho}\partial_j \left(\Pi^{ij}\rho\right)\,, \tag{1.3.22}$$

which would be exactly the Euler equation if the last term would be null. The term with the velocity dispersion couples this equation with the equation for the successive moment, this is typical of Boltzmann equations and gives an infinite system of equations. A method to close this system is to impose, for example, that the velocity doesn't depart from the mean value, i.e. $\Pi^{ij} = 0$. This condition is verified if $\Pi^{ij}$ keeps null for initial times and is actually true for Cold DM for a large rage of scales. In addition if the system is locally termalized the velocity dispersion becomes isotropic and in particular equal to the isotropic pressure $\Pi^{ij} = \delta^{ij}p$ and then also in this case we obtain the Euler equation, with a non vanishing pressure. Hence we found that in these cases (not so particular) the CDM can be actually described as a fluid [20].

## 1.4 Growth factor

In this section we want to define the growth factor, which is the quantity which describe the evolution of CDM perturbations in the linear regime. It is very important because using it as time variable simplifies the study of matter perturbations also outside the

linear regime.
Hence we have to linearize the equations describing the evolution of DM (1.2.13), (1.2.15) and (1.2.16).

$$\dot{\delta}_{DM} + \frac{1}{a}\nabla \cdot \mathbf{v}_{DM} = 0 \tag{1.4.1}$$

$$\dot{\mathbf{v}}_{DM} + H\mathbf{v}_{DM} = -\frac{1}{a}\nabla\Phi_{DM} \tag{1.4.2}$$

$$\nabla^2\Phi = 4\pi G a^2 \bar{\rho}_{DM}\delta_{DM} = \frac{3}{2}H_0^2\Omega_{0DM}a^2\frac{1}{a^3}\delta_{DM} \tag{1.4.3}$$

We can combine this three equation taking the time derivative of the continuity equation

$$\frac{\partial^2\delta_{DM}}{\partial t} + 2H\frac{\partial\delta_{DM}}{\partial t} = \frac{3}{2}\Omega_{0DM}H_0^2\frac{1}{a^3}\delta_{DM}\,. \tag{1.4.4}$$

The above second order differential equation describes the linear evolution of density perturbations of collisionless matter (DM) and is one of the fundamental equations within the linear theory of gravitational instability. The fact that it is a second order partial-differential equation has two important consequences. First that it has two solutions one growing and one decaying [20]

$$\delta_{DM} = \delta_1 + \delta_2\,. \tag{1.4.5}$$

And second the fact that are present only time derivatives means that the evolution of these solution is the same throughout the cosmic volume [20]. Thus they can be separated in a spatial varying function and in a time varying one, i.e $\delta = D(t)\Delta(\mathbf{x})$ or

$$\delta_1(\mathbf{x},t) = D_1(t)\Delta_1(\mathbf{x})\,, \quad \delta_2(\mathbf{x},t) = D_2(t)\Delta_2(\mathbf{x})\,. \tag{1.4.6}$$

Hence the time evolution of $D(t)$ is given by

$$\frac{\partial^2 D}{\partial t} + 2H\frac{\partial D}{\partial t} = \frac{3}{2}\Omega_{0DM}H_0^2\frac{1}{a^3}D\,. \tag{1.4.7}$$

This result brings the following important consequences for linear gravitational instability theories of collisionless matter [20]:

1. The density fluctuation $\delta$ will grow at the same rate at every location.
2. The topology of matter distribution will remain the same, i.e. the contours do not change in geometrical shape.

The density grow factor depends on the choice of the FRW Universe, i.e. on the cosmological background. These properties are enclosed in the scale factor $a$ and so also in the Hubble parameter $H$, which are present in the evolution equation (1.4.7). From now on we will use the name growth factor $D(t)$ just for the growing mode solution.
We compute now the growth factor for an Universe filled by baryons, cold dark matter and dark energy, in the form of the Cosmological constant. For such Universe the Hubble parameter is given by the relation

$$H^2(t) = H_0^2(\Omega_{0m}a^{-3} + \Omega_{0\Lambda} + (1-\Omega_0)a^{-2})\,, \tag{1.4.8}$$

where $\Omega_0 = \Omega_{0m} + \Omega_{0\Lambda}$ (we neglected the radiation contribution [20]) and the last term corresponds to the curvature of the Universe. Differentiating both once and twice the above expression we get

$$2H\dot{H} = H_0^2 H(-3\Omega_{0m}a^{-3} - 2\frac{1-\Omega_0}{a^2})\,, \tag{1.4.9}$$

$$\ddot{H} = H_0^2 H(\frac{9}{2}\Omega_{0m}a^{-3} + 2\frac{1-\Omega_0}{a^2})\,. \tag{1.4.10}$$

From the sum of this two equation we obtain

$$\ddot{H} + 2H\dot{H} = H_0^2 H\frac{3}{2}\Omega_{0m}a^{-3}\,. \tag{1.4.11}$$

Hence $H(t)$ evolves accordingly the same equation of the growth factor (1.4.7) in an Universe with collisonless matter. Multiplying the equation of evolution of $H$ by $D$ and the one of $D$ by $H$ and then subtracting the two

$$D\ddot{H} - \ddot{D}H + 2(\dot{H}D - \dot{D})H = 0 = a^2\frac{d}{dt}(\dot{D}H - D\dot{H}) + \frac{da^2}{dt}(\dot{D}H - D\dot{H}) \tag{1.4.12}$$

which can be rewritten as

$$\frac{d}{dt}\left[a^2H^2\frac{d}{dt}\left(\frac{D}{H}\right)\right] = 0\,, \tag{1.4.13}$$

which has as solution the integral equation

$$D(t) \propto H(t)\int_0^t \frac{dt}{a^2H^2}\,. \tag{1.4.14}$$

If we change time variables with the scale factor $a$

$$D(a) = \frac{5\Omega_{0m}H}{2H_0}\int_0^a \frac{da' H_0^3}{a'^3H^3} \tag{1.4.15}$$

where the proportionality factor is defined such as $\lim_{a\to 0} D \approx a$, because for early times the Universe will tend asymptotically to an Einstein-DeSitter Universe [20].
This can be computed using the fact that the early Universe was matter dominated so the Hubble parameter is approximable to $H^2 \approx H_0^2\Omega_{0m}a^{-3}$. Hence

$$D(a) \overset{a\to 0}{\approx} \frac{5\Omega_{0m}^{3/2}a^{-3/2}}{2}\int_0^a da'\frac{a'^{3/2}}{\Omega_{0m}^{3/2}} \approx a\,. \tag{1.4.16}$$

The general solution to (1.4.15) can be expressed in terms of the Gaussian hypergeometric functions ${}_2F_1$ as

$$D(a) = -\frac{1}{15\Omega_{0\Lambda}^{3/2}a^2\left(\Omega_{0m}+\Omega_{0\Lambda}a^3\right)}2\left(\frac{\Omega_{0\Lambda}a^3}{\Omega_{0m}}\right)^{3/2}\times \tag{1.4.17}$$
$$\times\left[\left(5\Omega_{0m}+2\Omega_{0\Lambda}a^3\right){}_2F_1\left(\frac{1}{2},\frac{5}{6};\frac{11}{6};-\frac{\Omega_{0\Lambda}a^3}{\Omega_{0m}}\right) - 8\Omega_{0m}\,{}_2F_1\left(-\frac{1}{2},\frac{5}{6};\frac{11}{6};-\frac{\Omega_{0\Lambda}a^3}{\Omega_{0m}}\right)\right]\,.$$

It's usefull to define also the ratio

$$f(a) = \frac{d\ln D}{d\ln a}\,, \tag{1.4.18}$$

called dimensionless linear growth.

## Flat Universe scenario

We proceed computing an approximate relation between the growth factor $D$ and the scale factor $a$ in a flat Universe. To compute $f$ is useful to rewrite (1.4.15) as

$$D \propto X^{1/2} a^{-1} \int_0^a da' X^{-3/2}\,, \tag{1.4.19}$$

with

$$X = 1 + \Omega_{0m}(a^{-1} - 1) + \Omega_{0\Lambda}(a^2 - 1) = \frac{H^2 a^2}{H_0^2}\,. \tag{1.4.20}$$

Then

$$\frac{d\ln D}{da} = \frac{1}{X}(\Omega_{0\Lambda} - \frac{\Omega_{0m}}{2a^2}) - \frac{1}{a} + \frac{X^{-3/2}}{\int_0^a da' X^{-3/2}} \tag{1.4.21}$$

and finally we can compute the dimensionless linear growth if function of the growth factor

$$f(\Omega_m, \Omega_\Lambda, a) = a\frac{d\ln D}{da} = \frac{H_0^2}{H^2}\left(\Omega_{0\Lambda} - \frac{\Omega_{0m}}{2a^3}\right) - 1 + \frac{5\Omega_{0m}H_0^2}{2a^2H^2D} = \tag{1.4.22}$$

$$= -1 - \frac{\Omega_m}{2} + \Omega_\Lambda + \frac{5a\Omega_m}{2D}\,. \tag{1.4.23}$$

The equation (1.4.17) is not a very manageable equation, so instead we can use as solution to the equations (1.4.15), (1.4.23) an approximation founded by [39] which is valid for a flat Universe. They found an approximate expression of $f$ today and assume it to be in a similar form at any time. This approximation is good for "big" values of $\Omega_m$ i.e. when the Universe was matter dominated, which is just the epoch we are studying.

$$f(z=0) \approx \Omega_{0m}^{0.6} + \frac{\Omega_{0\Lambda}}{70}\left(1 + \frac{\Omega_{0m}}{2}\right) \tag{1.4.24}$$

Then at any time

$$f(a) \approx \Omega_m^{0.6} + \frac{\Omega_\Lambda}{70}\left(1 + \frac{\Omega_m}{2}\right)\,. \tag{1.4.25}$$

Using (1.4.23) we obtain an expression for the growth factor [26]

$$D(a) \approx \frac{5\Omega_m}{2\left[\Omega_m^{0.6} + (1 + \Omega_m/2)\,\Omega_\Lambda/70 + 1 + \frac{\Omega_m}{2} - \Omega_\Lambda\right]}\, a = M(a)a\,. \tag{1.4.26}$$

Invert this relation to obtain $a$ in function of $D$ would be very difficult, but at early time we can find an approximate expression since in the limit $a \to 0$ we must have $a = D$. Thus we can think to use $a = D$ inside $M$ to don't increase the order of the solution, i.e.

$$a(D) = M^{-1}(a)D \approx M^{-1}(D)D\,, \tag{1.4.27}$$

where with $M(D)$ we mean that all the omegas are computed at "time" $D$, for example $\Omega_m \approx \Omega_{0m}(H_0/H)^2 D^{-3}$
If we do a Taylor expansion of (1.4.26) around $a = 0$ we can see how good is this

approximation, because at such times we expect $D = a$. Using $\Omega_m = \Omega_{0m}(H_0/H)^2 a^{-3} = \Omega_{0m}a^{-3}/(\Omega_{0m}a^{-3} + \Omega_{0\Lambda})$ and $\Omega_\Lambda = \Omega_{0\Lambda}(H_0/H)^2 = \Omega_{0\Lambda}/(\Omega_{0m}a^{-3} + \Omega_{0\Lambda})$ we obtain

$$D(a) \approx a - C\frac{\Omega_{0\Lambda}}{\Omega_{0m}}a^4 + \mathcal{O}(a^7)\,, \tag{1.4.28}$$

with $C = 0.168571$. Thus errors enters only at the $4^{th}$ power of $a$ and so are very small at early times.

In this chapter we introduced the basic principle of Cosmology and gravitational instability, for a more detailed discussion see e.g. the books [20, 56]. In particular we showed that the DM and baryon components of the Universe can be described as a fluid, for DM actually we had to use some approximation on the velocity dispersion (i.e. we neglect it). We also found an approximate relation (1.4.27) for relate the scale factor $a$ to the growth factor $D$, taking the basis from the works [26, 39].

# Chapter 2

# The Schrödinger-Poisson system

We introduce now a different approach to Large Scale Structure (LSS) formation respect to the ones more common in the literature, such as the Zel'dovich [79] and Adhesion [23] approximations or numerical studies such as cosmological N-body simulations [8] (these studies are limited to a Newtonian treatment of gravity) and relativistic perturbation theories (e.g. [75]), where general relativistic effects are considered. Those theories are based on the study via Lagrangian and Eulerian perturbation theory of a collisionless fluid, which represents the Cold Dark Matter (CDM) and can be extended to study also a system with baryons such as in [47]. They have some problems that can be overcome by studying the fluid with a wave-mechanical approach (namely via the Schrödinger equation). The main disadvantages are:

1. The Zel'dovich approximation breaks down at shell-crossing, where the density becomes infinite and the map between Lagrangian and Eulerian coordinate is singular.

2. The Adhesion approximation introduce a fictitious viscous term.

3. Even if N-body simulations provide the most accurate results in the description of LSS evolution, they are computationally expensive. Thus it is important to develop semi-analytical models too [67].

We will present a wave-mechanical method for the study of large-scale structure evolution which consists in the study of the coupled Schrödinger and Poisson equations. It was first suggested by [77] and then it showed great results for example in [67, 73, 80]. In the next section we will depict an intuitive way to pass from a fluid description to a wave-mechanical one through the Madelung transformation [43]. Instead in the section 2.3 we will present a clever way to relate the classic matter fields (density and velocity) to a wave-function through the use of distribution functions and Boltzmann equations, thus without pass through the fluid description which can have some problem when large velocity dispersions are present. Another advantage of the wave-mechanical model is that all the physical quantities are enclose in a single function, the wave-function, reducing so drastically the number of equations needed to solve. This also makes the model numerically competitive with N-body simulations.

## 2.1 From classical to quantum fluids

In this section we want to present the relation between the ordinary fluid description and the quantum mechanical one. In the following it will become evident that the relation between classical and quantum fluids holds until the motion is irrotational and not singular [37], in this regime, as we will show, there is a direct correspondence between the fluid equations and the Schrödinger equation. After the brake of this regime we can still relate the quantum wave-function to the properties of particles (e.g. density and velocity fields) through the use of a distribution function and so without pass through a fluid description, we will depict this method in Sect.2.3.
We begin with an important assumption, the velocity field is irrotational, i.e. $\mathbf{v} = -\nabla_{\mathbf{x}}\phi$ where $\phi$ is a general velocity potential. This is a reasonable assumption because the rotational part of the velocity decays fast under the Hubble flow as $a^{-1}$ in the linear regime of perturbations. We can show it from the Euler equation (1.2.14), the irrotational component of the velocity is orthogonal to gradients thus the right-hand side of the equation is null and also the term $\mathbf{v} \cdot \nabla_{\mathbf{x}}$, i.e.

$$\frac{\partial \mathbf{v}_{irr}}{\partial t} + H\mathbf{v}_{irr} = 0, \tag{2.1.1}$$

which using $H = \dot{a}/a$ gives $\mathbf{v}_{irr} \propto a^{-1}$, higher order terms could be a source for vorticity [7] hence this approximation is valid only at early times when vorticity has still to develop. Therefore even if there was any vortical velocity in the early Universe it decayed rapidly with the Universe expansion.
For be general we show the quantum-classical fluid relation for a general collisional fluid, which evolution in an expanding FRW universe is described by the equations (1.2.12), (1.2.14) and (1.2.16). From now on we will use the notation $\nabla = \nabla_{\mathbf{x}}$ for simplicity of notation.
If we substitute $\mathbf{v} = -\nabla\phi$ in the Euler equation (1.2.14), use (1.2.18) to express the pressure and take the first integral we get the Bernoulli or Hamilton-Jacobi equation

$$\dot{\phi} - \frac{1}{2a}\left(\nabla\phi\right)^2 = \frac{1}{a}V\,, \tag{2.1.2}$$

where

$$V = \Phi - aH\phi + \frac{\gamma}{\gamma - 1}A\rho^{\gamma-1}\,. \tag{2.1.3}$$

We can show the validity of this relation writing in components the Euler equation (1.2.14) and using (1.2.18) to express the pressure gradient in terms of the density. We use the notation $,_i = \frac{\partial}{\partial x^i}$ and the Einstein convention on repeated indexes.

$$\dot{\phi}_{,i} + H\phi_{,i} + \frac{1}{a}\phi_{,k}\,\phi_{,ki} = -\frac{1}{a}\Phi,i - \frac{1}{a}\frac{\gamma}{\gamma-1}A(\rho^{\gamma-1})_{,i}\ . \tag{2.1.4}$$

We can write the last term on the left-hand side as

$$\phi_{,k}\,\phi_{,ki} = \frac{1}{2}(\phi_{,k}\,\phi_{,k}\,)_{,i}\ . \tag{2.1.5}$$

Thus the Euler equation, in vectorial form, reads

$$\nabla\left(\dot{\phi} + H\phi - \frac{1}{2a}\left(\nabla\phi\right)^2\right) = -\frac{1}{a}\nabla\left(\Phi + \frac{\gamma}{\gamma-1}A\rho^{\gamma-1}\right) \tag{2.1.6}$$

and its first integral give the Bernoulli equation (2.1.2).
Now we want to switch to the quantum mechanical description of fluids. First we introduce a constant parameter $\nu$ with the same dimension of $\phi$ (and so of the kinematical viscosity), $L^2/T$, it is the phase space resolution in coordinates $\mathbf{x}$ and $\mathbf{v}$. This can be understood if we relate $\nu$ to the Planck constant $\hbar$ via $\nu = \hbar/m$ and then to a de Broglie wavelength $\lambda = \hbar/vm = \nu/v$, thus $\nu = \lambda v$ sets the resolution of the phase space. It is important to note that in this contest $\hbar$ is not necessary the proper Planck constant but just a parameter to set the resolution of the system, also $m$ is not necessary the mass of a particle but it is a parameter to obtain the right dimensions [13]. Due to this definition we will see that the parameter $\nu$ sets the magnitude of quantum effects, they are present on scales of the size of the de Broglie wavelength. Hence $\nu$ is artificially chosen to match the classical description by numerical simulation [51, 77]. Lastly we have to observe that in some case $\hbar$ and $m$ are treated actually as the Planck constant and a particle mass, this is the case of the study of exotic dark matter candidates as fuzzy dark matter, this theory is based on an ultra-light axion-light candidate ($m \sim 10^{-22} - 10^{-23}$) which then will have a very large de Broglie wavelength and it gives results comparable with N-body simulations of CDM on large scales [31]. Then we make the Madelung transformations [43]

$$1 + \delta = R^2 \qquad \psi = R\left(\boldsymbol{x}, t\right) e^{-i\phi/\nu} \,. \tag{2.1.7}$$

From this definition derives directly the non-negativity of the density function $\rho = \bar{\rho}|\psi|^2$, so the first problem, stated in the introduction, would be solved. We try to show, for now in a not expanding Universe, that the Schrödinger equation and the fluid equations are actually the same. If we substitute the wave-function $\psi$ in the Schrödinger equation (using for now just one spatial dimension for simplicity)

$$i\hbar\dot{\psi}\left(x,t\right) = \left(-\frac{\hbar^2}{2m}\frac{\partial^2}{\partial x^2} + V\left(x,t\right)\right)\psi\left(x,t\right) \,, \tag{2.1.8}$$

it gives, with the further substitution $\nu = \frac{\hbar}{m}$ in the Madelung definition of the wave-function,

$$\begin{aligned}\left[i\hbar\frac{\partial R}{\partial t} + Rm\frac{\partial \phi}{\partial x}\right] e^{-im\phi/\hbar} = \Bigg[-\frac{\hbar^2}{2m}\frac{\partial^2 R}{\partial x^2} + \frac{i\hbar}{2}\frac{\partial^2\phi}{\partial x^2}R + i\hbar\frac{\partial R}{\partial x}\frac{\partial\phi}{\partial x} + \\ + \frac{m}{2}\left(\frac{\partial\phi}{\partial x}\right)^2 R + V\,R\Bigg] e^{-im\phi/\hbar} \,.\end{aligned} \tag{2.1.9}$$

We can solve separately the real and imaginary parts of this equation.
Multiplying both sides of the imaginary part by $2R$:

$$2R\frac{\partial R}{\partial t} = +2R\frac{\partial R}{\partial x}\frac{\partial\phi}{\partial x} + R^2\frac{\partial^2\phi}{\partial x} \,, \tag{2.1.10}$$

that can be rewritten as

$$\frac{\partial R^2}{\partial t} = +\frac{\partial}{\partial x}\left(R^2\frac{\partial\phi}{\partial x}\right) \,, \tag{2.1.11}$$

which substituting $\rho = R^2$ and $\boldsymbol{v} = -\nabla\phi$ gives the continuity equation (1.2.12) in one dimensional case.
Instead the real part is

$$+mR\frac{\partial\phi}{\partial t} = \frac{m}{2}\left(\frac{\partial\phi}{\partial x}\right)^2 R - \frac{\hbar^2}{2m}\frac{\partial^2 R}{\partial x^2} + VR\,, \tag{2.1.12}$$

that can be rewritten as

$$\frac{\partial\phi}{\partial t} - \frac{1}{2}\left(\frac{\partial\phi}{\partial x}\right)^2 = \frac{1}{m}V(x,t) + Q(x,t)\,, \tag{2.1.13}$$

where

$$Q(x,t) = -\frac{\hbar^2}{2m^2}\frac{1}{R}\frac{\partial^2 R}{\partial x^2} \tag{2.1.14}$$

is called Bohm quantum potential and is a pure quantum term (in the limit $\hbar \to 0$ it vanishes). The equation (2.1.13) is the quantum version of the Hamilton-Jacobi equation (2.1.2) in a static Universe ($a = 1$) with the addition of the Bohm quantum potential and with the tranformation of the potential $V \to mV$.
So we have derived the equations that describe the evolution of a quantum fluid. Now instead we want to follow the opposite route: starting from the continuity, Euler and Poisson equations we want to derive the Schrödinger equation associated to them.
First we need to derive the expression for the gradient and Laplacian of $\psi$, this time using $\nu$ instead of $\hbar/m$:

$$\nabla\psi = \left(\nabla R - i\frac{R}{\nu}\nabla\phi\right)e^{-\frac{i\phi}{\nu}}\,, \tag{2.1.15}$$

$$\nabla^2\psi = \left[\nabla^2 R - \frac{i}{\nu}\left(R\nabla^2\phi + 2\nabla R\cdot\nabla\phi\right) - \frac{R}{\nu^2}(\nabla\phi)^2\right]e^{-\frac{i\phi}{\nu}}\,. \tag{2.1.16}$$

Using the continuity equation (2.1.11) written as

$$2\frac{\partial R}{\partial t} = \left(2\nabla R\cdot\nabla\phi + R\nabla^2\phi\right)\,, \tag{2.1.17}$$

we can simplify the expression of $\nabla^2\psi$ obtaining

$$\nabla^2\psi = \left[\nabla^2 R - \frac{2i}{\nu}\frac{\partial R}{\partial t} - \frac{R}{\nu^2}(\nabla\phi)^2\right]e^{-\frac{i\phi}{\nu}} \tag{2.1.18}$$

and rearranging the terms

$$(\nabla\phi)^2 = -\frac{\nu^2}{R}\nabla^2\psi e^{\frac{i\phi}{\nu}} + \frac{\nu^2}{R}\nabla^2 R - \frac{2i\nu}{R}\frac{\partial R}{\partial t}\,. \tag{2.1.19}$$

We need to compute also the time derivative of $\psi$

$$\frac{\partial\psi}{\partial t} = \left(\frac{\partial R}{\partial t} - \frac{iR}{\nu}\frac{\partial\phi}{\partial t}\right)e^{-\frac{i\phi}{\nu}}\,, \tag{2.1.20}$$

which gives

$$\frac{\partial\phi}{\partial t} = -\frac{i\nu}{R}\left(\frac{\partial R}{\partial t} - e^{\frac{i\phi}{\nu}}\frac{\partial\psi}{\partial t}\right) . \tag{2.1.21}$$

Replacing (2.1.19) and (2.1.21) in the Hamilton-Jacobi equation (2.1.2) and neglecting the expansion of the Universe we get:

$$\frac{i\nu}{R}\left(\frac{\partial R}{\partial t} - e^{\frac{i\phi}{\nu}}\frac{\partial\psi}{\partial t}\right) - \frac{1}{2}\left(\frac{\nu^2}{R}\nabla^2\psi e^{\frac{i\phi}{\nu}} - \frac{\nu^2}{R}\nabla^2 R + \frac{2i\nu}{R}\frac{\partial R}{\partial t}\right) = -V\,, \tag{2.1.22}$$

that can be written as

$$i\nu\frac{\partial\psi}{\partial t} = \frac{\nu^2}{2}\frac{\nabla^2 R}{R}\psi + \left(-\frac{\nu^2}{2}\nabla^2 + V\right)\psi\,. \tag{2.1.23}$$

This is the usual Schrödinger equation (in a non-expanding Universe) with an additional term, equal to minus the Bohm potential present in (2.1.13), usually called quantum pressure.

$$P = \frac{\nu^2}{2}\frac{\nabla^2 R}{R} \tag{2.1.24}$$

The name of this term can be better understood by observing how it arises as the Bohm potential $Q$. At this point we can also say more on the parameter $\nu$, that resembles the Planck constant of Quantum Mechanics. As we anticipated in the introduction of this chapter, because we are dealing with a classical system we treat $\nu$ as an adjustable parameter that controls the quantum pressure, this is more clear observing (2.1.13) and (2.1.14) where $\hbar \sim \nu$ appears only in front of $P = -Q$. The quantum pressure term acts as a regularizing term preventing the generations of multi-stream regions and singularities in the density field when particle trajectories cross, in a manner similar to the viscous term of the adhesion approximation [23]. The adhesion approximation consist in the addition of an artificial viscous term in the hydrodynamical equation, hence transforming the momentum equation in the Burgers' equation

$$\frac{D\mathbf{u}}{Dt} = \nu\nabla^2\mathbf{u}\,, \tag{2.1.25}$$

where here $\nu$ represents the kinematical viscosity and also in this case, since the viscosity is artificial, it is a controlled parameter to match N-body simulations. It can be shown that the quantum pressure has a similar effect, it is evident in particular in the free-particle approximation (which consist in neglect the external potentials in the Schrödinger equation) and which results we will depict in Sect.3.2. The comparison between the free-particle and the adhesion approximation is already deeply studied in literature, e.g. in [68]. The viscous term becomes large when particle trajectories intersect (shell-crossing), cancelling the component of the particle velocities perpendicular to the caustic thus particles are able to form stable structures. Since our system is composed of two "fluids" we have to be more precise in the multi-streaming notation, from the definition of the quantum pressure (2.1.24) it is clear that there is a pressure generated by each fluid and it depends only on the density field of the component which generates it. Hence we expect that it prevents the multi-streaming between different streams of the same fluid component, e.g. the DM

quantum pressure will prevent the shell-crossing and multi-streaming between different DM trajectories, this is caused by the fact that the quantum pressure of one component is enhanced by the overdensity of that single component. We could physically expect this result because for now there is no observational prove of an interaction (different from the gravitational one) between baryons and dark matter (it seems that even in the highly non-linear regime of perturbation, as inside galaxy clusters, there is no collisional interaction between baryons and DM [29]). Therefore the fact that a "mixed" quantum pressure does not arise can be interpreted as a adjunctive prove of efficiency of the Schrödinger-Poisson model in describing the evolution of LSS.
Then in this section we started describing a general quantum system with the usual Schrödinger equation and from that we derived the fluid equation; in the Hamilton-Jacobi (2.1.13) equation the Bohm potential arises in a position (and with the dimensions) usually taken by a pressure term. It's important to notice that we can take care of this term in two different ways:

- putting $Q$ in the Hamilton-Jacobi (2.1.13) and so dealing with the usual Schrödinger equation (2.1.8), i.e. considering a quantum fluid
- putting $Q$ in the Schrödinger equation (2.1.23) and keeping the usual classical fluids Hamilton-Jacobi equation

We observed also that the quantum effects, in particular the quantum pressure, are regularized by the choice of the phase space resolution $\nu$ [51]. Then we obtained a description of a fluid based just on a function $\psi$ and a resolution parameter $\nu$. This new description have a great potential in both analytical (e.g. [30, 67, 73]) and numerical (e.g. [77, 80]) descriptions of large-scale structure of the Universe.

## 2.2 CDM and ΛCDM Universe

### CDM Universe

Now we want to take care of the Universe expansion. We begin the study considering an Universe filled only by Cold Dark Matter (CDM), which is collisionless, and baryons, which experience a pressure. Later we will introduce also Dark Energy (as a cosmological constant) and see how the equation describing the evolution of LSS change.
First of all we rewrite the Euler (1.2.14) and Hamilton-Jacobi (2.1.2) equations in a more useful way as firstly done by Zel'dovich, using the two new variables:

$$\boldsymbol{u} = \frac{d\boldsymbol{x}}{da} \qquad \varphi = \frac{3}{2}\frac{t_*^2}{a_*^3}\Phi\,. \tag{2.2.1}$$

Note that in a matter dominated flat Universe from the expression of the Hubble parameter (1.4.8) the following equivalence is true

$$a^3H^2 = a^3H_0^2\Omega_{0m}a^{-3} = H_0^2\Omega_{0m} \tag{2.2.2}$$

and since the scale factor follows $a(t) = a_*\,(t/t_*)^{2/3}$ and then the Hubble parameter $H = \dot{a}/a = 2/(3t)$ with $a_*$ the scale factor at some set time $t_*$, the following relation holds

$$\frac{3}{2}\frac{t_*^2}{a_*^3} = \frac{2}{3a_*^3H_*^2} = \frac{2}{3\Omega_{0m}H_0^2}\,. \tag{2.2.3}$$

Hence we can rewrite the Euler equation in the new coordinates, for example for baryons,

$$\frac{D\mathbf{u}_b}{Da} = -\frac{3}{2a}\left[\mathbf{u}_b + \nabla\varphi + \left(\frac{3t_*^2}{2a_*^3}\right)\frac{\nabla P_b}{\rho_b}\right], \tag{2.2.4}$$

and doing the same for DM we obtain a similar equation, just without the pressure gradient. Expressing the velocity through its potential $\mathbf{u}_b = -\nabla\phi_b$ we can transform the Euler equation (2.2.4) in the Bernoulli equation

$$\frac{\partial\phi_b}{\partial a} - \frac{1}{2}(\nabla\phi_b)^2 = \frac{3}{2a}\left[\varphi - \phi_b + A'\frac{\gamma}{\gamma-1}\eta_b^{\gamma-1}\right], \tag{2.2.5}$$

where

$$A' = \frac{3t_*^2}{2a_*^3}\frac{k_b T_0(z)}{\mu m_p} \tag{2.2.6}$$

and we have done an abuse of notation, still calling $\phi$ the potential of $\boldsymbol{u}$. We can observe that the only difference between the Hamilton-Jacobi equation in an expanding Universe (2.2.5) and in a non-expanding one (2.1.2) is the substitution $t \to a$ in the time derivation and the use of a new potential

$$V + P = \frac{3}{2a}(-\phi + \varphi) + \frac{3}{2a}A'\frac{\gamma}{\gamma-1}\eta_b^{\gamma-1}. \tag{2.2.7}$$

So we can easly rewrite the baryons Schrödinger equation (2.1.23) in an expanding Universe as

$$i\nu\frac{\partial\psi_b(\mathbf{x},a)}{\partial a} = \left[Q_b - \frac{\nu^2}{2}\nabla^2 + V_b - \frac{3}{2a}\frac{\gamma A'}{\gamma-1}|\psi_b|^{2\gamma-2}\right]\psi_b \tag{2.2.8}$$

and similarly for DM, just neglecting the pressure term

$$i\nu\frac{\partial\psi_{DM}(\mathbf{x},a)}{\partial a} = \left[Q_{DM} - \frac{\nu^2}{2}\nabla^2 + V_{DM}\right]\psi_{DM}, \tag{2.2.9}$$

where

$$Q_{b,DM} = \frac{\nu^2}{2}\frac{\nabla^2\sqrt{1+\delta_{b,DM}}}{\sqrt{1+\delta_{b,DM}}} = \frac{\nu^2}{2}\frac{\nabla^2|\psi_{b,DM}|}{|\psi_{b,DM}|} \tag{2.2.10}$$

is the Quantum Pressure. We used the subscript $b, DM$ to indicate that we can write such quantity in a similar way for both DM and baryons, i.e. for a generic quantity $f_{b,DM} = c\,A_{b,DM}$ relative to baryons or DM, $c$ is a coefficient equal for both baryons and DM and $A_{b,DM}$ in another function which have different values if it is evaluated for the baryon or DM component

$$f_b = c\,A_b, \tag{2.2.11}$$

$$f_{DM} = c\,A_{DM}. \tag{2.2.12}$$

Clearly if $A_b = A_{DM}$ also $f_b = f_{DM}$. The "external" potential is

$$V_{b.DM} = \frac{3}{2a}(-\phi_{b,DM} + \varphi) \tag{2.2.13}$$

We still have to couple the Schrödinger equations to the Poisson equation, which can be expressed in the new variables (2.2.1) as

$$\nabla^2 \left( V_{DM} - \frac{3\nu}{2a} Arg\left(\psi_{DM}\right) \right) = \frac{3}{2a^2} \left( |\psi_{DM}|^2 - 1 \right) . \tag{2.2.14}$$

Where $Arg(\psi_{DM}) = -\phi_{DM}/\nu$ due to the Madelung definition of the wave-function (2.1.7) and we rewrite the baryons potential in terms of the DM one as

$$V_b = V_{DM} + \frac{3}{2a}\nu \left[ Arg(\psi_b) - Arg(\psi_{DM}) \right] = V_{DM} + \frac{3}{2a}\nu Arg\left(\psi_b/\psi_{DM}\right) . \tag{2.2.15}$$

Then the CDM-baryons system is fully described by the set of equations (2.2.8), (2.2.9) and (2.2.14), note that we almost halved the number of equation needed, this is a general property of the Schrödinger-Poisson model since the wave-function contains information on both the density and velocity fields [67].
So, as anticipated, we have now a density defined non-negative, as it should be, and also the problem of shell-crossing is solved because the wave-function $\psi$ has no singularities (this is not a property of just the Schrödinger model, also N-body simulations can describe the system after the shell-crossing without problems [8]).
We want now to make explicit the time dependence of the pressure coefficient $A'$, which is given by the baryon mean temperature $T_0(z)$. We use a simple law, but fairly general, of the type

$$T_0(z) \propto (1+z)^\alpha \propto a^{-\alpha} \tag{2.2.16}$$

with $\alpha \leq 1$, it is provided by experimental observations [47].
We can define an useful quantity for describe this coefficient, the "modified" Jeans wavenumber, from the Jeans wavenumber in the CDM Universe (we will compute it in the more general case of a ΛCDM Universe in App.A1), the Jeans wavenumber is a result of linear perturbation theory and it sets the scale for which the gravitational potential is strong enough to counter the baryon gas pressure and start the gravitational collapse of a matter region, i.e. for $k < k_J$ instabilities can grow, and thus sets the characteristic scale of pressure action [7]. In CDM-baryon dominated Universe it takes the form [47]

$$k_J^2 = \frac{3}{2} a^{-1} \frac{H_0^2 \Omega_{0m} \mu m_p}{\gamma k_b T_0(z)} . \tag{2.2.17}$$

Instead the modified Jeans wavenumber is defined in a way such as it is redshift indipendent (i.e. constant in time) [47]

$$\tilde{k}_J^2 = k_J^2 a^{1-\alpha} = \frac{3}{2} a^{-\alpha} \frac{H_0^2 \Omega_{0m} \mu m_p}{\gamma k_b T_0(z)} = \frac{3}{2\gamma A'} a^{-\alpha} , \tag{2.2.18}$$

where we used that in a matter dominated Universe $a^3/t^2 \sim a^3 H^2 = \texttt{const} \sim H_0^2 \Omega_{0m}^3$ as showed in (2.2.2). Note that only in the case $\alpha = 1$, i.e. $T_0 \propto a^{-1}$ the Jeans wavenumber is constant. Neglecting the expansion of the expansion of the Universe the comoving Jeans wavelength for a monoatomic gas ($\gamma = 5/3$) would have dimension [50]

$$\lambda_J = \frac{2\pi}{k_J} \approx 0.01 (\Omega_{b0} h^2)^{-1/2} Mpc \approx 0.06 Mpc , \tag{2.2.19}$$

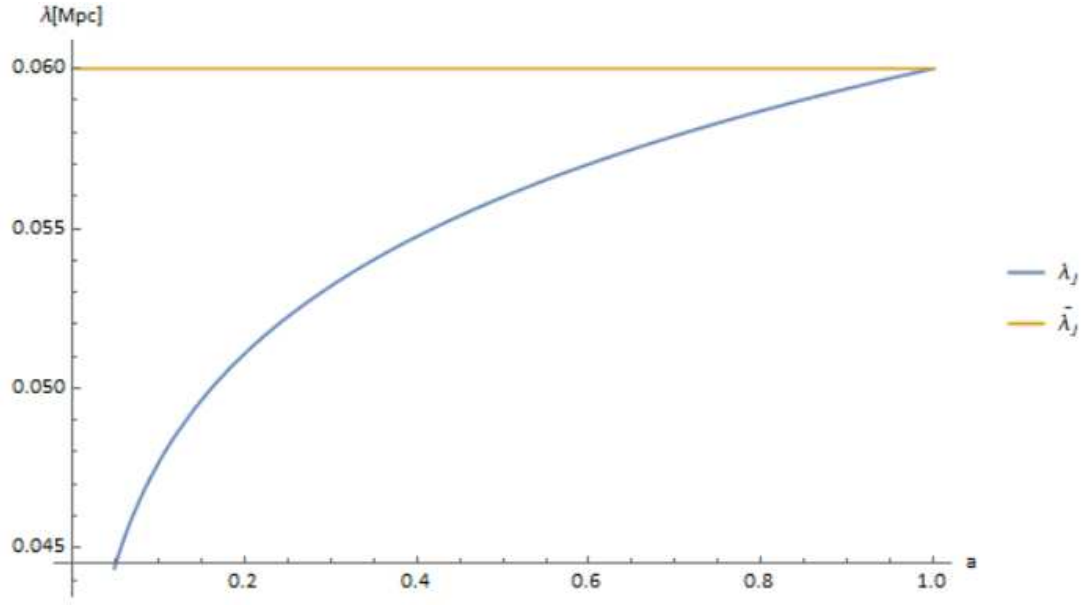


Figure 2.1: Time evolution of the comoving Jeans wavelength (blue line), it is compared to the modified comoving Jeans wavelength (orange line) for which is used the reference value (2.2.19). It is used $\alpha = 0.8$.

where in the last equality we used $\Omega_{b0} = 0.05$ and $h = 0.7$, which is a correction factor for the value of the Hubble constant $H_0$. We can keep this value as a reference dimension for $\tilde{k}_J^{-1}$ and show the time-evolution of the comoving Jeans wavelength in function of the scale factor $a$ in Fig.2.1, for example is used a temperature-redshift dependence of $\alpha = 0.8$. We can physically interpret $\tilde{k}_J$ such as it represents an effective scale for the gas pressure action which remains constant during the evolution of the pressure, this in turn can be interpreted such as only the pressure "magnitude" varies during the time evolution of the Universe instead its "range of action" remains constant.
Finally we can write the Schrödinger equation for baryons (2.2.8) as

$$i\nu\frac{\partial\psi_b(\mathbf{x},a)}{\partial a} = \left[Q_b - \frac{\nu^2}{2}\nabla^2 + V_b - \frac{9}{4a^{\alpha+1}}\frac{1}{\gamma-1}\frac{1}{\tilde{k}_J^2}\left|\psi_b\right|^{2\gamma-2}\right]\psi_b(\mathbf{x},a)\,. \tag{2.2.20}$$

Now the time dependence of the pressure term coefficient is factorized and take the simple form of $a^{-(\alpha+1)}$.

## ΛCDM Universe

To be more general we pass to the study of an Universe where is present also Dark Energy, modelled as a cosmological constant $\Lambda$. In this case is more useful to use the growth factor $D$ as time scale instead of the scale factor, thus we use the new variables [12] (with an abuse of notation respect the $\Lambda = 0$ case):

$$\varphi = \frac{2D\Phi}{3e(\Omega_{DM})a^2\dot{D}^2}, \qquad \mathbf{u} = \frac{d\mathbf{x}}{dD} = \frac{\mathbf{v}}{a\dot{D}}\,, \tag{2.2.21}$$

where $e(\Omega_{DM}) = \Omega_{DM}/f^2(\Omega_{DM})$, $f(\Omega_{DM})$ is defined in (1.4.18). Then using the growth factor $D$ as time we can rewrite the fluid equations for baryons as

$$\frac{\partial \mathbf{u}_b}{\partial D} + (\mathbf{u}_b \cdot \nabla)\mathbf{u}_b + \frac{3e(\Omega_{DM})}{2D}(\mathbf{u}_b + \nabla\varphi) + \frac{e(\Omega_{DM})}{a^2 D^2 H^2 \Omega_{DM}} \frac{\nabla P_b}{\rho_b} = 0\,, \tag{2.2.22}$$

$$\frac{\partial \delta_b}{\partial D} + \nabla \cdot [(1+\delta_b)\,\mathbf{u}_b] = 0\,, \tag{2.2.23}$$

$$\nabla^2\varphi - \frac{1}{D}\delta_{DM} = 0 \tag{2.2.24}$$

and similarly for DM. In the last equation, the Poisson one, we are neglecting the baryons self gravity as we have done in the course of this work since the baryon mass mean fraction is much smaller that the DM one.
As we have done before, assuming the velocity irrotational $\mathbf{u}_b = -\nabla\phi_b$, we can pass to an Hamilton-Jacobi equation for the velocity potential

$$\frac{\partial \phi_b}{\partial D} - \frac{1}{2}|\nabla\phi_b|^2 = \frac{3e(\Omega_{DM})}{2D}(\varphi - \phi_b) + \frac{e(\Omega_{DM})}{a^2 D^2 H^2 \Omega_{DM}} \frac{\gamma}{\gamma - 1} A \rho_b^{\gamma-1} = 0 \tag{2.2.25}$$

and then, since as in the $\Lambda = 0$ case the only difference from the Hamilton-Jacobi equation in a non-expanding Universe (2.1.2) is the change of the time variable and the definition of a new potential, we can easily write the Schrödinger equations

$$i\nu\frac{\partial \psi_b}{\partial D} = \left[-\frac{\nu^2}{2}\nabla^2 + V_b + Q_b + \frac{e(\Omega_{DM})A}{a^2 D^2 H^2 \Omega_{DM}} \frac{\gamma}{\gamma - 1}|\psi_b|^{2\gamma-2}\right]\psi_b\,, \tag{2.2.26}$$

$$i\nu\frac{\partial \psi_{DM}}{\partial D} = \left[-\frac{\nu^2}{2}\nabla^2 + V_{DM} + Q_{DM}\right]\psi_{DM}\,, \tag{2.2.27}$$

where

$$A = \frac{k_b T_0(z)}{\mu m_p}\,, \qquad V_{b,DM} = \frac{3e(\Omega_{DM})}{2D}(\varphi - \phi_{b,DM}) \tag{2.2.28}$$

and $Q$ is the already defined Quantum Pressure (2.2.10).
We have to couple it to the Poisson equation which after the Madelung transformations can be expressed as

$$\nabla^2\left[V_{DM} - \nu Arg[\psi_{DM}]\right] = \frac{3e(\Omega_{DM}}{2D^2}(|\psi_{DM}|^2 - 1) \tag{2.2.29}$$

and we relate the baryon potential to the DM one

$$V_b = V_{DM} + \nu Arg[\psi_b/\psi_{DM}]\,. \tag{2.2.30}$$

Thus our system is described by the three variables $\psi_{b,DM}$, $V_{DM}$ and by the three corresponding equations (2.2.26), (2.2.27) and (2.2.29). Hence we begun with a system of 5 equation and at the end we arrived to a system of just 3 equations.
We want to define a redshift independent wavenumber from the last term of the Schrödinger equation (2.2.26) as we have done in (2.2.18). Thus we have to study the coefficient of the pressure term to extrapolate its time dependence. From the relation for $H$ (1.4.8) in a flat Universe ($\Omega_0 = 1$) and using

$$\Omega_{i0} = \frac{8\pi G\rho_{i0}}{3H_0^2} \quad i = m, \Lambda\,, \tag{2.2.31}$$

we obtain

$$a^3H^2 = a^3\frac{8\pi G}{3}\left(\rho_{m,0}a^{-3} + \rho_{\Lambda,0}\right) = H_0^2\left(\Omega_{0m} + a^3\Omega_{0\Lambda}\right) \tag{2.2.32}$$

and so we write the pressure coefficient from (2.2.26) as

$$\frac{\gamma k_b T_0(z)}{\mu m_p(\gamma-1)}\frac{e(\Omega_{DM})}{D^2\Omega_{DM}}\frac{a}{H_0^2\Omega_{0m}}\frac{1}{1+a^3\frac{\Omega_{0\Lambda}}{\Omega_{0m}}}\,. \tag{2.2.33}$$

We can simplify this expression through the use of the Jeans wavenumber, as we have done in the CDM Universe scenario. We computed the evolution in time of the $k_J$ in the case of a ΛCDM Universe in App.A1.

$$k_J^2(D) = \frac{3a^2H^2\Omega_{DM}\mu m_p}{2\gamma k_b T_0(a)} = \frac{3H_0^2\Omega_{0m}\Omega_{DM}\mu m_p}{2a\gamma k_b T_0(a)}\left(1 + a^3\frac{\Omega_{0\Lambda}}{\Omega_{0m}}\right)\,, \tag{2.2.34}$$

where we used (2.2.32) to simplify $a^2H^2$. Now we have to use the relation between the growth factor $D$ and the scale factor $a$, which, at early times, we approximate to $a = M^{-1}(D)D$ with $M(D)$ defined in (1.4.27).

$$k_J^2(D) = \frac{3M(D)\mu m_p\Omega_{0m}H_0^2\Omega_{DM}(D)}{2D\gamma k_b T_0(D)}\left(1 + \frac{D^3}{M^3(D)}\frac{\Omega_{0\Lambda}}{\Omega_{0m}}\right)\,, \tag{2.2.35}$$

where $T_0(D) \propto a^{-\alpha} \propto \left(\frac{M(D)}{D}\right)^{\alpha}$ from (2.2.16). Then we can rewrite the pressure coefficient (2.2.33) as

$$\frac{3}{2e(\Omega_{DM})(\gamma-1)D^2k_J^2} \tag{2.2.36}$$

or if we define the modified Jeans wavenumber equivalent of (2.2.18) in the $\Lambda CDM$ Universe, which is time-independent,

$$\tilde{k}_J^2 = \left(\frac{M(D)}{D}\right)^{\alpha-1}\frac{k_J^2}{\Omega_{DM}(D)}\,, \tag{2.2.37}$$

as

$$\frac{3M^{\alpha-1}(D)}{2D^{\alpha+1}e(\Omega_{DM})\Omega_{DM}(\gamma-1)}\frac{1}{\tilde{k}_J^2}\,. \tag{2.2.38}$$

At early times the term $(D/M)^3(\Omega_{0\Lambda}/\Omega_{0m})$ present in (2.2.35) is negligible and so $\tilde{k}_J^2$ is constant in time, because we are expressing the temperature as (2.2.16).
Note that at early times we can use the same approximation we used in (1.4.27), i.e. use $a = D$ in the omegas, to express $f^2(D) = \Omega_{DM}/e(\Omega_{DM})$ from the $f(a)$ given by (1.4.25). Finally we can rewrite the baryon Schrödinger equation (2.2.26) as

$$i\nu\frac{\partial\psi_b}{\partial D} = \left[-\frac{\nu^2}{2}\nabla^2 + V_b + Q_b + \frac{3}{2}\frac{M^{\alpha-1}(D)}{D^{\alpha+1}}\left(\frac{f(D)}{\Omega_{DM}}\right)^2\frac{1}{\gamma-1}\frac{1}{\tilde{k}_J^2}|\psi_b|^{2\gamma-2}\right]\psi_b = \tag{2.2.39}$$

$$= \left[-\frac{\nu^2}{2}\nabla^2 + V_b + Q_b + W_b\right]\psi_b\,. \tag{2.2.40}$$

Note that is very similar to the equation in the $\Lambda = 0$ scenario, the only change is in the time dependence of the pressure coefficient

$$\frac{1}{a^{(\alpha+1)}} \to \frac{M^{\alpha-1}(D)f^2(D)}{D^{\alpha+1}\Omega_{DM}^2}\,. \tag{2.2.41}$$

Then the dynamics of the baryon-DM system is described by the set of equations

$$\begin{cases} i\nu\dfrac{\partial\psi_b}{\partial D} = \left[-\frac{\nu^2}{2}\nabla^2 + V_b + Q_b + W_b\right]\psi_b \\ i\nu\dfrac{\partial\psi_{DM}}{\partial D} = \left[-\frac{\nu^2}{2}\nabla^2 + V_{DM} + Q_{DM}\right]\psi_{DM} \\ \nabla^2\left[V_{DM} - \nu Arg[\psi_{DM}]\right] = \frac{3e(\Omega_{DM})}{2D^2}(|\psi_{DM}|^2 - 1) \end{cases} \tag{2.2.42}$$

with $V_b$ given by (2.2.30). All the ingredients to follow the evolution of the structure of the Universe are enclose in this system of equation. We want to derive a solution of this system in order to have a description of the evolution of density and velocity fields of both baryons and DM. We will see in the next section how to derive these fields from the wave function $\psi$.

## 2.3 Relation with observables

To relate the wave function with the usual fluid variables, which are the ones we can observe, there is a method more clever than the Madelung transformation [73]. We describe this method for a general wave-function $\psi$ beacuse it can be applied in the same way to both DM and baryons. We begin writing the Lagrangian for the system (remember that for DM we have to set $P = 0$), in the cosmic time it is

$$\mathcal{L}(\mathbf{x}, \dot{\mathbf{x}}, t) = \frac{1}{2}ma^2\dot{\mathbf{x}}^2 - m\Phi - m\frac{P}{\rho}\,. \tag{2.3.1}$$

As we stated in Sect.2.1 the mass $m$ is actually just a parameter needed to recover the correct dimensions, it is the real mass of a particles only in particular cases where we are considering a true quantum system (e.g. fuzzy dark matter [31]). Using the relations (2.2.21) we can write it in function of the growth factor $D$

$$\mathcal{L}(\mathbf{x}, \mathbf{x}', D) = \frac{1}{2}ma^2\dot{D}^2\mathbf{x}'^2 - m\frac{3e(\Omega_{DM})a^2\dot{D}^2}{2D}\varphi - m\frac{P}{\rho}\,, \tag{2.3.2}$$

where $\mathbf{x}' = \frac{\partial\mathbf{x}}{\partial D}$. From the Lagrangian we can define the conjugate momentum

$$\mathbf{p} = \nabla_{\mathbf{x}'}\mathcal{L} = ma^2\dot{D}^2\mathbf{x}' = ma^2\dot{D}^2\mathbf{u}\,. \tag{2.3.3}$$

Note that $a^2\dot{D}^2 = D^2a^2H^2\Omega_{DM}/e(\Omega_{DM})$ can be written in terms of $e(\Omega_{DM})$ but in this section we will keep the notation $a^2\dot{D}^2$ for compactness.
Then we construct a phase-space distribution function $f(\boldsymbol{x}, \boldsymbol{p})$ from the wave function $\psi$ using the Wigner function [78], which actually is a proper phase-space function only for scales bigger than $\nu$ because otherwise it can be not defined positive everywhere [72],

thus it is a qausi-probability function. But since we are interested in small values of $\nu$ this won't be a problem.

$$f_W(\mathbf{x},\mathbf{p},D) \equiv \int \frac{d^3x'}{(2\pi)^3} e^{-\frac{i}{\hbar}\frac{\mathbf{p}\cdot\mathbf{x'}}{a^2\dot{D}^2}} \psi(\mathbf{x}+\frac{1}{2}\mathbf{x'},D)\bar{\psi}(\mathbf{x}-\frac{1}{2}\mathbf{x'},D)\,. \tag{2.3.4}$$

In the exponential we can note that the following relation holds

$$\frac{1}{\hbar}\frac{\mathbf{p}}{a^2\dot{D}^2} = \frac{m\mathbf{u}}{\hbar} = \frac{\mathbf{u}}{\nu}\,. \tag{2.3.5}$$

Then the parameter $m$ is reincorporated inside the parameter $\nu$ as expected. Since is more common to use the momentum $\mathbf{p}$ in the distribution function we will set to unity the parameter $m$ so that we can directly use the parameter $\nu$ and do not worry for $m$ since it is always enclosed in $\nu$, i.e. the exponential will be

$$\exp\left[-\frac{i}{\nu}\frac{\mathbf{p}\cdot\mathbf{x'}}{a^2\dot{D}^2}\right]\,. \tag{2.3.6}$$

Anyway if needed (e.g. when we deal with real quantum systems) we can retrieve $m$ by dimensional arguments. From the form of this exponential it is clearer that the parameter $\nu$ choice corresponds to a coarse-graining, the integral is a sort of Fourier transform and $\nu$ select the resolution of the Fourier space, i.e. the phase space.
We make an additional change of variable $\mathbf{y} = \mathbf{x}'/\nu$ for have the Wigner distribution in a form more suitable to some analytical computation we will do in the course of this work.

$$f_W(\mathbf{x},\mathbf{p},D) = \int \frac{d^3y}{(2\pi)^3} e^{-i\frac{\mathbf{p}\cdot\mathbf{y}}{a^2\dot{D}^2}} \psi(\mathbf{x}+\frac{\nu}{2}\mathbf{y},D)\bar{\psi}(\mathbf{x}-\frac{\nu}{2}\mathbf{y},D)\,, \tag{2.3.7}$$

where the $\bar{\psi}$ indicates the complex conjugate of $\psi$. The Wigner distribution function has the virtue of providing information about the state of the system in phase space. This contrasts with the more conventional quantum representations, which may provide information about position only, or about momentum only, but not both together [3]. It can be a useful calculational tool. We have to observe that $f_W$ is not positive defined, hence it can have some problems in the location where it becomes negative [3]. In the original paper [78] Wigner used it to calculate the quantum corrections to the equation of state of a gas of interacting atoms. We will show that the first two momenta of the distribution correspond to the energy density and momentum.
An interesting property of the Wigner distribution is that it cannot be sharply peaked due to indeterminacy principle [3], i.e.

$$\int d^3p\, d^3x\, |f_W(\mathbf{x},\mathbf{p},D)|^2 \leq (2\pi\hbar)^{-1}\,. \tag{2.3.8}$$

Suppose that $f_w$ vanishes outside a region in the phase-space of area $A$, then the integral (2.3.8) yields $A^{-1}$ which means that the phase-space region must satisfy $A \geq 2\pi\hbar$. Since in our model $\hbar$ is not the real Planck constant but it is an artificial parameter related to the parameter $\nu$, it actually sets the resolution of the phase-space.
Wigner in [78] demonstrated that the evolution of $f_W$, constructed from $\psi$ satisfying a Schrödinger equation like

$$i\nu\frac{\partial\psi}{\partial D} = \left[-\frac{\nu^2}{2}\nabla^2 + V\right]\psi\,, \tag{2.3.9}$$

is described by a Boltzman-like equation up to second order in $\nu$, where the gradient of $V$ takes the place of the external forces. We can show it performing twice an integration by parts of the Schrödinger equation which yields [72]

$$\partial_D f_W = -\frac{\mathbf{p}}{a^2 D^2}\nabla_{\mathbf{x}} f_W + \frac{i}{\nu}\int \frac{d^3x'}{(\pi\nu)^3}\exp\left[\frac{i}{\nu}\mathbf{p}\cdot\mathbf{x}'\right]\times$$
$$\times\left(V(\mathbf{x}+\frac{1}{2}\mathbf{x}') - V(\mathbf{x}-\frac{1}{2}\mathbf{x}')\right)\psi(\mathbf{x}-\frac{1}{2}\mathbf{x}')\bar{\psi}(\mathbf{x}+\frac{1}{2}\mathbf{x}')\,. \tag{2.3.10}$$

To express the last term in terms of the Wigner function we have to Taylor expand the difference between the potentials $V$ around $\mathbf{x}$ [3].

$$V(\mathbf{x}+\frac{1}{2}\mathbf{x}') - V(\mathbf{x}-\frac{1}{2}\mathbf{x}') = \sum_{n=odd}\frac{2\partial_x^{(n)}V(\mathbf{x})}{n!}\left(\frac{1}{2}\mathbf{x'}\right)^n\,. \tag{2.3.11}$$

The difference between the $(\mathbf{x}'/2)^n$ can be rewritten as $-i\nu\partial_p^{(n)}\exp[i\mathbf{p}\cdot\mathbf{x'}/\nu]/(2^n)$ [3]. After resumming the various terms we can write the evolution of the Wigner function as [3]

$$\partial_D f_W = -\frac{\mathbf{p}}{a^2\dot{D}^2}\nabla_{\mathbf{x}} f_W + \sum_{n=odd}\frac{1}{n!}\left(-\frac{1}{2}i\nu\right)^{n-1}\partial_x^{(n)}V\partial_p^{(n)}f_W\,. \tag{2.3.12}$$

This equation at leading order differs from the Vlaslov (or collisonless-Boltzmann) equation only by a term proportional to $\nu^2$ [72], if we call $f$ a general distribution function solving the Vlaslov equation with an Hamiltonian $H = T + V_{eff}$ we can write [72]

$$\partial_D(f_W - f) \simeq \frac{\nu^2}{24}\partial_{x_i}\partial_{x_j}\nabla_{\mathbf{x}}V_{eff}\partial_{p_i}\partial_{p_j}\nabla_{\mathbf{p}}f_W + \mathcal{O}(\nu^4)\,. \tag{2.3.13}$$

This difference has a similar nature with respect to the appearance of the quantum pressure in the fluid treatment of Sect.2.1, hence also when working with the Wigner distribution we have to keep $\nu$ small to don't encounter quantum artefacts. Thus we found that using the Wigner function we are actually following a Boltzmann description of baryons and DM, which is better suited in the study od dark matter with respect to the fluid description we depicted in Cap.1.2. In other words, the Wigner function describes the distribution of particles which evolve accordingly the collisionless Boltzmann (Vlaslov) equation.
The Wigner function is constructed in a way such as the normalized density $\eta = 1+\delta$ and the mean peculiar momentum $\boldsymbol{j} = (1+\delta)\,\boldsymbol{u}$ are obtained as the two first kinetic moments of $f_W$ (in ordinary QM interpretation they corresponds respectively to the *probability density* and the conserved *probability flux* [73]).

$$\eta^W(x) = \int d^3p\, f_W(x,\boldsymbol{p}) = |\psi|^2\,, \tag{2.3.14a}$$

$$\boldsymbol{j}^W(x) = \int d^3p\,\frac{\boldsymbol{p}}{a^2\dot{D}^2}f_W(x,\boldsymbol{p}) = \frac{i\nu}{2}\left[\psi\nabla\bar{\psi} - \bar{\psi}\nabla\psi\right]\,, \tag{2.3.14b}$$

where we used the notation $x = (\boldsymbol{x}, D)$ to take care of the dependece on time. Note that with those definitions the velocity can be written as the gradient of the phase of the

wave function ($\boldsymbol{u} = -\nabla\phi$ with $\psi = \sqrt{\eta}e^{-i\phi/\nu}$) if and only if the amplitude and phase are sufficiently smooth [73]. So after shell-crossing, which causes strong oscillatory behaviour, the velocity can be no more irrotational and the vorticity can be easily extracted from $f_W$ using the kinetic moments for the definition of the velocity $\boldsymbol{u}^W = \boldsymbol{j}^W/\eta^W$. Hence the potential $\phi$ describes just the irrotational component of the velocity and we have to use the definition of velocity through the kinetic momenta of $f_W$ to have a full description of velocity. Thus we encoded simultaneously the density and velocity information in a single function $f_W$.
We show now that in the semi-classical limit ($\nu \to 0$) the Wigner function recover the distribution function of a perfect fluid. We have to be particularly careful in doing so because also the wave function depends on $\nu$ in its phase. We'll see now that taking this limit of the solutions of the Wigner function (2.3.7) we get the phase-space function of a perfect fluid

$$\begin{aligned}\lim_{\nu\to 0} f_W =& \lim_{\nu\to 0}\int \frac{d^3x'}{(2\pi)^3} e^{-\frac{i\boldsymbol{p}\cdot\boldsymbol{x}'}{a^2\dot{D}^2}} \sqrt{\eta\left(\boldsymbol{x}+\frac{\nu}{2}\boldsymbol{x}'\right)\eta\left(\boldsymbol{x}-\frac{\nu}{2}\boldsymbol{x}'\right)}\times \\ &\times \exp\left[-\frac{i}{\nu}\left(\phi\left(\boldsymbol{x}+\frac{\nu}{2}\boldsymbol{x}'\right)-\phi\left(\boldsymbol{x}-\frac{\nu}{2}\boldsymbol{x}'\right)\right)\right] = \\ =& \int \frac{d^3x'}{(2\pi)^3} e^{\left(-\frac{i\boldsymbol{p}}{a^2\dot{D}^2} - i\frac{\nabla\phi(\boldsymbol{x})}{\nu}\right)\cdot\boldsymbol{x}'}\eta(\boldsymbol{x})\end{aligned}$$

$$\lim_{\nu\to 0} f_W(x,\boldsymbol{p}) = \eta(x)\,\delta_D^{(3)}\left(\frac{\boldsymbol{p}}{a^2\dot{D}^2} - \boldsymbol{u}(x)\right) = f_{fl}(x,\boldsymbol{p}) \tag{2.3.15}$$

Note that despite the $\nu$ prefactor in (2.3.14b) the peculiar velocity is non-zero, this is due to the dependence of $\psi$ on $\nu$. We can also formulate the perfect fluid distribution function in Lagrangian coordinates using mass conservation $\delta = 1/J - 1$, where $J$ is the determinant of the Jacobian $x_{i,j}$ of the coordinate map between Lagrangian ($\mathbf{q}$) and Eulerian ($\mathbf{x}$) frames, in the following way

$$\eta(\boldsymbol{x}) = \int d^3x\, J^{-1}\delta_D^{(3)}(\boldsymbol{x}-\boldsymbol{q}-\boldsymbol{\xi}(\boldsymbol{q})) = \int d^3q\,\delta_D^{(3)}(\boldsymbol{x}-\boldsymbol{q}-\boldsymbol{\xi}(\boldsymbol{q}))$$

where the integration over the Dirac delta is needed to conserve the information on the particle trajectories and $\xi$ is the displacement between Eulerian and Lagrangian coordinates, thus we obtain

$$f_{fl}(x,\boldsymbol{p}) = \int d^3q\,\delta_D^{(3)}(\boldsymbol{x}-\boldsymbol{q}-\boldsymbol{\xi}(\boldsymbol{q}))\,\delta_D^{(3)}\left(\frac{\boldsymbol{p}}{a^2\dot{D}^2} - \boldsymbol{u}^L(\boldsymbol{q})\right) \tag{2.3.16}$$

where $\boldsymbol{u}^L$ is the Lagrangian velocity of the fluid. Then in the semi-classical limit $\nu \to 0$ the Wigner distribution resembles the classical fluid distribution [73].
For overcome the possible negativity of the Wigner distribution we could define a coarse-grained Wigner distribution . One possibility is to use the Husimi distribution [32, 72] defined as

$$f_H(\mathbf{x},\mathbf{u},D) = \frac{1}{(2\pi\sigma_x\sigma_u)^3}\int d^3x'd^3u' e^{-\frac{(\mathbf{x}-\mathbf{x}')^2}{2\sigma_x^2}} e^{-\frac{(\mathbf{u}-\mathbf{u}')^2}{2\sigma_u^2}} f_W(\mathbf{x}',\mathbf{u}',D)\,, \tag{2.3.17}$$

where $\sigma_x$ and $\sigma_u$ are the resolution in position and velocity of the phase-space and in the Wigner function we pass from the use of the momentum $\mathbf{p}$ to the use of the velocity $\mathbf{u}$ thanks to the relation (2.3.3) as we showed previously. Since we already had the coarse-graining parameter $\nu$, these three parameters cannot be independent. The velocity resolution is defined in function of the other two parameters as [37]

$$\sigma_u = \frac{\nu}{2\sigma_x}\,. \tag{2.3.18}$$

Hence in this representation we can separately set the resolution of position and velocity spaces, but we always have to satisfy the constraint $\sigma_x\sigma_u = \nu/2$. The Husimi distribution then can be interpreted as the probability density for the system to occupy a fuzzy region in phase space, of half-widths $\sigma_x$ and $\sigma_u$, centered at $(\mathbf{x}, \mathbf{p})$. In the limit $\sigma_x \to 0$ the distribution function becomes vanishingly narrow in position, and so approximates a position eigenfunction. Alternatively, in the limit $\sigma_x \to \infty$ it approximates a momentum eigenfunction. Thus the Husimi representation, like the Wigner representation, is intermediate between the position and momentum representations [3].
The Husimi distribution is a Gaussian filtered Wigner distribution and is everywhere positive [37]. This property of the Wigner function may explain why it has been found to provide a qualitatively useful description of phase space structures, even though it has no probability interpretation due to its not-positiveness. Any strongly pronounced feature of the Husimi distribution will also show up in the Wigner function, although the latter may also contain unphysical structures [3]. [11] showed that a Gaussian coarse-grained Wigner function has to satisfy the condition $\sigma_x\sigma_u \geq \nu/2$ for be positive defined, therefore the Husimi representation picks the smallest sufficient $\sigma_u$ for a positive phase space distribution given a $\sigma_x$ and $\nu$ [72], or in other words $\nu$ set the best possible velocity resolution $\sigma_u$ given the position resolution $\sigma_x$.
Another good feature of the Husimi distribution is that it can be directly define from the wave-function, and so without the need to sample the quite heavy oscillating Wigner function to construct its coarse-grained function [72], in the following way [3, 37].

$$K_H(\mathbf{x}, \mathbf{u}, D) = \frac{\exp\left[-\frac{(\mathbf{x}-\mathbf{x}')^2}{4\sigma_x^2} - \frac{i}{\nu}\mathbf{u}\cdot\mathbf{x}'\right]}{(2\pi\nu)^{(\mathcal{D}/2)}(2\pi\sigma_x^2)^{\mathcal{D}/4}}\,, \tag{2.3.19}$$

$$\psi_H(\mathbf{x}, \mathbf{u}, D) = \int d^{\mathcal{D}}x'\, K_H(\mathbf{x}, \mathbf{u}, D)\psi(\mathbf{x}', D)\,, \tag{2.3.20}$$

$$f_H(\mathbf{x}, \mathbf{u}, D) = |\psi_H(\mathbf{x}, \mathbf{u}, D)|^2\,, \tag{2.3.21}$$

where $\mathcal{D}$ is the dimension of the coordinate space and it is already used the definition of the velocity resolution (2.3.18). Then we can choose to construct the Husimi function directly from the wave-function or using the Wigner distribution depending on what is simpler for the case under study, usually for numerical codes is faster the direct approach. As we have done for the Wigner distribution we can show that the Husimi distribution follows a Vlaslov like equation up to order $\mathcal{O}(\nu^2)$ [72].
We can relate the observables to the wave function through the Husimi function in the same way of the Wigner one, i.e. thanks to the momenta of the distribution. Actually it results that the momenta of the Husimi distribution are just the coarse-grained Wigner momenta [72], as one could have expected. It is then useful to define a coarse-graining

operator in the following way [37]

$$\bar{f}(D,\mathbf{x},\mathbf{u}) = \int \frac{d^3x'd^3u'}{(2\pi\sigma_x\sigma_u)^3} e^{-\frac{(\mathbf{x}-\mathbf{x}')^2}{2\sigma_x^2}-\frac{(\mathbf{u}-\mathbf{u}')^2}{2\sigma_u^2}} f(D,\mathbf{x}',\mathbf{u}') = e^{\frac{\sigma_x^2}{2}\Delta_x+\frac{\sigma_u^2}{2}\Delta_u}\{f\}\,. \tag{2.3.22}$$

Then the first two momenta of the Husimi distribution results [37]

$$\eta^H = e^{\frac{\sigma_x^2}{2}\Delta_x}\{\eta^W\} = e^{\frac{\sigma_x^2}{2}\Delta_x}\{|\psi|^2\}\,, \tag{2.3.23}$$

$$\mathbf{j}^H = \eta^H\mathbf{u}^H = e^{\frac{\sigma_x^2}{2}\Delta_x}\{\mathbf{j}^W\} = e^{\frac{\sigma_x^2}{2}\Delta_x}\{\frac{i\nu}{2}\left[\psi\nabla\bar{\psi}-\bar{\psi}\nabla\psi\right]\}\,. \tag{2.3.24}$$

It is found that higher momenta depend also on the velocity coarse-graining [72].

## 2.4 Rotational flows

Thanks to the definition of the velocity field through the first order momentum of the Wigner distribution (2.3.14) we no longer have to make the approximation of irrotational flow. The potential $\phi$ still describes the irrotational component of the velocity but a vortical term can arise too. Actually even for an initial irrotational flow, in two or more dimension, an effective vorticity arises after shell-crossing, i.e. after two or more fluid trajectories cross. This vorticity, in classical collisionless dynamics, is generated by a density weighted averaging of the multistream velocities. The velocity field can be decomposed in two terms

$$\mathbf{u} = \mathbf{u}_\parallel + \mathbf{u}_\perp \tag{2.4.1}$$

where $\mathbf{u}_\parallel = -\nabla\phi$ is the irrotational component and $\mathbf{u}_\perp \perp \nabla\phi$ is the rotational component of the velocity field. The vorticity $\boldsymbol{\omega}$ is defined as the curl of the velocity, i.e.

$$\boldsymbol{\omega} = \nabla\times\mathbf{u} \tag{2.4.2}$$

Clearly the irrotational velocity $\mathbf{u}_\parallel$ doesn't contribute to the vorticity.
We showed in Sect.2.1 that the rotational component of the peculiar velocity decays rapidly as $a^{-1}$ in the linear regime of perturbations. Now thanks to the wave-mechanical model we can investigate the velocity field also outside the linear or the irrotational regime. We would like to understand if also in the classical description is possible the arising of vortical motion, to do so it is easier to work with the vorticity $\boldsymbol{\omega}$ instead of the rotational peculiar velocity $\mathbf{u}_\perp$, therefore if we take the curl of the Euler equation (1.2.14) for a collisional fluid we obtain the time evolution equation for the vorticity [7].

$$\frac{\partial\boldsymbol{\omega}}{\partial D} + \frac{3e(\Omega_{DM})}{2D}\boldsymbol{\omega} = \nabla\times(\mathbf{u}\times\boldsymbol{\omega}) - \frac{e(\Omega_{DM})}{a^2D^2H^2\Omega_{DM}}\frac{(\nabla\rho)\times(\nabla P)}{\rho^2}\,, \tag{2.4.3}$$

where we used the property of the vectorial product $\mathbf{a}\times(\mathbf{b}\times\mathbf{c}) = \mathbf{b}(\mathbf{a}\cdot\mathbf{c}) - \mathbf{c}(\mathbf{a}\cdot\mathbf{b})$. The last term is called baroclinity and it is present only for the baryon component since the dark matter has no pressure. The terms on the right-hand side generates the vorticity, instead on the left-hand side the Hubble drag tends to damp it. Hence we expect to encounter some vorticity in the evolution of the Universe both in the DM and in the baryon fluids when their perturbations reach the non-linear regime.

Note that with our simple model of the baryon gas pressure, i.e. a barotropic pressure, the baroclinic term vanishes since $\nabla P \propto \nabla\rho$ (1.2.18). The barotropic assumption take its basis on the fact that we can express also the temperature evolution in function of the density perturbations [48] $T \propto (1+\delta_b)^{\gamma-1}$ and so we expect that with the right choice of the adiabatic index $\gamma$ we can recover the correct vorticity which would be generated by the baroclinic term in the presence of a more general equation of state for the pressure. Hence in our model the vorticity in the DM and in the baryon fluid is produce in the same way, i.e. by averaging nearby fluid streams [73].
Another important consequence of the equation (2.4.3) is the Kelvin-Helmoltz theorem [27, 42] for the conservation of vorticity flux, which derives directly from the Stoke's theorem. It states that if the baroclinic term vanishes [7]

$$\mathcal{I} = \oint_{C(D)} \mathbf{u}\cdot d\mathbf{x} = \int_S (\nabla\times\mathbf{u}) d\mathbf{S} \quad \text{is a integral invariant}\,, \tag{2.4.4}$$

i.e. $\frac{d\mathcal{I}}{dD} = 0$.
$C(D)$ are the curves in configuration space that follow the inviscid flow, they describe also the boundary of a surface $S$ and $d\mathbf{S}$ is its corresponding oriented surface element. This means that the flux of vorticity is conserved and vortex lines move with the fluid. Due to the invariance of (2.4.4) we can compute $\mathcal{I}$ at the initial time and since we are considering a flow initially irrotational we have $\mathcal{I} = 0$ at any time.
This theorem holds always for DM because it is collisonless, instead for the baryons it breaks in the non-linear regime since the baroclinity term will become large, anyway as we stated before in our simple model the baroclinity vanishes also for baryons and so the theorem is valid for both the fluid components.
The physical motivation of this invariance can be understood in our cosmological context by observing that from the Zel'dovich approximation (which is recovered by our wave-mechanical study as we will show in Sect.3.2) for an inviscid flow the displacement field between Lagrangian and Eulerian coordinates (and so the velocity which is its time derivative) before shell-crossing is sourced by the gradient of the gravitational potential and so has zero vorticity. After shell-crossing in the multi-stream regime each stream is gravitationally coupled with the others but the displacement is still given by the gradient of a gravitational potential, thus there is still no source of vorticity. However there is generally an effective vorticity that arises from averaging over the multiple streams [73].
The Kelvin-Helmoltz theorem (2.4.4), which is a classical hydrodynamics theorem, can be generalized to a quantum mechanical description. In [14] Damnsky and Sacha showed that $\mathcal{I}$ is also an invariant under the evolution with a quantum Hamiltonian (i.e under Schrödinger function) if one ensures that the integral contour goes only through regions where the velocity is well defined over all its evolution.
We have to be careful because $\mathcal{I}$ has to be null for initially irrotational systems, but it is a global condition of zero vorticity. Since in quantum system vorticity is quantized, vorticity can be only produced in pairs [63], called rotons, with opposite topological charges such as

$$\mathcal{I} = \frac{1}{2\pi\nu}\oint_{C(D)} \mathbf{u}\cdot d\mathbf{x} = \frac{1}{2\pi\nu}\oint_{C(D)} \nabla\phi\cdot d\mathbf{x} = n_+ - n_- = 0 \quad n_\pm \in \mathcal{N} \tag{2.4.5}$$

where $n_+$ is the number of vortices with positive charge, instead $n_-$ is the one of negative charged vortices.

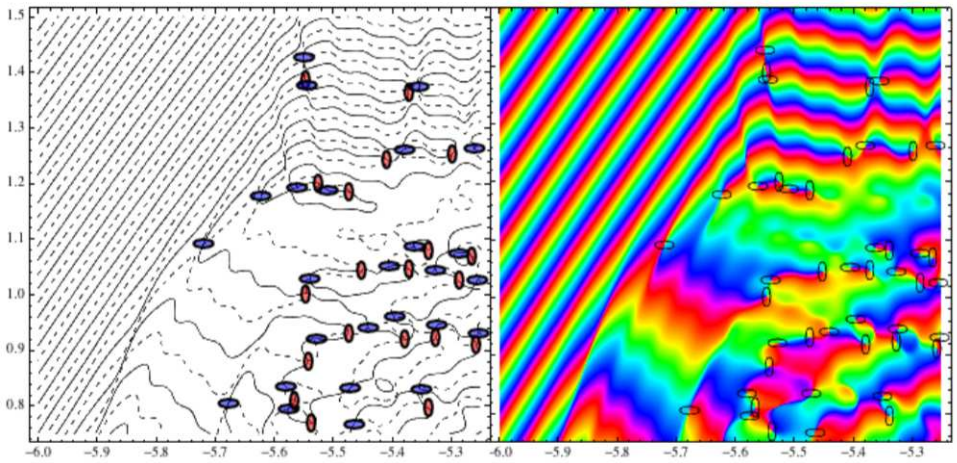


Figure 2.2: The solid curves show the zeros of $Re[\psi]$ and dashed curves the zeros of $Im[\psi]$. The zeros of $\psi$ are the crossing of the two curves and encircled by ellipses. The same ellipses are shown on to right panel, which shows the phase $\phi/\nu$ of the wave function. The color and orientation of the ellipses correspond to the orientation of the circulation: blue/horizontal (red/vertical) corresponds to negative (positive) winding number. This figure is provided by [37], for any further detail check the main text.

While in classical fluid dynamics vorticity arises from averaging of multi-stream velocity, in the quantum picture the wave function is always single valued so vorticity can only arise from topological defects where the phase factor $\phi/\nu$ undergoes a localized phase jump of integer multiples of $2\pi$, which could be interpreted as that the wave function overlaps with itself. In three dimensions the defects are line-like and form a network of vortex lines [37]. This permits us to relate vorticity to the irrotational velocity $\mathbf{u} = -\nabla\phi$ through [37, 38]

$$\nabla \times \nabla\phi = \hat{z} 2\pi\nu \sum_{i}^{N_{vort}} n_i \delta_D^{(2)}(\mathbf{x}^{(2)} - \mathbf{x}_i^{(2)}) \,, \tag{2.4.6}$$

where for simplicity we chose the vortex lines along the $\hat{z}$ direction, we denoted with $\mathbf{x}^{(2)}$ the coordinates on the plane orthogonal to the vortex line and with $\mathbf{x}_i^{(2)}$ the position of the vortex $i$ in this plane [38]. The defects can have more complicated forms, e.g. vortex rings, but the contribution to the vorticity would be provided by the topological charge in a similar way to (2.4.6) just with a more complex expression in the Dirac delta [38].

In Fig.2.2 [37] show that vortices are identified with phase singularities, which in turn are identified with zeros of the amplitude. This is because singularities of the phase are related to singularities of the Madelung transformation (2.1.7) which happen where the wave-function vanishes [30]. The first panel shows in dashed and dotted the zeros of $Re[\psi]$ and $Im[\psi]$. Points where both types of zeros cross are places where $\psi$ is also zero and where we expect the arising of vortices. We mark the zeros of $\psi$ with ellipses. Drawing the same ellipses on the right panel of Fig.2.2, that is the plot of the phase $\phi/\nu$ we observe that all these points carry non-zero circulation with precisely $|n| = 1$ [37]. Color and orientation denote the sign of $n$, with blue/horizontal $n = -1$ and red/vertical $n = 1$.
Another interesting fact on vorticity was observed by Gross in [21], on the basis of the Feynman's [18, 19] and Onsager's [55] works. We study the flow in a multiply connected

region, for example it could be a flow between concentric cylinders, and we call $R$ the inner radius of this region. An ideal classical vortex line has vorticity zero everywhere beside on the singular vortex line and the vortex has a characteristic value of the velocity of $1/R$. Quantum mechanically the $1/R$ behaviour of the velocity can persist in the limit $R \to 0$ only if the real part of the wave-functions drops to zero on the vortex line, otherwise the kinetic velocity would become infinite. But due to the uncertainty principle there must be limitations on the definition of the singular vortex line, which thus spreads out. Hence one expects a core in which the density will become small but not necessary null and in which the velocity will be finite. The vorticity should spread out over the core and should decay rapidly and in a continuous way to zero leaving the core [21].
In the previous section we show that the velocity field is better described by the first moment of the Husimi function (2.3.24) instead by the Madelung transformation. Since the Husimi function applies a coarse-graining to the wave-function we expect that this operation would generate some trivial vorticity [37]. The vorticity can be easily computed if we rewrite the smoothed Husimi velocity (2.3.24) as [37]

$$\eta^H \mathbf{u}^H = \eta^H \exp\left(\sigma_x^2 \overleftarrow{\nabla}\overrightarrow{\nabla}\right) \nabla\bar{\phi}\,, \tag{2.4.7}$$

where $\bar{\phi} = e^{\frac{1}{2}\sigma_x^2 \Delta_x}\phi$ is the coarse-grained phase or velocity potential. Taylor expanding $\nabla \times \mathbf{u}_H$ to leading order in $\sigma_x$ it is found [37]

$$(\nabla \times \mathbf{u}^H)_i = \delta_{i,z}\frac{\sigma_u}{\sigma_x}\sum_j^{N_{vort}} n_j \exp\left[\frac{(\mathbf{x}-\mathbf{x}_j)^2}{2\sigma_x^2}\right] + \sigma_x^2\left(\nabla\frac{\eta^H_{,i}}{\eta^H} \times \nabla\bar{\phi}_{,i}\right) + \mathcal{O}(\sigma_x^4)\,. \tag{2.4.8}$$

From this expression it is clear that the vorticity predicted by the Schrödinger-Poisson model is dominated by quantum vortices for small $\sigma_x$, i.e. at small scales where we could expect that quantum effects are more relevant. Increasing the spatial resolution parameter $\sigma_x$ these quantum effects are smoothed out and the vorticity is dominated by the "artificial" vorticity generated by the coarse-graining operation [37]. Therefore the Husimi coarse-grained vorticity arises in a similar to the vorticity predicted by classic cosmologic perturbation theory, i.e. by the averaging of multiple streams [73].
In Fig.2.3 [37] overplot the vortices generated by the defects of the wave-function (2.4.6) (plotted in Fig.2.2) on the coarse-grained vorticity obtained by (2.4.8). In the top panel we use a very small smoothing scale, which is clearly too small to be in good correspondence with the CDM vorticity shown on the left [37]. However, it clarifies that reducing $\sigma_x$ to ever smaller values makes $\nabla \times \mathbf{u}^H$ more and more dominated by the quantum vortices (2.4.6), whereas letting $\sigma_x$ to flow to large enough values that give good correspondence to the coarse-grained CDM, the vortices are not visible and loose their apparent correlation with $\nabla \times \mathbf{u}^H$ [37].

The same results on vorticity are recovered by the work [73]. The vorticity $\omega = \nabla \times \mathbf{u}^{\mathbf{W}}$ is obtained from the kinetic moment (2.3.14) of the Wigner distribution and is numerically computed through the Fourier decomposition of the curl, i.e.

$$\boldsymbol{\omega} = \mathcal{F}^{-1}\left[-i\mathbf{k} \times \mathcal{F}\left(\frac{\mathbf{j}^W}{\eta^W}\right)\right]\,, \tag{2.4.9}$$

where to compute $\mathcal{F}$ is used a fast Fourier transform (FFT). Since the vortices are point-like (due to their topological defect nature), the inverse FFT produces heavy ringing. In

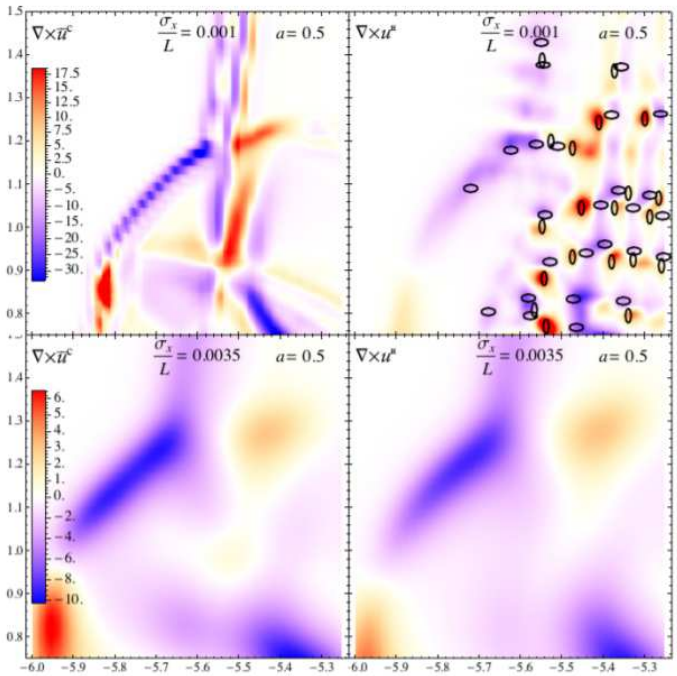


Figure 2.3: Coarse-grained vorticity (2.4.8). Upper panels are for $\sigma_x = 0.001L = 0.02$Mpc with $L = 20$Mpc the size of the simulation, lower panels for $\sigma_z = 0.0035L = 0.07$Mpc. Left panels show the results of ColdDICE simulation for CDM, right panels those of the Schrödinger model (ScM). Overplotted on the right are the locations of the vortices identified by the zeros of the wave-function. This figure is provided by [37], for any further detail check the main text.

order to avoid convolving transverse and longitudinal velocity components we can filter the velocity field with a Gaussian $\exp\left(-\frac{k^2}{k_s^2}\right)$, where $k_s$ is a filter scale, directly in Fourier space, so the vorticity can be computed as

$$\boldsymbol{\omega} = \mathcal{F}^{-1}\left[-i\mathbf{k}\times\mathcal{F}\left(\frac{\mathbf{j}^W}{\eta^W}\right)e^{-\left(\frac{k}{k_s}\right)^2}\right]. \tag{2.4.10}$$

This filter could be avoided using the Husimi distribution but anyway would give similar results since both the methods employ a Gaussian filtering.
Ulheman and collaborators confronted the result of the Schrödinger-Poisson description (applied to a CDM Universe), in particular of the free particle approximation which we will present in Sect.3.2, with respect to the classic Lagrangian Perturbation theory (LPT), i.e. the Zel'dovich approximation. For the LPT prediction of vorticity generation they used the method of [24] to explicit carry out the multi-stream average, which is the source of vorticity in this picture.
In Fig.2.4 [73] presented a two-dimensional computation of vorticity using as initial velocity potential

$$\phi_i(q_1, q_2) = -2\cos(q_1 + \cos(q_2)) \tag{2.4.11}$$

which represents a strongly phased plane wave, and as reference scale for the filtering the Nyquist wave-number[1] $k_{Ny}$. From Fig.2.4 second panel from the left, which corresponds to a representation of vortices for small smoothing scales, it is clear that in two dimensions vortices are point-like objects, which have positive (red) or negative (blue) sign, and also that they are concentrated around the caustic [73]. Comparing this panel with the one on its left, which describes the wave function, we can observe that vortices are always associated with dark regions, i.e where the amplitude of $\psi$ (and so the density) vanishes. As before discussed vorticity global conservation implies (here is treated only CDM so there is no baroclinity) that vortices has to be produced in pairs with opposite topological charge, this effect is clearly visible in Fig.2.4. Furthermore for larger softening (third panel from left) it becomes obvious that, averaging over these quantum vortices, one obtain a large-scale limit which is very similar to the vorticity pattern obtained by ZA (right-most panel).

Hence we have found that in our quantum mechanical theory of LSS evolution the arise of vorticity is possible, provided that the vortices are generated in pairs of opposite topological charge [73](until the non-linear regime of baryon perturbations for which is no more needed the global conservation of vorticity). These quantum vortices are found in regions of vanishing density as theoretically predicted [37, 73]. We found also that using large filtering scale the predictions of the wave-mechanical approach are in good agreement with the classical results of LPT [37, 73].

[1]The Nyquist wavenumber is equal to half the spatial sampling distance, in other fields is more used the respective frequency which is half the sampling rate

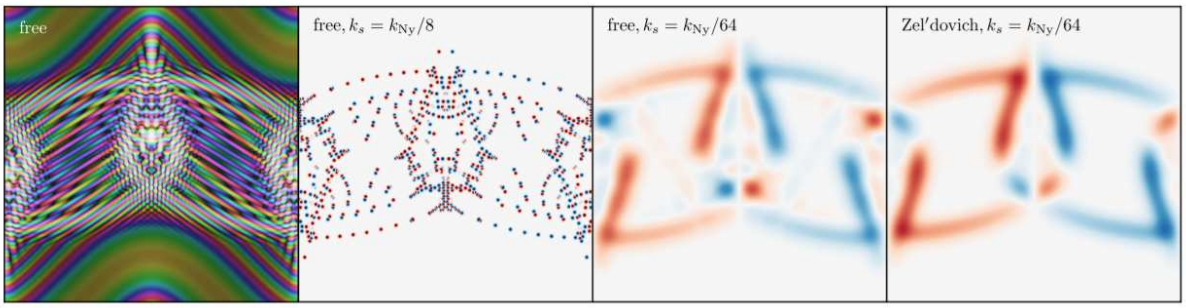


Figure 2.4: Representation of the wave function $\psi$ (left panel, shown using domain coloring), as well of the vorticity $\omega$ (other panels), using the 2D initial conditions $\delta_i = 0$, $\phi_i(q_1, q_2) = -2\cos(q_1 + \cos(q_2))$. The second and third panels from the left show the vorticity obtained using the free particle approximation, filtered with a Gaussian filter in Fourier space on scales of 1/8 and 1/64 the Nyquist wave number to highlight both the large-scale transversal modes and the topological defects from which they arises. The right-most panel shows the corresponding vorticity using the Zel'dovich approximation with a smoothing to facilitate comparison to the large-scale free particle solution shown next to it. The simulation is done for times much later than the shell-crossing $D = 1$ and with $\nu = 0.05$. This figure is provided by [73], for any further detail check the main text.

# Chapter 3

# Perturbation Theory

There is no hope to find an analytic solution of the system of equations (2.2.42) but if we assume that the "potential" part of these Schrödinger equation is smaller respect to the kinetic term (the potential components are all generated by perturbations so we expect it to be right) we can find an approximate solution using quantum perturbation theory [67]. Short and Coles used this method in [67] for find a solution of the Schrödinger-Poisson system in a static Universe, we will extend this approach to an expanding Universe. They obtained results in agreement with other approaches but they observed that we have to be careful on which value assign to $\nu$. If it is too small the perturbation theory can be no longer valid [67], hence if we take the semi-classical limit $\nu \to 0$ we have to be particularly careful to don't broke the perturbative behaviour, i.e. when higher order terms of the perturbative expansion have the same order of magnitude of the $0^{th}$-order term. This will be more clear looking to the expansion (3.0.31) of the external potential. Here the objective is to find a general solution of a Schrödinger equation with a timespace-dependent potential $\Phi(\mathbf{x}, D)$ and then we particularize the solution to our cosmological problem described by the Schrödinger-Poisson system (2.2.42). We neglect the quantum pressure (2.1.14) as did [67], i.e. we study a quantum-like fluid, because since it goes as $\nabla\psi/|\psi|$ it can give problems to the perturbative expansion where $|\psi| = 0$ and $\nabla\psi \neq 0$. We expect that this condition can happen, in particular it is related to quantum vorticity as we will show in Chap.5. This can be easily understood from the fact that the presence of the quantum pressure in the Schrödinger equation implies that we are modelling a classical fluid and so no quantum vortices are expected. Instead if we neglect the quantum pressure we are modelling the cosmological fluids as a quantum fluid, they can be a real quantum fluid as FDM [31] or a classical fluid which description is recovered by the correct choice of the parameter $\nu$, which selects the magnitude of the quantum pressure (2.1.14) [67].
Hence the potential term in the Schrödinger equation will be given by the "Poisson" potential ((2.2.29) for DM and (2.2.30) for baryons) and by the gas pressure ($W_b$ in (2.2.40)) for the baryon component.

$$\Phi_{DM} = V_{DM}\,, \tag{3.0.1}$$

$$\Phi_b = V_b + W_b\,. \tag{3.0.2}$$

Before starting the pertubation theory we have to make another important observation. Since the baryon gas pressure is expected to have a big impact on the dynamics on scales

smaller than the Jeans wavelength (see App.A1) we expect that in such scales it cannot be considered as a perturbative correction to the kinetic energy. i.e. for scales $k >> k_J$ the term $W_b$ should be included in the "free-particle" Hamiltonian $\hat{H}_0$ togheter with the kinetic energy and we should apply the perturbation theory over this Hamiltonian in function of the small correction given by the potential $V$. Since the Schrödinger equation describing this baryon "free-particle" Hamiltonian would require numerical computation to obtain a solution, we restrict the perturbation theory of this chapter to scales $k \lesssim k_J$ such as the baryon gas pressure can considered as a perturbative term with respect to the kinetic energy. This can be done selecting a proper coarse-graining length in the Husimi distribution (2.3.17), i.e. $\sigma_x > \lambda_J$. Anyway these scales are also the most interesting since are the one for which Jeans instability predicts that the bounded structures we see today can form trough gravitational collapse [50].
In the following chapter instead we will develop a full numerical method for the study of the Schrödinger-Poisson system, following the Solid state physics work [5], and so we will not anymore restrict to scales bigger than the Jeans one.
Now we begin with the study of the general Schrödinger equation

$$i\nu\frac{\partial\psi}{\partial D} = \left[-\frac{\nu^2}{2}\nabla^2 + \Phi\right]\psi\,. \tag{3.0.3}$$

For simplicity of computation we use the ket representation and we report only the results in the position representation using the relation

$$\psi(\mathbf{x}, D) = \langle\mathbf{x}|\psi(D)\rangle\ . \tag{3.0.4}$$

We want to solve pertubartively (3.0.3) using the fact that the potential $\Phi$ is small. First of all we need to solve the general free-particle Scrhödinger equation, i.e. neglecting the spacetime-dependent potential $\Phi$.

$$i\nu\frac{\partial\psi}{\partial D} = -\frac{\nu^2}{2}\nabla^2\psi \tag{3.0.5}$$

The Hamiltonian describing this system is called free particle Hamiltonian and is equal to

$$\hat{H}_0 = -\frac{\nu^2}{2}\nabla\,. \tag{3.0.6}$$

We can define the evolution of the wave-fuction from the initial state ket $|\psi_i\rangle = |\psi(D_i)\rangle$ via

$$|\psi(D)\rangle = \hat{U}_0(D, D_i)\,|\psi_i\rangle\ , \tag{3.0.7}$$

where $\hat{U}_0(D, D_i)$ is called free-particle time-evolution operator. If we substitute (3.0.7) in the free Schrödinger equation we obtain an equation which defines $\hat{U}_0$

$$i\nu\frac{d}{dt}\hat{U}_0(D, D_i) = \hat{H}_0\hat{U}_0(D, D_i)\,. \tag{3.0.8}$$

Since the free Hamiltonian $\hat{H}_0$ is independent from time the equation can be integrated directly giving

$$\hat{U}_0(D, D_i) = \exp\left[\frac{-i(D - D_i)\hat{H}_0}{\nu}\right]\ . \tag{3.0.9}$$

Hence the free particle evolution operator $\hat{U}_0(D, D_i)$ satisfies the following properties [60]

$$\hat{U}_0^\dagger \hat{U}_0 = \hat{U}_0 \hat{U}_0^\dagger = I \quad \text{unitary} \tag{3.0.10}$$

$$\hat{U}_0(D, D_i) = \hat{U}_0(D, D_1)\hat{U}_0(D_1, D_i) \tag{3.0.11}$$

$$\hat{U}_0(D_i, D_i) = I \tag{3.0.12}$$

$$\hat{U}_0(D, D_i)\hat{U}_0(D_i, D) = I \tag{3.0.13}$$

$$\hat{U}_0(D_i, D) = \hat{U}_0^{-1}(D, D_i) = \hat{U}_0^\dagger(D, D_i) \tag{3.0.14}$$

where $\hat{U}_0^\dagger$ is the adjoint operator of $\hat{U}_0$.
It is important to introduce the eigestates and eigenkets of the free Hamiltonian $\hat{H}_0$. They are defined from the eigenproblem

$$\hat{H}_0 \left|n^{(0)}\right\rangle = E_n^{(0)} \left|n^{(0)}\right\rangle \,, \tag{3.0.15}$$

where $\left|n^{(0)}\right\rangle$ are the eigenkets and $E_n^{(0)}$ the eigenstates of $\hat{H}_0$. In the following we will study our system in a box of size $L$ with periodic boundary conditions, which we define in a more rigorous way in the following section. Hence it is as to think that the Universe is filled by the repetition of this box, if its dimension are enough big this would be an accurate approximation of the whole Universe due to its homogeneity and isotropy. For now we just say that the states of the free Hamiltonian are discretized due to the periodic boundary conditions [2], we will show that this is true in the one-dimensional case (3.1.11). Anyway it is easy to pass from the discrete to the continuous case using integrals instead of sums. The eigenkets are a complete set i.e.

$$\sum_n \left|n^{(0)}\right\rangle \left\langle n^{(0)}\right| = I \,. \tag{3.0.16}$$

And they form an orthonormal basis, i.e. the eigenkets are orthogonal to each other

$$\langle n^{(0)} | m^{(0)} \rangle = \delta_{n,m} \,, \tag{3.0.17}$$

where $\delta_{n,m}$ is the Kronecker delta. We use this basis to expand the initial state ket

$$\left|\psi_i\right\rangle = \sum_n s_n \left|n^{(0)}\right\rangle \tag{3.0.18}$$

in terms of orthonormal eigenkets $\left|n^{(0)}\right\rangle$ of $\hat{H}_0$, The coefficients of the expansion are defined by

$$s_n \equiv \langle n^{(0)} | \psi_i \rangle \,. \tag{3.0.19}$$

If we find the eigenstates $E_n^{(0)}$ and eigenvectors $\left|n^{(0)}\right\rangle$ of the free particle Hamiltonian solving the eigenproblem (3.0.15) we can then compute the free wave function $\left|\psi_0\right\rangle$ at any time using (3.0.7) and (3.0.18).

$$\left|\psi_0(D)\right\rangle = \sum_n s_n \hat{U}_0(D, D_i) \left|n^{(0)}\right\rangle \,. \tag{3.0.20}$$

To study the higher order terms of the perturbation theory we have to add the time dependent potential, i.e. we have to study the Hamiltonian $\hat{H}(D) = \hat{H}_0 + \Phi(D)$. As before we can relate the evolution of the wave-function to the initial ket via

$$\left|\psi(D)\right\rangle = \hat{U}(D, D_i) \left|\psi_i\right\rangle \,. \tag{3.0.21}$$

Since we are using the full Hamiltonian the wave-function contains all the terms of the perturbative expansion. To divide it in the different order terms we need first to expand the time-evolution operator in a perturbative series. $\hat{U}(D, D_i)$ is defined by the Schrödinger equation

$$i\nu \frac{d}{dD}\hat{U}(D, D_i) = \hat{H}(D)\hat{U}(D, D_i)\,. \tag{3.0.22}$$

Hence we need to find a perturbative solution of this equation.
Also now that we are treating a system defined by the full Hamiltonian with the time-dependent potential the initial ket can still be described by the expansion (3.0.18) in terms of the eigenkets $|n^{(0)}\rangle$ of the free particle Hamiltonian $\hat{H}_0$, because they still form an orthonormal base.
Differently from the non interacting case we can no longer directly integrate (3.0.22) to find $\hat{U}(D, D_i)$ but we can use time-dependent perturbation theory. Until now we used the Schrödinger picture of quantum mechanics but for the perturbation theory is easier to use the Interaction picture. We define a ket in the interaction picture from the ket in the Schrödinger one as [60]

$$|\psi(D)\rangle^{(I)} = \hat{U}_0^\dagger(D, D_i)\,|\psi(D)\rangle\ , \tag{3.0.23}$$

where the dagger denotes the adjoint operator and the superscript (I) denotes quantities in the interaction picture. Note from the definition of $\hat{U}_0$ (3.0.9) the interaction and the Schrödinger kets coincide at initial time because $\hat{U}_0(D_i, D_i) = I$. It is straightforward to show that in the interaction picture a general state ket evolves through [60]

$$i\nu \frac{d}{dD}\,|\psi(D)\rangle^{(I)} = \hat{\Phi}^{(I)}(D)\,|\psi(D)\rangle^{(I)}\ , \tag{3.0.24}$$

where $\hat{\Phi}^{(I)}(D) = \hat{U}_0^\dagger(D, D_i)\Phi(D)\hat{U}_0(D, D_i)$.
This can be shown from (3.0.23):

$$\begin{aligned}
i\nu \frac{d}{dD}\,|\psi(D)\rangle^{(I)} =& i\nu \frac{d}{dD}\left(\hat{U}_0^\dagger(D, D_i)\,|\psi(D)\rangle\right) = \\
=& \left(-\hat{H}_0\hat{U}_0^\dagger(D, D_i) + \hat{U}_0^\dagger(D, D_i) i\nu \frac{d}{dD}\right)|\psi(D)\rangle = \\
=& \left(-\hat{H}_0\hat{U}_0^\dagger(D, D_i) + \hat{U}_0^\dagger(D, D_i)\hat{H}\hat{U}_0(D, D_i)\hat{U}_0^\dagger(D, D_i)\right)|\psi(D)\rangle = \\
=& \left(\hat{U}_0^\dagger(D, D_i)\Phi(\hat{D})\hat{U}_0(D, D_i)\right)\hat{U}_0^\dagger(D, D_i)\,|\psi(D)\rangle = \\
=& 1, \hat{\Phi}^{(I)}(D)\,|\psi(D)\rangle^{(I)}\ ,
\end{aligned}$$

where between the third and forth line we used the fact that $\hat{U}_0$ and $\hat{H}_0$ commute, i.e. $\left[\hat{U}_0, \hat{H}_0\right] = \hat{U}_0\hat{H}_0 - \hat{H}_0\hat{U}_0 = 0$ [60].
Our objective is to determine a perturbative expansion of the time-evolution operator $\hat{U}(D, D_i)$ in the Schrödinger picture, to do that we need first to find an expansion for the time-evolution operator in the interaction picture, we can write the evolution of the wave-function in this new representation as [60]

$$|\psi(D)\rangle^{(I)} = \hat{U}^{(I)}(D, D_i)\,|\psi_i\rangle^{(I)} = \hat{U}^{(I)}(D, D_i)\,|\psi_i\rangle\ , \tag{3.0.25}$$

where

$$\hat{U}^{(I)}(D, D_i) = \hat{U}_0^{\dagger}(D, D_i)\hat{U}(D, D_i)\,. \tag{3.0.26}$$

As before we can constraint the time-evolution operator in the interaction picture from the Scrhödinger equation (3.0.24) [60]

$$i\nu\frac{d}{dD}\hat{U}^{(I)}(D, D_i) = \hat{\Phi}^{(I)}(D)\hat{U}^{(I)}(D, D_i)\,, \tag{3.0.27}$$

with initial condition $\hat{U}^{(I)}(D_i, D_i) = I$ with $I$ the identity operator. The equation (3.0.27) is equivalent to its integral form

$$\hat{U}^{(I)}(D, D_i) = I - \frac{i}{\nu}\int_{D_i}^{D} dD'\hat{\Phi}^{(I)}(D')\hat{U}^{(I)}(D', D_i)\,. \tag{3.0.28}$$

The integral equation (3.0.28) provides a convenient mean of determining a perturbation expansion for $\hat{U}^{(I)}(D, D_i)$. We can solve it in an iterative way, i.e. at the zeroth order we neglect the external potential $\hat{\Phi}^{(I)} = 0$

$$\hat{U}^{(I)}(D, D_i) = I + \mathcal{O}(\Phi)\,. \tag{3.0.29}$$

At first order we use the $0^{th}$-order solution (3.0.29) inside the integral to don't increase the order of the solution

$$\hat{U}^{(I)}(D, D_i) = I - \frac{i}{\nu}\int_{D_i}^{D} dD'\hat{\Phi}^{(I)}(D') + \mathcal{O}(\Phi^2)\,. \tag{3.0.30}$$

To keep care of second order terms in $\hat{\Phi}$ we have to use the solution up to first order (3.0.30) in the integral.

$$\begin{aligned}\hat{U}^{(I)}(D, D_i) =& I - \frac{i}{\nu}\int_{D_i}^{D} dD'\hat{\Phi}^{(I)}(D') + \\ &- \frac{1}{\nu^2}\int_{D_i}^{D} dD'\int_{D_i}^{D'} dD''\hat{\Phi}^{(I)}(D')\hat{\Phi}^{(I)}(D'') + \mathcal{O}(\Phi^3)\,.\end{aligned} \tag{3.0.31}$$

We could proceed to higher orders following this procedure and it is easy to see that we would obtain up to the n-th order [60]

$$\begin{aligned}\hat{U}^{(I)}(D, D_i) =& 1 - \frac{i}{\nu}\int_{D_i}^{D} dD'\hat{\Phi}^{(I)}(D') + ... + \\ &+ \left(\frac{-i}{\nu}\right)^n \int_{D_i}^{D} dD'dD_2...dD_n\hat{\Phi}^{(I)}(D')...\hat{\Phi}^{(I)}(D_n)\,.\end{aligned} \tag{3.0.32}$$

We can express it in a more compact way observing that the following two integrals are equivalent because they span the same space [60]

$$-\frac{1}{\nu^2}\int_{D_i}^{D} dD'\int_{D_i}^{D'} dD''\hat{\Phi}^{(I)}(D')\hat{\Phi}^{(I)}(D'')\,, \tag{3.0.33}$$

$$-\frac{1}{\nu^2}\int_{D_i}^{D} dD''\int_{D''}^{D} dD'\hat{\Phi}^{(I)}(D')\hat{\Phi}^{(I)}(D'')\,. \tag{3.0.34}$$

Thus we can write, for example, the second order term of the expansion as

$$\frac{1}{2}\left[-\frac{1}{\nu^2}\int_{D_i}^{D}dD'\int_{D_i}^{D'}dD''\hat{\Phi}^{(I)}(D')\hat{\Phi}^{(I)}(D'')-\frac{1}{\nu^2}\int_{D_i}^{D}dD''\int_{D''}^{D}dD'\hat{\Phi}^{(I)}(D')\hat{\Phi}^{(I)}(D'')\right]=$$
$$=\frac{1}{2!}\left(\frac{-i}{\nu}\right)^2\int_{D_i}^{D}dD'\int_{D_i}^{D}dD''\left[\Theta(D'-D'')\hat{\Phi}^{(I)}(D')\hat{\Phi}^{(I)}(D'')+\right.$$
$$\left.+\Theta(D''-D')\hat{\Phi}^{(I)}(D'')\hat{\Phi}^{(I)}(D')\right],. \tag{3.0.35}$$

If we define the time-ordered product of operators as

$$T\left[A(D_1)B(D_2)\right]=\begin{cases}A(D_1)B(D_2) & D_1>D_2\\ B(D_2)A(D_1) & D_2>D_1\end{cases} \tag{3.0.36}$$

we can rewrite (3.0.35) as

$$\frac{1}{2!}\left(\frac{i}{\nu}\right)^2\int_{D_i}^{D}dD_1dD_2T\left[\hat{\Phi}^{(I)}(D_1)\hat{\Phi}^{(I)}(D_2)\right] \tag{3.0.37}$$

and thus the whole expansion of the time evolution operator is

$$\hat{U}^{(I)}(D,D_i)=\sum_{n=0}^{\infty}\frac{1}{n!}\left(\frac{i}{\nu}\right)^n\int_{D_i}^{D}dD_1...dD_nT\left[\Phi^{(I)}(D_1)...\hat{\Phi}^{(I)}(D_n)\right]. \tag{3.0.38}$$

Since the time ordering operation can be taken outside the integral [60] we obtain the expansion of an exponential, i.e.

$$\hat{U}^{(I)}(D,D_i)=T\left[\exp\left\{-\frac{i}{\nu}\int_{D_i}^{D}dD'\hat{\Phi}^{(I)}(D')\right\}\right]. \tag{3.0.39}$$

This is the most general expression of the time-evolution operator, of which is made large use in quantum mechanics [60] and when it is computed in the time interval $[D_i, D_0]$ it is called scattering matrix $S = U^{(I)}(D_i, D_o)$ which describes the full time-evolution of the initial state from initial time $D = D_i$ until today $D = D_0$.
In this work we will not investigate the small corrections given by these higher order terms. In this more general part we keep up to second order terms in the potential, but when we need to particularize to our cosmological problem we will limit ourselves to first order corrections.
Since our observables are related, through the Husimi distribution (2.3.17), to the wave-function in the Schrödinger picture we want to come back to this representation. We obtain the corresponding time-evolution operator in the Schrödinger picture from (3.0.23)

$$|\psi(D)\rangle=\hat{U}_0(D,D_i)\hat{U}^{(I)}(D,D_i)\,|\psi_i\rangle\ , \tag{3.0.40}$$

thus

$$\hat{U}(D,D_i)=\hat{U}_0(D,D_i)\hat{U}^{(I)}(D,D_i)\,. \tag{3.0.41}$$

Then, using the following property of the time-evolution operator $\hat{U}_0(D, D_i)\hat{U}_0^\dagger(D', D_i) = \hat{U}_0(D, D_i)\hat{U}_0(D_i, D') = \hat{U}_0(D, D')$ and the expansion (3.0.31), we write the time evolution operator in the Schrödinger picture as

$$\hat{U}(D, D_i) = \sum_{j=0}^{2} \hat{U}_j(D, D_i) + \mathcal{O}(\hat{\Phi}^3) \tag{3.0.42}$$

up to second order [67], with $\hat{U}_0(D, D_i)$ equal to the free particle evolution operator (3.0.9),

$$\hat{U}_1(D, D_i) = -\frac{i}{\nu}\int_{D_i}^{D} dD' \hat{U}_0(D, D')\hat{\Phi}(D')\hat{U}_0(D', D_i) \tag{3.0.43}$$

and

$$\hat{U_2} = -\frac{1}{\nu^2}\int_{D_i}^{D} dD' \int_{D_i}^{D'} dD'' \hat{U}_0(D, D')\hat{\Phi}(D')\hat{U}_0(D', D'')\hat{\Phi}(D'')\hat{U}_0(D'', D_i)\,. \tag{3.0.44}$$

Thus we can write the wave function as a series expansion similarly to (3.0.42)

$$|\psi(D)\rangle = \sum_{j=0}^{\infty} |\psi^{(j)}(D)\rangle = \sum_{j=0}^{\infty} \hat{U}_j(D, D_i)\,|\psi_i\rangle\ , \tag{3.0.45}$$

where, using the expansion in terms of the free Hamiltonian eigenkets (3.0.18), at the zeroth order we recover the free particle solution (3.0.20) and the first order term is

$$|\psi^{(1)}(D)\rangle = \sum_n s_n \hat{U}_1(D, D_i)\,|n^{(0)}\rangle \tag{3.0.46}$$

then at linear order in the potential $\Phi$ we can express the solution of the Schrödinger equation (3.0.3) as

$$|\psi(D)\rangle = |\psi^{(0)}(D)\rangle + |\psi^{(1)}(D)\rangle + \mathcal{O}(\hat{\Phi}^2) \tag{3.0.47}$$

We have still to express our solution in the position representation. We begin defining the free-energy eigenfunctions $\phi_n^{(0)} = \langle x|n^{(0)}\rangle$, then we find

$$\begin{aligned}
\psi^{(1)}(\mathbf{x}, t) &= \sum_n s_n \langle \mathbf{x}|\, U_1(D, D_i)\,|n^{(0)}\rangle = \\
&= \sum_n s_n \int_{D_i}^{D} dD' \,\langle \mathbf{x}|\, e^{-i(D-D')\hat{H}_0/\nu}\hat{\Phi}(D')e^{-i(D'-D_i)\hat{H}_0/\nu}\,|n^{(0)}\rangle = \\
&= \sum_n s_n \int_{D_i}^{D} dD' \,\langle \mathbf{x}|\, e^{-i(D-D')\hat{H}_0/\nu}\hat{\Phi}(D')\,|n^{(0)}\rangle\, e^{-i(D'-D_i)E_n/\nu} = \\
&= \sum_n s_n \sum_m \int_{D_i}^{D} dD' \,\langle \mathbf{x}|\, |m^{(0)}\rangle \langle m^{(0)}|\, e^{-i(D-D')\hat{H}_0/\nu}\hat{\Phi}(D')\,|n^{(0)}\rangle\, e^{-i(D'-D_i)E_n/\nu} = \\
&= \sum_n s_n \sum_m \int_{D_i}^{D} dD' \phi_m^{(0)} \,\langle m^{(0)}|\, e^{-i(D-D')\hat{H}_0/\nu}\hat{\Phi}(D')\,|n^{(0)}\rangle\, e^{-i(D'-D_i)E_n/\nu} = \\
&= \sum_n s_n \sum_m \int_{D_i}^{D} dD' \phi_m^{(0)} e^{-i(D-D')E_m/\nu} \,\langle m^{(0)}|\, \hat{\Phi}(D')\,|n^{(0)}\rangle\, e^{-i(D'-D_i)E_n/\nu}
\end{aligned}$$

where we used the completness property of the eigenket base $\sum_m |m^{(0)}\rangle \langle m^{(0)}| = I$. We can define the "potential" tensor

$$\Phi_{m,n}(D') = \langle m^{(0)}| \hat{\Phi}(D') |n^{(0)}\rangle = \int d^3y\, d^3z \, \langle m^{(0)}| |\mathbf{y}\rangle \langle \mathbf{y}| \hat{\Phi}(D') |\mathbf{z}\rangle \langle \mathbf{z}| |n^{(0)}\rangle = \\ = \int \bar{\phi}_m^{(0)}(\mathbf{y}) \Phi(\mathbf{y}, D') \phi_n^{(0)}(\mathbf{y}) d^3\, y \tag{3.0.48}$$

where we use the fact the our potential $\Phi$ doesn't affect the spatial dependence. Finally we can write the first order correction of the wave-function as

$$\psi^{(1)}(\mathbf{x}, D) = -\frac{i}{\nu} \sum_n s_n \sum_m \mathcal{I}_{m,n} \phi_m^{(0)}\,, \tag{3.0.49}$$

with

$$\mathcal{I}_{m,n}(\mathbf{x}, D) = \int_{D_i}^{D} dD'(\mathbf{x}) \exp\left[\frac{-i(D - D')E_m^{(0)}}{\nu}\right] \Phi_{m,n}(D') \exp\left[\frac{-i(D' - D_i)E_n^{(0)}}{\nu}\right]. \tag{3.0.50}$$

Thanks to the prefactor $1/\nu$ in (3.0.49) we can understand why we have to be careful in taking small $\nu$, the perturbation $\psi^{(1)}$ can become big and if it reaches the value of the unperturbed $\psi^{(0)}$ the whole perturbation theory is no more valid [67].
To particularize this solution to our Schrödinger-Poisson system is sufficient to define the two potentials for DM and baryons

$$\Phi_{DM} = V_{DM} \tag{3.0.51}$$

$$\Phi_b = V_b + W_b \tag{3.0.52}$$

with $V_b$ given by (2.2.30) in terms of the DM potential.
Hence the expression (3.0.49), once taken in account the proper potential, gives the amount of correction (at first order in the potential) to the baryons or DM distribution with respect to the free particle solution, i.e. considering baryons and DM as non interacting particles. In the section 2.3 we showed how to relate the wave-function to the physical observables, e.g. the density and velocity fields. In the following we want to apply those concepts to the wave-function derived from perturbation theory.

## 3.1 One dimensional solution

Since at linear order the distribution of baryons and DM is known with good accuracy [47, 54] we would like to compare our solution with the linear order solution obtained in the fluid representation of cosmic matter, to do so we need to express explicitly the wave-function such as we can pass to the fluid observables. For the simplicity of computation we find a solution in a 1D space for an initial overdensity of the form

$$\delta_i(q) = \delta_a \cos\left(\frac{2\pi q}{d}\right)\,, \tag{3.1.1}$$

where $0 < |\delta_a| \leq 1$ to ensure that the initial density field is everywhere non-negative. Anyway we will show in the next section that the results of this one-dimensional case are

easily generalized to the three-dimensional space and to more general initial conditions. Since plane-symmetry implies that the quantity under consideration is one dimensional we can think of be studying a plane-symmetric density perturbation [67]. Beside simplicity the restriction to the one dimensional case has another advantage, the Zel'dovich approximation [79] is exact for DM in 1D until shell-crossing thus comparing our solution with respect to it is an important test.
Thanks to the homogeneity of the Universe on very large scales instead of an infinite space we can consider a segment of dimension $L$ (which can be directly generalize to the three dimensional case of a box of side $L$) equipped with periodic boundary conditions at each extremity, defined such as $L = Nd$ with $N$ big and $d$ the wavelength of the initial overdensity. Since we are studying only scales bigger than the Jeans wavelength for keep the baryon pressure small we have to impose that the size of the box is much bigger than the Jeans one $L >> \lambda_J$ or $N >> \lambda_J/d$.
We can find the initial gravitational potential solving the Poisson equation (2.2.24) at the initial time

$$\varphi_i(q) = -\frac{\delta_a}{D_i}\left(\frac{d}{2\pi}\right)^2 \cos\left(\frac{2\pi q}{d}\right) . \tag{3.1.2}$$

Now that we have set the initial conditions we can come back to our perturbative problem. We have to find first the solution in the free-particle ($0^{th}$-order) case, we need to solve the eigenproblem (3.0.15) to obtain the eigenvector basis of the free particle Hamiltonian $\hat{H}_0 = -(\nu^2/2)\nabla^2$, which is easier in the position representation (remember that at a general time we have to use the Eulerian coordinates $\mathbf{x}$, only at the initial time we have $\mathbf{x} = \mathbf{q}$, that is why the initial condition depends only on the Lagrangian coordinates). Thus in one dimension

$$\langle x|\, \hat{H}_0\, |n^{(0)}\rangle = \langle x|\, E_n^{(0)}\, |n^{(0)}\rangle \tag{3.1.3}$$

$$-\frac{\nu^2}{2}\frac{d^2}{dx^2}\langle x|n^{(0)}\rangle = E_n^{(0)}\langle x|n^{(0)}\rangle \tag{3.1.4}$$

$$-\frac{\nu^2}{2}\frac{d^2\phi_n^{(0)}}{dx^2}(x) = E_n^{(0)}\phi_n^{(0)}(x)\,, \tag{3.1.5}$$

with solution

$$\phi_n^{(0)}(x) = \frac{1}{L^{1/2}}\exp\left(ix\sqrt{\frac{2E_n^{(0)}}{\nu^2}}\right) . \tag{3.1.6}$$

The prefactor $(1/L)^{1/2}$ comes from the normalization of the eigenfunctions. Since we are working in a space equipped of periodic boundary conditions, if we impose them

$$\phi_n^{(0)}(0) = \phi_n^{(0)}(L) \tag{3.1.7}$$

$$1 = \exp\left(iL\sqrt{\frac{2E_n^{(0)}}{\nu^2}}\right) , \tag{3.1.8}$$

which has for solution

$$\sqrt{\frac{2E_n^{(0)}}{\nu^2}} = \frac{2n\pi}{L}\,, \tag{3.1.9}$$

with $n$ an integer. The energy eigenfunction $\phi_n^{(0)}$ are also eigenfunction of the momentum operator $\hat{P}$:

$$\begin{aligned}\hat{P}\,|\phi_n^{(0)}\rangle &= -i\frac{\partial}{\partial x}\phi_n^{(0)} = p_n\phi_n^{(0)}\\ p_n &= \nu k_n = \frac{2n\pi\nu}{L}\\ k_n &= \frac{2n\pi}{L} \equiv \sqrt{\frac{2E_n^{(0)}}{\nu^2}}\,,\end{aligned} \tag{3.1.10}$$

where we used the de Broglie relation through momentum and wave number of a particle/wave in the second line. Hence we can express the free particle eigenvectors in function of the discrete wavenumber $k_n$ in the simple form

$$\phi_n^{(0)}(x) = \frac{1}{L^{1/2}}\exp(ik_n x)\,. \tag{3.1.11}$$

Hence the free particle eigenstates are static sinusoidal (plane waves) states with associated energy

$$E_n^{(0)} = \frac{2n^2\pi^2\nu^2}{L^2} = \frac{\nu^2 k_n^2}{2} \geq 0\,, \tag{3.1.12}$$

which is positive defined and quantized. Actually the quantization is due to the choice of a box with periodic boundary conditions, if there were no boundaries $k$ would be not discretized and so the energy levels would be continuous [60].
We shall now study the evolution of the free particle wave-function from its initial state, which is related to the free Hamiltonian eigenvectors through (3.0.20). In the position representation we obtain

$$\begin{aligned}\psi^{(0)}(x,D) = \langle x|\psi^{(0)}(D)\rangle &= \sum_n s_n \langle x|\exp\left[\frac{-i(D-D_i)\hat{H}_0}{\nu}\right]|n^{(0)}\rangle =\\ &= \sum_n s_n \exp\left[\frac{-i(D-D_i)E_n^{(0)}}{\nu}\right]\phi_n^{(0)}(x)\,.\end{aligned} \tag{3.1.13}$$

The expansion coefficients $s_n = \langle n^{(0)}|\psi_i\rangle$ are given by

$$s_n = \int_0^L dq\,\langle n^{(0)}|q\rangle\,\langle q|\psi_i\rangle = \int_0^L \bar{\phi}_n^{(0)}(q)\psi_i(q)dq\,. \tag{3.1.14}$$

We can divide the segment $L$ in N small segments of dimension $d$ [67]

$$s_n = \sum_{j=0}^{N-1}\int_{jd}^{(j+1)d}\bar{\phi}_n^{(0)}(q)\psi_i(q)dq \tag{3.1.15}$$

We make a change of variable $q' = q - jd$. Then the initial wave-function, which is defined by the Madelung transformation $\psi_i = (1+\delta_i)^{1/2}\exp(-i\phi_i/\nu)$, is periodic of period $d$. This comes from the initial conditions on the overdensity and from the fact that the initial velocity potential is itself periodic of period $d$. We can show that computing the

Hamilton-Jacobi equation (2.2.25) at initial time. The initial velocity potential is function only of the initial density and gravitational potential and their derivatives, which are all periodic functions. Thus the initial wave-function is not affected by the change of variable. For the free particle eigenfunction instead we have

$$\bar{\phi}_n^{(0)}(q' + jd) = \frac{1}{L^{1/2}} \exp\left[-ik_n q - ik_n jd\right] = \bar{\phi}_n^{(0)}(q') e^{-ijk_n d} \,. \tag{3.1.16}$$

Hence

$$s_n = \int_0^d \bar{\phi}_n^{(0)}(q') \psi_i(q') dq' \sum_{j=0}^{N-1} \exp(-ijk_n d) \tag{3.1.17}$$

However thanks to the definition of $k_n = 2n\pi/d$ the exponential is equal to one and so the sum over it gives simply $N$.

$$s_n = N \int_0^d \bar{\phi}_n^{(0)}(q') \psi_i(q') dq' \tag{3.1.18}$$

From the form of the eigenfucntions (3.1.11) follows that the expansion coefficients are simply found by taking the Fourier transform of the initial wave-function [67], i.e.

$$s_n(k_n) = \sqrt{\frac{2\pi}{L}} \psi_i(k_n) \tag{3.1.19}$$

Thus we can express the free particle wave-function as

$$\psi_0(x, D) = \sum_n \psi_i(k_n) \exp\left[\frac{-i(D - D_i) E_n^{(0)}}{\nu}\right] \phi_n^{(0)}(x) \,, \tag{3.1.20}$$

which is totally set by its initial state $\psi_i$.
Now we want to compute the first-order correction to the wave-function, we begin computing the potential tensor $\Phi_{n.m}$ (3.0.48). Using the expression of the eigenfunctions (3.1.11) we can express also this quantity as a Fourier transform

$$\Phi_{n,m} = \frac{1}{L} \int_0^L e^{-ik_p y} \Phi(D', y) = \frac{\sqrt{2\pi}}{L} \Phi(D', k_p) \,, \tag{3.1.21}$$

where $k_p = k_m - k_n$. To simplify the computations we can approximate the eigenstates of the free energy as continuous such as we can use integrals instead of series

$$\sum_n \to \frac{L}{2\pi} \int_{\frac{2\pi}{L}}^{\infty} dk_n \,. \tag{3.1.22}$$

This is a common procedure in Statistical Mechanics. We show now how this relation is made. If the dimension of the system $L$ is big the distance $\Delta k_n$ between the wavenumbers $k_n$ defined by the eigenstates of the free Hamiltonian would be small $\Delta k_n \to 0$. Thus we can express the sum as an integral in the following manner

$$\sum_{k_n} = \sum_{k_n} \frac{\Delta k_n}{\Delta k_n} \to \frac{1}{\Delta k_n} \int_{\frac{2\pi}{L}}^{\infty} dk_n \tag{3.1.23}$$

and the wavenumber interval is set by the dimension of the system [2], i.e.

$$\Delta k_n = \frac{2\pi}{L}\,. \tag{3.1.24}$$

Hence, from the expression of the free Hamiltonian eigenfunction (3.1.11) and of the expansion coefficient $s_n$ (3.1.19), the first two terms of the perturbative expansion of the wave-function are

$$\psi^{(1)}_{b,DM}(x,D) = -\frac{i}{\nu}\frac{1}{2\pi}\int_{D_i}^{D} dD' \int_{\frac{2\pi}{L}}^{\infty} dk_n \int_{\frac{2\pi}{L}}^{\infty} dk_m e^{ik_m x}\psi_i^{b,DM}(k_n)\times \\ \times \exp\left[\frac{-i(D-D')\nu k_m^2}{2}\right]\Phi_{b,DM}(D',k_p)\exp\left[\frac{-i(D'-D_i)\nu k_n^2}{2}\right] \tag{3.1.25}$$

and

$$\psi^{(0)}_{b,DM}(x,D) = \frac{1}{\sqrt{2\pi}}\int_{\frac{2\pi}{L}}^{\infty} dk_n \psi_i^{b,DM}(k_n)\exp\left[-i\frac{(D-D_i)\nu k_n^2}{2}\right]\exp\left(ik_n x\right) \tag{3.1.26}$$

These expressions are still too complex to compute analytically the fluid observables, we need to make some approximations or do a numerical computation. We explore this two possibilities in the next sections.

## 3.2 Free particle solution

For now we limit ourselves to the study of the $0^{th}$-order solution, i.e. we neglect the contribution of the "external potential" $\Phi$. Hence we are describing a free particle and the solution will be the same for both DM and baryons since we are neglecting the pressure. We have to remember that this is true only on the scales we are considering ($k < k_J$), otherwise the pressure can have some contribution even at the $0^{th}$-order.
In the semi-classical limit (or after coarse-graining) $\nu \to 0$ (we want it to be small but still different from zero otherwise the perturbation theory would be no more valid) this solution resembles the Zel'dovich approximation [73,79], instead for a finite value of $\nu$ the free particle approximation gives similar results to the adhesion approximation [23,67,73] but in this case we will need numerical computations. The study of the semi-classical limit is easier if we write the integral in the Fourier space of (3.1.26) as an integral in the position space by means of the equipartition theorem.
Since the following relations hold

$$\exp\left[-i\frac{(D-D_i)\nu k_n^2}{2}\right] = \frac{1}{(2\pi)^{1/2}}\int_0^L dy \frac{\exp\left[\frac{i}{2\nu}\frac{y^2}{D-D_i}\right]}{\sqrt{i(D-D_i)\nu}} e^{-ik_n y}\,, \tag{3.2.1}$$

$$\psi_i(k_n) = \frac{1}{(2\pi)^{1/2}}\int_0^L dy \psi_i(y) e^{-ik_n y}\,, \tag{3.2.2}$$

we can write (3.1.26) as (we won't write again the 0-th index because we are considering just this order in this section)

$$\psi(x,D) = \frac{1}{(2\pi)^{1/2}} \int_{\frac{2\pi}{q}}^{\infty} dk_n e^{ik_n x} \int_0^L \frac{dy}{(2\pi)^{1/2}} \psi_i(y) e^{-ik_n y} \int_0^L \frac{ds}{(2\pi)^{1/2}} \frac{\exp\left[\frac{i}{2\nu}\frac{s^2}{D-D_i}\right]}{\sqrt{i(D-D_i)\nu}} e^{-ik_n s} =$$

$$= \frac{1}{(2\pi)^{1/2}} \int dy \int ds \psi_i(y) \frac{\exp\left[\frac{i}{2\nu}\frac{s^2}{D-D_i}\right]}{\sqrt{i(D-D_i)\nu}} \delta^{(D)}(x-s-y) =$$

$$= \frac{1}{(2\pi)^{1/2}} \int ds \psi_i(x-s) \frac{\exp\left[\frac{i}{2\nu}\frac{s^2}{D-D_i}\right]}{\sqrt{i(D-D_i)\nu}} .$$

If we make the change of variable $q = x - s$ we obtain

$$\psi(x,D) = \frac{1}{(2\pi)^{1/2}} \int_0^L dq \psi_i(q) \frac{\exp\left[\frac{i}{2\nu}\frac{(x-q)^2}{D-D_i}\right]}{\sqrt{i(D-D_i)\nu}} = \int_0^L dq K_0(x,D;q,D_i)\psi_i(q) , \qquad (3.2.3)$$

where

$$K_0(x,D;q,D_i) = \frac{\exp\left[\frac{i}{2\nu}\frac{(x-q)^2}{D-D_i}\right]}{\sqrt{2\pi i(D-D_i)\nu}} \qquad (3.2.4)$$

is the kernel or propagator for a free particle, it defines the probability to have a particle in the position x at the time D knowing that it was in q at time $D_i$. Then the wave-function is defined by integrating this probability over all the possible starting points $q$. This is a common result of path-integrals description of Quantum Mechanics [28], within which usually the perturbation theory is applied to the propagator instead of the time-evolution operator $\hat{U}(D, D_i)$. In general the propagator is defined as

$$K(\mathbf{x}, D|\mathbf{q}, D_i) = \int_{\mathbf{q}}^{\mathbf{x}(\mathbf{q})} \mathcal{D}\mathbf{x}(D) e^{\frac{i}{\nu}S(\mathbf{x},\mathbf{q},D)} , \qquad (3.2.5)$$

where the integral is over all the possible paths connecting the points $\mathbf{q}$ and $\mathbf{x}$, i.e. it is a path-integral [28]. $S(\mathbf{x}, \mathbf{q}, D)$ is the Action, defined as

$$S(\mathbf{x}, \mathbf{q}, D) = \int_{D_i}^{D} dD' L(\mathbf{x}, \dot{\mathbf{x}}, D) \qquad (3.2.6)$$

and $L(\mathbf{x}, \dot{\mathbf{x}}, D)$ is the Lagrangian of the system under study. We could have obtained the same results of the free particle approximation applying perturbation theory to this propagator [28].

We can also pass to the 3-dimensional description just using vectors for positions and taking the third power of the square root in the denominator of the kernel to account for the normalization of the kernel. In this simple situation we can actually study our system in a case more general than a box with periodic boundary condition, we can expand our treatment to the study of the "whole" Universe at the same time and neglect surface effects at the borders set by the cosmological horizon. Hence we will let our spatial coordinates vary in the interval $[-\infty, +\infty]$. The results will not change thanks to the homogeneity of

the background Universe, it is just easier to deal with the integrals when they span the interval $[-\infty, +\infty]$.

$$\psi(\mathbf{x}, D) = \int d^3q \psi_i(\mathbf{q}) \frac{\exp\left[\frac{i}{2\nu}\frac{(\mathbf{x}-\mathbf{q})^2}{D-D_i}\right]}{\left[2\pi i(D-D_i)\nu\right]^{3/2}} . \tag{3.2.7}$$

For simplicity of notation we set the initial "time" to 0, i.e. $D_i = 0$, for a more accurate description we should use as initial time the time of baryon recombination [25] but here we want to test our model and not to compute a refined simulation of LSS evolution so the approximation $D_i = 0$ is sufficient [73]. First of all we need to set the initial conditions, in this simple case we can use conditions more general and more physical than the simple sinusoid (3.1.1) used by [67]. We expect that at the beginning the density fluctuations were very small, because just passed from the quantum state to a macroscopical one thanks to inflation(this is proven also by CMB observations) [20]. They will grow later thanks to the effect of gravity, the initial velocity potential can instead be set by the Euler equation (2.2.22). We should use the values of density and velocity of baryon and DM at the epoch of baryon recombination as initial conditions [25], it is proven that at this time baryons and DM was not identically distributed in the Universe [9], since DM decoupled before from radiation with respect to baryons and also because DM does not experience a gas pressure. In the works [9,25] the authors depicted several methods to obtain accurate initial conditions when both DM and baryon evolution is involved. Anyway for now we can keep the initial conditions generic, i.e.

$$\psi_i^{DM}(\mathbf{q}) = \delta_{DM}^{(in)}(\mathbf{q}) e^{-\frac{i}{\nu}\phi_{DM}^{(in)}(\mathbf{q})} , \qquad \psi_i^b(\mathbf{q}) = \delta_b^{(in)}(\mathbf{q}) e^{-\frac{i}{\nu}\phi_b^{(in)}(\mathbf{q})} , \tag{3.2.8}$$

because, as said for the choice of the initial time, here we want just to test our model and not to compute a refined simulation so we can keep us the most general as possible. From now on we solve the free particle approximation for a general component and so we do not use the subscript $b$ or $DM$. For recover the baryon or DM result is sufficient to use the respective initial conditions since the evolution described by the free particle approximation is the same. We say once more that this is true because we are considering scales bigger than the Jeans one such as the baryon gas pressure will enter in the next order of the QPT expansion, which we study in the next section. As a matter of facts from the equation of state (1.2.17) we obtained the pressure contribution $W_b$ in the baryon Schrödinger equation (2.2.40) which is proportional to $1/k_J(D)^2$ or to the modified Jeans wavenumber $1/\tilde{k}_J^2$ which is time independent. We want to keep this term small (with respect to the kinetic energy) such as we can include it in the perturbative potential $\Phi_b$ (3.0.2), to do so we can use the results of Jeans instability theory which says that the pressure contributions are negligible over scales bigger than the Jeans one (see e.g App.A1). Hence using the Husimi coarse-graining $\sigma_x$ we can limit ourselves to scales bigger than the modified Jeans length $\tilde{\lambda}_J = 2\pi/\tilde{k}_J$, which is the biggest Jeans scale over all the time-evolution (see e.g. Fig.2.1 where we depicted the evolution of $\lambda_j$ and $\tilde{\lambda}_J$ in an Universe with no Dark Energy $\Lambda$), i.e. we study scales

$$k < \frac{1}{\sigma_x} < \tilde{k}_J . \tag{3.2.9}$$

Now we compute the Wigner distribution (2.3.7) for relate the wave-function to the fluid observable. Later we will compute the Husimi distribution (2.3.17) coarse-graining the

Wigner function and so compare the results of these two phase-space distributions. Anyway we must use the Husimi function due to what we say on baryon pressure and scale selection.

$$f_W^0(\mathbf{x},D)=\int\frac{d^3x'}{(2\pi)^3}e^{-i\frac{\mathbf{p}\cdot\mathbf{x}'}{(aD)^2}}\int d^3q\psi_i(\mathbf{q})\frac{\exp\left[\frac{i}{2\nu}\frac{(\mathbf{x}+\frac{\nu}{2}\mathbf{x}'-\mathbf{q})^2}{D}\right]}{(2\pi iD\nu)^{3/2}}\times$$
$$\times\int d^3q'\psi_i(\mathbf{q}')\frac{\exp\left[-\frac{i}{2\nu}\frac{(\mathbf{x}-\frac{\nu}{2}\mathbf{x}'-\mathbf{q}')^2}{D}\right]}{(2\pi iD\nu)^{3/2}}\,. \tag{3.2.10}$$

The integrals over $\boldsymbol{q}$ and $\boldsymbol{q}'$ can be simplified by the change of variables:

$$\boldsymbol{q}_+=\frac{\boldsymbol{q}+\boldsymbol{q}'}{2}\,,\qquad\qquad \boldsymbol{q}_-=\boldsymbol{q}-\boldsymbol{q}'\,. \tag{3.2.11}$$

So $f_W$ becomes

$$f_W^0(\mathbf{x},D)=\int\frac{d^3x'}{(2\pi)^3}\int\frac{d^3q_+d^3q_-}{(2iD\pi\nu)^3}\delta^{(in)}(\mathbf{q}_++\frac{\mathbf{q}_-}{2})\delta^{(in)}(\mathbf{q}_+-\frac{\mathbf{q}_-}{2})\times \tag{3.2.12}$$
$$\times\exp\left[i\boldsymbol{x}'\cdot\left(-\frac{\boldsymbol{p}}{a^2\dot{D}^2}+\frac{\boldsymbol{x}-\boldsymbol{q}_+}{D}\right)\right]\exp\left\{-\frac{i}{D\nu}\left[\boldsymbol{q}_-\cdot(\boldsymbol{x}-\boldsymbol{q}_+)+D\delta\phi\left(\boldsymbol{q}_+,\boldsymbol{q}_-\right)\right]\right\}\,,$$

where we defined

$$\delta\phi\left(\boldsymbol{q}_+,\boldsymbol{q}_-\right)=\phi^{(in)}\left(\boldsymbol{q}_++\frac{\boldsymbol{q}_-}{2}\right)-\phi^{(in)}\left(\boldsymbol{q}_+-\frac{\boldsymbol{q}_-}{2}\right)\,. \tag{3.2.13}$$

As we anticipated we can find an analytical solution for the free particle system only in the semi-classical limit ($\nu\to 0$), where for the DM component we expect to recover the results of the classical perturbation theory applied to the fluid description [73] and, as we will show, we actually recover the Zel'dovich approximation [79]. We will not recover baryon classical linear perturbation theory as [47] because we are totally neglecting the pressure effects, for a more accurate description of baryon we need to go to the next order of the QPT, which we present in the next section. In this limit the second complex exponent in (3.2.12) will vary very quickly, and so cancels its contributions, unless $\boldsymbol{q}_-$ is small [73]. Thus we can approximate $\delta\phi$ expanding it around small $\boldsymbol{q}_-$

$$\delta\phi(\mathbf{q}_+,\mathbf{q}_-)\sim\boldsymbol{q}_-\cdot\nabla\phi^{(in)}\left(\boldsymbol{q}_+\right)+\mathcal{O}\left(\boldsymbol{q}_-^3\right)\,, \tag{3.2.14}$$

where the even terms of the expansion cancels due to the opposite sign of the two terms in (3.2.13). Also the product between the $\delta^{(in)}$ is approximated by small $\mathbf{q}_-$ as

$$\delta^{(in)}\left(\mathbf{q}_++\frac{\mathbf{q}_-}{2}\right)\delta^{(in)}\left(\mathbf{q}_+-\frac{\mathbf{q}_-}{2}\right)\sim{\delta^{(in)}}^2(\mathbf{q}_+)+\mathcal{O}(\mathbf{q}_-^2)\,. \tag{3.2.15}$$

Therefore the Wigner function becomes

$$\lim_{\nu\to0}f_W^0(\mathbf{x},D)=\lim_{\nu\to0}\int\frac{d^3x'}{(2\pi)^3}\int\frac{d^3q_+d^3q_-}{(2iD\pi\nu)^3}{\delta^{(in)}}^2(\mathbf{q}_+)\exp\left[i\boldsymbol{x}'\cdot\left(-\frac{\boldsymbol{p}}{a^2\dot{D}^2}+\frac{\boldsymbol{x}-\boldsymbol{q}_+}{D}\right)\right]\times$$
$$\times\exp\left\{-\frac{i}{D\nu}\left[\boldsymbol{q}_-\cdot\left(\boldsymbol{x}-\boldsymbol{q}_++D\nabla\phi^{(in)}(\mathbf{q}_+)\right)\right]\right\}\,. \tag{3.2.16}$$

Then integrating over $\boldsymbol{x}'$ and $\boldsymbol{q}_-$ gives simply Dirac delta functions and if we recall the remaining integration variable $\boldsymbol{q}_+ = \boldsymbol{q}$ we obtain the following expression for the Wigner function [73]

$$\lim_{\nu\to 0} f_W^0(\boldsymbol{x},\boldsymbol{p}) = \int d^3q\, {\delta^{(in)}}^2(\mathbf{q})\delta_D^{(3)}\left[\boldsymbol{x} - \boldsymbol{q} + D\nabla\phi^{(in)}(\boldsymbol{q})\right]\, \delta_D^{(3)}\left[\frac{\boldsymbol{p}}{a^2\dot{D}^2} + \nabla\phi^{(in)}(\boldsymbol{q})\right]. \tag{3.2.17}$$

Here we can make an additional comment on the semi-classical limit, we showed the difference between the classical Vlaslov distribution function $f$ and the Wigner function in (2.3.12) and it goes like

$$\frac{d}{dD}(f_W - f) \propto \nu^2\partial_{\mathbf{x}}^3\Phi\,, \tag{3.2.18}$$

where we used the equivalence between the effective potential of (2.3.12) and the $\Phi$ we defined in (3.0.1),(3.0.2). The semi-classical limit is recovered when the right-hand side of (3.2.18) goes to 0, this clearly happens if $\nu \to 0$. But there is another condition which can bring us nearer to the semi-classical limit leaving unchanged $\nu$, since the external potential $\Phi$ is sourced by perturbations it was smaller and slowly varying at the Universe early times when perturbations where still in the linear regime [56], hence also the limit $D \to 0$ would correspond to the semi-classical limit. Therefore to keep both the possible behaviours we should define the semi-classical limit as

$$D\nu \to 0 \quad \Rightarrow \quad f_W \sim f\,. \tag{3.2.19}$$

The same arguments are valid using the Husimi distribution because it develops a similar difference from the Vlaslov distribution $f$ [72]. Note that this new definition of the semi-classical limit does not change the results (3.2.17) because they are provided by the "behaviour" of perturbations at initial time (3.2.14) and (3.2.15), but we have defined more formally the semi-classical limit and it will be very useful in the study of the higher order terms of QPT since the limit $\nu \to 0$ would destroy the perturbative expansion due to the $1/\nu^n$ scaling of the n-th order term (3.0.38).
Comparing the result (3.2.17) with the general distribution function in Lagrangian coordinates (2.3.16) we can directly read off the displacement and the velocity which would be obtained from the Wigner distribution [73].

$$\boldsymbol{x}_0^W(\mathbf{q}, D) = \mathbf{q} - D\nabla\phi^{(in)}(\boldsymbol{q})\,, \tag{3.2.20}$$

$$\boldsymbol{u}_0^W(\boldsymbol{q}) = -\nabla\phi^{(in)}(\boldsymbol{q})\,. \tag{3.2.21}$$

From the equation of motion (3.2.20) we can immediately obtain the density function through the conservation of mass (1.2.20)

$$\delta_0(\mathbf{x}, D) + 1 = (1 + \delta^{(in)}(\mathbf{q}))\left(\frac{\partial\mathbf{x}}{\partial\mathbf{q}}\right)^{-1} = (1 + \delta^{(in)}(\mathbf{q}))\left(1 - D\frac{\partial^2\phi^{(in)}}{\partial\mathbf{q}^2}\right)^{-1}, \tag{3.2.22}$$

where with $\partial^2\phi^{(in)}/\partial\mathbf{q}^2$ we mean the determinant of the Hessian.
These solutions are exactly the same ones obtained from the Zel'dovich approximation [79] if we use the same initial conditions, i.e.

$$\delta_{DM}^{(in)}(\mathbf{q}) = 0 \qquad \phi_{DM}^{(in)}(\mathbf{q}) = \varphi^{(in)}(\mathbf{q})\,, \tag{3.2.23}$$

$$\delta_b^{(in)}(\mathbf{q}) = 0 \qquad \phi_b^{(in)}(\mathbf{q}) = \varphi^{(in)}(\mathbf{q})\,, \tag{3.2.24}$$

where we extended the DM initial conditions to be the same for both DM and baryons. This is unphysical for baryons [9] but we use this simple model to give the idea that under the free particle approximation DM and baryons behave in the same way. We have to remember that this is true only because we are considering scales bigger than the Jeans wavelength and so pressure effects are small and appear only in higher order terms of the perturbation theory, as we will depict in the following section. These initial conditions are justified for DM if the linear approximation of the Euler equation and negligible initial density fluctuations are assumed [73], the peculiar gravitational potential $\varphi^{(in)}(\mathbf{q})$ should be then estimate by observation of the DM distribution at recombination. Instead they are not well suited for baryons because they neglect initial pressure effects and the fact that baryons decoupled from radiation later than DM.
Thus in the semi-classical limit and to the leading order in perturbation theory we reproduce results from classical fluid dynamics. Anyway after shell-crossing we cannot use any more the conservation of mass to compute the density because it is no more valid after the Jacobian of coordinate transformation $\mathbf{q} \to \mathbf{x}$ becomes singular, i.e. at shell-crossing. Let's see now what results would give the Husimi distribution, we have to coarse-grain the Wigner function (3.2.12) as in (2.3.17). We use the definition of the conjugate momentum (2.3.3) to write the Wigner distribution in function of the velocity field.

$$\begin{aligned} f_H^0(\mathbf{x},\mathbf{u},D) &= \lim_{\nu\to 0}\frac{1}{(2\pi\sigma_x\sigma_u)^3}\int d^3x'd^3u'\, e^{-\frac{(\mathbf{x}-\mathbf{x}')^2}{2\sigma_x^2}} e^{-\frac{(\mathbf{u}-\mathbf{u}')^2}{2\sigma_u^2}} f_W^0(\mathbf{x}',\mathbf{u}',D) = \\ &= \lim_{\nu\to 0}\frac{1}{(2\pi\sigma_x\sigma_u)^3}\int d^3x'd^3u'd^3q\, e^{-\frac{(\mathbf{x}-\mathbf{x}')^2}{2\sigma_x^2}} e^{-\frac{(\mathbf{u}-\mathbf{u}')^2}{2\sigma_u^2}} {\delta^{(in)}}^2(\mathbf{q})\times \\ &\quad \times \delta_D^{(3)}\left[\boldsymbol{x}' - \boldsymbol{q} + D\nabla\phi^{(in)}(\boldsymbol{q})\right]\, \delta_D^{(3)}\left[\boldsymbol{u}' + \nabla\phi^{(in)}(\boldsymbol{q})\right] = \\ &= \lim_{\nu\to 0}\int d^3q\, {\delta^{(in)}}^2(\mathbf{q})\frac{\exp\left[-\frac{(\mathbf{x}-\mathbf{x}_0^W)^2}{2\sigma_x^2}\right]\exp\left[-\frac{(\mathbf{u}-\mathbf{u}_0^W)^2}{2\sigma_u^2}\right]}{(2\pi\sigma_x\sigma_u)^3}\,, \end{aligned} \tag{3.2.25}$$

where in the second line we used the previous results of the Wigner semi-classical limit since we can still use the smallness of $\nu$ e $\mathbf{q}_-$ to compute the integrals. From the second line $\nu$ is still present in $\sigma_u = \nu/(2\sigma_x)$. We can compute the density as its $0^{th}$-order momentum, i.e.

$$\eta_0^H(\mathbf{x},D) = \int d^3u f_H^0(\mathbf{x},\mathbf{u},D) = \int d^3q\, {\delta^{(in)}}^2(\mathbf{q})\frac{\exp\left[-\frac{(\mathbf{x}-\mathbf{x}_0^W(\mathbf{q}))^2}{2\sigma_x^2}\right]}{(2\pi\sigma_x^2)^{3/2}}\,. \tag{3.2.26}$$

Hence the resulting density field is just a Gaussian distribution centered on the Wigner trajectories (3.2.20) (and so on the Zel'dovich one) with a variance given by the position resolution $\sigma_x$. Defined in this way the density field does not diverge anymore at shell-crossing, it remains well defined for the whole evolution of the particle trajectories. Anyway this semi-classical result cannot predict the correct dynamics after the shell-crossing event because it continues to follow the Zel'dovich approximation and so the particles which encountered in the shell-crossing will not stick together.
We can compute also the coarse-grained velocity field from the Husimi function

$$\eta_0^H\mathbf{u}_0^H = \int d^3u\,\mathbf{u} f_H^0(\mathbf{x},\mathbf{u},D)\,. \tag{3.2.27}$$

Therefore the velocity field predict by the Husimi distribution is equal to the Wigner, we could expect it because in the semi-classical limit the velocity resolution is $\sigma_u = \nu/(2\sigma_x) \to 0$ and so no coarse-graining is performed over the velocity.
If we do not limit our study to the semi-classical regime the free particle approximation is able to investigate also the after shell-crossing regime and so the multi-stream regime [73]. Thus we have to keep $\nu$ finite and small such there is still some coarse-grain procedure acting on the velocity field, the problem is that for study this regime we have to compute the wave-function from (3.2.7) numerically, we will show later some simulations of the free particle solution. Instead the Zel'dovich approximation breaks at shell-crossing because it doesn't predict any multi-stream regime, the particles continue to free stream after the caustic, which is unphysical [79].
Note that one could obtain the same results in the semi-classical limit using the stationary-phase approximation (SPA) [34] , which is just equivalent to a Wick rotation of the saddle-point approximation, for computing directly $\psi_0$ from (3.2.3) and then use this result to compute the displacement and the Lagrangian velocity field through the moments of the Wigner distribution (2.3.14) or of the Husimi distribution (2.3.23), (2.3.24). For completness we report here the general (three-dimensional) result of SPA, which is treated more rigorously in App. A2.

$$I(\lambda) = (2\pi\lambda)^{-3/2} \int d^3q\, h(\boldsymbol{q}) \exp\left[\frac{i}{\lambda} g(\boldsymbol{q})\right], \tag{3.2.28}$$

$$\lim_{\lambda\to 0} I(\lambda) = \sum_{\boldsymbol{q}_c} \frac{h(\boldsymbol{q}_c) \exp\left[\frac{i}{\lambda} g(\boldsymbol{q}_c)\right]}{|det(H_{ij})|^{1/2}} \exp\left[\frac{i\pi}{4} \operatorname{sign}(H_{ij})\right], \tag{3.2.29}$$

where the sum is over the critical points $\boldsymbol{q}_c$ of $g(\boldsymbol{q})$ and $H_{ij}$ is its Hessian. This approximation is inspired by the fact that in the limit $\lambda \to 0$ the exponential term oscillates rapidly and tends to cancel out, thus only the points more stable, i.e. the stationary points of $g(\mathbf{q})$, are not negligible.
We define the following quantities using the initial conditions (3.2.23) (3.2.24) and the expression for $\psi$ (3.2.7)

$$\lambda = D\nu\,, \tag{3.2.30}$$

$$h(\mathbf{q}) = \sqrt{\eta^{(in)}} = 1\,, \tag{3.2.31}$$

$$g(\mathbf{q}) = \frac{(\mathbf{x}-\mathbf{q})^2}{2} - D\phi^{(in)}(\mathbf{q})\,. \tag{3.2.32}$$

Observe that the limit $\lambda \to 0$ recovers perfectly the more formal definition of the semi-classical limit we showed in (3.2.19), contrarily to the usual $\nu \to 0$. Then we can find the minimum of g as

$$\frac{\partial g}{\partial q^i} = -(x-q)_i - D\partial_i\phi^{(in)}(\mathbf{q}) = 0 \;\to\; q_{ci} = x_i + D\partial_i\phi^{(in)}(\mathbf{q}) \tag{3.2.33}$$

and its Hessian

$$H_{ij} = \delta_{ij} - D\partial_i\partial_j\phi^{(in)}(\mathbf{q})\,. \tag{3.2.34}$$

Thus we can write the wave function as

$$\psi_0^{SPA}(\mathbf{x}(\mathbf{q},D),D) \overset{D\nu\to 0}{=} \exp\left[\frac{i}{\nu}\left(\frac{D(\nabla\phi^{(in)}(\mathbf{q}))^2}{2}-\phi^{(in)}(\mathbf{q})\right)\right]\frac{1+i\,\mathrm{sign}\,H_{ij}}{2}\times \\ \times\left[1-D\det[\partial_i\partial_j\phi^{(in)}(\mathbf{q})]\right]^{-1/2}. \quad (3.2.35)$$

It's clear that the square modulus of this expression recover the same result for the overdensity (3.2.22). And the minimum condition (3.2.33) gives the equation of motion

$$\mathbf{x}=\mathbf{q}-D\nabla\phi^{(in)}(\mathbf{q})\,. \quad (3.2.36)$$

We need to compute also the gradient of the wave-function to obtain the velocity field through (2.3.14b). To find an accurate result we first compute the gradient from the general expression of the free particle wave-function (3.2.7) and then we apply the stationary phase approximation.

$$\nabla_{\mathbf{x}}\psi_0(\mathbf{x},D)=\frac{i}{\nu D}\int d^3q(\mathbf{x}-\mathbf{q})\frac{\exp\left[\frac{i}{2\nu D}\left((\mathbf{x}-\mathbf{q})^2-2\phi^{(in)}(\mathbf{q})\right)\right]}{(2\pi iD\nu)^{3/2}}\,. \quad (3.2.37)$$

Now we can apply the SPA ansatz (3.2.29). We should define all the various quantities but we can observe that they are all the same of the ones applied to $\psi_0$ beside the function $h(\mathbf{q})$, which becomes

$$\mathbf{h}(\mathbf{q})=\frac{i}{\nu D}(\mathbf{x}-\mathbf{q})\,. \quad (3.2.38)$$

Since the function $g(\mathbf{q})$ is the same also the minima $\mathbf{q}_c$ are the same that in the previous case (3.2.33), thus apply the stationary phase approximation we obtain

$$\nabla_{\mathbf{x}}\psi_0(\mathbf{q}_c(\mathbf{x},D))=-\frac{i}{\nu}\nabla_{\mathbf{q}}\phi^{(in)}(\mathbf{q})\psi_0(\mathbf{q}_c(\mathbf{x},D))\,. \quad (3.2.39)$$

Hence from the relation (2.3.14b) we obtain the Wigner momentum

$$\mathbf{j}^W(\mathbf{x}(\mathbf{q},D),D)=\eta(\mathbf{x}(\mathbf{q},D),D)\mathbf{u}(\mathbf{x}(\mathbf{q},D),D)=\frac{i\nu}{2}\left[\psi_0\nabla_{\mathbf{x}}\bar{\psi}_0-\bar{\psi}_0\nabla_{\mathbf{x}}\psi_0\right]= \\ =-\nabla_{\mathbf{q}}\phi^{(in)}(\mathbf{q})|\psi_0(\mathbf{q}_c(\mathbf{x},D))|^2=-\nabla_{\mathbf{q}}\phi^{(in)}(\mathbf{q})\eta(\mathbf{x}(\mathbf{q},D),D)\,, \quad (3.2.40)$$

the velocity field

$$\mathbf{u}^W(\mathbf{x}(\mathbf{q},D),D)=-\nabla_{\mathbf{q}}\phi^{(in)}(\mathbf{q}) \quad (3.2.41)$$

and the velocity potential

$$\phi(\mathbf{x}(\mathbf{q},D),D)=\phi^{(in)}(\mathbf{q}) \quad (3.2.42)$$

Hence we found that the stationary phase approximation gives the same results of (3.2.20), (3.2.21) and so of the Zel'dovich approximation [73]. Then as we showed previously we can apply the Gaussian filtering to obtain the Husimi results.
We will use all this results for investigate the higher orders of the perturbation theory. Instead in the following subsection we report some interesting simulation which studies the behaviour of the free particle approximation outside the semi-classical regime.

### 3.2.1 Numerical simulations

To investigate the evolution of the LSS density after shell-crossing times we no longer can limit ourselves to the semi-classical regime $D\nu \to 0$ but we have to study in its completeness the evolution of the wave-function through the free particle propagator defined by (3.1.26) in the Fourier space or by (3.2.3) in the coordinate space. Usually in numerical codes is more used the Fourier description.
We present now some simulations for the case of one-dimensional space divided in segments with periodic boundary conditions as we described in Sect.3.1 and presented in [67], the initial conditions are sinusoidal given by (3.1.1).
If we define the dimensionless comoving coordinate $\bar{x} = x/d$, where $d$ is the wavelength of the initial density perturbation, we obtain that the free particle wave-function (3.1.26) depends only on the parameter $\Gamma = \nu/d^2$ [67]. Since the Zel'dovich approximation in one dimension is exact and in the semi-classical limit the free particle approximation recovers it also our approximation is exact for $\Gamma \to 0$ [67]. Here we want to keep $\Gamma$ finite and not null but from the semi-classical limit observations we can expect that the free particle approximation behaviour would be optimized by the smallest possible value of $\Gamma$ [67].
Since we will test our solution on a discrete grid there is a lower bound $\Gamma_c$ on the value of $\Gamma$. The minimum possible sampling rate, called Nyquist rate, is defined as the the rate for which the phase change between two neighbouring grid points must be less than or equal to $\pi$ radians, otherwise the phase is not sufficiently sampled and aliasing effects cause the free-particle method to break down [67]. Hence we expect our problem to be optimized for $\Gamma = \Gamma_c$. From the initial conditions the amplitude of the phase of the initial wave-function, i.e. the initial velocity potential, is $\approx \delta_a$ thus we can define the optimal value of the $\Gamma$ parameter as $\Gamma_c = \delta_a/(2\pi^2)N_g$ where $N_g$ is the number of points on the grid [67].
Another important consideration is that since in the free particle approximation the quantum pressure is missing from the Schrödinger equation the dynamics directly take care of its effect, i.e. it is like have an additional pressure-like term in the Bernoulli equation, as we stated in the introduction of Chapter 2. As we will see from the simulations the quantum pressure has a regularizing effect, it oppose to the gravitational collapse preventing the formation of a caustic in a way similar to the fictitious viscous term of the Adhesion approximation [23, 68]. Since in the free particle approximation it is not present any "external" potential it is important to confront the magnitude of the quantum pressure with respect to the one of the convective term $\mathcal{C}(\mathbf{x}, D) = -|\nabla\phi|^2/2$, in this manner we can understand when the effect of the quantum pressure is negligible or not [67]. Note also that the quantum pressure $Q \propto \nu^2 \propto \Gamma^2$, hence its magnitude will depend on the value of the coarse-graining parameter.

In the following we will report numerical solutions provided by [67] for decreasing parameter $\Gamma$, so we can see the effect of the different values of it. In these simulations the initial amplitude is set to $\delta_a = 0.01$ and the grid is divide in $N_g = 512$ point, thus the optimal parameter is $\Gamma_c = 1 \times 10^{-6}$. From the value of the amplitude of the initial fluctuations is possible to derive the shell-crossing time predicted by the Zel'dovich approximation and so by the free particle one in the semi-classical limit. It corresponds to the time when the

overdensity (3.2.22) diverges, i.e. for

$$D_{SC} - D_i = \left( \frac{\partial^2 \varphi^{(in)}}{\partial \mathbf{q}^2} \right)^{-1} = \left( \frac{\delta_i}{D_i} \right)^{-1} = \frac{D_i}{\delta_a} \,, \tag{3.2.43}$$

where we used the fact that in the linear regime $\phi^{(in)} \sim \varphi^{(in)}$, which is the initial conditions used by Zel'dovich [79] for find the shell-crossing. In the second equivalence we used the Poisson equation at initial time. From the values set by [67] of $\delta_a = 0.01$ and $D_i = 1$ we obtain a shell-crossing growth factor $D_{SC} = 101$.
We begin assuming $\Gamma = 1$ with Fig.3.1. On the left side the evolution of the free particle density field with $\delta = |\psi|^2 - 1$ is showed in the interval $0 \leq x \leq d$, because we constructed the density field such as it is periodic with comoving period $d$. We observe that the density fluctuation field simply oscillates about the mean value $\bar{\delta} = 0$ and so there is no net growth of the initial density perturbation, this is an effect of the quantum pressure [67]. In the right-hand side the quantum pressure and the convective term magnitudes are confronted and it is immediate to see that the pressure term always dominates beside when the overdensity momentarily pass through 0. Hence it seems like the density growth is inhibited by the quantum pressure [67]. It is somewhat reminiscent of the effect of gas pressure [67], as Jeans showed (and it is briefly presented in App.A1) the gravitational collapse is stopped for any Fourier mode of the overdensity with wavenumber bigger than a critical one, called Jeans wavenumber. This modes undergo damped oscillations rather than growth, like the free particle overdensity for $\Gamma = 1$ (or bigger) in Fig.3.1. Anyway we have to state that the quantum and the gas pressure cannot be considered as effects of the same nature because the gas pressure is actually a pressure which the gas feels, meanwhile the quantum pressure is a pure quantum effect which arise from our wave-mechanical treatment of gravitational instability [67].
Since $Q \propto \Gamma^2$ (2.1.14) we expect that its effect will be less significant as $\Gamma$ decreases. In Fig.3.2 a plot with the same structure of Fig.3.1 is shown, but this time with the coarse-graining parameter set to $\Gamma = 1.4 \times 10^{-3}$. From the left panels (a) and (b) of Fig. 3.2 we can observe the free particle density grow as expect until $D = D_{SC}/2$, the matter flows towards initially over-dense regions. But this growth is too small to follow the one of the Zel'dovich approximation, the effect of the quantum pressure is still to strong [67]. At times $D > D_{SC}/2$ the growth stops and somewhere the density actually start to decay, this is because the quantum pressure has started to grow, overcoming the convective term, and so suppressing the gravitational collapse and the density growth. This cause that at times near shell-crossing $D \approx D_{SC}$ there is a large discrepancy between the results of the free particle approximation and the Zel'dovich one. Thus also for this value of $\Gamma$ there is a good correspondence between the two approximation only at early times, when the density is still small and so the quantum pressure.
In [67] Short and Coles found that the quantum pressure never becomes large enough to stop the growth of the density perturbations for values of $\Gamma \leq 1.4 \times 10^{-3}$, but in high density region the collapse is still strongly suppressed and so there is a poor match between the free particle and the Zel'dovich approximations.
As the coarse-graining parameter approaches its optimal value $\Gamma \to \Gamma_c$ the suppression effect of the pressure diminish and the agreement between the free particle and the Zel'dovich approximations improves. In Fig.3.3 it is reported the case $\Gamma = \Gamma_c = 1 \times 10^{-6}$. Now there is a good match between the two approximation at any time, the quantum

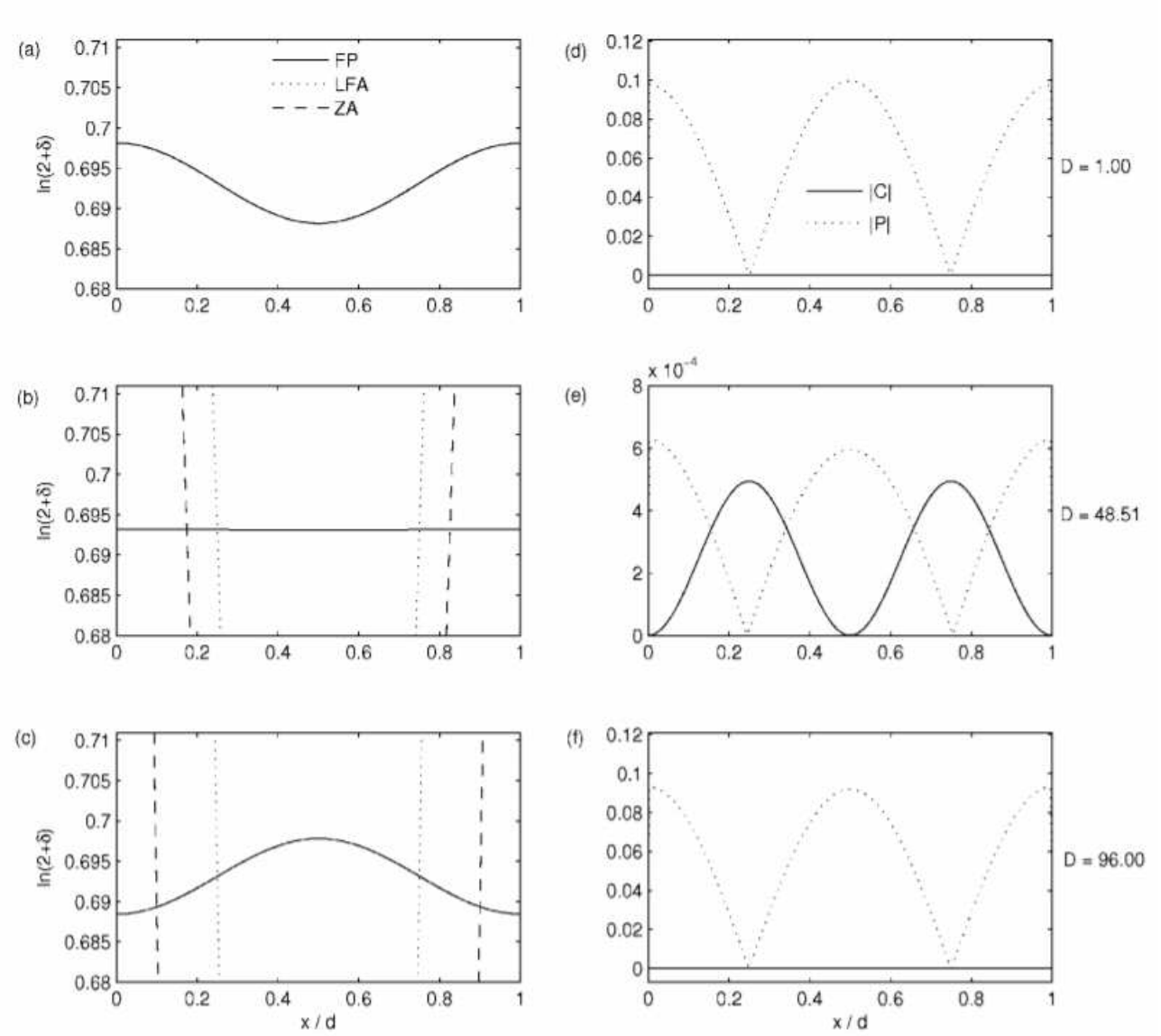


Figure 3.1: Evolution of a plane-symmetric sinusoidal density perturbation in an expanding CDM-dominated universe. The amplitude of the initial density fluctuation is $\delta_a = 0.01$. The left-hand plots show the density fields obtained from the free-particle approximation (FP), the linearized fluid approach (LFA) and the Zeldovich approximation (ZA) at three different values of the linear growth factor. The parameter $\Gamma = 1$ in the free-particle approximation. The right-hand plots show the corresponding evolution of the magnitudes of the convective (C) and quantum pressure (P) terms, in units of $d^2$. This figure is provided by [67], for any further detail check the main text.

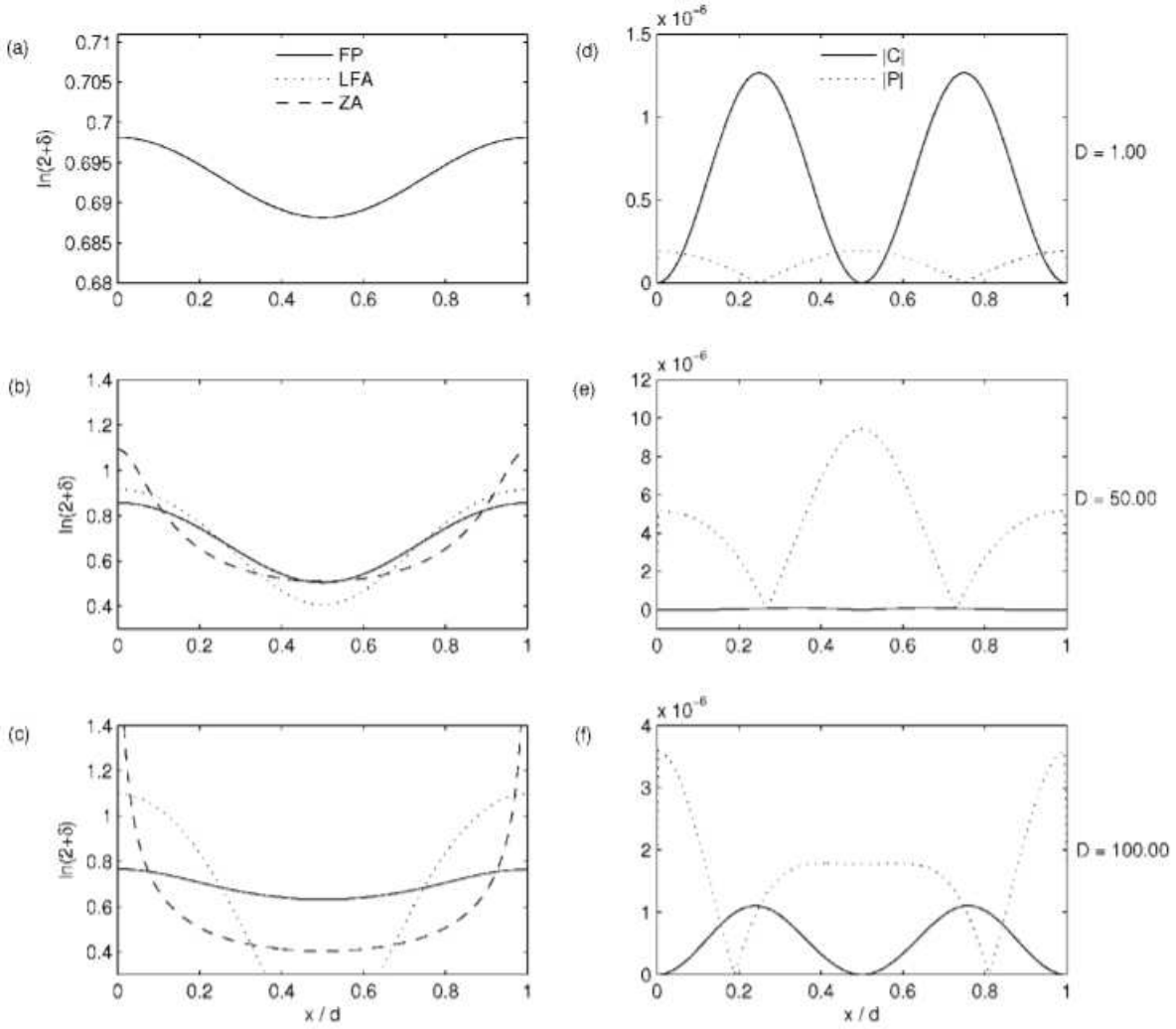


Figure 3.2: Evolution of a plane-symmetric sinusoidal density perturbation in an expanding CDM-dominated universe. The layout of the plots is as in Fig. 3.1; the only difference is that the parameter $\Gamma = 1.4 \times 10^{-3}$ in the free-particle approximation. This figure is provided by [67], for any further detail check the main text.

pressure is suppressed even in high-density regions [67]. It is very important to note that, unlike the Zel'dovich approximation, the free particle approximation leads to a density field that remains well behaved at shell-crossing [67]. From the right-hand side it is immediately evident that the convective term dominates the quantum pressure at any time. Anyway even if the quantum pressure is small it is not 0 because we are using a finite $\Gamma$ and so it has still a role in the collapse dynamic, it is due to its presence that the density field doesn't diverge at shell-crossing and it remains well defined [67].

Another interesting simulation of the free particle approximation was done by Porqueres and collaborators in [58]. They called the wave-mechanical method propagator perturbation theory, because our perturbation theory on the Hamiltonian can be seen as a perturbation theory on the propagator defined in (3.2.5). To compute the free particle solution they exploited the numerical use of discrete Fourier transforms (DFT) and circular

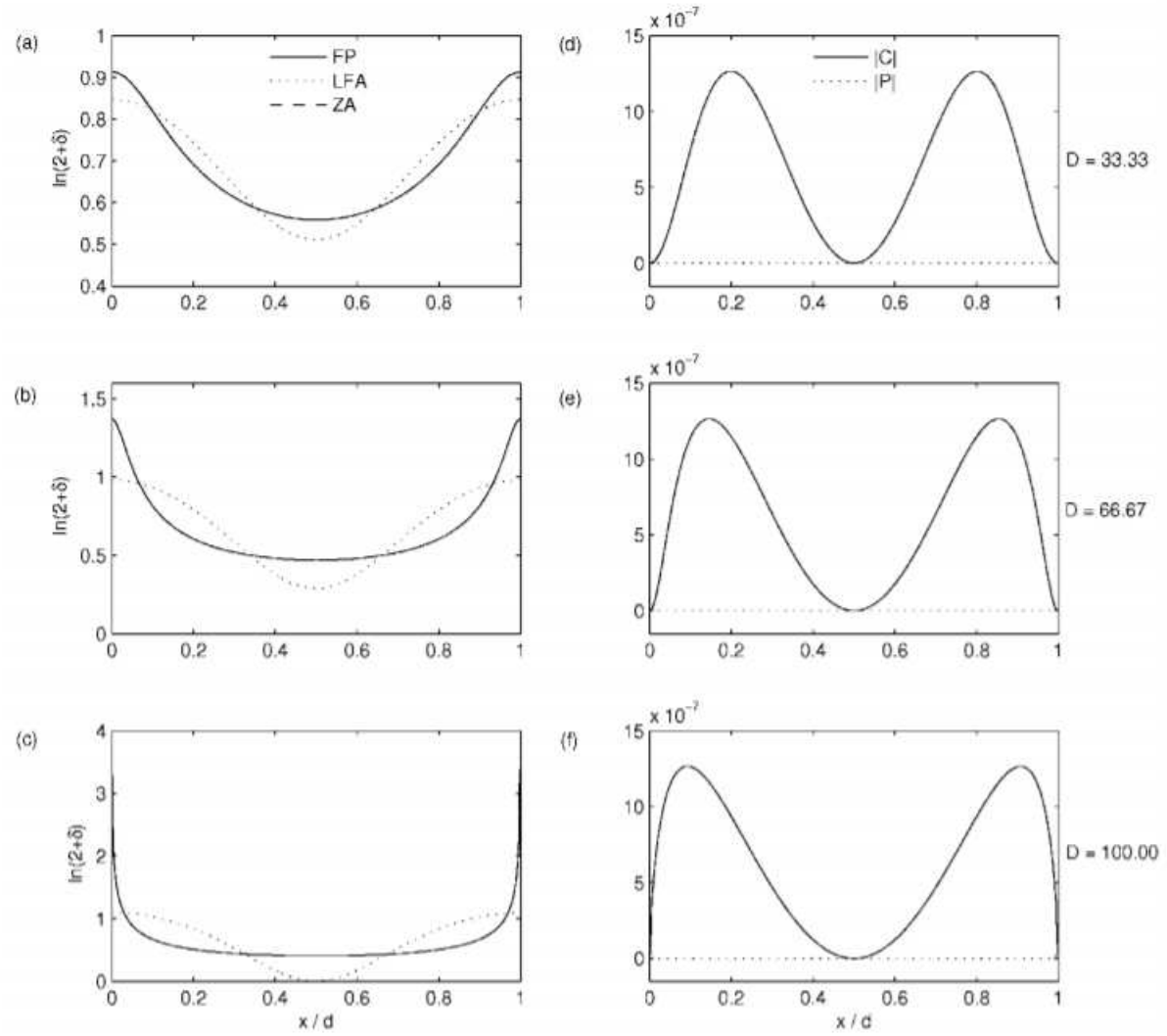


Figure 3.3: Evolution of a plane-symmetric sinusoidal density perturbation in an expanding CDM-dominated universe. The layout of the plots is as in Fig. 3.1; the only difference is that the parameter $\Gamma = \Gamma_c = 1 \times 10^{-6}$ in the free-particle approximation. This figure is provided by [67], for any further detail check the main text.

convolution on a periodic domain, i.e. they computed (3.1.26) as

$$\psi_0(\mathbf{x}, D) = DFT^{-1}\left[\exp\left(-i\nu\frac{k^2}{2}D\right) DFT\left[e^{-\frac{i}{\nu}\phi_i}\right]\right], \tag{3.2.44}$$

where they used as initial conditions $\delta_i = 0,\ \phi_i$.
In [58] they noted that cosmological observations are made in a redshifted space instead of the comoving physical space. Specifically, a particle is not observed to be at its Eulerian position $\mathbf{x}$ but instead at its redshift space position $\mathbf{s}$, because of deviations from pure Hubble expansion, due to peculiar velocities. They find that they can pass from the comoving physical space to the redshift one using a new propagator in addition to the ordinary one (3.2.5), we report their method in App.A3.
In Fig.3.4 (provided by [58]) we report a comparison between the density fields obtained with the Zel'dovich (ZA) and the PPT (free particle) approximations in comoving physical space (top panels) and in redshift space (bottom panels). It is immediately noted that PPT and ZA generate the same structures in the density distribution both in real and in redshift space [58]. At the far right we show the quasar flux field F, i.e. the matter distribution inferred by observations of the Ly-$\alpha$ forest, modelled through the fluctuating Gunn-Peterson approximation [22]. From the comparison of this last panels with the Zel'dovich and free particle (PPT) approximations it is clear the wave-mechanical approach provide a good model of density distribution [58].

We want to present a last numerical simulation of the free particle approximation, it is provided by [73] and it describes some interesting features of the wave-function evolution after shell-crossing. This simulation is done for a Universe filled just by cold dark matter (CDM), hence the growth factor is equivalent to the scale factor $D \equiv a$. Fig.3.5 shows the evolution of the free particle wave-function in one-dimension with initial conditions

$$\psi_i(q) = e^{-\frac{i}{\nu}\phi_i(q)}, \qquad \phi_i(q) = -\cos(q)\,. \tag{3.2.45}$$

The domain colouring technique is used in the plot to assign a unique color to each point in the complex plane, this representation method is described in [76]. The amplitude of the wave-function is mapped by the brightness and the phase by the color hue for each point in the space-time $(x, a)$.
From Fig.3.5 is evident that after shell-crossing, for $a > a_{sc}$, interference patterns arise. This is due to the fact that when two (or more) fluid trajectories cross, i.e. at shell-crossing, the wave-functions corresponding to the different trajectories overlap giving rise to the interference patterns [73]. The interference patterns are related to the effective vortical motion depicted in Sect.2.4 and which arises after shell-crossing due to an averaging of the different fluid trajectories. In this region of space-time we have the transition from the single-stream to the multi-stream regime. This latter regime can be quite well described by the free particle approximation choosing an optimal value of $\nu$ [73].

Hence through these numerical simulations we have found that the free particle approximation resembles very well the Zel'dovich approximation before shell-crossing (and this implies that our approximation is well behaved since the Zel'dovich approximation is exact in one-dimension before shell-crossing) and that our approximation is still valid after shell-crossing behaving in a way similar to the Adhesion approximation [23, 68] but

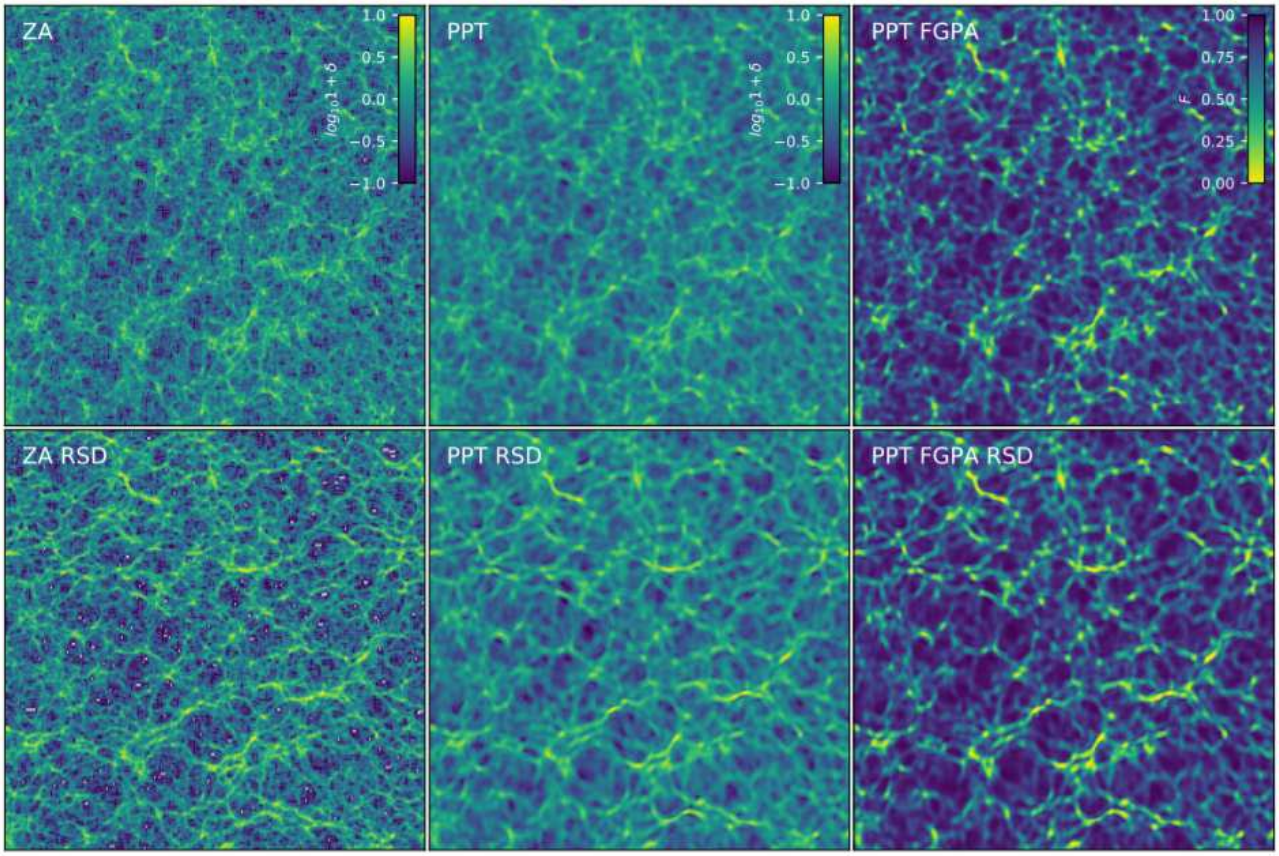


Figure 3.4: Density fields (left and middle column) and quasar flux field in the FGP approximation (right column) in physical space (top panels) and in redshift space (bottom panels), with the line-of-sight direction upwards. The leftmost panels use the Zel'dovich approximation and CIC deposit, the others use the PPT formalism. In all cases we used $256^3$ resolution elements, the box size (and extent of each image) used for this comparison is $256h^{-1}$Mpc at $z = 2.5$. The thickness of the projected slice is $2h^{-1}$Mpc and white pixels in the CIC panels indicate zero particles deposited. This figure is provided by [58], for any further detail check the main text.

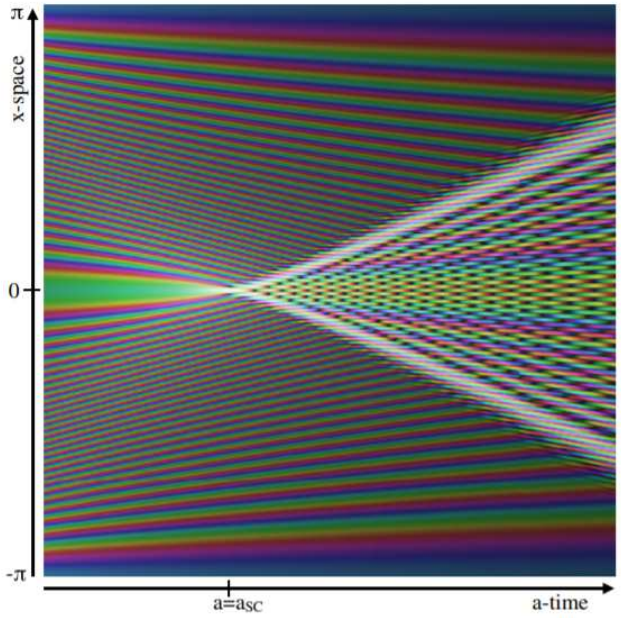


Figure 3.5: Time evolution of the free particle wave-function with 1D initial data given by (3.2.45), with $\nu = 0.01$ and evolved using a grid of 1024 cells in a CDM Universe. Using domain colouring the plot shows both the wave-function amplitude, in terms of the brightness as $0.5^{|\psi|}$, and the phase through the colour hue. Thus lines at constant colour corresponds to lines at constant phase. For times $a > a_{sc}$ a interference pattern arises due to multi-streaming. This figure is provided by [73], for any further detail check the main text.

without the need of introduce a fictitious viscous term, the quantum pressure takes its place.

## 3.3 First order solution

Now we want to investigate the successive order of the perturbation theory. Similarly to the free particle case, the small effects of the quantum pressure are implicit in the discussion since is is not present in the underling Schrödinger equation (3.0.3). But it can be retrieved implicitly by numerical simulations as shown for the free particle approximation [67] in the previous section. Also in the section we will keep the generic initial conditions (3.2.8), thus we obtain a general results which describes the evolution of any initial condition. For physical initial conditions one should follow the work [9, 25], which depict how to find accurate initial condition whene studying a mixed baryon-DM system.
We start solving the DM Schrödinger equation following the quantum perturbation theory. From the Poisson equation (2.2.29) we can express the potential $\Phi_{DM}$ as

$$\Phi_{DM}(D', k_p) = \left( \nu \mathcal{F}_{k_p}[Arg(\psi_{DM}(D', y)] - \frac{3e(\Omega_{DM})}{2D'^2} \frac{1}{k_p^2} \left( |\psi_{DM}|^2(D', k_p) - \delta^{(D)}(k_p) \right) \right) , \tag{3.3.1}$$

where $\mathcal{F}_{k_p}$ is the Fourier transform and $\delta^{(D)}$ the Dirac delta.
Inserting this expression in the first order correction (3.1.25) to the DM wave-function we

get an integral equation defining the DM wave-function at linear order in the potential $\Phi_{DM}$. We observe that the potential $\Phi_{DM}$ is totally set by $\psi_{DM}$ and, since we don't want to increase the order of the perturbative solution, we can use the free particle wave-function (3.1.26) in the definition of $\Phi$ (3.3.1).
In the same way we can obtain a similar equation defining the baryon wave-function, but this time the potential will depend on both $\psi_{DM}$ and $\psi_b$, because we assumed that the gravitation potential is generated by the DM. Using (2.2.30) we can write the potential $\Phi_b$ in the Fourier space as

$$\Phi_b(D', k_p) = \left(\nu \mathcal{F}_{k_p}[Arg(\psi_b(D', y)] - \frac{3e(\Omega_{DM})}{2D'^2}\frac{1}{k_p^2}\left(|\psi_{DM}|^2(D', k_p) - \delta^{(D)}(k_p)\right)\right) + \\ + \frac{3}{2}\frac{M^{\alpha-1}(D')}{D'^{\alpha+1}}\left(\frac{f(D')}{\Omega_{DM}(D')}\right)^2 \frac{1}{\gamma - 1}\frac{1}{\tilde{k}_J^2}|\psi_b|^{2\gamma-2}(D', k_p)\,, \tag{3.3.2}$$

where the expression for $M$ and $f$ are given respectively by (1.4.26) and (1.4.25). Then as before if we insert this expression in (3.1.25) we obtain an integral equation for $\psi_b^{(1)}(x, D)$. We could use again the equipartition theorem to write the first-order correction to the wave-function (3.1.25) in the phase space, in terms of the free particle kernel. But, since the potentials are easier to write in the Fourier space due to the form of the Poisson equation, we stick to the momentum integral. Anyway we can write it in a more compact way using the Fourier transform of the free particle kernel (3.2.4).

$$\psi_{b,DM}^{(1)}(x, D) = -\frac{i}{\nu}\frac{1}{2\pi}\int_{D_i}^{D} dD' \int_{\frac{2\pi}{L}}^{\infty} dk_n \int_{\frac{2\pi}{L}}^{\infty} dk_m e^{-ik_m x}\psi_i^{b,DM}(k_n)\times \\ \times K_0(k_m, D; D')\Phi_{b,DM}(D', k_m - k_n)K_0(k_n, D'; D_i)\,. \tag{3.3.3}$$

Now is easier to give a physical meaning to this integral. The term $K_0(k_m, D; D') \times$ $\times \Phi_{b,DM}(D', k_m - k_n)K_0(k_n, D'; D_i)$ means that the particle evolves from the time $D_i$ as a free one until the time D' with momentum $k_n$, at the time D' is scattered by the potential $\Phi(D', k_m - k_n)$ and then evolves again as a free particle until the time D with momentum $k_m$. The complete form of the probability of evolution is given by integrating this term over all possible combination of D' and $k_n$, which are all the possible alternatives of points in the Fourier space where the "scattering" may have taken place.
This is a common result of the path-integral formulation of quantum perturbation theory [28]. If we would go to upper order in the perturbation theory there would be more scatterings, the same number as the order of the perturbation term, and still between each scattering the particle can be considered free.
As we said for dark matter, we can use the free particle solution as the wave-function inside the integral to do not increase the order of the solution.
The expression of $\psi^{(1)}$ through Fourier transforms can be very useful for numerical studies but it is not analytically tractable. We can try to find an analytical solution in the semi-classical limit $D\nu \to 0$ using the stationary phase approximation. We have to observe immediately that it is a very crude approximation because of the $i/\nu$ prefactor in the wave-function (3.0.3). We deal with it anyway because it could still give some interesting result on very big scales where the perturbation are expected to be the smallest and so

the perturbation theory can be still a crude approximation of the real behaviour. In order to use SPA we have to pass to the coordinate space because we need the fast oscillating exponentials with the $\nu$ at the denominator. Hence as we have done with the free particle approximation we can use the convolution theorem and derive the following expression for the first order correction to the wave-function.

$$\psi^{(1)}_{b,DM}(\mathbf{x},D) = -\frac{i}{\nu}\int_{D_i}^{D} dD' \int d^3x' d^3q K_0(\mathbf{x},D;\mathbf{x}',D')\Phi_{b,DM}(\mathbf{x}',D')K_0(\mathbf{x}',D';\mathbf{q},D_i)\psi_i(\mathbf{q}) = \\ = -\frac{i}{\nu}\int_{D_i}^{D} dD' \int d^3x' d^3q K_0(\mathbf{x},D;\mathbf{x}',D')\Phi_{b,DM}(\mathbf{x}',D')\psi_0(\mathbf{x}',D')\,, \tag{3.3.4}$$

where the external potential is given by

$$\Phi_{DM}(\mathbf{x}',D') = \nu Arg(\psi_{DM}(\mathbf{x}',D')) - \frac{3e(\Omega_{DM})}{2D'^2}\nabla^{-2}\left(|\psi_{DM}|^2(\mathbf{x}',D')-1\right)\,, \tag{3.3.5}$$

$$\Phi_b(\mathbf{x}',D') = \nu Arg(\psi_b(\mathbf{x}',D')) - \frac{3e(\Omega_{DM})}{2D'^2}\nabla^{-2}\left(|\psi_{DM}|^2(\mathbf{x}',D')-1\right) + \\ + \frac{3}{2}\frac{M^{\alpha-1}(D')}{D'^{\alpha+1}}\left(\frac{f(D')}{\Omega_{DM}(D')}\right)^2\frac{1}{\gamma-1}\frac{1}{\tilde{k}_J^2}|\psi_b(\mathbf{x}',D')|^{2\gamma-2}\,. \tag{3.3.6}$$

Here we directly generalized to the three dimensional case and we used the inverse Laplace operator $\nabla^{-2}$ to write the potential $V_{b,DM}$ from the Poisson equation (2.2.29). We have to observe that semi-classical limit $D\nu \to 0$ actually corresponds to $\lambda \to 0$ because $D' < D$. Since we don't want to increase the order of the solution we can use the results of the free particle approximation for the quantities inside the potential $\Phi$, remember that $\nu Arg(\psi) = -\phi$. Then, for small $\nu$, we can apply SPA to solve the spatial integrals. We study the case of a general potential $\Phi$ and later we will particularize the results to the baryons or DM. Since we have two integrals we have to use SPA two times, we begin with the integral in $\mathbf{q}$ but this integral is just the definition of the free particle wave-function (3.2.7) and thus SPA gives the same result obtained in the previous section (3.2.35) with the stationary condition

$$\mathbf{q} = \mathbf{x}' + D'\nabla_{\mathbf{q}}\phi^{(in)}(\mathbf{q})\,, \tag{3.3.7}$$

where we have chose as initial time $D_i = 0$. For the integral in $\mathbf{x}'$ we define the new variables from the SPA ansatz (3.2.29)

$$\lambda = \nu(D-D')\,, \tag{3.3.8}$$

$$h(\mathbf{x}') = \frac{\Phi(\mathbf{x}',D')}{\sqrt{\delta_0(\mathbf{x}'(\mathbf{q},D'),D')}}\,, \tag{3.3.9}$$

$$g(\mathbf{x}') = (\mathbf{x}-\mathbf{x}')^2 + (D-D')\left(\frac{D'(\nabla\phi^{(in)}(\mathbf{q}))^2}{2} - \phi^{(in)}(\mathbf{q})\right)\,, \tag{3.3.10}$$

where $\delta_0(\mathbf{x}'(\mathbf{q},D'),D')$ is the overdensity for the SPA free particle approximation (3.2.22). The stationary points of $g(\mathbf{x}')$ are given in components by

$$x_c^{i'} = x^i - (D-D')D'\partial^i\partial^k\phi^{(in)}(\mathbf{q})\partial_k\phi^{(in)}(\mathbf{q}) + (D-D')\partial^i\phi^{(in)}(\mathbf{q})\,, \tag{3.3.11}$$

where the partial derivations should be respect to $\mathbf{x}'$ but, since they are applied to the initial velocity potential, the stationary condition (3.3.7) at initial time leads to $\nabla_{\mathbf{x}'} = \nabla_{\mathbf{q}}$. We need to compute also the Hessian of $g(\mathbf{q})$

$$H_{ij} = \delta_{ij} + (D - D')D'\partial_j \left[\partial_i\partial^k\phi^{(in)}(\mathbf{q})\partial_k\phi^{(in)}(\mathbf{q})\right] - (D - D')\partial^j\partial^i\phi^{(in)}(\mathbf{q})\,. \tag{3.3.12}$$

Finally we can write the first order correction as

$$\begin{aligned}\psi^{(1)}_{SPA}(\mathbf{x}(\mathbf{q}, D), D) = \lim_{D\nu\to 0} -\frac{i}{\nu}\int_0^D dD' \frac{\Phi(\mathbf{x}(\mathbf{q}, D'), D')}{\delta_0^{1/2}(\mathbf{x}(\mathbf{q}, D'), D')}\times \\ \times \frac{e^{\frac{i}{\nu(D-D')}g(\mathbf{x}'_c)}}{|1 + \det\left[(D - D')D'\partial_j\left[\partial_i\partial^k\phi^{(in)}(\mathbf{q})\partial_k\phi^{(in)}(\mathbf{q})\right] - (D - D')\partial^j\partial^i\phi^{(in)}(\mathbf{q})\right]|^{1/2}}\end{aligned} \tag{3.3.13}$$

$$\begin{aligned}= \lim_{D\nu\to 0} -\frac{i}{\nu}\int_0^D dD'\psi_0^{SPA}(\mathbf{x}(\mathbf{q}, D'), D')\times \\ \times \frac{\Phi(\mathbf{x}(\mathbf{q}, D'), D')}{|1 + \det\left[(D - D')D'\partial_j\left[\partial_i\partial^k\phi^{(in)}(\mathbf{q})\partial_k\phi^{(in)}(\mathbf{q})\right] - (D - D')\partial^j\partial^i\phi^{(in)}(\mathbf{q})\right]|^{1/2}}\times \\ \times \exp\left[\frac{i}{2\nu}\left(D'\partial_i\partial^k\phi^{(in)}(\mathbf{q})\partial_k\phi^{(in)}(\mathbf{q}) - \partial^i\phi^{(in)}(\mathbf{q})\right)^2\right]\,,\end{aligned} \tag{3.3.14}$$

where we expressed $\mathbf{x}$ in function of $\mathbf{q}$ thanks to the two stationary conditions, which together give

$$x^i = q^i + (D - D')D'\partial^i\partial^k\phi^{(in)}(\mathbf{q})\partial_k\phi^{(in)}(\mathbf{q}) - D\partial^i\phi^{(in)}(\mathbf{q}) \tag{3.3.15}$$

Unfortunately this equation is not the equation of motion of our system because there is still a time-integral in the wave-function expression (3.3.14). This last integration cannot be solved analytically and it is left to a numerical treatment. Due to the exploding behviour of $1/\nu$ after the numerical integration we have to compare (3.3.14) with the semi-classical result of the free particle approximation (3.2.35) and we must keep only the scales where the free particle term is the dominant one. we have to observe to that using this SPA approximation only at very early times the semi-classical limit condition $D\nu \to 0$ with $D$ very small can permit us to keep $\nu$ bigger and so prevent the spoiling of the perturbative expansion. Hence in the semi-classical limit we can obtain results only on these scales or times (which have to be investigated by numerical studies), these results would be far from accurate but could still give the idea on some features present in the dynamics due to the presence of the external potential $\Phi$.
Then we should apply the Husimi filtering (2.3.19), which we expect to behave as in the free particle approximation, i.e. no filtering over the velocities due to the semi-classical limit $D\nu \to 0$ and the density distribution will be a Gaussian distribution centered on the Wigner particle trajectories. The spatial resolution instead has to be set such as the perturbation theory is still valid as we observed above. These results could superclass the free particle approximation but only on very big scales so we expect them to be not very interesting. The numerical results from the study of QPT with a finite $\nu$ would be far more interesting and we expect them to be able to investigates results until the neighbourhoods of the Jeans scale.

Applying numerical methods to the results of the perturbation theory up to first order would permit us to predict the distribution of baryons and dark matter over the Universe. From the drift-kick-drift form of the first-order propagator (3.3.3), (3.3.5), (3.3.6) we expect that the locations where the potential kick is more relevant corresponds to higher-density loci predicted by the free particle approximation, since the components of the potentials are bigger for higher density $|\psi|^2$. Hence we expect that the numerical simulation would be less computationally requiring respect a full N-body simulation.

# Chapter 4

# Time-splitting spectral approximation

In the previous chapter we found that even if we make several approximation and study the Schrödinger-Poisson system (2.2.42) with quantum perturbation theory at the end we need numerical computations to obtain physical results. Hence we want now to present a numerical method which solves directly the Schrödinger equation without the need of the perturbative expansion. Therefore we do need any more to restrict on scales much bigger to the Jeans wavelength to keep baryon pressure small as in the previous chapter, the pressure effects can be fully developed by the numerical code. In this chapter we present in particular an approximation which seems to be very useful to solve numerically the Schrödinger equations, this approximation is commonly used in the solid state physics field for example in the study of Bose-Einstein condensates (BEC). We apply the time-splitting spectral approximation to a general nonlinear Schrödinger equation (NLS) in the semi-classical regime $\nu \to 0$, then we will particularize the solution to describe our baryon-DM system (2.2.42). An overview of this method is described in [5], where a series of numerical studies for particular realizations of the nonlinear Schrödinger equation are presented. We have to make an important observation on the semi-classical limit, since this numerical method was develop for Solid state physics studies it uses the common semi-classical limit $\nu \to 0$ and not the more physical in our particular cosmological study (3.2.19) $D\nu \to 0$. Anyway this is not a problem since this numerical method is able to investigate also late times (see e.g. the gravitational collapse presented in Fig.4.4) and so we do not need to limit ourselves to early times as we did for the semi-classical limit of the higher order QPT in Sect.3.3.
We search for a solution of the following nonlinear Schrödinger equation

$$i\nu\psi^\nu_D + \frac{\nu^2}{2}\nabla^2\psi^\nu - V(\mathbf{x}, D)\psi^\nu - h(|\psi^\nu|^2, D)\psi^\nu - \nu\tau(D)Arg[\psi^\nu]\psi^\nu = 0\,, \tag{4.0.1}$$

where the superscript $\nu$ indicates functions which depend on $\nu$ itself, $\psi^\nu_D \equiv \frac{\partial\psi^\nu}{\partial D}$, $V(\mathbf{x}, D)$ is a general real potential (in the original article [5] it is a electrostatic potential), $h(|\psi^\nu|^2, D)$ is a real-valued smooth function and $\tau(D)$ is a relaxation rate. We can relate this Schrödinger equation to our cosmological problem comparing it with the Schrödinger-

Poisson system (2.2.42):

$$V_{b,DM}(\mathbf{x},D) = \frac{3e(\Omega_{DM})}{2D}\varphi(\mathbf{x},D)\,, \tag{4.0.2}$$

$$\tau_{b,DM}(D) = \frac{3e(\Omega_{DM})}{2D}\,, \tag{4.0.3}$$

$$h(|\psi^\nu(\mathbf{x},D)|^2,D) = \begin{cases} 0 & \text{for DM} \\ \frac{3}{2}\frac{M^{\alpha-1}(D)}{D^{\alpha+1}}\left(\frac{f(D)}{\Omega_{DM}}\right)^2 \frac{1}{\gamma-1}\frac{1}{\tilde{k}_J^2}|\psi_b(\mathbf{x},D)|^{2(\gamma-1)} & \text{for baryons} \end{cases}, \tag{4.0.4}$$

where $e(\Omega_{DM}) = \Omega_{DM}/f(D)^2$ and $f(D)$ is given by (1.4.25) with the relation between $a$ and $D$ given by (1.4.26) and we made an abuse of notation calling $V_{b,DM}$ the gravitational potential, in the previous chapters it contained also the term $\nu\tau(D)Arg[\psi^\nu]$. Since the baryon potential $V_b$ is provided by the gravitational potential, which is sourced by the DM distribution through the Poisson equation (2.2.24), we will have to solve first the Schrödinger equation for DM and then the baryons one. From this comparison with our cosmological quantities it is clear that the relaxation rate $\tau(D)$ corresponds to the effects of the Hubble drag due to the expansion of the Universe; the $h(|\psi^\nu(x,D)|^2,D)$ corresponds to a pressure and the potential $V$ simply to the gravitational potential.
We need to set also the initial conditions

$$\psi^\nu(\mathbf{x},D=0) = \psi_i^\nu(\mathbf{x})\,, \tag{4.0.5}$$

which then have to be divided in the DM and baryon cases.
We have to observe that the quantum pressure is not present in the NLS (4.0.1), thus its effect is implicit and it will be directly seen in the particle dynamics as observed in the simulations of the free particle approximation [67].
We keep the Madelung definition of the wave function (2.1.7), for which the following definitions hold

$$\nu Arg[\psi^\nu(\mathbf{x},D)] = -\phi^\nu(\mathbf{x},D)\,, \tag{4.0.6}$$

$$-\nabla\phi^\nu(\mathbf{x},D) = \frac{J_W^\nu(\mathbf{x},D)}{\eta_W^\nu(\mathbf{x},D)}\,. \tag{4.0.7}$$

with $\eta_W^\nu(\mathbf{x},D)$ and $J_W^\nu(\mathbf{x},D)$ computed from the wave-function through the Wigner function as in (2.3.14), we can apply the Husimi filtering a posteriori as shown for the free particle simulation in Sect.3.2 for the semi-classical regime. These two functions are called quadratic macroscopic quantities due to their quadratic proportionality with respect to the wave-function. The nonlinear Schrödinger equation (4.0.1) covers many situation studied in Solid State Physics such as [5]:

- $V \equiv 0$, $h(\rho) = \beta_\nu\rho$ and $\tau = 0$: it is the cubic NLS, called the focusing NLS when $\beta_\nu < 0$ and the defocusing NLS if $\beta_\nu > 0$.
- $V = \frac{\omega}{2}|\mathbf{x}|^2$ with $\omega > 0$ a constant, $h(\rho) = \rho$ and $\tau = 0$: it is called Gross-Pitaevskii equation (GPE) and it is related to Bose-Einstein condensate (BEC).
- $V$, $h$ general and $\tau > 0$: the system is equivalent to a current-relaxed quantum hydrodynamical system for $\rho^\nu$ and $J^\nu$, this is the case on which we are interested and we showed how to relate the hydrodynamical and the Schrödinger systems in Sect. 2.1.

From mathematical studies of the NLS (4.0.1) it is well known that (4.0.1) propagates oscillations in space and time preventing $\psi^\nu$ from converging strongly as $\nu \to 0$ [5]. This oscillatory nature of the solutions of the Schrödinger equation in the semi-classical regime leads to some problem in the numerical analysis. Even for stable numerical approximation (or under mesh size and time step restrictions which guarantee stability) the oscillations may pollute the solution in such a way that the quadratic macroscopic quantities ($\eta^\nu$ and $J^\nu$) and other physical observables come out completely wrong unless the spatial-temporal oscillations are fully resolved numerically [5], i.e. using many grid points per wave length of order $\mathcal{O}(\nu)$. In [45, 46] they found that the best combination of time and space discretizations, which guarantees good approximations to all smooth observables for small but finite $\nu$, is provided by

$$\text{mesh size} \quad l = o(\nu)\,, \tag{4.0.8}$$

$$\text{time step} \quad t = o(\nu)\,. \tag{4.0.9}$$

If these conditions are not fulfilled the observable inferred by the numerical analysis would not correctly describe the real system [5].

## 4.1 One dimensional case

We introduce the time-splitting Fourier spectral approximation of the nonlinear Schrödinger equations in one space dimension, for simplicity of notation. Later we will show hot it can be generalized to a three-dimensional space. We study a periodic system, which can be described in the spatial interval $x \in [a, b]$, with periodic boundary conditions

$$\psi^\nu(a, D) = \psi^\nu(b, D)\,, \tag{4.1.1}$$

$$\psi^\nu_x(a, D) = \psi^\nu_x(b, D)\,, \tag{4.1.2}$$

with $\psi_x \equiv \partial_x \psi^\nu$. For be consistent with Chap. 3 we set the boundaries as

$$a = 0\,, \qquad b = L\,. \tag{4.1.3}$$

We define the spatial mesh size $l = \Delta x > 0$ as $l = (b - a)/M = L/M$ with $M$ an even positive integer. We call the time step $t = \Delta D > 0$ and let the grid points and the time steps be

$$x_j \equiv a + jl = jl, \quad j = 0, 1, ..., M\,. \tag{4.1.4}$$

$$D_n \equiv nt, \quad n = 0, 1, 2, ...\,. \tag{4.1.5}$$

We call $\Psi^{\nu,n}_j$ the approximation of the wave-function in a space-time step $(j, n)$ $\Psi^\nu(x_j, D_n)$ and $\mathbf{\Psi}^{\nu,n}$ the solution vector at time $D = D_n = nt$ with as components the approximation at each grid point $\Psi^{\nu,n}_j$.
The time-splitting spectral method take its basis from solve the NLS equation (4.0.1) from time $D = D_n$ to time $D = D_{n+1}$ in two steps. First one solves the "kinetic" part of the nonlinear Schrödinger equation [5]

$$i\nu\psi^\nu_D + \frac{\nu^2}{2}\psi^\nu_{xx} = 0\,, \tag{4.1.6}$$

for one time step of length $t$. We already know the solution of this equation, it is the free particle approximation which was presented in Sect.3.2. Then one solves [5]

$$i\nu\psi^{\nu}_{D} - V(x,D)\psi^{\nu} - h(|\psi^{\nu}|^2, D)\psi^{\nu} - \nu\tau(D)Arg(\psi^{\nu})\psi^{\nu} = 0\,, \tag{4.1.7}$$

for the same time step $[D_n, D_{n+1}]$. We can observe that the Schrödinger-like equation (4.1.7) leaves the norm of the wave-function $|\psi^{\nu}|$ invariant in time during the time step [5]. It is shown in the following way

$$\begin{aligned}\partial_D(|\psi^{\nu}|^2) &= 2Re[\psi^{\nu}_{D}\bar{\psi}^{\nu}] = \\ &= -\frac{2}{\nu}Re\left[i\left(V(x,D) + h(|\psi^{\nu}|^2, D) + \nu\tau(D)Arg[\psi^{\nu}]\right)|\psi^{\nu}|^2\right] = 0\,.\end{aligned} \tag{4.1.8}$$

This means that the norm of the wave-function during a time step evolves accordingly the free particle solution of (4.1.6). Hence, for solve (4.1.7), we can set the norm of $\psi^{\nu}$ at a given time inside the time step, for example at $D_n$ $|\psi^{\nu}(x, D_n)|$.
Thanks to this invariance we can set the wave-function through the Madelung definition (2.1.7) to [5]

$$\psi^{\nu}(x,D) = |\psi^{\nu}(x,D_n)| \exp\left(-\frac{i}{\nu}\phi^{\nu}(x,D)\right), \qquad D \in [D_n, D_n + 1]\,. \tag{4.1.9}$$

Therefore the differential equation (4.1.7) becomes

$$\phi^{\nu}_{D}(x,D) + \tau(D)\phi^{\nu}(x,D) - V(x,D) - h(|\psi^{\nu}(x,D_n)|^2, D) = 0\,. \tag{4.1.10}$$

If we differentiate with respect to $x$ this equation we obtain a differential equation for the kinetic momentum $J^{\nu}(x,D)$, defined in (4.0.7),

$$J^{\nu}_{D}(x,D) + \tau(D)J^{\nu}(x,D) + [V_x(x,D) + h_x(|\psi^{\nu}(x,D_n)|^2, D)]\eta(x,D_n) = 0\,. \tag{4.1.11}$$

The equation (4.1.11) is a first order differential equation of the type

$$y_t(t) + b(t)y(t) = g(t)\,, \tag{4.1.12}$$

with $b(t)$, $g(t)$ continuous functions. It has as general integral

$$y(t) = e^{-A(t)}\left[y_0 + \int_{t_0}^{t} ds\, g(s)e^{A(s)}\right], \tag{4.1.13}$$

with initial conditions $y_0 = y(t=0)$ and

$$A(t) = \int_{t_0}^{t} ds\, b(s)\,. \tag{4.1.14}$$

Comparing the two differential equations (4.1.11), (4.1.12) we can make the following definitions

$$b(D) = \tau(D)\,, \tag{4.1.15}$$

$$g(D) = -\left[V_x(x,D) + h_x(|\psi^{\nu}(x,D_n)|^2, D)\right]\eta(x,D_n)\,. \tag{4.1.16}$$

It is arrived the moment of specialize this solution to the dynamics of the baryon-DM system. Comparing the NLS (4.0.1) with the Schrödinger equations describing DM (2.2.27) and baryons (2.2.40) we can define the various terms of the time-splitting spectral approximation in one dimension.

$$V_{b,DM}(x,D) = \frac{3e(\Omega_{DM})}{2D}\varphi(x,D)\,, \tag{4.1.17}$$

$$\tau_{b,DM}(D) = \frac{3e(\Omega_{DM})}{2D}\,, \tag{4.1.18}$$

$$h(|\psi^{\nu}(x,D)|^2,D) = \begin{cases} 0 & \text{for DM} \\ \frac{3}{2}\frac{M^{\alpha-1}(D)}{D^{\alpha+1}}\left(\frac{f(D)}{\Omega_{DM}}\right)^2 \frac{1}{\gamma-1}\frac{1}{k_J^2}|\psi_b(x,D)|^{2(\gamma-1)} & \text{for baryons} \end{cases}, \tag{4.1.19}$$

where $e(\Omega_{DM}) = \Omega_{DM}/f(D)^2$ and $f(D)$ is given by (1.4.25) with the relation between $a$ and $D$ give by (1.4.26). We can observe that, since the norm of the wave-function is constant in a time step, the time-dependence of the gravitational potential $V$ is easily determined by the Poisson equation

$$V(|\psi^{\nu}_{DM}(x,D_n)|^2,D) = \frac{3e(\Omega_{DM}(D))}{2D^2}\nabla^{-2}(|\psi^{\nu}_{DM}(x,D_n)|^2-1)\,. \tag{4.1.20}$$

We can now find the solution of the differential equation (4.1.11). First we need to compute

$$A(D) = \int_{D_n}^{D}\frac{3e(\Omega_{DM})}{2D'}dD'\,. \tag{4.1.21}$$

Then we obtain the kinetic moment in the time interval $D \in [D_n, D_{n+1}]$

$$\begin{aligned} J^{\nu}_{b,DM} =& e^{-\int_{D_n}^{D}\frac{3e(\Omega_{DM})}{2D'}dD'}\left[J^{\nu}_{b,DM}(x,D_n)+\right. \\ &-\int_{D_n}^{D}dD'\left[V_x(|\psi^{\nu}_{DM}(x,D_n)|^2,D')+\right. \\ &\left.\left.+h_x^{b,DM}(|\psi^{\nu}_{b,DM}(x,D_n)|^2,D')\right]\eta_{b,DM}(x,D_n)e^{\int_{D_n}^{D'}\frac{3e(\Omega_{DM})}{2D"}dD"}\right]. \end{aligned} \tag{4.1.22}$$

From this solution we can obtain the phase of the wave-function, i.e. the velocity potential $\phi_x^{\nu,b,DM}(x,D) = -J^{\nu}_{b,DM}/\eta^{\nu}_{b,DM}(x,D_n)$ in the time step under study.

$$\begin{aligned} \phi^{\nu}_{b,DM}(x,D) =& -e^{-\int_{D_n}^{D}\frac{3e(\Omega_{DM})}{2D'}dD'}\int_0^x dy\,\nu Im\left(\frac{\psi_y^{\nu,b,DM}(y,D_n)}{\psi^{\nu}_{b,DM}(y,D_n)}\right)+ \\ &+\int_{D_n}^{D}dD'\left[V(|\psi^{\nu}_{DM}(x,D_n)|^2,D')+\right. \\ &\left.+h_{b,DM}(|\psi^{\nu}_{b,DM}(x,D_n)|^2,D')\right]e^{\int_{D_n}^{D'}\frac{3e(\Omega_{DM})}{2D"}dD"}\,, \end{aligned} \tag{4.1.23}$$

where we expressed $J^{\nu}_{b,DM}(x,D_n)$ as

$$J^{\nu}_{b,DM}(x,D_n) = \nu Im\left(\frac{\psi_x^{\nu,b,DM}(x,D_n)}{\psi^{\nu}_{b,DM}(x,D_n)}\right)\eta^{\nu}_{b,DM}(x,D_n)\,. \tag{4.1.24}$$

Substituting (4.1.23) in (4.1.9) we obtain the solution of the potential part of the nonlinear Schrödinger equation (4.1.7).
To combine the time steps from time $D_n$ to $D_{n+1}$ we use the Strang splitting method [71]. It consists in a three step approach: first it evolves the initial state through the solution of (4.1.7) for a time step long $\Delta D/2 = t/2$; then this state is evolved for a time step $t$ following the solution of (4.1.6), i.e. the free particle one; finally to obtain the true final state we need another evolution for half time step $t/2$ following the solution of (4.1.7). Applying this method from the initial state $\psi_i$ and iterating it we recover the wave-function at any time $D$. We can show how the Strang splitting method is applied to our baryons-DM system in particular for a time step $[D_n, D_{n+1}]$. First we evolve the state $\Psi_j^{\nu,n}$, which is the approximated wave-function obtained by the use of the time-splitting spectral approximation to previous time steps, through the potential solution of (4.1.7) for a time step $t/2$.

$$\Psi_{j,b,DM}^{\nu,*} = |\Psi_{j,b,DM}^{\nu,n}| \exp\left[-i\left(-\mathcal{S}_j^{\nu}(\Psi_{b,DM}^{\nu,n}, \frac{t}{2}) + \right.\right. \\ \left.\left. + \frac{i}{\nu}\int_{D_n}^{D_n+t/2} dD' \left[V(|\Psi_{j,DM}^{\nu,n}|^2, D') + h_{b,DM}(|\Psi_{j,b,DM}^{\nu,n}|^2, D')\right] e^{\int_{D_n}^{D'} \frac{3e(\Omega_{DM})}{2D"} dD"}\right)\right], \tag{4.1.25}$$

where we defined

$$\mathcal{S}_j^{\nu,n}(\Psi^{\nu,n}, \frac{t}{2}) \equiv e^{-\int_{D_n}^{D_n+t/2} \frac{3e(\Omega_{DM})}{2D'} dD'} \int_0^{x_j} dy\, Im\left(\frac{\Psi_y^{\nu,b,DM}(y, D_n)}{\Psi_{b,DM}^{\nu}(y, D_n)}\right) \tag{4.1.26}$$

and we compute it using the approximate wave-function obtained from the previous step [71]. Now we have to evolve this state through the free particle approximation, which can be expressed through a discrete Fourier decomposition as [5], for a whole time step $t$.

$$\Psi_{j,b,DM}^{\nu,**} = \frac{1}{M}\sum_{p=-M/2}^{M/2-1} \exp\left[-\frac{i\nu k_p^2 t}{2}\right] \tilde{\Psi}_{p,b,DM}^{\nu,*} e^{-ik_p x_j}\,, \tag{4.1.27}$$

which resembles (3.1.20) but with a different spatial spacing. We defined the Fourier coefficients of $\Psi_j^{\nu,*}$ as

$$\tilde{\Psi}_p^{\nu,*} = \sum_{j=0}^{M-1} \Psi_j^{\nu,*} e^{-ik_p x_j}\,, \quad p = -\frac{M}{2}, ..., \frac{M}{2} - 1\,, \tag{4.1.28}$$

where $k_p = (2\pi p)/l$. Finally we can recover the final state at time $D_n$ reapplying the solution (4.1.23) of (4.1.7).

$$\Psi_{j,b,DM}^{\nu,n+1} = |\Psi_{j,b,DM}^{\nu,**}| \exp\left[-i\left(-\mathcal{S}_j^{\nu}(\Psi_{b,DM}^{\nu,**}, \frac{t}{2}) + \right.\right. \\ \left.\left. + \frac{i}{\nu}\int_{D_n+t/2}^{D_{n+1}} dD' \left[V(|\Psi_{j,DM}^{\nu,**}|^2, D') + h_{b,DM}(|\Psi_{j,b,DM}^{\nu,**}|^2, D')\right] e^{\int_{D_n+t/2}^{D'} \frac{3e(\Omega_{DM})}{2D"} dD"}\right)\right]. \tag{4.1.29}$$

Hence with this three-step procedure we have evolved the wave-function from time $D_n$ to time $D_{n+1}$.
A numerical method to obtain $\mathcal{S}_j^\nu(\Psi, D)$ is the composite trapezoidal rule [5]

$$\mathcal{S}_j^\nu(\Psi, D) = e^{-\int_{D_n}^{D} \frac{3e(\Omega_{DM})}{2D'} dD'} \sum_{l=1}^{j} \frac{l}{2} Im\left( \frac{D_x^S \Psi|_{x=x_l-1}}{U_{l-1}} + \frac{D_x^S \Psi|_{x=x_l}}{U_l} \right) , \tag{4.1.30}$$

with

$$j = 1, 2, ..., M\,, \qquad S_0(\Psi, t) = 0$$

and where $D_x^S$ is the spectral approximation of $\partial_x$ [5], i.e.

$$D_x^S \Psi|_{x=x_j} = \frac{1}{M} \sum_{p=-M/2}^{M/2-1} i k_p \tilde{\Psi} e^{i k_p x_j}\,. \tag{4.1.31}$$

We can observe that this scheme is somewhat similar to the propagator scheme resulting from quantum perturbation theory. In the previous chapter from QPT we found that the wave-function evolves first as following the free particle solution then the external potential is applied and finally it follows again the free particle approximation, this is commonly called a drift-kick-drift scheme. The Strang splitting method instead consist in a kick-drift-kick scheme, more similar to the one presented in [73] in the study of the first order correction in the propagator of CDM, anyway we expect that the two schemes will be similar. Applying first the free particle approximation and then the potential solution or the opposite would be exactly the same if and only if the kinetic operator and the potential one commute, i.e. if

$$\left[ -\frac{\nu^2}{2} \nabla^2, \Phi(x, D) \right] = 0\,, \tag{4.1.32}$$

with $\Phi(x, D) = V(x, D) + h(|\psi^\nu|^2, D) + \nu\tau(D) Arg[\psi^\nu]$ and where the commutator is such defined $[A, B] = AB - BA$. But the commutator is different from 0 due to the spatial dependence of the potential operator. Hence we expect that the difference between the schemes kick-drift-kick and drift-kick-drift to be of the order of the commutator applied to the wave function, this is the error between the choice of one or the other scheme. Since the potential term, in our cosmological study, is provided by perturbations over the background Universe this term is small and so the error is. For the time-splitting spectral approximation we prefer to use the scheme kick-drift-kick because in this way the norm of the wave-function changes just one time, it is constant for the "potential solution" as showed in (4.1.8) thus the norm evolve only when the free particle approximation is applied [5].
In [5] Bao and collaborators noted an important fact, the use of the trapezoidal rule to compute $\mathcal{S}_j^\nu$ leads to the lost of spectral accuracy in space in the case $\tau \neq 0$. However the spatial accuracy can be improved using higher order numerical integration for approximating the integral in the definition of $\mathcal{S}_j^\nu$ [5]. We reported anyway this simple numerical method because it is the method used by [5] to make some interesting numerical studies of the nonlinear Schrödinger equation (4.0.1) when studying the case $\tau = 0$. Observing

the NLS (4.0.1) and the meaning of $\tau$ in our cosmological study it is immediately understood that neglecting the $\tau$ term is equivalent to neglect the Universe expansion and its dumping effect on the density growth.
We could easily generalize the just presented one-dimensional time-splitting spectral approximation to three-dimension. To do so is sufficient to discretize the space with spatial steps over three arbitrary orthogonal axis defining the space, i.e. we have to generalize (4.1.4) to

$$x_i^1 = a^1 + l^1 i\,, \qquad i = 0, 1, ..., M\,; \tag{4.1.33}$$
$$x_j^2 = a^2 + l^2 j\,, \qquad j = 0, 1, ..., M\,; \tag{4.1.34}$$
$$x_k^3 = a^3 + l^3 k\,, \qquad k = 0, 1, ..., M\,; \tag{4.1.35}$$

where we called $(x^1, x^2, x^3)$ the coordinates of the space, defined the spatial interval with periodic boundary condition as $\mathbf{x} \in [\mathbf{a}, \mathbf{b}]$ and the spatial step $\Delta\mathbf{x} = \mathbf{l} = (\mathbf{b} - \mathbf{a})/M$.
With such definitions we can call $\Psi_{i,j,k}^{\nu,n}$ the approximation of the wave-function in a space-time step (i,j,k; n) $\Psi^{\nu}(x_i^1, x_j^2, x_k^3; D_n)$ and $\mathbf{\Psi}^{\nu,\mathbf{n}}$ the solution tensor at time $D = D_n = nt$ with as components the approximation at each grid point $\Psi_{i,j,k}^{\nu,n}$. Now we should just follow the same procedure done in the one-dimensional case to derive the time-splitting spectral approximation of the three-dimensional generalization of the nonlinear Schrödinger equation (4.0.1).

## 4.2 Numerical simulations

We report now two interesting simulation made by Bao and collaborators and described in [5] and one simulation made by [80] in which they used a Strang splitting method to study the evolution of the gravitational collapse of DM. In [5] they assumed that the relaxation rate $\tau$ is constant in time, this leads to an easier solution of the nonlinear Schrödinger equation (4.1.7) with

$$A(D) = \tau(D - D_n)\,. \tag{4.2.1}$$

More for every simulation they used the space interval $x \in [-8, 8]$, instead of the interval $[0, L]$ which we used to be consistent with the previous chapter, which is large enough for computations such as the periodic boundary conditions don't introduce a significant aliasing error relative to the whole space problem [5]. The first example we want to report is the case of a cubic nonlinearity with confining potential: $V(x) = \frac{\omega x^2}{2}$, $h(\rho) = \beta\rho$ and $\tau = 0$, where $\rho = \bar{\rho}\eta$. This NLS is usually called Gross-Pitaevskii equation (GPE) and it is related to Bose-Einstein condensates [5] and corresponds to a particular choice of $\gamma = 2$. BEC occurs when interacting trapped bosons are cooled down to a temperature below the critical one, then all the particles fall in the same quantum mechanical ground state [38]. The GPE describes the evolution of this ground state due to a change in the trap frequencies [5]. This example is interesting mainly for the following reason. To understand it we need to observe that there are two different interpretations of the Schrödinger-Poisson description of CDM. One can think at it as a field theoretical approximation to the classic Boltzmann description, as we have done until now. Or it can be interpreted as a distinct description of DM known as fuzzy dark matter [31, 80], in which structure formation is

driven by BEC trapped in its own gravitational potential and where the expansion of the space sets the time dependent interaction strength [80] (in this example we are loosing this last property due to $\tau = 0$). The following initial conditions are chosen [5]

$$\sqrt{\eta_i(x)} = e^{-x^2}\,, \qquad \phi_i(x) = \log\left(e^x + e^{-x}\right)\,. \tag{4.2.2}$$

Fig. 4.1 shows the density $\rho^\nu = \eta^\nu = |\psi^\nu|^2$ (here we set $\bar{\rho} = 1$ to be consistent with the notation of [5] simulations) of the solutions in space-time for the defocusing nonlinearity, i.e. $\beta = 1$, with $\nu = 0.025$ and for different $\omega$'s. It is clear that the confinement becomes stronger as $\omega$, and so the potential, increases. These over-dense regions correspond to regions of structure formation due to, in our cosmological counter part, the attractive effect of the gravitational potential. The potential-well $V(x) = \omega x^2/2$ can be interpreted as a very simple model of the attractive gravitational potential nearby shell-crossing.

The second numerical simulation we want to report from [5] studies the defocusing case with $V = 0$, $h(\eta) = (\gamma/(\gamma-1))\eta^{\gamma-1}$, which in our cosmological description corresponds to a baryonic gas in an Universe with negligible peculiar gravitational potential. A sort of free particle approximation smoothed by the gas pressure. More the time-dependent coefficient of the gas pressure is neglect in this computation, i.e. it is set to 1.
We use the following initial conditions [5]

$$\sqrt{\eta_i(x)} = e^{-x^2}\,, \qquad \phi_i(x) = \frac{1}{e^{3x} + e^{-3x}}\,. \tag{4.2.3}$$

For comparison with the Schrödinger solution Bao solved also the equivalent hydrodynamical system (related through the Madelung transformation) by the use of the second-order relaxed scheme [35]. Fig. 4.2 shows the solution of the defocusing nonlinear equation in the hydrodynamical description, labelled as SHDE, and in the Schrödinger representation, the other lines, for various values of $\nu \equiv \epsilon$. In this figure the energy density is called position density and the time $D \equiv t$ for be consistent with [5] notation. From Fig. 4.2 we can observe that when the hydrodynamical solution is smooth the two observables of the nonlinear Schrödinger equation (4.0.1) converge to the solution of the formal hydrodynamical limit for $\nu \to 0$ [5]. The hydrodynamical solution is smooth before breaking, before the caustic occurs, which for this simulation happens between the times $D = 0.2$ and $D = 1.4$ for most of the values of $\tau$ (only for $\tau = 10.0$ at $D = 1.4$ no caustic has still occurred) [5], since the larger is $\tau$ later the caustic occurs. After the hydrodynamical solution brakes, i.e. when two or more fluid trajectories cross (shell-crossing event), in the Schrödinger solution an oscillatory behaviour arises. This is naturally explained by the fact that the waves in the Schrödinger description represents particles thus when trajectories cross the waves create interference patterns, as already seen in Fig. 3.5. In Fig. 4.3 we reported the evolution of the energy density from the solution of the NLS with $\nu \equiv \epsilon = 0.01$, $\gamma = 1.4$ and for different values of $\tau$. It is difficult to observe the net effect of the pressure comparing this figure with Fig.4.1 because here there isn't the confining potential, anyway we can observe that the density distribution is smooth even at shell-crossing (apart from the oscillatory behaviour).

Another interesting numerical computation of the fuzzy dark matter evolution (BEC) is provided by [80], in which Zimmerman and collaborators applied the Strang time-splitting

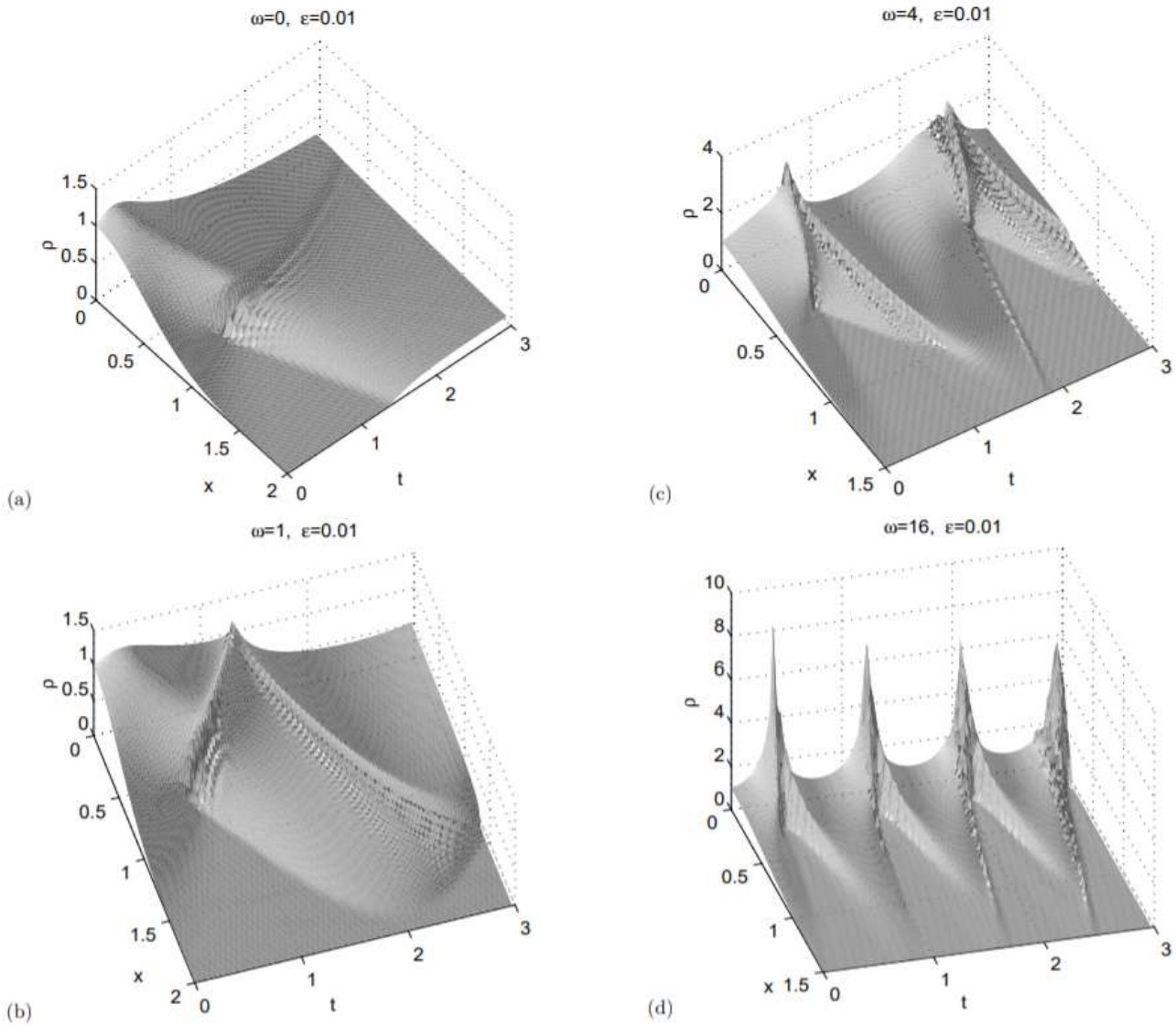


Figure 4.1: Evolution of the energy density for the defocusing case ($\beta = 1$) of GPE with $\nu = \epsilon = 0.01$, (a) $\omega = 0$, (b) $\omega = 1.0$, (c) $\omega = 4.0$, (d) $\omega = 16.0$. Here we used the notation $\rho \equiv \eta$ and $t \equiv D$. This figure is provided by [5], for any further detail check the main text.

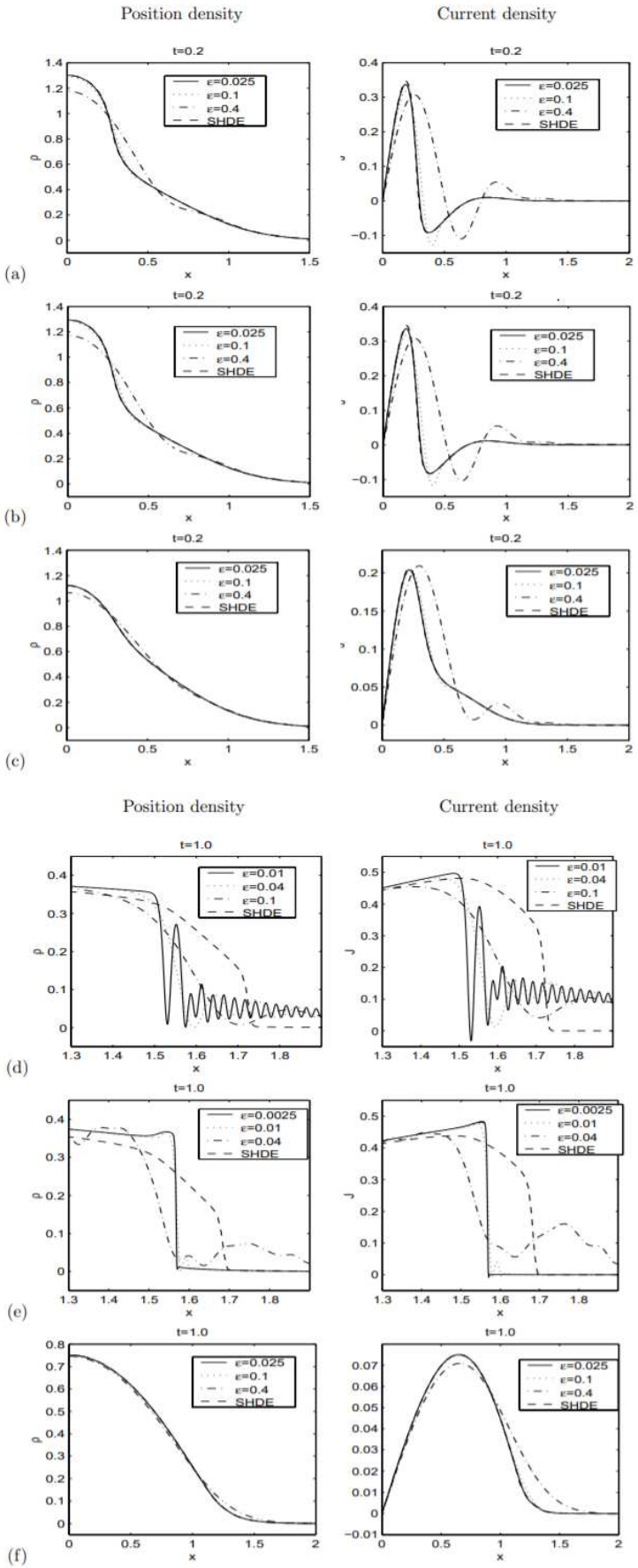


Figure 4.2: Numerical solution for the defocusing nonlinearity with $V = 0$, $h(\eta) = (\gamma/(\gamma - 1))\eta^{\gamma-1}$. Here, to be consistent with [5] we made the following redefinitions: energy density≡position density, $\nu \equiv \epsilon$ and $\eta \equiv \rho$. (a) $\tau = 0.0$, (b) $\tau = 0.2$, (c) $\tau = 10.0$. (d) $\tau = 0.0$, (e) $\tau = 0.2$, (f) $\tau = 10.0$. For the top panels $D = 0.2$, for the bottom ones $D = 1.0$. For all panels $\gamma = 2.0$. Here SHDE stands for the hydrodynamical solution of the problem.

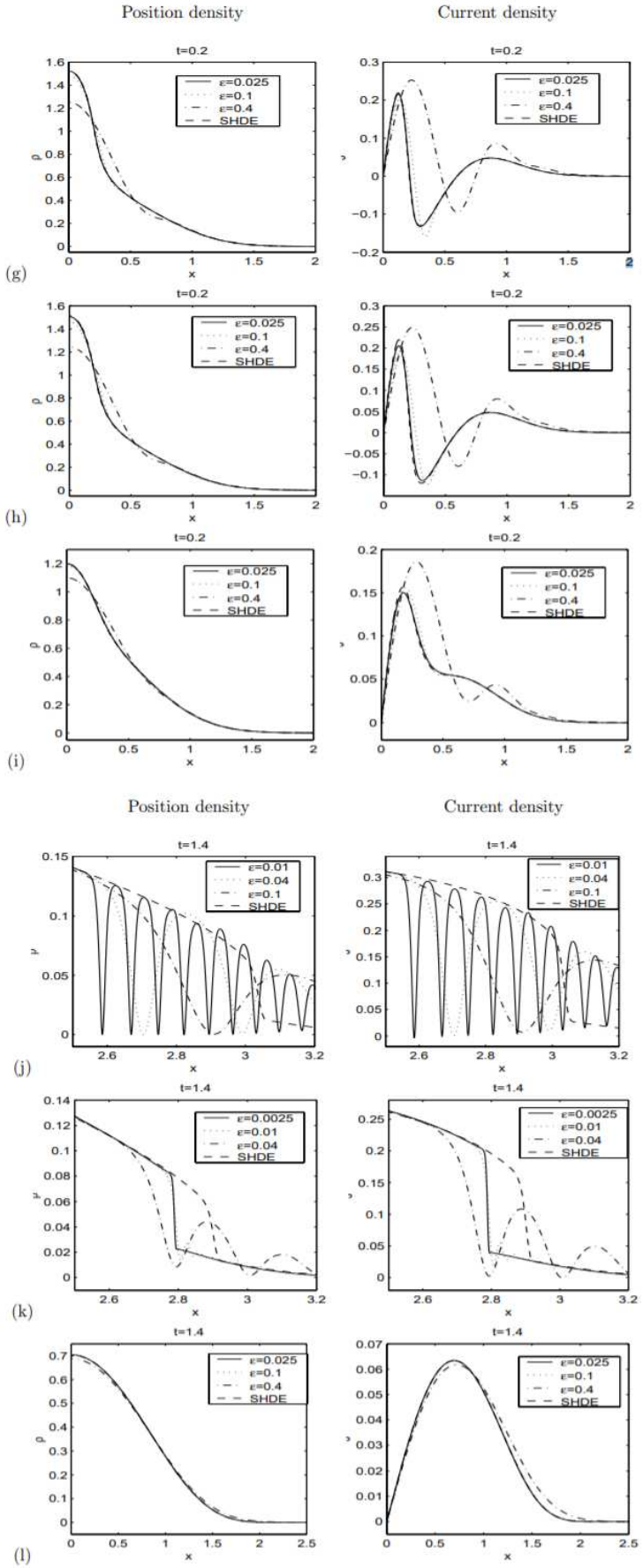


Figure 4.2: (cont.) (g) $\tau = 0.0$, (h) $\tau = 0.2$, (i) $\tau = 10.0$, (j) $\tau = 0.0$, (k) $\tau = 0.2$, (l) $\tau = 10.0$. For the top panels $D = 0.2$, for the bottom ones $D = 1.4$. For all panels $\gamma = 1.4$. These figures are provided by [5], for any further detail check the main text.

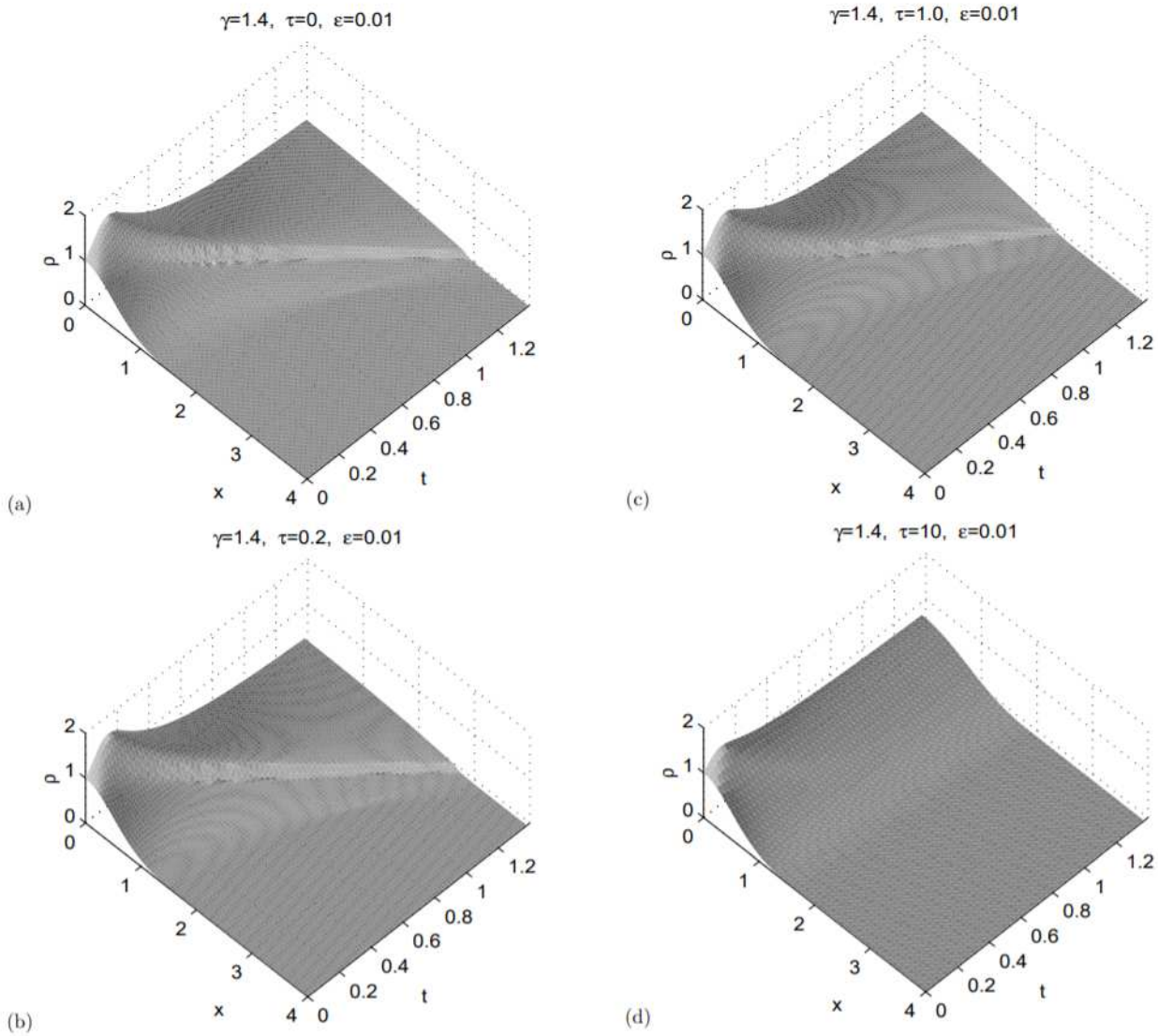


Figure 4.3: Evolution of the energy density $\rho = \bar{\rho}\eta = \eta$ for the defocusing NLS with $V = 0$, $h(\eta) = \frac{\gamma}{\gamma-1}\eta^{\gamma-1}$. We set $\nu \equiv \epsilon = 0.01$ and $\gamma = 1.4$ and use the notation of [5] $D \equiv t$. The evolution is represented for different values of $\tau$ (a)$\tau = 0.0$, (b) $\tau = 0.2$, (c) $\tau = 1.0$, (d) $\tau = 10.0$. This figure is provided by [5], for any further detail check the main text.

method [71] to the Schrödinger-Poisson system describing the DM in cosmological time $t$. Thus they studied the Schrödinger-Poisson system [80]

$$i\nu\frac{\partial\psi_{DM}}{\partial t} = \left[-\frac{\nu^2}{2a^2(t)}\nabla^2 + V_{DM}\right]\psi_{DM}\,, \tag{4.2.4}$$

$$\nabla^2 V_{DM} = \frac{4\pi G\rho_{m0}}{a(t)}(|\psi_{DM}|^2 - 1)\,. \tag{4.2.5}$$

Note that the quantum pressure (2.1.14) is not present in the Schrödinger equation, thus its effects will be implicit in this discussion but directly seen in the dynamics [67].
They solved this system in one-dimension using the dimensionless coordinates

$$x' = \frac{1}{\nu^{1/2}}\left(\frac{3}{2}H_0^2\Omega_{m0}\right)^{1/4} x\,, \tag{4.2.6}$$

$$dt' = \frac{1}{a^2(t)}\left(\frac{3}{2}H_0^2\Omega_{m0}\right)^{1/2} dt\,. \tag{4.2.7}$$

The potential in the Schrödinger equation then becomes

$$V' = \frac{a}{\nu}\left(\frac{3}{2}H_0^2\Omega_{m0}\right)^{-1/2} V\,. \tag{4.2.8}$$

Finally we write the Schrödinger-Poisson system in the new dimensionless coordinates (dropping the primes) [80]

$$i\frac{\partial\psi_{DM}}{\partial t} = \left[-\frac{1}{2}\frac{\partial^2}{\partial x^2} + a(t)V_{DM}(|\psi_{DM}|^2)\right]\psi_{DM}\,, \tag{4.2.9}$$

$$\partial_x^2 V_{DM} = |\psi_{DM}|^2 - 1\,. \tag{4.2.10}$$

They studied these equations in a box with periodic boundary conditions $x \in [-L/2, L/2)$, where $L$ is the box length in dimensionless units. The problem is discretized with a spatial grid of $N$ points separated by $\Delta x = L/N$ and so we store the wave-function and the potential values only at the grid point. For the simulation we will report in the following, [80] used in particular $L = 100$, $N = 2^{14}$, the coarse-graining parameter $\nu = 1$ and a spatial resolution of the Husimi distribution (2.3.17) $\sigma_x = \sqrt{2}$, such as it is equal to the velocity resolution due to the relation $\sigma_u = \nu/(2\sigma_x)$. They chose as initial conditions

$$\psi_i(x) = \sqrt{A\cos\left(\frac{2\pi}{L}x\right) + 1}\,, \qquad A = -0.1\,, \tag{4.2.11}$$

with vanishing initial velocity. The potential is computed from the Poisson equation by means of Fourier transformations [80]:

$$V(|\psi_{DM}|^2) = \mathcal{F}^{-1}\left[-\frac{1}{k^2}\mathcal{F}\left[|\psi_{DM}|^2 - 1\right]\right]\,. \tag{4.2.12}$$

Small $k$ corresponds to very large scale where the Universe is homogeneous, hence $\delta_{DM} = |\psi_{DM}|^2 - 1 = 0$, which implies that no singularity is found at $k = 0$ [80].

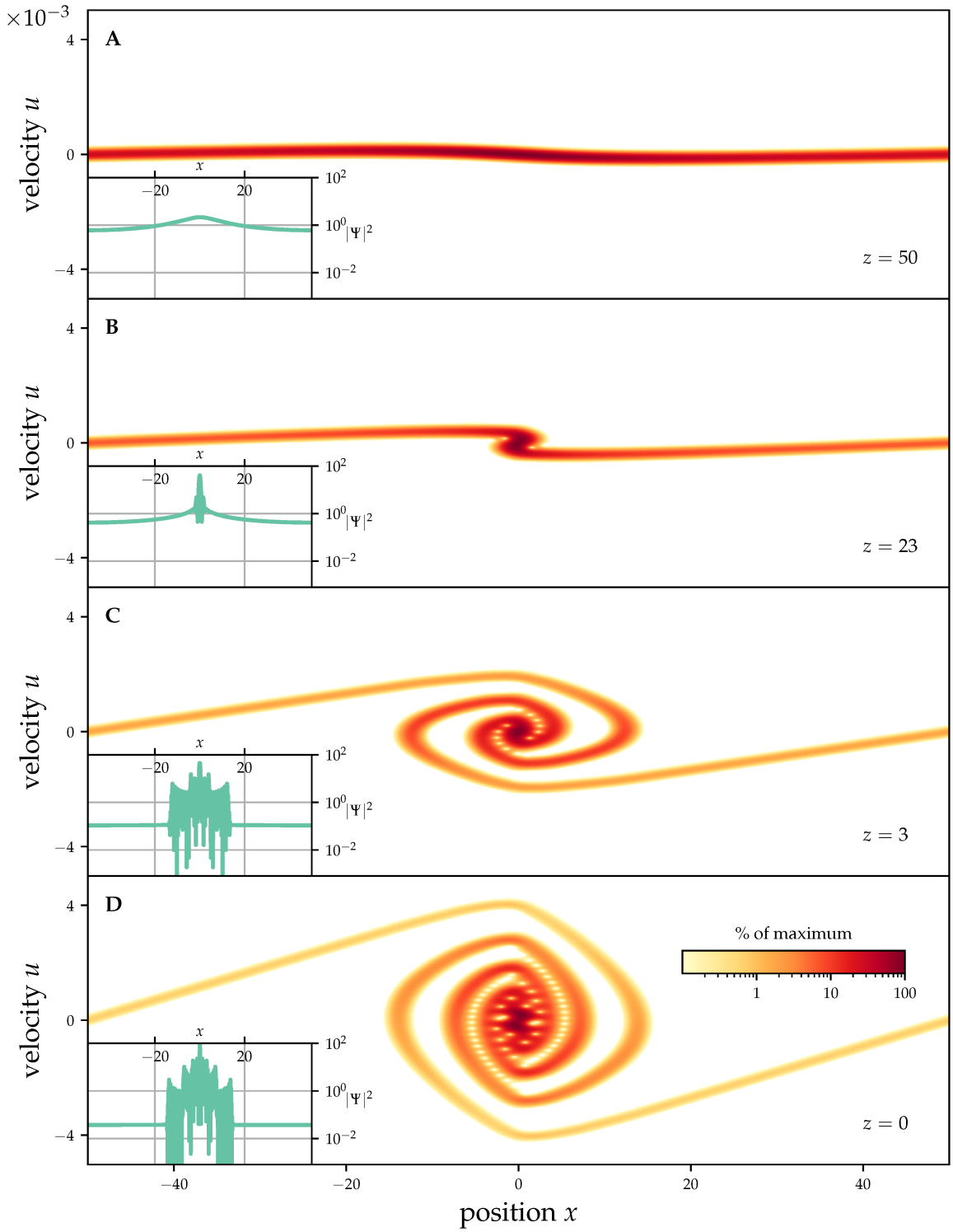


Figure 4.4: Gravitational collapse of a sinusoidal density perturbation in an expanding background cosmology with $\Omega_{m0} = 0.3$. Panel (A) depicts a snapshot in the single-stream regime which ends with a shell crossing shown in panel (B). Matter accumulation continues during the multi-stream evolution in panel (C) and (D). Note that the collapse is not completed in panel D as matter still falls to the center. All distributions are normalized to their current maximum value. The insets illustrate the associated, unsmoothed density contrast on a logarithmic scale. This figure is provided by [80], for any further detail check the main text.

The simulation reported in Fig.4.4 studies the collapse evolution of a perturbation and it starts from redshift $z_i = 500$, at which [80] make sure that the perturbation begins its gravitational collapse right at the onset of the integration. In particular the velocity field obtained from the Husimi distribution (2.3.17) is showed for four characteristic evolutionary stages. The panel (A) depicts the single stream situation in the linear growth regime of the overdensity. Here, matter slowly starts to fall into the gravitational well until both streams of matter meet at its origin and form a shell crossing in phase space, shown in the panel (B). At this point in time the distribution becomes perpendicular to the spatial axis [80] (i.e. shell-crossing happens) and the classical dust model breaks down. As noted before the Schrödinger-Poisson model is insensitive to such events and comfortably evolves the system forward into the multi stream regime shown in the panel (C) [80]. Finally the panel (D) depicts the situation at present time $z = 0$, where matter of outer regions is still in free fall to the center of gravity [80].
From classical analysis one expects the approach of a dynamical equilibrium state, which is characterized by the fact that the virial theorem holds. In particular in our case of a perturbation gravitational collapse we would have expected a stationary core surrounded by a circularly shaped halo of matter in phase space but our phase-space distribution in the panel (D) of Fig.4.4 does not yet show a complete relaxation to an equilibrium state [80]. This result is common in literature, for example in [65] the evolution of the CDM distribution is followed by means of the Vlaslov equation (collisionless Boltzmann equation). They found that the gravitational collapse is described similarly as in Fig.4.4 . At late times the gravitational potential approaches a stationary state, instead the spiral curve describing the velocity field continues to wind up indefinitely [65]. This unphysical fact can easily explained in the following way: a state supported on a smooth curve in phase space formally has an infinite number of particles, but it never becomes stationary in a pointwise sense. It just weakly converges to the stationary solution as the number of point/particles under-study tends to infinity, i.e. $N \to +\infty$ where $N$ is the number of grid points [65]. This problem can be solved through coarse-graining, thanks to it we can make a continuous description of the spiral and the collapse eventually end at some time, leading to a stationary solution [80].

### 4.2.1 Quantum virial theorem

Since we observed that the evolution of perturbation in the LSS density can eventually lead to a gravitational collapse and to a dynamical equilibrium state, we would investigates the properties of this state. We stated that it is characterized by the virial theorem [65,80] and, since we are studying a quantum fluid (or modelling a classical one with a wave-mechanical approach), we want to present the quantum analogue of the classical virial theorem. Following the work of [40] we need first to derive the Ehrenfest theorem for the evolution of an observable or better of its expectation value. We denote the expectation value of an observable $A$ as

$$< A >= \langle \psi(D)| \, A \, |\psi(D)\rangle \ . \tag{4.2.13}$$

We wrote explicitly only the time dependence of the wave-function because we are interested in the evolution in time of the observable (we keep using the growth factor as time).

The time evolution of the states of the system is governed by the Schrödinger equation

$$i\nu\,|\dot{\psi}(D)\rangle = \hat{H}\,|\psi(D)\rangle\ , \tag{4.2.14}$$

with the Hamiltonian operator $\hat{H} = \hat{P}^2/2 + \hat{V}$ given by the momentum operator $\hat{\mathbf{P}}$ and a generic potential $\hat{V}$, which in the study of baryons will include also the gas pressure. We can now compute the time evolution of the expectation value of a generic observable

$$\frac{d < A >}{dD} = \frac{1}{i\nu}\,\langle\psi|\,A\hat{H} - \hat{H}A\,|\psi\rangle + \langle\psi|\,\frac{\partial A}{\partial D}\,|\psi\rangle \tag{4.2.15}$$

or in a more compact form [40]

$$\frac{d < A >}{dD} = \frac{1}{i\nu}\,\langle\psi|\,[A, \hat{H}]\,|\psi\rangle + < \frac{\partial A}{\partial D} > \ . \tag{4.2.16}$$

This result is called Ehrenfest theorem and it useful to describe the time-evolution of the expectation value of an observable.
For a system of $N$ particles we can define the expectation value of the quantum virial [40] as

$$G_Q = \sum_{i=1}^{N}\sum_{k=1}^{3} < \hat{P}_i^k \cdot \hat{R}_i^k >\,, \tag{4.2.17}$$

where $i$ denotes the particles, $k$ the spatial coordinates and $\hat{\mathbf{R}}$ is the position operator. In classical mechanics the time average of the time derivative of the virial is null, from this conservation the classical virial theorem is obtained [40]

$$2\overline{(T)}_\infty = -\overline{\left(\sum_{i=1}^{N}\mathbf{r}_i\cdot\mathbf{F}_i\right)}_\infty\ , \tag{4.2.18}$$

where $\overline{(T)}_\infty$ is the time average over infinite times [40]. We want now to compute the time derivative of the quantum virial $G_Q$ using the Ehrenfest theorem (4.2.15), note that since we are studying a system at equilibrium the position and momentum operators have not any dependence on time [40], so

$$\frac{d\,G_Q}{dD} = \frac{1}{i\nu}\sum_{i=1}^{N}\sum_{k=1}^{3}\langle\Big[\hat{P}_i^k\cdot\hat{R}_i^k, \hat{H}\Big]\rangle\,. \tag{4.2.19}$$

First we compute the commutator with the kinetic term of the Hamiltonian, i.e.

$$\begin{aligned}[\hat{P}_i^k\cdot\hat{R}_i^k, \hat{P}_i^{k^2}] &= \hat{P}_i^k\hat{R}_i^k\hat{P}_i^{k^2} - \hat{P}_i^{k^3}\hat{R}_i^k = \hat{P}_i^k(\hat{R}_i^k\hat{P}_i^{k^2} - \hat{P}_i^{k^2}\hat{R}_i^k) = \\ &= \hat{P}_i^k((i\nu + \hat{P}_i^k\hat{R}_i^k)\hat{P}_i^k - \hat{P}_i^k(\hat{R}_i^k\hat{P}_i^k - i\nu)) = 2i\nu\hat{P}_i^{k^2}\,,\end{aligned} \tag{4.2.20}$$

where in the last line we used $[\hat{R}, \hat{P}] = i\nu$, which is a common result of quantum mechanics [40]. For the commutator $[G_Q, V]$ is easier to use the position representation [40]

$$\begin{aligned}[\hat{P}_i^k\hat{R}_i^k, V] &= \frac{\nu}{i}\left(\frac{\partial}{\partial R_i^k}R_i^kV - V\frac{\partial}{\partial R_i^k}R_i^k\right) = \\ &= \frac{\nu}{i}\left(V + R_i^k(\frac{\partial V}{\partial R_i^k}) + R_i^kV\frac{\partial}{\partial R_i^k} - V - VR_i^k\frac{\partial}{\partial R_i^k}\right) = \\ &= \frac{\nu}{i}R_i^k\frac{\partial V}{\partial R_i^k}\,.\end{aligned} \tag{4.2.21}$$

Hence the time derivative of the quantum virial is

$$\frac{d\,G_Q}{dD} = \sum_i \sum_k \langle \hat{P}_i^{k^2} \rangle - \sum_i \sum_k \langle R_i^k \frac{\partial V}{\partial R_i^k} \rangle \,. \tag{4.2.22}$$

The first term is clearly two times the expectation value of the system kinetic energy $T = \sum_i \sum_k \langle \hat{P}_i^{k^2}/2 \rangle$. If we take the time average over an infinite period a bound system in its rest frame must satisfies

$$\overline{\left( \frac{d\,G_Q}{dD} \right)}_\infty = 0 \,, \tag{4.2.23}$$

because $\hat{\mathbf{R}}_i$ and $\hat{\mathbf{P}}_i$ must be bounded [40]. From this conservative law derive the quantum virial theorem, using the Ehrenfest theorem to compute the time-derivative of the quantum virial [40],

$$2\overline{(T)}_\infty = \overline{\left( \sum_{i=1}^{N} \sum_{k=1}^{3} \langle R_i^k \frac{\partial V}{\partial R_i^k} \rangle \right)}_\infty \,. \tag{4.2.24}$$

We recovered the virial theorem in the exact same formulation as in classical mechanics except for the fact that the kinetic energy and potential term have to be replaced by their expectation values. This is the condition which define the dynamical equilibrium of a quantum system [40], such as the one which will form after the gravitational collapse described in Fig.4.4 [80]. We have to remark that here $V$ is a general potential, which will include also the gas pressure when we consider the baryon matter component.

Hence in this chapter we found that the Strang splitting-time approximation applied to the Schrödinger-Poisson system can give good numerical results in the description of the evolution of the large-scale structure of the Universe. We showed that this approximation have already given nice results for the description of DM in the fuzzy/BEC form, in particular it was able to follow the whole gravitational collapse of a perturbation as showed in Fig.4.4 [80]. We observed also that this method could provide an useful numerical algorithm for describing the evolution of baryons density distribution, as a matter of fact we showed that this approach was able to reproduce hydrodynamical results, at least for a system where the only meaningful contribution was the one of the gas pressure [5], before shell-crossing and it was able to predict also the oscillatory behaviour after the caustic event [5], providing a way to study the multi-stream regime.
Thus we expect that a more involved numerical computation, studying the full solution of the nonlinear Schrödinger equation with the Strang splitting method [71] presented in the previous section, will provide very good results in the description of the evolution of the large-scale structure of the Universe.

# Chapter 5

# Vorticity as a probe for FDM

In the previous chapters we presented two methods to follow the evolution of the structure of the Universe through the solution of the Schrödinger-Poisson system (2.2.42). The first method is semi-analytical and it consists in solving perturbatively the Schrödinger equation via quantum perturbation theory, once the results are found anyway we need numerical integration to compute them. The second method instead is purely numerical and it is based on time-splitting techniques for solve the non-linear Schrödinger equation. In this chapter we depart from the main argument of this work, i.e. the evolution of baryons under the gravitational potential of CDM. Here we stop studying baryons and CDM and instead we study DM in the from of ultra-light axion-like particles (FDM) [30]. We then apply the Schrödinger model we described in Chapter 2 to a quantum single-fluid. This is another interesting application of the Schrödinger model in cosmology. In particular we will depict some features related to quantum vorticity (following the work [30]) which if observed in DM halos could be a probe for this kind of DM candidates [1, 30].

We have seen that the evolution of the initial perturbations in the density field can lead to gravitationally bound structures (e.g. the dark matter halo of Fig.4.4). In this chapter our purpose is to study this structures at dynamical equilibrium and in particular the formation and evolution of quantum vortices. This will continue the introduction to rotational motions we made in Sect.2.4 and we will follow the work [30], where Hui and collaborators studied the dynamics of vortices in light dark matter.
We observe from the relation between fluid equations and the Schrödinger one in Sect.2.1 that the Schrödinger model, which we studied in the previous chapters, can describe both classical fluids using $\nu$ as an adjustable parameter and quantum fluid where $\nu = \hbar/m$ is the Planck constant rescaled by the particle mass. For light dark matter candidates (as axion-like particles [31]) the Schrödinger model we presented in the previous chapters describes a real quantum fluid, hence $\hbar$ and $m$ takes their ordinary mean of Planck constant and particle mass. The parameter $\nu = \hbar/m$, which in this context can be interpreted as a reduced Planck constant, keeps providing the phase-space resolution scale through the use of the Husimi distribution (2.3.17). For very light particles the $\nu$ parameter sets a macroscopic scale at which quantum effects are still present, usually the scale of quantum effects is set by the De Broglie wavelength [30] (later in this chapter we will investigate better how this scale is set) $\lambda_{dB} = 2\pi\nu/\tilde{v}$, with $\tilde{v}$ the characteristic velocity of

the structure under study (e.g. a DM halo). Since we adopted in Chapter 2 the Husimi function (2.3.17) as the phase-space distribution the characteristic velocity should be of the order of the velocity resolution (it is the dispersion around the mean value of velocity) $\tilde{v} \sim \sigma_u$, hence the de Broglie wavelength is given by $\lambda_{dB} \sim 2\pi\nu/\sigma_u$.Here $\nu$ is no more a free parameter so the velocity resolution (which is left free) sets the value of the spatial resolution through $\sigma_x\sigma_u = \nu/2$ (2.3.18), therefore $\sigma_x$ results set to $\sigma_x \sim \lambda_{dB}/(4\pi)$. Since the spatial coarse-graining results a bit smaller than the typical length $\lambda_{dB}$ over which quantum effects are present we expect that they are resolved enough to be observable in the phase-space distribution [66]. For example the typical value of the de Broglie wavelength inside a dark matter halo for a DM candidate with mass $m = 6 \times 10^{-24}$eV is $\lambda_{dB} \sim 0.06\,\mathrm{Mpc}$ which is a significant fraction of the typical size of a galaxy [30]. This mass, used by [30] mainly to have a better resolution due to the large $\lambda_{dB}$ is a bit smaller than the more commonly predicted FDM masses, a recent work [44] constraint the mass from the observational data of the rotation curve of the Milky Way (MW) galaxy finding $m = 2.5^{+3.6}_{-2.0} \times 10^{-21}\,\mathrm{eV}$ from their model , which have a $\lambda_{dB} \sim 0.0025\,\mathrm{kpc}$ if the typical velocity would be the same of the case studied by [30] and it has to be compared with the diameter of the Milky way stellar disk $\sim 52 - 61\,\mathrm{kpc}$ [62]. And giving a lower bound $m \geq 10^{-23}\,\mathrm{eV}$ [44]. A theoretical lower bound for the mass range can be provided by the study of the inner gravitational potential of the Milky way $m \lesssim 10^{-19}\,\mathrm{eV}$ [6]. These ultra-light dark matter candidates are usually called fuzzy dark matter (FDM) [31].
We will see later that the quantum vortices predicted size is comparable with the de Broglie wavelength [30], and then we expect to survive to the coarse-graining procedure and to be observable as sub-structures in DM halos [30]. Thus in the following we want to investigate the properties of quantum vortices in order to use them as a probe for FDM, i.e. if sub-structures with the properties of quantum vortices will be found by DM halos observation it would be one more reason for the FDM hypothesis.
Since in the self-gravitating DM approximation, i.e. neglecting the baryon gravitational potential, the DM component does not feel the baryon component in this chapter we can concentrate ourselves to the study of a single-fluid model in order to study the quantum vortices properties. We know that the baryon fluid is not formed by ultra-light particles but by protons (and electrons), then this study is restricted to DM. For be more general as possible we will provide results for both a collisonless DM and a collisonal one, thanks to the results we obtained from the baryon study in the previous chapters, thus extending the work [30] to the possibility of the presence of pressure effects. The study of pressure effect for DM is justified by the fact that the effects of velocity dispersion can be modelled by an effective pressure, in particular it would be possible also to define a Jeans wavelength related to the velocity dispersion [57]. For be consistent with the previous chapter we will keep the equation of state (1.2.17), but since we will show in the following that corrections due to the pressure presence are mostly related to the size of the Jeans wavelength we expect that it would not be difficult to generalize our results to a different equation of state. In the following we will refer to this problem as just pressure, but we have to remember that it is actually generated by dark matter velocity dispersion.
We have seen that in the non-linear regime of perturbations the fact that the matter density field is given by the modulus square of the wave-function $\rho = \bar{\rho}|\psi|^2$ leads to interference patters, as shown for example by the free particle approximation in Fig.3.5, thus a galactic halo, which forms after shell-crossing and so in the non-linear regime, typically

consists of a superposition of $\psi$ waves leading to order unity fluctuations in the mass density field [30].
In Sect.2.4 we showed that the vortices can arise in regions of null density [37], hence we are particularly interested in the destructive interferences between $\psi$s which can generate the conditions necessary to the creation of vortices. These destructive loci behave essentially like topological defects around which the phase of the wave-function, i.e. the velocity potential, jumps or has a non-trivial winding [30]. At this point we can already make an important observation: gravity is fundamental in the vortices generation because it is under its effect that the density perturbations grow in the non-linear regime up to a point to form sufficiently strong interference to make the density vanish [30]. But once the vortices arose, the gravitational effects are negligible at least near the vortex lines since there the matter density is very low [30]. Anyway later we will treat this observation more rigorously. We would like also to remember here that the Kelvin-Helmholtz theorem for the conservation of the vorticity flux (2.4.4) is a global condition, locally the vorticity does not have to be conserved if the flow intersect a point where the fluid parametrization (density and velocity) is ill-defined, i.e. a topological defect [73].
Since the wave-function is a function of $\mathcal{D}$ spatial variables, the vanishing of either its real or imaginary part generically occurs along a co-dimension one surface. These two surfaces will generically intersect along a co-dimension two surface, i.e. a string in $\mathcal{D} = 3$. These strings are vortices from the fluid perspective [30]. Since these surfaces generically are infinite also the intersection string is but it would be unphysical to have vorticity which spreads out up to infinity, thus we expect these strings to close up in vortex rings [30]. In lower dimensions (or in non-generic circumstances in three spatial dimensions) the total wave-function can vanish along a lower co-dimension surface, leading to the appearance of a domain wall [30]. In the following we will able to show that the phase and density close to a defect behave in characteristic ways.
In the vorticity study we will apply a crude approximation, we neglect the self-interaction of dark matter, i.e. both the gravitational potential and the pressure (this term will have a more involved study since its effects are ruled by the Jeans wavelength, thus we will show that on some scale it is important to keep trace of its action), which actually is related to velocity dispersion. We can justify this approximation from the fact that near vortex lines the matter density is very low, thus both the gravitational potential (given by the Poisson equation (2.2.24)) [30] and the pressure (1.2.17) will be small. We will see later how far from the vortex line this approximation holds. The opposite regime (called Thomas-Fermi regime) is well studied in literature [4,10,36,61,69,81] for BEC DM, where self-interactions dominates over the quantum pressure [30]. But for weakly-coupled dark matter is the "free particle" regime which is more interesting on galactic scales [30].

## 5.1 Near-defect regime

We have seen in the introduction to this chapter that defects are present in the fluid variables where the wave-function vanishes and so the matter density. Even if the dynamics of the defects is in general very complicated because is described by the non-linear Schrödinger-Poisson system, in the neighbourhoods of the defect we can depict an universal behaviour of the defects thanks to the vanishing wave-function. Since in this region the matter density field is very low we assume that the gravitational potential and the

gas pressure are negligible, thus the following treatment of the defects would be valid for both collisional (as we stated in the introduction here DM is not collisional but we model velocity dispersion as pressure, for simplicity we use anyway the notation collisional) and collisionless DM. In Sect.5.4 we will depict the correction due to pressure effects for collisional DM.

## Domain walls in $\mathcal{D} = 1$

It is instructive to begin from the simplest case, i.e. the study of a defect in one spatial dimension. We want to show that the behaviour of the fluid variables in the vicinity of the defect are universal. In this dimension the defect can have only co-dimension one and thus it is a wall [30].
We assume that the density vanishes at some arbitrary time $D$ and at the point $x = 0$, hence both the imaginary and the real part of the wave-function have to vanish at this point of space-time. Now for simplicity we study a static configuration, which does not any more evolve in time. In the nearby of the defect $x = 0$ we can Taylor expand the wave-function around its null value $\psi(0) = 0$

$$\psi(x) \sim x\partial_x\psi(0) + \mathcal{O}(x^2)\,, \tag{5.1.1}$$

where we assumed that $\partial_x\psi(0) \neq 0$ and the higher-order corrections are negligible at small distances from $x = 0$ [30]. In order for $\psi$ to be well-defined when passing from the 0 its phase must jump by $\pi$ (or an odd integer multiple of $\pi$), so that $\psi$ changes its sign crossing $x = 0$. This indicates that there is a wall defect in $x = 0$ [30].
From the Taylor expansion we can also extract the behaviour of the density near the defect [30],

$$\rho = \bar{\rho}|\psi|^2 \sim x^2\,. \tag{5.1.2}$$

Hence the fluid density grows like $x^2$ in the neighbourhood of the defect and this result derive just by the fact that the wave-function vanishes at the defect, but not its spatial derivative, therefore it is quite general [30].

## Higher dimension defects

In dimensions higher then one the condition for the vanish of the real and the imaginary parts of the wave-function set the co-dimension of the defects to two, i.e. each condition corresponds to a two dimensional surface [30]. Therefore the defects, which are given by the intersection of these two surfaces, are lines. Since we assume that at the infinity there is no vorticity we expect these lines to close in vortex rings. This is consistent for example with our expectation that dark matter haloes (or baryon galaxy clusters) are of finite size and thus are able to support only vortex loops of finite extent [30].
Following the study of one-dimensional defects we can Taylor expand the wave-function in the vicinity of a point where the wave-function vanishes, we choose arbitrary this point to be the origin $\mathbf{x} = 0$ (we keep studying static configurations).

$$\psi(\mathbf{x}) \sim \mathbf{x} \cdot \nabla\psi(0) + ... \tag{5.1.3}$$

Since in this higher-dimensional case the wave-function vanished along a whole line the wave-function spatial derivative has to vanish along the line direction. Without loss of

generality we take the tangent to the line to be pointing along the $z$ direction (we are just defining a reference frame). We can also introduce a set of complex coordinates in the transverse plane [30]:

$$\chi \equiv x + iy\,, \qquad \bar{\chi} \equiv x - iy\,. \tag{5.1.4}$$

Then we can rewrite the Taylor expansion in the new coordinates as

$$\psi(\chi, \bar{\chi}) \sim \chi\bar{\partial}\psi(0) + \bar{\chi}\partial\psi(0) + ... \simeq a\chi + b\bar{\chi} + ....\,, \tag{5.1.5}$$

where $\bar{\partial} = \frac{\partial}{\partial\bar{\chi}}$. Since the derivative $\partial\psi(0)$ and $\bar{\partial}\psi(0)$ are just constants we renamed them as $a$ and $b$ for shortness of notation. From the fact that $\mathbf{x} = 0$ is a zero of $\psi$ and from the argument principle, generalized to harmonic complex function [16], it can be shown that when $|a| > |b|$ the phase winds by $+2\pi$ as we traverse a circle enclosing the origin (and so the defect), while in the case $|a| < |b|$ the winding is $-2\pi$ [30]. Hence both of these cases describe vortices with winding $+1$ or $-1$.
Then we can obtain the behaviour of the density field in the vicinity of the defects as we have done for the 1-dimensional wall.

$$\rho \sim \bar{\rho}|\psi|^2 \sim Ax^2 + By^2 + Cxy\,, \tag{5.1.6}$$

where the parameters $A, B, C$ can be solved from $a, b$ but their precise form is not important, in any way they are constants. Hence the density scales roughly as $\sim r_\perp^2$, where $r_\perp$ is the radius in the cylindrical coordinates (i.e. the distance from the vortex), but it is not in general axially symmetric [30]. Lines of constant density are ellipses in the plane transverse to the vortex. We can also extrapolate a rough estimate for the velocity profile near the defect deriving the velocity field from the first moment of the Wigner distribution (2.3.14).

$$|\mathbf{u}^W| = \frac{1}{|\psi|^2}\left|\psi\nabla\bar{\psi} - \bar{\psi}\nabla\psi\right| \sim \frac{\nabla\psi}{\psi} \sim r_\perp^{-1} \tag{5.1.7}$$

The Husimi velocity (2.3.24) would correspond to a coarse-graining of this result and we expect that if the spatial resolution does not exceed the near-defect region (where we can neglect pressure and gravity) the velocity scaling is conserved. For the ultra-light particles we are studying in this chapter (FDM) the quantum effects are present on scales which are a considerable fraction of galaxy size [30], thus we expect that the near-defect regime survives to coarse-graining, at least using a suitable spatial resolution.
Therefore from the velocity scaling we expect the fluid to have very high velocities near the vortices.
We still have to consider the case $|a| = |b|$, this time the defect is not a vortex but it is a domain wall, where the phase jumps by $\pi$ as we cross the wall [30]. Lastly if $|a| = |b| = 0$ we should keep the next order term in the Taylor expansion (5.1.3) and the defect is typically a vortex of higher winding [30].
Using these simple results we can infer also the non-static configurations. First we note that the time derivative of the wave-function is, obviously, provided by the Schrödinger equation, which in the proximity of the defect we can approximate to

$$i\nu\frac{\partial}{\partial D}\psi(\mathbf{x}, D) \simeq -\frac{\nu^2}{2}\nabla^2\psi - \frac{3e(\Omega_{DM})}{2D}\phi\,. \tag{5.1.8}$$

To keep the problem simple enough to be tractable with analytical tools we limit our study (in this non-static case) to scales small enough to neglect the effects of the Universe expansion. This approximation is good enough for the gravitational bound objects as for example galactic halos [30].
In this scenario the growth factor is constant so we should use the cosmological time, and more the velocity potential does not appear in the potential term in the right-hand side of the Schrödinger equation. Then the Schrödinger equation (2.1.23) in a non-expanding Universe with our previous approximations reads

$$i\nu\frac{\partial}{\partial t}\psi(\mathbf{x},t) \simeq -\frac{\nu^2}{2}\nabla^2\psi(\mathbf{x},t)\,. \tag{5.1.9}$$

Finally we can Taylor expand the wave-function near the defect at $\mathbf{x}=0,\ t=0$.

$$\psi(\mathbf{x},t) \simeq t\frac{\partial\psi(0)}{\partial t} + \mathbf{x}\cdot\nabla\psi(0) \sim \frac{i\nu t}{2}\nabla^2\psi(0) + \mathbf{x}\cdot\nabla\psi(0) + \dots\,, \tag{5.1.10}$$

where 0 denotes the origin of both space and time. As before near the defect we can neglect higher order terms if we assume that the first order ones are not null [30]. We can find the location of the defect if we set (5.1.10) to 0 for small spatial and time deviations [30], i.e. $\mathbf{x}\sim\Delta\mathbf{x}$ and $t\sim\Delta t$. In this manner we can obtain the vortex velocity, it is the velocity of the vortex and not of the surrounding fluid because we imposed $\psi=0$ which defines the defect.

$$\dot{\mathbf{x}}\cdot\nabla\psi(0) = -\frac{i\nu}{2}\nabla^2\psi(0) \tag{5.1.11}$$

By dimensional arguments we can obtain the velocity scaling [30], we call $R$ the characteristic scale over which the configurations varies,

$$v_{vortex} \sim \frac{\nu}{R} \tag{5.1.12}$$

For curved vortices the characteristic scale is of order of the curvature, hence we expect that the velocity is inversely proportional to the radius of the curvature of the vortex $R$. This is a common result in superfluids, where smaller vortex loops move faster [30].

### 5.1.1 Vortex neighbourhood

Now we have to answer to the important question on the limits in the validity of the assumption of negligible gravitational potential and gas pressure. To understand where the effects of this last two terms stop to be negligible we have to compare them with respect to the kinetic term of the Schrödinger equation, i.e. the Laplacian. We want to study structures at equilibrium, which are characterized by the virial theorem (4.2.24). Since in the present work we are not interested in the description of what happens far away from the vortex but just to where we can neglect gravity and pressure we can consider only the combined effect of these two quantities in an effective potential $V_{effective}$. We make a crude confront between this effective potential and the Laplacian by means of dimensional arguments. Clearly the Laplacian term has dimension $\nu^2R^{-2}$. For the potential instead we use the virial theorem (4.2.24).

$$R\times R^{-1}V_{effective} \sim V_{effective} \sim 2T \sim \tilde{v}^2\,, \tag{5.1.13}$$

where $\tilde{v}$ is the characteristic comoving peculiar velocity of the virialized structure surrounding the vortex. This characteristic velocity is of the same order of the velocity dispersion $\sigma_u$ which characterize the phase-space resolution in the Husimi distribution (2.3.17), hence we can assume $\tilde{v} \sim \sigma_u$. We can relate the velocity to an effective de Broglie wavelength related to the coarse-graining scale through the parameter $\nu$.

$$\lambda_{dB} \equiv \frac{h}{mv} = \frac{2\pi\nu}{\tilde{v}} \sim \frac{2\pi\nu}{\sigma_u}\,, \tag{5.1.14}$$

where $h$ is the Planck constant and we used the fact that we defined $\nu = \hbar/m$. Then the effective potential in terms of the de Broglie wavelength is $V_{effective} \sim \nu^2\lambda_{dB}^{-2}$. The limit of the near-defect regime is found equating this last expression with the kinetic term of the Schrödinger equation $\nu^2 R^{-2}$ which gives

$$R \sim \lambda_{dB}\,. \tag{5.1.15}$$

Then we found that this simple regime ends at a distance equal to the de Broglie wavelength from the vortex [30]. Outside this region the effects of the gravitational potential and of the gas pressure will change the scaling of the density field and we expect this density field to vanish again far away from the vortex, for example as $r_\perp$ exceeds the size of the halo [30].
Another important observation is that this results is exact only for virialized structures. For structure which have not yet reached the virialization also the Jeans scale has a role in determining the dynamics, we know that for scales bigger than $\lambda_J$ gravity dominates the effective DM pressure and leads the region to a gravitational collapse and eventually to virialization [64]. Therefore we expect that during this collapsing regime the eventually arose vortices do not follows the properties stated previously. Instead for scales smaller than the Jeans wave-length the pressure dominates the gravity and so we expect that the pressure can destroy the quantum vortices, since they are seen as sub-structures in a DM structure and the pressure can avoid their formation as in Jeans gravitational instability theory [50]. In Sect.5.4 we will study the region near the critical behaviour $\lambda_{dB} \gtrsim \lambda_J$ such that the pressure term is not exploding (as it will on smaller scales due to Jeans instability theory [50]) but it gives competing contribution to the dynamics with respect to the kinetic energy (as expected by Jeans instability theory [50]). Instead in the regime $\lambda_{dB} < \lambda_J$ we expect that the pressure interdicts the formation of the vortices as it prevents the formation of bounded structures in the Jeans instability theory [50], always following the results of Jeans theory we expect that for $\lambda_{dB} >> \lambda_J$ the pressure is negligible with respect to gravity and so the results of collisionless FDM [30] holds also for FDM with not negligible velocity dispersion in this last regime. We will depict in Sect.5.4 the pressure corrections to the near-defect properties in the regime $\lambda_{dB} \gtrsim \lambda_J$.
Since here the coarse-graining is done on about the de Broglie scale, $\sigma_x \sim \lambda_{dB}/4\pi$ due to the phase-space resolution condition (2.3.18) $\sigma_x\sigma_u = \nu/2$ as we already mentioned in the introduction at the chapter, it will not introduce additional regime of solutions with respect to the already mentioned $\lambda_{dB} \lessgtr \lambda_J$.
All the results we derived in this section are universal in the regime $\lambda_{dB} >> \lambda_J$, i.e. do not depend on boundary conditions (e.g. the form of the external potential) or on initial conditions. They hold for any vortex/defect after its generation.

## 5.2 Simple vortex solutions

In the previous section we presented some universal properties of vortices and of the fluid near them, since in this region the effects of gravity and pressure are negligible. In this section we want to show that solutions to the Schrödinger equation with these properties actually exist, even if there were no vortices at the beginning. The pressure effect will be investigated in Sect.5.4.
We continue to limit our study to the low-density region, neglecting gravity and pressure, so the problem is analytically tractable. Therefore we need to solve just the Schrödinger equations and not the Poisson one. We have to continue to use also the approximation we introduced in the study of non-static configuration, i.e. we study scales small enough to neglect the expansion of the Universe. Thus we use the cosmological time instead of the growth factor. With these assumptions we will able to study the fluid flow pattern around a vortex ring.

### Domain walls

We begin searching solutions that describe domain walls, we have seen that generally these defects arise in one spatial dimension but also in some particular case in three dimensions (anyway this is not the case of a gravitational collapse [30]).
If we focus on a static defect in one dimension in the low-density region the Schrödinger equation takes the simple form

$$\partial_x^2 \psi = 0\,, \tag{5.2.1}$$

with general solution [30]

$$\psi = x + b\,, \tag{5.2.2}$$

where $b$ is a constant. We can set $b = 0$ choosing the origin appropriately, which means that the defect appear at $x = 0$ where $\psi$ and $\rho$ vanish. To make more apparent the properties of the defect we rewrite $\psi$ as an amplitude and a phase [30]

$$\psi = |x| e^{i\theta},. \tag{5.2.3}$$

The phase jumps from $-\pi$ for $x < 0$ to $+\pi$ for $x > 0$. Then we recovered the expected properties from the previous section treatment, i.e.

- $\rho \propto |\psi|^2 \propto x^2$ where $|x|$ is the distance to the defect.
- The phase jumps around the defect from $-\pi$ to $+\pi$-

But this solution has an evident problem, the density diverges far away from the defect. We expect that the gravitational interactions will correct this irregularity at infinity, leaving unchanged the behaviour of density and velocity near the defect [30].

### Vortex rings

Since vortices are localized at the intersection where both the real and imaginary parts of the wave-function vanish, we can visualize the evolution of vortex configurations by considering how these vanishing loci evolve in time.
Here we will study only static-configuration because are the only ones admitting analytical

solutions. When keeping the time evolution in the near-defect region the Schrödinger equation describes the free particle approximation which need (outside the semi-classical limit) a numerical solution as we showed in Cap.3.
The simplest solution in three dimension should be an infinitely long straight vortex [30], thus we begin looking for a time-independent axial-symmetric solution. Hence we have to solve a Laplace-like equation in the $xy$ plane. It is convenient to work in the complex coordinates we defined in (5.1.4), then the Schrödinger equation becomes [30]

$$\partial\bar{\partial}\psi(\chi,\bar{\chi}) = 0\,. \tag{5.2.4}$$

This equation is solved by an arbitrary (anti-)holomorphic function, e.g. $\psi \propto \chi^n$ with $n$ an integer [30]. This solution has a zero of order $n$ in $x = y = 0$ and thus describes a vortex with winding $n$, due to the argument principle [16]. Similarly the anti-holomorphic solutions $\psi \propto \bar{\chi}^n$ describe anti-vortices of winding $-n$ [30].
If we study the simplest vortex, of winding 1, which is described by the wave-function

$$\psi = \chi = x + iy\,, \tag{5.2.5}$$

we observe that the real part vanishes over the $yz$ plane located at $x = 0$ and the imaginary part over the $xz$ plane at $y = 0$. Therefore the defect, given by the intersection of these two planes is a line along the $z$ axis. For any purely holomorphic or anti-holomorphic vortices the velocity flow is circular around the position of the defect and it winds $+n$ or $-n$ time as we travel in a closed loop [30].
We can study also more complicated solutions of (5.2.4), for example an admixture of a vortex and anti-vortex solutions [30]

$$\psi \propto \chi + \alpha\bar{\chi}\,. \tag{5.2.6}$$

Similarly as in (5.1.5) in the previous section the solution will behave differently for different values of $\alpha$. For $\alpha < 1$ this describes a winding $n = 1$ solution with an elliptical velocity. For $\alpha > 1$ it describes a winding $n = -1$ vortex again with elliptical velocity. In the degenerate case $\alpha = 1$ the wave-function is purely real and thus this solution describes a domain wall in the $yz$ plane where the phase jumps by $\pi$ as we cross the wall [30].
Hence we showed that the Schrödinger-Poisson system, in the vicinity of the defects, actually admit solution with the properties we described in the previous section. We did not show any solution for the non-static case because it is not possible to obtain analytical solutions. Anyway this case corresponds to the free particle approximation and from the numerical simulation made by [73] and reported in Fig.3.5 we actually see that vortices of winding $n = \pm 1$ arise in regions of vanishing density.

## Moving vortices

Until this point we found only stationary vortex configurations as solutions of the Schrödinger equation, but we can exploit the symmetries of this equation to obtain at least solutions with vortices moving at constant velocity [30]. A Schrödinger group transformation is defined as a transformation under which the wave-function continues to satisfy the Schrödinger equation, i.e.

$$\psi \to T[\psi] \equiv \tilde{\psi} \;\text{ with } i\nu\dot{\tilde{\psi}} = H\tilde{\psi}\,. \tag{5.2.7}$$

In general these transformations can act quite non-trivially on the wave-function and lead to the most variegate vortex motions, for a more in depth study of Schrödinger transformations check [53]. If we restrict to constant velocity motions we only need the transformation of the wave-function under Galilean boosts [30]:

$$\psi(\mathbf{x},t) \to \exp\left(-i\mathbf{x}\cdot\mathbf{v} - \frac{i}{2}v^2 t\right)\psi(\mathbf{x}+\mathbf{v}t,t) \tag{5.2.8}$$

where we keep neglecting the Universe expansion and so we use the cosmological time. The velocity $\mathbf{v} = d\mathbf{x}/dt$ is the boost parameter. Since the gravitational potential and the pressure do not contain any derivatives it is immediate to see that this transformation is invariant under the combined action of the time derivative and of the Laplacian and so under the Schrödinger equation. We can show for example the effect of this boost on an infinitely long vortex, with boost parameter $v$ in the $x$ direction [30]

$$\psi(\mathbf{x},t) = \exp\left(-ixv - \frac{i}{2}v^2 t\right)(x + vt + iy)\,. \tag{5.2.9}$$

Hence now the vortex moves with velocity $-v$ along $x$. Note that actually the whole fluid is boosted under these particular transformations, so they do not represent solutions where only the vortex is moving through a fluid at rest [30]. Beside be so simple these solutions can lead us to interesting observations on vortex motions.
The infinitely long vortex lines, as (5.2.9), are the simplest configurations, and they capture some important aspects of the physics, but we do not expect that these precise configurations will arise in dark matter haloes or in baryon bounded structures, which are of finite extent. As we have seen a more realistic situation is the one of vortex loops. Therefore we would like to observe the properties of these rings, at least in some simple scenario. The simplest example is given by [30]

$$\psi(\mathbf{x},t) = r_\perp^2 - \frac{l^2}{4} + 2i\left(-az + \frac{t}{q}\right)\,, \tag{5.2.10}$$

where $r_\perp^2 = x^2 + y^2$, $a$ and $l$ are parameters with units of length, $q$ has dimension $[t/L^2]$. The real part of the wave-function vanishes on a cylinder centered in the $z$ axis and with diameter $l$, instead the imaginary part vanishes on the $xy$ plane with a $z$ coordinate that increases at a constant rate with time. The vortex is given by the intersection of these two surfaces and then it is a ring of radius $l/2$ moving at $v_{ring} = (aq)^{-1}$ in the $+z$ direction. Note that this velocity is the speed of the ring as measured relative to the rest frame of the fluid very far from the vortex [30].
To understand the properties of the density and velocity fields near the vortex we should study the wave-function (5.2.10) in a region such as $r_\perp = l/2 + \delta r_\perp$. At the initial time $t = 0$ the near-ring wave-function is [30]

$$\psi(\mathbf{x},0) = l\delta r_\perp - 2aiz\,. \tag{5.2.11}$$

From the variables $(\delta r_\perp, z)$ we can define a plane and describe it with the complex coordinates [30]

$$u = \delta r_\perp + iz\,, \quad \bar{u} = \delta r_\perp - iz\,. \tag{5.2.12}$$

Then (5.2.11) becomes

$$\psi(u, \bar{u}, 0) = (l/2 - a)u + (l/2 + a)\bar{u}\,. \tag{5.2.13}$$

As we previously saw a flow around a ring described by such wave-function is elliptical for a generic value of $a$, corresponding to a mix of a vortex and anti-vortex, but it will always have winding $-1$ because the coefficient of $\bar{u}$ is always the greatest. For $a = l/2$, the near-ring geometry is precisely that of a pure vortex of winding $-1$ and in this case, there is a relation between the size of the ring and its velocity, $v_{ring} \sim (ql)^{-1}$, which is consistent with the results obtained by the Taylor expansion in the previous section and with the behaviour of superfluid vortex rings [30]. We do not expect realistic vortex rings to be circular, but anyway we generically expect the characteristic scale that governs the dynamics, $a$, to continue to be $a \sim l$, so that the relation between size and velocity persists [30].
We pass now to the study of the density profile near the vortex. Very close to the ring, where (5.2.11) holds, the density grows as $r_\perp^2$ as expected [30]. However very far from the ring we have to use the full wave-function (5.2.10) and the density field is anisotropic. In particular on the plane of the ring the density grows like $r_\perp^4$, instead in the transverse direction it grows just as $z^2$. Anyway these scaling depend on the fact that the ring in the solution lies in a plane, thus we do not expect them to hold in more realistic situations [30]. The only robust result is the $r_\perp^2$ behaviour of the density in vicinity of the ring, which is provided by the smallness of the distance from the ring $\delta r_\perp$ [30].
Another interesting fact on vortices is the fact that they can appear and disappear dynamically. We can analytically observe this property considering the nucleation of a vortex ring. For example we can study the wave-function [30]

$$\psi(\mathbf{x}, t) = r^2 - \frac{l^2}{4} + i\left(-lz + 3\frac{t}{q}\right)\,, \tag{5.2.14}$$

where $r^2 = x^2 + y^2 + z^2$. The real part of the wave-function vanishes over the surface of a sphere and the imaginary part over a plane moving in the $z$ direction. Hence this solution describes the nucleation of a vortex ring at $x = y = 0, z = -l/2$ at $t = -ql^2/6$, the ring moves in the $z$ direction with velocity $v = 3/(ql)$ and its radius at height $z$ is given by $R = \sqrt{l^2/4 - z^2}$. At time $t = ql^2/6$ the vortex re-combines and annihilates. We expect that the velocity of the vortex increases as the size of the ring decreases. This property is recovered because, besides the velocity along $z$ being constant, the $v_x$ and $v_y$ components of the velocity change as a function of its size, when the ring shrinks to 0 the velocity actually becomes very large [30].
Until this point we showed simple solutions of the Schrödinger equation for illustrate the main properties of vortices. In Sect.2.4 we showed that in a quantum fluid the vortices have to arises in couples with opposite winding. Then we want to show that such solutions actually exist. For example we can take a wave-function of the form [30]

$$\psi(\mathbf{x}, t) = x^2 + y^2 - \frac{l^2}{4} + 2i\left(-\frac{lx}{2} + \frac{t}{q}\right)\,. \tag{5.2.15}$$

The real part vanishes over a cylinder of radius $l/2$ with center in the $z$ axis and the imaginary part over a $yz$ plane moving with time. For $t > -ql^2/4$ no vortex is present, at

$t = -ql^2/4$ a vortex-antivortex pair nucleate at $x = -l/2, y = 0$ [30]. They move around the ring $x^2 + y^2 = l^2/4$ in opposite directions and recombine at $t = ql^2/4$, after which they annihilate. Thus the nucleation of a vortex-antivortex pair is actually a solution of the Schrödinger equation, but in a real scenario it would take a much more complicated form with respect to (5.2.15) [30].
The last case we want to investigate is the intersection between two vortices. The generic behaviour of the analytic solutions we have considered so far is for the vortices to reconnect whenever they come into contact, as opposed to becoming frustrated and forming a defect network. We can describe the collision between two vortex lines with the wavefunction [30]

$$\psi(\mathbf{x}, t) = (x + iy)(y + iz) - \frac{t}{q}\,. \tag{5.2.16}$$

At $t = 0$ this describes two vortex lines oriented along the $z$ and $x$ axes which intersect at the origin. Instead if we watch the full time evolution it describes two cusped vortices coming together to the point $\mathbf{x} = 0$ at time $t = 0$, at this time the two cusped vortices are indistinguishable from two infinitely long vortex lines intersecting. Also for more complex configurations, involving vortex rings, the pinch off behaviour at the intersection seems to hold [30].

## 5.3 Numerical simulations

To show that all the vortex properties present in the previous section actually appears in cosmological scenarios we present some numerical simulations done by [30]. Hui and collaborators numerical studied with the "SPoS" code [41] the Schrödinger-Poisson system in three spatial dimensions for DM only. In order to study the vortex rings in detail, they focused on simulations with a small box size (such as have a good spatial resolution) and somewhat artificial initial conditions chosen to result in a collapsed halo. In all cases they studied, there are no vortices in the initial conditions. Yet, vortices generically appear after the gravitational collapse brings about a superposition of waves in a virialized halo [30]. To identify vortex lines in a simulation output we need to look for location of high vorticity $\boldsymbol{\omega} = \nabla \times \mathbf{v}$. Since we showed that vortices arise in region of vanishing density we imagine that we could use also such condition in order to search for vortices. But from the simulations [30] observed that sometimes regions with low density also have a small vorticity, hence the small density condition alone is not a sufficiently robust indicator of vortex lines. Therefore the search via high-vorticity regions is more precise.
After a vortex line is identified we should check that the phase does have the required characteristic winding around it. This is an important feature because, given limited resolution, it might be difficult to verify that a particular point has low density or high vorticity, but the winding phase is something that can be checked in the neighbourhood of that point and is therefore robust. Then [30] grouped the discrete grid points corresponding to high vorticity $\boldsymbol{\omega}$ into vortex lines using DBSCAN (Density-Based Spatial Clustering of Applications with Noise) algorithm [17].
We begin the numerical study with a fairly simple configuration with some symmetries, an halo (remember that the simulations here presented regard just collisionless dark matter) which forms from the coalescence of four evenly spaced density peaks. The three-dimensional computational box in which the simulation is ran has a length of $L = 0.5$Mpc

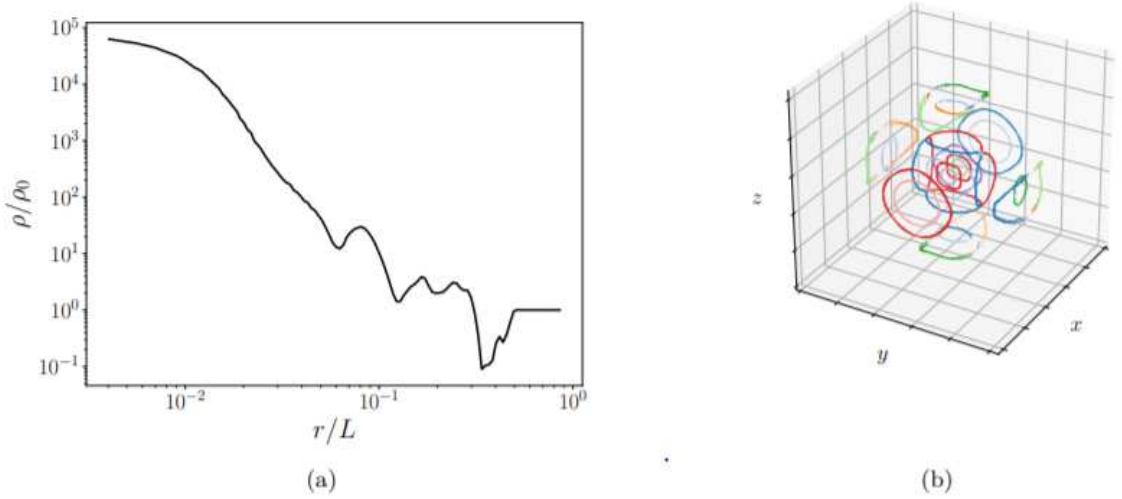


Figure 5.1: Numerical simulation of a halo formed from the collapse and merger of a symmetric configuration of four Gaussian peaks. (a) Spherically averaged density profile (as a function of radius) of the virialized halo that forms from the coalescence of the peaks. (b) Vortex rings formed in the same halo. This figure is provided by [30], for any further detail check the main text.

on each side. Hui used dark matter particle of very low mass $m = 6 \times 10^{-24}$eV, which is consistent with the fuzzy DM proposal. Anyway all the results we derived in the previous sections are mass independent thus we expect that also the properties observed in the simulations are not limited to the mass scale in consideration. Setting the mass to a so low value has the advantage that the de Broglie wavelength is well-resolved already with a simulation grid of $256^3$ points [30]. As we assumed in the derivation of the vortex properties, the Universe background expansion is neglected in the simulation. On the scales under consideration this assumption holds quite well because the expansion effect is by far not the dominant one [30]. The density peaks are initialized to a Gaussian profile

$$\rho = 250\bar{\rho} \exp\left[-\left(\frac{\mathbf{r} - \mathbf{r}_c}{r_0}\right)^2\right], \tag{5.3.1}$$

where $r_0 = 0.05L$ is the radius of the Gaussian core, $\mathbf{r}_c$ denotes the position of the peak's center and $\bar{\rho}$ is the background density.
The beginning configuration is set such as the four peaks are placed on the vertices of a square chosen to lie in the $x = 0$ plane and centered at the origin, with a side length of $L/10$. The initial wave-function is chose to be real $\psi = \sqrt{\rho/\bar{\rho}}$, thus both the initial velocity and initial angular momentum are null. The simulation results are presented in Fig.5.1, provided by [30]. The panel (a) shows the density profile of the quasi-stationary dark matter halo that forms from the merging of the four initial peaks under the influence of gravity. A soliton core, i.e. a region characterized by a coherent and stable configuration of the DM where the density is almost constant, is formed in the inner region of size

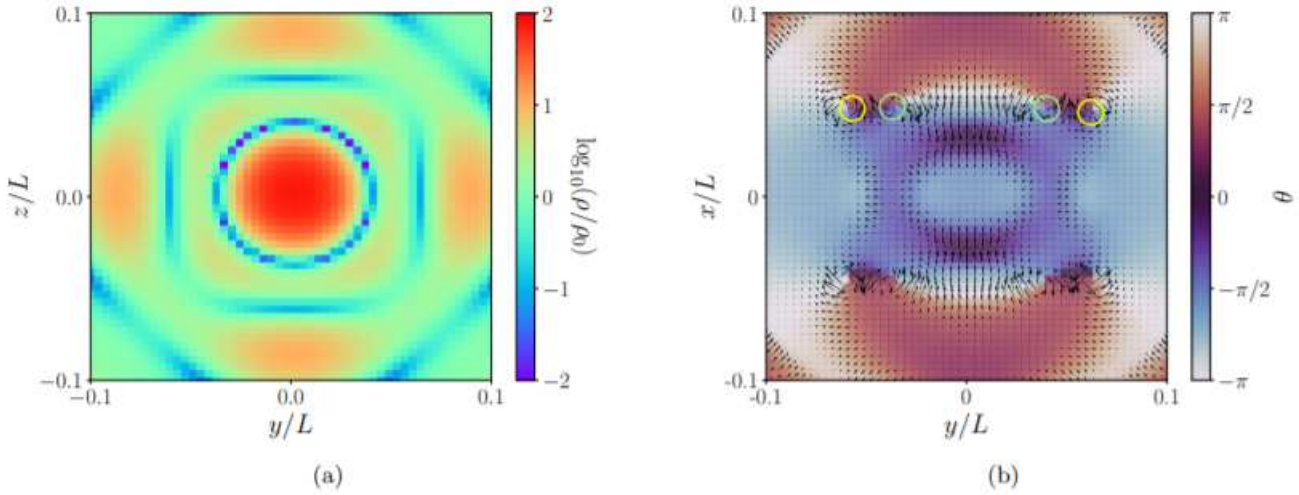


Figure 5.2: More detailed views of a halo depicted in Figure 5.1, formed from collapse of a symmetric configuration of four Gaussian peaks. (a) A zoomed-in slice of the density field in the $yz$ plane at $x = 0.05L$, showing vortex rings (where the density vanishes) observed near the halo center. (b) A zoomed-in slice of the phase $\Theta$ in the $yx$ plane at $z = 0$. The colors show the phase value and the arrows trace the velocity field in the plane. The green and yellow circles indicate where the circular and square vortex rings in the left panel intersect the $z = 0$ plane. Note that there is a pair of such rings at $x = 0.05L$, and a pair at $x = -0.05L$, due to the symmetric nature of the initial condition. This figure is provided by [30], for any further detail check the main text.

$r \sim 0.01L$, this is a common wave-mechanical features of FDM [30] and this inner profile is found to fit very well the cores observed in some dwarf galaxies [49]. Instead in the outer region the density falls approximately as $r^{-3}$ [30], this scaling fits quite well the Navarro-Frenk-White (NFW) [52] profile which is the most commonly used profile for DM halos and it derives from fitting N-body simulations.
The (b) panel of Fig.5.1 shows the vortex lines identified in the collapsed halo with the previously described method. Since the soliton core is smooth and dense the vortices can be found only outside it [30]. As expected from the previous considerations we have done on the defects in three dimensions, all the vortex lines found are in the form of vortex rings, there is no straight line.
From the measure of the three-dimensional velocity dispersion of the halo outside the soliton core [30] inferred a de Broglie wavelength of $\lambda_{dB} \equiv (2\pi)/(m\sigma_u) \approx 0.12L$. We have to observe that the soliton core size of $\sim 0.01L$ is in closer to $\lambda_{dB}/(2\pi)$ rather than just $\lambda_{dB}$, so a bit smaller than expected. Another interesting fact is that Hui and collaborators showed that it is possible to predict the number of vortices per de Broglie volume ($\lambda_{dB}^3$), it should be about 1 for de Broglie volume, and their prediction was of $\sim 19$ rings with respect to the 20 rings found in the simulated halo.
In Fig.5.2 [30] presented two zoomed-in slices of the DM halo of Fig.5.1 for the density and phase fields. The panel (a) shows the density slice in the $yz$ plane at $x = 0.05L$, the magnitude is represented by the color. Since the halo is generated from symmetric initial conditions the plane at $x = -0.05L$ looks similar. Near the high density center

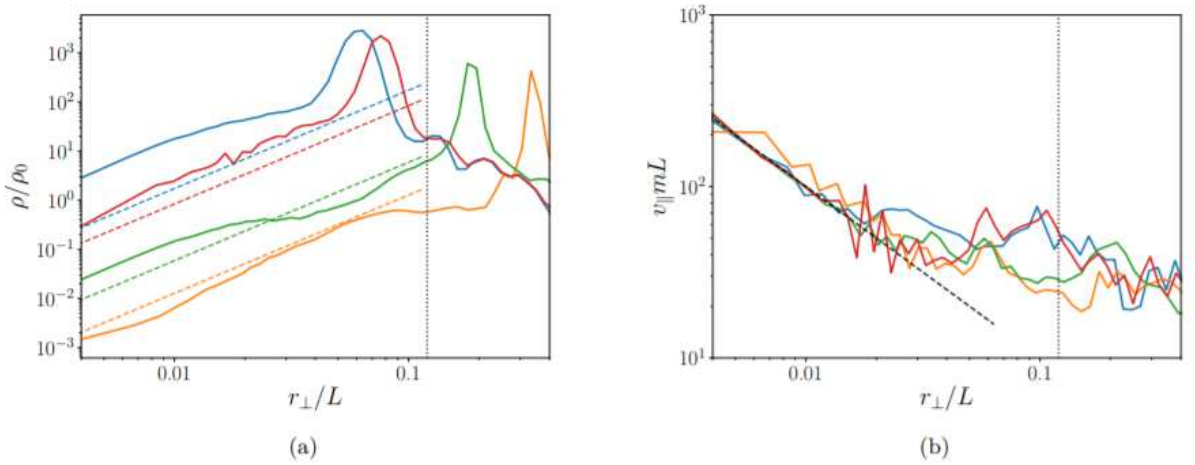


Figure 5.3: Density and velocity profiles around four vortices in of Fig.5.1(b). The profiles are cross-sectional, in the sense that they depict (circularly averaged) profiles on a plane perpendicular to the vortex, intersecting the vortex at some point. (a) Density profiles (solid lines) in the radial direction; the dashed lines indicate $\rho_{local}(r_\perp/\lambda_{dB})^2$, where $\rho_{local}$ is the mean density interior to the location of the vortex, and $r_\perp$ is the distance to the vortex line. This shows that the near-vortex density profiles obey the expected $r_\perp^2$ scaling. (b) Velocity profiles (solid lines); the black dashed line shows the tangential (circulation) velocity $v_\parallel \sim 1/r_\perp$. The vertical dotted line in both panels shows the scale of $\lambda_{dB}$. Lines of the same color on the left and right correspond to the same vortex. This figure is provided by [30], for any further detail check the main text.

we can observe a circle and a square loop of low density (in blue), these correspond to two vortex rings. The panel (b) shows the phase on the $yx$ plane at $z = 0$, its magnitude is represented by the color and the arrows indicate the velocity field projected on the plane. The green and the yellow circles shows respectively where the circular and the square vortices intersect the $z = 0$ plane, clearly there is a symmetry between the points at $x = 0.05L$ and the points at $x = -0.05L$. From this plot we can observe as the phase smoothly varies from $-\pi$ to $+\pi$ around each vortex, with winding number $\pm 1$ (the velocity around the green and yellow circles rotates in opposite directions) hence the quantum Kelvin-Helmholtz theorem (2.4.5) is respected.

Lastly we would like to see if the $r_\perp^2$ scaling of the density and the $r_\perp^{-1}$ of the velocity in the vicinity of the vortex are present in the numerical simulation. Hui and collaborators plotted in Fig.5.3 the density and velocity profiles close to four different vortices seen in the halo presented in Fig.5.1, here each vortex is defined by a color. The profiles are on a plane oriented perpendicular to the local vortex line direction at the intersection between it and the plane, then the profiles are also circularly averaged around the vortex [30]. The panel (a) shows the density profile as a function of the distance from the vortex $r_\perp$. As comparison to the simulation profile for each vortex the expected density profile $\rho = \rho_{local}(r_\perp/\lambda_{dB})^2$ is plotted as a dashed line, where $\rho_{local}$ is the mean mass density at radii smaller than the location of the corresponding vortex. We can thus observe that the $r_\perp^2$ scaling is a good approximation close to the vortex but it generally breaks before $r_\perp$ reaches the de Broglie scale (represented by the vertical dotted line in Fig.5.3). For

all the vortex bumps are present in the density profile, these correspond to distances at which one encounter the high-density halo core [30]. The panel (b) shows the tangential velocity $v_\parallel$ this time as comparison is reported the profile $v_\parallel = 1/(mr_\perp)$. Also in this case the expected profile describes well the simulation results near the vortex and it ends again before reaching the de Broglie scale.
To be sure that all the properties we have seen for the halo depicted in Fig.5.1 does not arise just from the symmetric initial condition, [30] studied also a halo resulting from the coalescence of 10 initially identical peaks randomly placed close to the center of the simulation box. They found that all the feature founded with the symmetric initial conditions are conserved, the vortices are just less symmetric.
For clarity we report here all the features we found in the study of vortices and the velocity and the density fields around it [30].

- All vortices close in loops.
- The phase winds in the cross-section of each line with winding number $n = \pm 1$.
- The density profile scales as $r_\perp^2$ near the vortex.
- The velocity profile scales as $r_\perp^{-1}$ near the vortex.
- The number density of vortices is roughly one per de Broglie volume $\lambda_{dB}^3$.

Hence we confirmed the theoretical properties depicted in the previous sections with numerical simulations for dark matter. If these properties would be confirmed observationally it would be a prove for the possibility of the existence of axion-like dark matter (FDM).

## 5.4 Pressure effects

In the previous sections we depicted the properties of vortices and of the density and velocity fields near them following the work [30]. We additionally observed that in this near-defect regime we expect the collisional and the collisionless DM to behave similarly. In particular we showed that this regime holds for distances from the vortex smaller than an effective de Broglie wave-length in the case of virialized structure. But we know from the Jeans gravitational instability theory (briefly depicted in App.A1) that the gravitational collapse and so the generation of bound structures is not expected to happen on scales smaller than the Jeans wavelength $\lambda_J = 2\pi/k_J$ due to the effects of the gas pressure (which actually is free streaming caused by velocity dispersion). Since vortices can be interpreted as sub-structures in the halo [1] we expect that they cannot form if $\lambda_{dB} << \lambda_J$. Instead for scales comparable with the Jeans wavelength $\lambda_{dB} \leq \lambda_J$ we expect that vortices can still form but their dynamics and the nearby fluid are influenced by pressure effects. We begin showing that the velocity dispersion actually give rise to a Jeans scale as gas pressure would. We started the study of CDM neglecting its effects into the Euler-like equation (1.3.22), now we want to study it via Jeans gravitational instability as we have done for gas pressure in App.A1, in doing so we follow the work [64].
The Jeans gravitational instability studies the evolution of perturbations in the linear regime, in this regime the dispersion velocity tensor is constant and given by the three

dimensional initial fluid dispersion $\Pi_{ij} = \sigma^2 \delta_{ij}$ [64], thus the linearised (1.3.22) is

$$\dot{v}_i + H v_i = -\frac{1}{a}\partial_i \Phi_{DM} - \frac{\sigma^2}{a\rho}\partial_i \rho \,. \tag{5.4.1}$$

If we multiply this equation by $\rho$ and take its divergence, and we insert it in the time-derivative of the continuity equation (1.3.18), we obtain at linear order

$$\frac{\partial^2 \delta}{\partial t^2} + 2H\frac{\partial \delta}{\partial t} = \frac{1}{a^2}\nabla^2 \Phi + \frac{\sigma^2}{a^2}\nabla^2(1+\delta) \,. \tag{5.4.2}$$

Then using the Poisson equation (1.2.16) for express the gravitational potential we obtain

$$\frac{\partial^2 \delta}{\partial t^2} + 2H\frac{\partial \delta}{\partial t} = 4\pi G \bar{\rho}_{DM}\delta + \frac{\sigma^2}{a^2}\nabla^2 \delta \,. \tag{5.4.3}$$

This equation describes the evolution of linear perturbation under the effect of gravity and initial velocity dispersion. Since we are treating linear perturbation we can expand them as a sum of plane waves [64], i.e.

$$\delta(\mathbf{x}, t) = \frac{1}{(2\pi)^{3/2}} \int d^3k \delta_{\mathbf{k}}(t) e^{i\mathbf{k}\cdot\mathbf{x}} \tag{5.4.4}$$

and we search for solution of the form [50]

$$\delta_{\mathbf{k}}(t) = \delta_{\mathbf{k}} e^{i\omega t} \,. \tag{5.4.5}$$

Therefore we can rewrite the equation (5.4.3) as

$$\omega^2 - 2iH\omega = -4\pi G \bar{\rho}_{DM} + \frac{\sigma^2 k^2}{a^2} \,. \tag{5.4.6}$$

Since we are studying the quantum vortices in a region small enough to neglect the Universe expansion, we have to impose $H = 0$ and we can set $a = 1$. Then we obtain the dispersion equation

$$\omega^2 = -4\pi G \bar{\rho}_{DM} + \sigma^2 k^2 \,. \tag{5.4.7}$$

From the definition (5.4.5) we observe that the perturbations can grow in time only if $\omega$ is imaginary. Then we can define a critical scale between the oscillatory regime ($\omega^2 > 0$) and the unstable regime ($\omega^2 < 0$), as we have done for the Jeans scale in App.A1.

$$k_J^2 = \frac{4\pi G \bar{\rho}_{DM}}{\sigma^2} \,, \tag{5.4.8}$$

which is similar to the Jeans wavenumber in a static background Universe where the velocity dispersion $\sigma$ takes the place of the sound speed $c_s$ [64]. Thus we have shown that the dark matter velocity dispersion acts on perturbations in a similar way to gas pressure. We come back now to our Schrödinger model and to the study of quantum vortices. Here we do not limit ourselves to linear perturbations, hence velocity dispersion cannot be considered a constant any more. Since [15] showed that in DM halos the velocity dispersion can be represented by an isotropic pressure by the relation

$$P(\mathbf{x}) = \frac{1}{3}\rho(\mathbf{x})\sigma^2(\mathbf{x}) \tag{5.4.9}$$

with $\Pi_{ij}(\mathbf{x}) = \delta_{ij}\sigma^2(\mathbf{x})$ and $P$ is the isotropic pressure, we can note that, beside the 1/3 factor the Euler equation (1.3.22) would be the same of the baryon one (1.2.14). Hence in the following we will model the velocity dispersion with a gas pressure using the results we obtained with the baryons Schrödinger equation.
As we stated before, for keep the problem analytically tractable we study regions small enough to neglect the Universe expansion, then is useful to rewrite the Schrödinger equation for a collisional fluid using cosmological time $t$ in an non-expanding Universe as we first did in (2.1.23).

$$i\nu\frac{\partial\psi}{\partial t} = -\frac{\nu^2}{2}\nabla^2\psi + \Phi + A|\psi|^{2\gamma-2}\psi\,, \tag{5.4.10}$$

where

$$A = \frac{\gamma}{\gamma-1}\frac{\bar{\rho}_{DM}k_BT_0}{m}\,. \tag{5.4.11}$$

We neglected the quantum pressure in the Schrödinger equation thus its effects will be present implicitly in the dynamics. In this case it will not be strongly suppressed by the choice of a proper $\nu$, since we are treating a real quantum system with $\nu = \hbar/m$. The Jeans wavenumber for collisional DM perturbations over a static background Universe is [7]

$$k_J^2 = \frac{4\pi G\bar{\rho}_{DM}}{c_s^2} = \frac{3H_0^2\Omega_{0DM}}{2}\frac{m}{\gamma k_BT_0}\,, \tag{5.4.12}$$

where we used $c_s^2 = \frac{\gamma k_BT_0}{m}$. Note that the form of the Jeans wavenumber is similar to the one obtained from the velocity dispersion (5.4.8) with the sound speed $c_S$ instead of the velocity dispersion $\sigma$. We will use this model of pressure and Jeans wavenumber for study the effects DM velocity dispersion on quantum vortices, this is just a simple approximation but it will make evident how the results depend on the ratio $\lambda_{dB}/\lambda_J$. Hence we can rewrite the coefficient $A$ as

$$A = \frac{3H_0^2}{2(\gamma-1)}\Omega_{0DM}\bar{\rho}_{DM}\frac{1}{k_J^2}\,. \tag{5.4.13}$$

In the case $\lambda_{dB} >> \lambda_J$ we expect that the results found in the previous sections are still valid since on such scales the pressure effects are still negligible, due to Jeans instability theory [50].
Instead for $\lambda_{dB} < \lambda_J$ we expect that the gas pressure, due to its stabilizing role, can destroy the vortices. Actually it is not a stabilizing effect due to pressure but the particles tends to free stream out the vortex and destroy it due to velocity dispersion [64]. We want to study the regime $\lambda_{dB} \gtrsim \lambda_J$ such as the pressure term is not big enough to dominates the dynamics but it is still a competing factor with respect to the kinetic energy (always following the results of Jeans instability [50]), hence it will introduce corrections over the properties we depicted in the previous sections. To investigate this last scenario we study the collisional fluid near a defect through the Taylor expansion of the wave-function. We will not study the regime $\lambda_{dB} < \lambda_J$ because it requires numerical solutions due to the complex form of the pressure term.

## Static configurations

We begin our study with the simplest configuration possible, i.e. a static one in a one-dimensional space. In this scenario the wave-function has to satisfy the equation

$$\frac{\nu^2}{2}\partial_x^2\psi = \frac{3H_0^2}{2(\gamma-1)}\Omega_{0DM}\bar{\rho}_{DM}\frac{1}{k_J^2}|\psi|^{2\gamma-2}\psi\,. \tag{5.4.14}$$

If we assume the defect to be at $x = 0$ ($\psi(0) = 0$) we can Taylor expand the wave-function around it, this time we cannot neglect second order terms due to the pressure effects

$$\begin{aligned}\psi(x) &\sim x\partial_x\psi(0) + \frac{x^2}{2}\partial_x^2\psi(0) \sim x\partial_x\psi(0) + \frac{3\Omega_{0DM}\bar{\rho}_{DM}}{2(\gamma-1)}\frac{H_0^2x^2}{\nu^2k_J^2}\psi^{2\gamma-1} \sim \\ &\sim x\partial_x\psi(0) + \frac{3\Omega_{0DM}\bar{\rho}_{DM}}{2(\gamma-1)}\frac{H_0^2x^2}{\nu^2k_J^2}\left(x\partial_x\psi(0)\right)^{2\gamma-1}\,,\end{aligned} \tag{5.4.15}$$

where in the last line we used the first order expansion of the wave-function to keep the expression at the lowest order possible. From this expansion we can deduct the approximate scaling of the density field

$$\rho = \bar{\rho}\psi \sim x^2\left(1 + C^2\left(\frac{H_0^2x}{\nu^2k_J^2}\right)^2x^{4\gamma-2} + ...\right)\,, \tag{5.4.16}$$

with

$$C = \frac{3\Omega_{0DM}\bar{\rho}_{DM}}{2(\gamma-1)}\,. \tag{5.4.17}$$

Since this relation holds in the neighbourhoods of $x = 0$ we observe as the pressure introduce a small corrective term to the density profile. We can study also the velocity field, which is roughly given by

$$v \sim \frac{\partial_x\psi}{\psi} \sim \frac{\left(1 + C\frac{H_0^2x}{\nu^2k_J^2}x^{2\gamma-1}\right) + C\frac{H_0^2x^{2\gamma}}{\nu^2k_J^2}}{x\left(1 + C\frac{H_0^2x}{\nu^2k_J^2}x^{2\gamma-1}\right)} \sim \frac{1}{x}\left(1 + C^2\left(\frac{H_0x^\gamma}{\nu k_J}\right)^2 + ...\right)\,. \tag{5.4.18}$$

The pressure provides a small correction to the near-defect velocity profile, which depends on both the coarse-graining and Jeans scales. Actually we can rewrite the coefficient of the spatial correction as

$$\frac{H_0}{\nu k_J} = \frac{H_0}{\sigma_u}\frac{\lambda_J}{\lambda_{dB}}\,, \tag{5.4.19}$$

which is big in the case $\lambda_{dB} < \lambda_J$ as expected.
We do not study also the three dimensional case for static configuration because it is much more computationally involved with respect to the one dimensional case. Anyway we can think that, similarly to the collisionless case we studied before [30], the density and velocity field scaling will be mostly like to the one-dimensional case in function of the distance from the vortex $r_\perp$, but generally not isotropic.

## Dynamical configurations

Now we want to investigate the dynamical case, here we start directly from the three dimensional case which, since we will use only dimensional arguments to study the vortex velocity, is simple enough in terms of the pressure correction. The time evolution of the wave-function in the vicinity of the defects is given by

$$i\nu\frac{\partial\psi}{\partial t} = -\frac{\nu^2}{2}\nabla^2\psi + \frac{3H_0^2}{2(\gamma-1)}\Omega_{0DM}\bar{\rho}_{DM}\frac{1}{k_J^2}|\psi|^{2\gamma-2}\psi\,. \tag{5.4.20}$$

If we assume the defect to be at the origin of space-time ($\mathbf{x}=0, t=0$) we can Taylor expand the wave-function around it

$$\begin{aligned}\psi(\mathbf{x},t) \approx\, & t\frac{\partial\psi}{\partial t}(0) + \mathbf{x}\cdot\nabla\psi(0) + \frac{1}{2}\mathbf{x}^T\mathbf{H}(0)\mathbf{x} + \frac{1}{2}t^2\frac{\partial^2\psi}{\partial t^2}(0) + t\frac{\partial\psi}{\partial t}(0)\mathbf{x}\cdot\nabla\psi(0) + ... \sim \\ \sim\, & \frac{it\nu}{2}\nabla^2\psi(0) - \frac{it}{\nu}C\frac{H_0^2}{k_J^2}\psi^{2\gamma-1} + \mathbf{x}\cdot\nabla\psi(0) + \frac{1}{2}\mathbf{x}^T\mathbf{H}(0)\mathbf{x} - \frac{t^2\nu^2}{4}\nabla^2\nabla^2\psi(0) + \\ & + \frac{it\nu}{2}\nabla^2\psi(0)\mathbf{x}\cdot\nabla\psi(0) + ... \sim \\ \sim\, & \frac{it\nu}{2}\nabla^2\psi(0) + \mathbf{x}\cdot\nabla\psi(0) - \frac{it}{\nu}C\frac{H_0^2}{k_J^2}\left(\frac{it\nu}{2}\nabla^2\psi(0) + \mathbf{x}\cdot\nabla\psi(0)\right)^{2\gamma-1} + \\ & + \frac{1}{2}\mathbf{x}^T\mathbf{H}(0)\mathbf{x} - \frac{t^2\nu^2}{4}\nabla^2\nabla^2\psi(0) + \frac{it\nu}{2}\nabla^2\psi(0)\mathbf{x}\cdot\nabla\psi(0) + ...\,,\end{aligned} \tag{5.4.21}$$

where in the last line we used the first order correction to keep the lowest order possible in $\psi^{2\gamma-1}$ and we defined $C$ in (5.4.17). To investigate the vortex properties we can impose $\psi = 0$ and $\mathbf{x} = \Delta\mathbf{x} \to 0$, $t = \Delta t \to 0$ as we did for the collisionless case [30]. We then obtain

$$\begin{aligned}\mathbf{v}\cdot\nabla\psi(0) + \mathbf{v}^T\mathbf{H}(0)\Delta\mathbf{x} \sim & \frac{i}{\nu}C\frac{H_0^2}{k_J^2}\left(\frac{i\Delta t\,\nu}{2}\nabla^2\psi(0) + \Delta\mathbf{x}\cdot\nabla\psi(0)\right)^{2\gamma-1} - \frac{i\nu}{2}\nabla^2\psi(0) + \\ & + \frac{\Delta t\,\nu^2}{4}\nabla^2\nabla^2\psi(0) - \frac{i\nu}{2}\nabla^2\psi(0)\Delta\mathbf{x}\cdot\nabla\psi(0) + ...\end{aligned} \tag{5.4.22}$$

where $\mathbf{v}$ is the vortex velocity. We can estimate it through dimensional arguments, we call $R$ the characteristic dimension of the vortex.

$$\begin{aligned}v\left(\frac{\Delta x}{R^2} + \frac{1}{R}\right) \sim\, & \frac{\nu}{R^2} - C\frac{H_0^2}{\nu k_J^2}\Delta x^{2\gamma-1}\left(\frac{\nu}{vR^2} + \frac{1}{R}\right)^{2\gamma-1} - \frac{\Delta t\,\nu^2}{R^4} - \frac{\Delta x\,\nu}{R^3} + ... \\ \frac{v}{R}\left(1 + \frac{\Delta x}{R}\right) \overset{v\sim\nu/R}{\sim}\, & \frac{\nu}{R^2} - C\frac{H_0^2}{\nu k_J^2}\Delta x^{2\gamma-1}\left(\frac{R}{2}\right)^{1-2\gamma} - \frac{\Delta t\,\nu^2}{R^4} - \frac{\Delta x\,\nu}{R^3} + ... \\ v_{vortex} \sim\, & \frac{\nu}{R}\left[1 - 2\frac{\Delta x}{R} - C\left(\frac{H_0 R}{\nu k_J}\right)^2\left(\frac{2\Delta x}{R}\right)^{2\gamma-1} - \frac{\Delta t\,\nu}{R^2} + ...\right],\end{aligned} \tag{5.4.23}$$

where in the second line we used the first order solution for the vortex velocity $v = \nu/R$. As done by [30] for the collisionless case for obtain a more formal solution one should split the wave-function in its real and imaginary parts and keep them separate but, [30] showed

that the scaling can be roughly estimate by the coefficients dimensions without give much importance to real and imaginary splitting, therefore we limit to this rough estimate too. Like before due to the coefficient $(\nu k_J)^{-1} = \lambda_J/(\sigma_u \lambda_{dB})$ the pressure correction is the dominant term for $\lambda_{dB} << \lambda_J$ as expected. Since we are limiting ourselves to the regime $\lambda_{dB} \gtrsim \lambda_J$ the pressure term is not exploding but it provides a not negligible correction in the vortex dynamics.
The quantity $\Delta x$ represents the shrinking of the dimension of the vortex, we expect it to be large when the vortex nucleates or annihilates since at these points its form (and its velocity) changes rapidly with respect to its characteristic dimension $R$, as seen in the examples of Sect.5.2. The same argument is valid for the last term of the expansion since also the vortex position in time changes rapidly there. Hence we expect the pressure effects to be relevant mostly near these events, also the correction from second order terms is of the same nature. The minus sign in front of the correction implies that the pressure tends to slow down the vortex and so to suppress its formation, we expect that it can be possible that in certain regions (from Jeans instability theory [50] we expect it to be where $\lambda_{dB} << \lambda_J$) the pressure is strong enough to prevent the vortex formation. But we should investigate numerically this regime since to obtain this solution we assumed that the pressure is not the leading term in the wave-function evolution, which is true for the scale under consideration $\lambda_{dB} \gtrsim \lambda_J$. Anyway the model here depicted is able only to study the vortices after their formation and not to predict under which condition they can form, therefore we are not able to show when the pressure is strong enough to deny vortices nucleation.

Then this chapter departed a bit from the main argument of this work, i.e. study the baryon evolution through the Schrödinger equations; here we depicted the properties of quantum vortices and of the fluid around them studying a single-fluid Schrödinger model for a real quantum fluid, which is composed by ultra-light ($10^{-23} \lesssim m \lesssim 10^{-19}$ [6, 62]) axion-like particles, following the work [30]. In the last section we extended the previous results of [30] studying also the possibility of having a large velocity dispersion modelled as a pressure, which could destroy the quantum vortices, and for which investigation we used some of the results obtained from the baryon theory. We limited our study of collisional FDM to scales $\lambda_{dB} \gtrsim \lambda_J$ in order to can consider the pressure small but not negligible, the regime $\lambda_{dB} < \lambda_J$ would require a numerical study which here we did not develop. In the studied regime we found that pressure slow down vortices and the fluid around them. These particles are possible candidates for DM and are known under the name of fuzzy DM [31]. If sub-structures with the depicted characteristic would be observed in DM halos it can be a probe for this kind of DM candidates, the works [1, 30] noted that an efficient way of observe these sub-structures would be through gravitational lensing.

# Chapter 6

# Conclusions

In this work we presented a model for the description of the evolution of the large-scale structure of the Universe (LSS). In particular we modelled the two matter components of the Universe, baryons (collisional) and dark matter (collisionless), as a quantum fluid described by the system of Schrödinger-Poisson equations (2.2.42). In this model the Planck constant is a parameter which value can be set arbitrary, actually it appears always rescaled by the mass $m$ (which it is also an arbitrary parameter of the model) in the quantity $\nu = \hbar/m$ (hence we actually couple $\hbar$ and $m$ in a single parameter). This parameter sets the phase-space resolution, as it is clarified by the definitions of the phase-space distributions of Wigner (2.3.7) and Husimi (2.3.17). This approach, beside modelling classical matter through the choice of $\nu$, is useful to describe also a "new" candidate for dark matter, an ultra-light axion-like particle in a Bose-Einstein condensate (BEC) state commonly called fuzzy DM (FDM) [31], in this case $\hbar$ and $m$ are not parameter but the proper quantities. This wave-mechanical method, pioneered by [77], provides both a numerically competitive alternative to N-body simulation [77, 80] and semi-analytical results [67, 73]. Until now it was used only for the description of the evolution of DM and only recently [59] applied the Schrödinger description to a two-component fluid, but both collisionless. We, taking the inspiration from the DM description, extended this model to the study of a two-component fluid made of baryons and DM. Hence, differently to the literature, we had to take care of pressure effects (described by the equation of state (1.2.17)) in the Schrödinger-Poisson system.
After the introductory chapter 1, in the second chapter we depicted how the wave-mechanical description provided by the Schrödinger-Poisson system is related to the classic description of baryons and DM, we showed that this is possible in two different ways. We can relate the density and irrotational velocity fields of DM (baryons) to a wave-function $\psi_{DM}$ ($\psi_b$) through the Madelung transformation [43], in this way we showed that the Schrödinger equation is related to the continuity and Euler equations. In this way in the Euler equation appears an adjunctive term, which is purely quantistic, the quantum pressure (2.1.14). This term has a regularizing action similar to a classical pressure and its magnitude is set by the choice of the parameter $\nu$ [67]. The second way to relate the Schrödinger-Poisson system to the classical description of the matter components of the Universe is through the use of phase-space distribution, in particular we presented the Wigner (which is not positive defined) and the Husimi (which is positive defined and

so preferable) following the works [37, 72]. In the definition of the Husimi distribution (2.3.17) we add a new coarse-graining parameter $\sigma_x$ and define $\sigma_u = \nu/(2\sigma_x)$ such as we can choose the phase-space resolution in both the position and velocity directions with the limiting condition $\sigma_x\sigma_u = \nu/2$. We showed, always following the works [37, 72], that these two distribution are related to a Vlaslov equation up to terms of order $\mathcal{O}(\nu^2)$, hence for small values of the parameter $\nu$ we are following a Boltzmann description of baryons and DM which is preferable to the fluid description because DM (being collisionless) is only approximatively described by the fluid Euler equation [20].
Following the work [37] in Sect.2.4 we showed that if we define the velocity from the first order momentum of the Husimi distribution (2.3.24) we are able to compute the vorticity just from the wave-function $\psi$. This vorticity is sources by two components: one is purely quantistic and it arises over the defects of the wave-function due to the winding of the phase, the other one arises from the coarse-graining of the wave-function applied by the Husimi function in a manner similar to the vorticity in the classical description which arises from the averaging of different fluid trajectories [73]. We showed also that the quantum vorticity is cancelled by bigger spatial coarse-graining and over this bigger scale the Schrödinger model predictions of the DM vorticity are in agreement with the classical prediction of CDM [37], see e.g. Fig.2.3. We expect that if numerical simulation would be done also the vorticity predicted for the baryon component would be in agreement with the classical results, at least in the regions where the assumed equation of state (1.2.17) is valid.
In the Chapter 3 we presented a solution of the Schrödinger-Poisson system through the use of quantum perturbation theory (QPT), we followed the idea of [67] and extended it to the study of a time-dependent potential in the expanding Universe. The work [67] studied a single-fluid model with DM, instead we have a two-fluid composed by baryons and DM hence we had to include also the pressure in the potential part of the Schrödinger equation. To keep the pressure a perturbative term with respect to the kinetic energy we had to limit the QPT study to scales above the Jeans wavelength. We showed how the $0^{th}$-order term of the perturbative expansion, the free particle solution (3.2.7), recover the Zel'dovich approximation in the semi-classical limit $D\nu \to 0$ [67, 73], which is a good test of the Schrödinger model since the Zel'dovich approximation is exact in one dimension before shell-crossing. Instead if $\nu$ is kept small but finite we showed that the free particle approximation is able to surpass the shell-crossing without encounter any singularity thanks to the regularizing effects of the quantum pressure in a way similar to the classical Adhesion approximation [68], this solution is able also to investigate the multi-stream regime after the shell-crossing event [73] but it has to be computed numerically. Then we found the first order correction due to the gravitational potential, Universe expansion and gas pressure (3.3.3). This was the first time a gas pressure and the Universe expansion was studied with the QPT, [67] limited to a static Universe with only DM and so no pressure terms. The result (3.3.3) have the common form of first order QPT correction. In fact the propagator of the wave-function consists in evolving the particle as free and with momentum $\mathbf{k}_n$ from initial time to an intermediate time $D'$, where the effective potential "kick" the particle to momentum $\mathbf{k}_m$, then the particle is once again evolved as free till the time $D$, this is usually called a drift-kick-drift scheme. The propagator actually consist in the integration of this evolution over all possible $D'$ and $\mathbf{k}_n$. This result, which is expressed in the Fourier space, can be numerically competitive with a

full hydrodynamical code. Then we tried to find an analytical result in the semi-classical limit $D\nu \to 0$ using the stationary phase approximation (SPA) obtaining (3.3.14), which however need still a numerical integration over all the possible choice of the time $D'$ when the effective potential kicks the particle.
In the chapter 4 we presented a numerical method for obtain solutions of the Schrödinger-Poisson system, we followed the Solid state physics work [5] and particularized it to our cosmological problem, it consists to apply the Strang time-splitting approximation [71] to the non-linear Schrödinger equation describing the evolution of baryons or DM. It consists in evolve the wave-function first through the solution of the "potential" Schrödinger equation (4.1.7), then with the free particle Schrödinger equation (4.1.6) and again with the potential one. This evolution is repeated for small spatial intervals. In this case the kick-drift-kick scheme is favourable to the drift-kick-drift because the norm of the wave-function does not evolve during a time interval under the "potential" Schrödinger equation (4.1.7) [5]. We then reported some numerical simulations which show as this method is well suited to our cosmological problem. [5] showed (e.g. in Fig.4.2) that the numerical code recovers hydrodynamical results in the case of a particle which feels only the pressure. We reported also a simulation by [80] where a similar code is used to describe the gravitational collapse of DM and the formation of an halo (e.g. see Fig.4.4). Hence this method seems promising in the study of LSS evolution also in our case of a baryon-DM system.
Finally in the chapter 5 we departed from the main argument of this work (the baryon LSS evolution) for present some properties of quantum fluids, studied as a single-fluid under the Schrödinger-Poisson system, which can be a probe for the axion-like candidates of DM (FDM). In particular we studied the properties of quantum vortices inside bounded structures, e.g. DM halos, following the work [30]. This is interesting because for ultra-light axion-like candidates of DM (FDM) the quantum vortices are expected to persist over observable scales [30]. As a matter of facts since the FDM candidate is actually a quantum fluid $\hbar$ and $m$ are interpreted as the Planck constant and particle mass, we showed also that quantum vortices are expected arise over scales comparable with the de Broglie wavelength $\lambda_{dB} = \nu/\sigma_u$, where $\sigma_u$ is the velocity resolution of the Husimi phase-space distribution which is related to the characteristic velocity of the structure under study as its velocity dispersion, and so for such small masses they are expected to be present on scales big enough to be observable [30]. Therefore the observation of the properties of quantum vortices, which can be seen as sub-structures in DM halos, can be a probe for fuzzy dark matter [1, 30]. Since these effects are expected only in DM in this chapter we neglected the baryons and studied a single-fluid of FDM. We extended the results of [30] to the presence of velocity dispersion, which we modelled as a pressure with an associated Jeans wavelength [15, 64], in particular we modelled the pressure as the barotropic pressure we used for baryons (1.2.17). We have to stress the fact that this is just a simple approximation, which is justified by the fact that the magnitude of the pressure (dispersion) effects is mostly set by the scale, for a more rigorous treatment of the relation between velocity dispersion and an effective pressure see e.g. [57]. In the regime $\lambda_{dB} \gtrsim \lambda_J$ we found that the "pressure" gives correction to the vortices, tending to slow them down and so we expect that this can contrast their formation. For $\lambda_{dB} < \lambda_J$ the pressure corrections of our simple model explodes and becomes the dominant contribution in the dynamics of vortices and the fluid around them. But, since in the derivation of these

results we assumed the pressure to be small, we cannot actually investigate the regime $\lambda_{dB} < \lambda_J$, for which is required a numerical study. We expect that such a study could find that for such regime quantum vortices cannot form due to pressure effects (which actually represents the free streaming of DM particles) in a manner similar to the Jeans instability theory for the formation of structure under gravitational collapse [50]. Finally the main properties of quantum vortices and the fluid around them are

- All vortices close in loops. [30]
- The phase winds in the cross-section of each line with winding number $n = \pm 1$. [30]
- The density profile scales as $r_\perp^2$ near the vortex. [30]
- The velocity profile scales as $r_\perp^{-1}$ near the vortex. [30]
- The number density of vortices is roughly one per de Broglie volume $\lambda_{dB}^3$. [30]
- Dispersion velocity introduces a term proportional to $\lambda_J/\lambda_{dB}$ which tends to dump vortex velocity and fluid density around them.

If these features would be observed in DM halos it can be considered as a probe for fuzzy dark matter, i.e. ultra-light axion-like particles, which makes up the missing part of the Universe matter, or a part of it.

# Appendices

## A1 Jeans wavenumber

Here we want to compute the Jeans wavenumber for a collisional fluid (baryons) in an Universe with present the Cosmological constant $\Lambda$. Historically Jeans studied perturbations over a static background Universe and he found that these perturbations can grow if the effect of gravity exceeds the balancing effect of pressures. The grow of perturbations happens when the scales are bigger than the Jeans scale $\lambda_J = 2\pi/k_J$, which is defined as the scale for which the instability forces are in equilibrium with the stability ones. We want now pass to the study of the Jeans instability for an expanding background Universe, thus also the expansion forces has to be taken in account in the compute of the equilibrium state. To do so we need to study the gravitational instability of a region of the Universe filled by the baryon fluid by the study of the linear regime of the perturbed fluid equations (2.2.22), (2.2.23) coupled with the Poisson equation

$$D\nabla^2\varphi_b - \delta_b = 0\,. \tag{A1.1}$$

Where $\varphi_b$ is the peculiar gravitational potential generated by the baryons, from now in this section we omit the subscript b for indicate baryons because we are considering an Universe region filled by them (plus $\Lambda$).
Id we keep only linear terms in perturbations in the fluid equations (2.2.22), (2.2.23) we obtain

$$\dot{\delta}(\mathbf{x}, D) + \nabla \cdot \mathbf{u}(\mathbf{x}, D) = 0\,, \tag{A1.2}$$

$$\dot{\mathbf{u}}(\mathbf{x}, D) + \frac{3e(\Omega_{DM})}{2D}(\mathbf{u} + \nabla\varphi) + \frac{e(\Omega_{DM})}{a^2D^2H^2\Omega_{DM}}\frac{\nabla P}{\rho} = 0\,. \tag{A1.3}$$

Since we want to make a linear approximation we can express every quantity as a combination of plane waves so that is easier to solve differential equations, for example

$$\delta(\mathbf{x}, D) = \frac{1}{(2\pi)^3}\int e^{i\mathbf{k}\cdot\mathbf{x}}\delta_{\mathbf{k}}(D)d^3k\,. \tag{A1.4}$$

We search for solutions which time dependence is of the form

$$\delta_{\mathbf{k}}(D) = \delta_{\mathbf{k}}e^{i\omega D}\,. \tag{A1.5}$$

Then if we use this dependences in the linear equations and we assume the pressure barotropic and given by (1.2.17), In general the pressure $P(\rho, s)$ depends on both the

energy density and the entropy, for its perturbations over the homogeneous Universe we have

$$P(\mathbf{x}, D) = \bar{P}(D) + \delta P(\mathbf{x}, D)\,, \tag{A1.6}$$

$$\delta P = \left.\frac{\partial P}{\partial \rho}\right|_s \delta\rho + \left.\frac{\partial P}{\partial s}\right|_\rho \delta s = c_s^2 \delta\rho + \left.\frac{\partial P}{\partial s}\right|_\rho \delta s\,, \tag{A1.7}$$

where $\bar{P}(D)$ is the background pressure and $s$ is the entropy per unit mass. Assume the density barotropic correspond to neglect the entropy dependence of the pressure $P(\rho)$. From the definition of the barotropic pressure (1.2.17) we can compute the adiabatic sound speed $c_s^2$:

$$c_s^2 = \left(\frac{dP}{d\rho}\right)_{\bar{\rho}} = \frac{\gamma k_b T_0}{\mu m_p}\,. \tag{A1.8}$$

Hence we obtain

$$\omega\delta_{\mathbf{k}} + \mathbf{k}\cdot\mathbf{u}_{\mathbf{k}} = 0\,, \tag{A1.9}$$

$$\omega\mathbf{u}_{\mathbf{k}} + \frac{3e(\Omega_{DM})}{2D}(-i\mathbf{u}_{\mathbf{k}} + \mathbf{k}\varphi_{\mathbf{k}}) + \frac{e(\Omega_{DM})c_s^2\mathbf{k}}{D^2a^2H^2\Omega_{DM}}\delta_{\mathbf{k}} = 0\,, \tag{A1.10}$$

$$Dk^2\varphi_{\mathbf{k}} + \delta_{\mathbf{k}} = 0\,. \tag{A1.11}$$

To have non trivial solution the determinant of the matrix made by the coefficients of the above three equations has to be null, thus we have

$$\det\begin{bmatrix} \omega & \mathbf{k} & 0 \\ \frac{e(\Omega_{DM})c_s^2\mathbf{k}}{D^2a^2H^2\Omega_{DM}} & \omega - i\frac{3e(\Omega_{DM})}{2D} & \frac{3e(\Omega_{DM})}{2D}\mathbf{k} \\ 1 & 0 & Dk^2 \end{bmatrix} = 0$$

$$k^2\omega^2 - ik^2\frac{3e(\Omega_{DM})}{2D}\omega - k^2\left(\frac{e(\Omega_{DM})k^2c_s^2}{D^2a^2H^2\Omega_{DM}} - \frac{3e(\Omega_{DM})}{2D^2}\right) = 0\,. \tag{A1.12}$$

The equation (A1.12) is called dispersion relation and the Jeans wavelength is defined as the wavelength for which $\omega = 0$. This is the critical wavelength between the regime of instability ($\omega^2 < 0$) and of acoustic waves ($\omega^2 > 0$) [50]. Hence we have found

$$k_J^2 = \frac{3a^2H^2\Omega_{DM}\mu m_p}{2\gamma k_B T_0} \tag{A1.13}$$

where we used $c_s^2 = (\gamma k_b T_0)/(\mu m_p)$. For scales bigger than $\lambda_J = 2\pi/k_J$ the perturbations are growing in amplitude, instead on smaller scales the perturbations are oscillating sound waves. Hence the Jeans wavelength represents the scale at which there is the transition between these two regimes [50].

## A2 Stationary phase approximation

The stationary phase approximation is a basic principle of asymptotic analysis stated already by Stokes and Kelvin. This method relies on the cancellation of sinusoids with rapidly varying phase. If many sinusoids have the same phase and are added together

they add constructively, otherwise if these sinusoids have phases which rapidly change with the frequency they will add incoherently, which can generate constructive or destructive addition at different times.
We will show how this method works in the simplest case in our study, i.e. in the free particle approximation. We want to solve the integral defining the free particle wave function (3.2.7), which we report here

$$\psi(\mathbf{x}, D) = \int d^3q \psi_i(\mathbf{q}) \frac{\exp\left[\frac{i}{2\nu}\frac{(\mathbf{x}-\mathbf{q})^2}{D-D_i}\right]}{(2\pi i(D-D_i)\nu)^{3/2}} = \\ = \int d^3q \sqrt{1+\delta_i(\mathbf{q})} \frac{\exp\left[\frac{i}{\nu}\left(\frac{(\mathbf{x}-\mathbf{q})^2}{2(D-D_i)} - \phi_i(\mathbf{q})\right)\right]}{(2\pi i(D-D_i)\nu)^{3/2}}, \tag{A2.1}$$

where we used the Madelung definition of the wave-function $\psi = \sqrt{1+\delta}e^{-i\phi/\nu}$. It is clear that this integral is over sinusoids of phase

$$\frac{1}{\nu}\left(\frac{(\mathbf{x}-\mathbf{q})^2}{2(D-D_i)} - \phi_i(\mathbf{q})\right). \tag{A2.2}$$

Since we are interested in the semi-classical limit $\nu \to 0$ the phase is rapidly varying. Thus the dominant contribution to the integral comes from the points where the phase varies least rapidly in $\mathbf{q}$, i.e. at the stationary points. For compactness of the notation we introduce the function

$$g(\mathbf{q}) = \frac{(\mathbf{x}-\mathbf{q})^2}{2(D-D_i)} - \phi_i(\mathbf{q}), \tag{A2.3}$$

where we wrote explicitly only the dependence in $\mathbf{q}$ because the integral is over it only. The stationary points $\mathbf{q}_c$ satisfies the conditions $g_{,j}(\mathbf{q}_c) = 0$, which leads to

$$\mathbf{q}_c = \mathbf{x} - (D-D_i)\nabla_{\mathbf{q}}\phi_i(\mathbf{q}_c). \tag{A2.4}$$

We can Taylor-expand the function $g$ about the stationary point $\mathbf{q}_c$

$$g(\mathbf{q}) = g(\mathbf{q}_c) + \frac{1}{2}\sum_{k=1}^{3}\sum_{l=1}^{3}(q_k - q_k^c)g_{,kl}(\mathbf{q}_c)(q_l - q_l^c) + \mathcal{O}((\mathbf{q}-\mathbf{q}_c)^3), \tag{A2.5}$$

where we used the fact that $g_{,k}(\mathbf{q}_c) = 0$. If we substitute this expansion in the integral (A2.1) we obtain

$$\psi(\mathbf{x}, D) = \sum_{q_c} \frac{(1+\delta_i(\mathbf{q}_c))^{1/2}}{(2\pi i(D-D_i)\nu)^{3/2}} \exp\left[\frac{i}{\nu}g(\mathbf{q}_c)\right] \int d^3p \exp\left[-\frac{1}{2}\mathbf{p}^T\mathbf{M}(\mathbf{q}_c)\mathbf{p}\right], \tag{A2.6}$$

where we computed also the amplitude $(1+\delta_i(\mathbf{q}_c))^{1/2}$ at the stationary points since from these points the most relevant contribution comes and we made the change of variable $\mathbf{p} = \mathbf{q} - \mathbf{q}_c$. We defined the complex matrix $M_{kl}(\mathbf{q}_c) = -ig_{,kl}(\mathbf{q}_c)/\nu$ and the superscript $T$ indicates a transpose vector.
The remaining integral is a three-dimensional complex Gaussian integral ($\mathbf{M}$ is a purely imaginary quantity) which can be evaluated using standard techniques

$$\int d^3p \exp\left[-\frac{1}{2}\mathbf{p}^T\mathbf{M}(\mathbf{q}_c)\mathbf{p}\right] = \left(\frac{(2\pi)^3}{\det\mathbf{M}(\mathbf{q}_c)}\right)^{1/2} \exp\left[\frac{i\pi}{4}\,\mathrm{sign}\,(Im\,\mathbf{M})\right], \tag{A2.7}$$

where $Im\,\mathbf{M}$ is the imaginary part of the matrix $\mathbf{M}$. Thus we have obtained the wave-function under the SPA

$$\psi(\mathbf{x}, D) = \sum_{q_c} \frac{(1+\delta_i(\mathbf{q}_c))^{1/2}}{(2\pi i(D-D_i)\nu)^{3/2}} \exp\left[\frac{i}{\nu} g(\mathbf{q}_c)\right] \left(\frac{(2\pi)^3}{\det \mathbf{M}(\mathbf{q}_c)}\right)^{1/2} \exp\left[-\frac{i\pi}{4}\,\mathrm{sign}\,(Im\,\mathbf{M})\right] . \tag{A2.8}$$

In order the relation (A2.7) to hold we need $\det[\mathbf{M}(\mathbf{q}_c)] \neq 0$, this implies that this relation is true only before shell-crossing. We can show that in the following manner, first note that the definition of the function $g(\mathbf{q})$ (A2.3) implies

$$g_{,kl}\,(\mathbf{q}) = \frac{H_{kl}(\mathbf{q})}{D-D_i} \qquad H_{kl} = \delta_{kl} - (D-D_i)\phi_{,kl}\ . \tag{A2.9}$$

Thus we can express $\mathbf{M}$ and its determinant through the new matrix $\mathbf{H}$ as

$$\mathbf{M}(\mathbf{q}_c) = -\frac{i}{\nu(D-D_i)}\mathbf{H}(\mathbf{q}_c)\,, \tag{A2.10}$$

$$\det[\mathbf{M}(\mathbf{q}_c)] = \frac{i}{\nu^3(D-D_i)^3}\det[\mathbf{H}(\mathbf{q}_c)]\,. \tag{A2.11}$$

Since $\mathbf{H}$ is also the Jacobian of the coordinate transformation between Lagrangian $\mathbf{q}$ and Eulerian $\mathbf{x}$ coordinates, defined by the stationariness condition (A2.4), it is non zero before shell-crossing occurs. Because before shell-crossing only one particle can depart from the point $\mathbf{q}$ and arrive at the point $\mathbf{x}$ at time $D$ we can assume that there is only one stationary point $\mathbf{q}_c$ satisfying the condition (A2.4), hence we can neglect the sum over the stationary point in (A2.8).
Finally the wave-function resulting from the stationary phase approximation is

$$\psi_{SPA}(\mathbf{x}, D) = \left(\frac{1+\delta_i(\mathbf{q}_c)}{\det[\mathbf{H}(\mathbf{q}_c)]}\right)^{1/2} \exp\left[\frac{i}{\nu} g(\mathbf{q}_c)\right] \exp\left[\frac{i\pi}{4}\,\mathrm{sign}\,(Im\,\mathbf{H})\right] . \tag{A2.12}$$

# A3 Redshift space propagator

Porqueres and collaborators observed in [58] that, since all cosmological observations are made in a redshift space rather than in a comoving physical one, it would be helpful to have an "instrument" for translate directly our theoretical results in the redshift space.
We assume the approximation of a distant observer, which implies that the redshift distortion can be chose to coincide with a single Cartesian axis. We can summarize the redshift effect as the fact that we doesn't observe a particle in its Eulerian position $\mathbf{x}$ but instead in its redshift space position $\mathbf{s}$, due to the deviations from the Hubble flow caused by our peculiar motion. In Lagrangian perturbation theories (LPT), as the Zel'dovich approximation [79], we can describe this effect as [58]

$$\mathbf{s} = \mathbf{x} + f(D)\,(\boldsymbol{\Xi}\cdot\hat{\mathbf{e}}_{\mathbf{LOS}})\,\hat{e}_{LOS}\,, \tag{A3.1}$$

where $\hat{e}_{LOS}$ is a unit vector pointing along the line-of-sight, $\boldsymbol{\Xi}$ is the displacement field between Lagrangian and Eulerian coordinates, $\boldsymbol{\Xi} \equiv \mathbf{x} - \mathbf{q}$, and $f = d\log D/d\log a$ is defined in (1.4.18). This is quite obviously simply a velocity dependent displacement, and

it can therefore be trivially included in an additional propagator from Eulerian to redshift space, hence with the same form of the free particle propagator (3.2.4), given as [58]

$$K_{RSD}(\mathbf{s};\mathbf{x},D) = N\exp\left[\frac{i}{\nu}\frac{((\mathbf{s}-\mathbf{x})\cdot\hat{e}_{LOS})^2}{2f(D)(D-D_i)}\right], \tag{A3.2}$$

with $N$ a normalisation factor that has to be suitably chosen [58]. Thus to find the wave-function, and then all the observables, in the redshift space we have to apply this propagator to the solution in comoving physical space [58], i.e.

$$\psi(\mathbf{s},D) = \int d^3x K_{RSD}(\mathbf{s};\mathbf{x},D)\psi(\mathbf{x},D)\,. \tag{A3.3}$$

Actually it is possible to define a single propagator which brings the particle from the initial (Lagrangian) position to the position in the redshift space at time $D$ [58]. For example we can define it for the free particle approximation from the free propagator (3.2.4).

$$\psi(\mathbf{s},D) = \int d^3x d^3q K_{RSD}(\mathbf{s};\mathbf{x},D)K_0(\mathbf{x},D;\mathbf{q},D_i)\psi_i(\mathbf{q})\,, \tag{A3.4}$$

We can express the product of the two propagators as a single one in the Fourier space using the convolution theorem, i.e.

$$\begin{aligned}\psi(\mathbf{s},D) &= \int d^3q d^3x \frac{d^3t}{\sqrt{2\pi}}\frac{d^3u}{\sqrt{2\pi}}\frac{d^3v}{\sqrt{2\pi}} e^{i\mathbf{t}\cdot\mathbf{q}} e^{i\mathbf{u}(\mathbf{x}-\mathbf{q})} e^{i\mathbf{v}\cdot[(\mathbf{s}-\mathbf{x})\cdot\hat{e}_{LOS}]\hat{e}_{LOS}}\psi_i(\mathbf{t}) e^{-\frac{i\nu}{2}(D-D_i)u^2} e^{-\frac{i\nu}{2}(D-D_i)v^2} = \\ &= \frac{1}{\sqrt{2\pi}}\int d^3v \psi_i((\mathbf{v}\cdot\hat{e}_{LOS})\hat{e}_{LOS}) e^{-\frac{i\nu}{2}(D-D_i)\left[(\mathbf{v}\cdot\hat{e}_{LOS})^2+v^2\right]} e^{i(\mathbf{v}\cdot\hat{e}_{LOS})(\mathbf{s}\cdot\hat{e}_{LOS})} \\ &= \frac{1}{\sqrt{2\pi}}\int d^3k e^{i\mathbf{k}\cdot[\hat{e}_{LOS}(\mathbf{s}\cdot\hat{e}_{LOS})]}\psi_i(\mathbf{k})K_{RL}(\mathbf{k},D)\end{aligned} \tag{A3.5}$$

where in the last line we made the change of variable $\mathbf{k} = (\mathbf{v}\cdot\hat{e}_{LOS})\hat{e}_{LOS}$. Thus we found that we can express the free particle propagator from Lagrangian to redshift coordinates in the Fourier space as [58]

$$K_{RL}(\mathbf{k},D) = \exp\left[-\frac{i\nu}{2}\left(k^2 + f(D)(\mathbf{k}\cdot\hat{e}_{LOS})^2\right)(D-D_i)\right]. \tag{A3.6}$$

From the form of the Fourier transform in (A3.5) $\mathbf{k}\cdot[\hat{e}_{LOS}(\mathbf{s}\cdot\hat{e}_{LOS})]$ it's clear that the propagator affects only the points along the line of sight, i.e. in the directions orthogonal to the line of sight the redshift and the Eulerian space coincide, this is due to the distant observer approximation we made.

# Bibliography


[1] Stephon Alexander, Sergei Gleyzer, Evan McDonough, Michael W. Toomey, and Emanuele Usai. Deep Learning the Morphology of Dark Matter Substructure. *Astrophys. J.*, 893:15, 2020.

[2] John Dirk Walecka Alexander L. Fetter. *Quantum theory of many-particle systems.* Pure and Applied Physics. Mcgraw-Hill College, first edition edition, 1971.

[3] Leslie E Ballentine. *Quantum Mechanics in Phase Space*, chapter Chapter 15, pages 406–420. World Scientific, 2014.

[4] N. Banik and P. Sikivie. Axions and the galactic angular momentum distribution. *Phys. Rev. D*, 88:123517, Dec 2013.

[5] Weizhu Bao, Shi Jin, and Peter A. Markowich. Numerical study of time-splitting spectral discretizations of nonlinear schrödinger equations in the semiclassical regimes. *SIAM Journal on Scientific Computing*, 25(1):27–64, 2003.

[6] Nitsan Bar, Diego Blas, Kfir Blum, and Sergey Sibiryakov. Galactic rotation curves versus ultralight dark matter: Implications of the soliton-host halo relation. *Phys. Rev. D*, 98(8):083027, 2018.

[7] Edmund Bertschinger. Cosmological dynamics: Course 1. In *Les Houches Summer School on Cosmology and Large Scale Structure (Session 60)*, pages 273–348, 8 1993.

[8] Edmund Bertschinger and James M. Gelb. Cosmological n-body simulations. *Computers in Physics*, 5(2):164–179, 1991.

[9] Simeon Bird, Yu Feng, Christian Pedersen, and Andreu Font-Ribera. More accurate simulations with separate initial conditions for baryons and dark matter. *JCAP*, 06:002, 2020.

[10] Mark N Brook and Peter Coles. Gravitational stability of vortices in bose-einstein condensate dark matter, 2009.

[11] "N.D. Cartwright". A non-negative wigner-type distribution. *Physica A: Statistical Mechanics and its Applications*, 83(1):210 – 212, 1976.

[12] Paolo Catelan, Francesco Lucchin, Sabino Matarrese, and Lauro Moscardini. Eulerian perturbation theory in non-flat universes: second-order approximation. *Monthly Notices of the Royal Astronomical Society*, 276(1):39–56, 09 1995.

[13] Peter Coles and Kate Spencer. A wave-mechanical approach to cosmic structure formation. *Monthly Notices of the Royal Astronomical Society*, 342, 12 2002.

[14] Bogdan Damski and Krzysztof Sacha. Changes of the topological charge of vortices. *Journal of Physics A: Mathematical and General*, 36, 02 2002.

[15] H.J. de Vega and N.G. Sanchez. The Dark Matter distribution function and Halo Thermalization from the Eddington equation in Galaxies. *Int. J. Mod. Phys. A*, 31(13):1650073, 2016.

[16] Peter Duren, Walter Hengartner, and Richard S. Laugesen. The argument principle for harmonic functions. *The American Mathematical Monthly*, 103(5):411–415, 1996.

[17] Martin Ester, Hans-Peter Kriegel, Jörg Sander, and Xiaowei Xu. A density-based algorithm for discovering clusters in large spatial databases with noise. pages 226–231. AAAI Press, 1996.

[18] R.P. Feynman. Progress in low temperature physics. 1955.

[19] R.P. Feynman. Excitations in liquid helium. *Physica*, 24:18 – 26, 1958.

[20] Peter Coles Francesco Lucchin. *Cosmology: the origin and evolution of cosmic structure*. Wiley, 2 edition, 2002.

[21] E. P. Gross. Structure of a quantized vortex in boson systems. *Il Nuovo Cimento*, 20(3):454–477, May 1961.

[22] James E. Gunn and Bruce A. Peterson. On the Density of Neutral Hydrogen in Intergalactic Space. *Astrophysical journal*, 142:1633–1636, November 1965.

[23] S Gurbatov, A Saichev, and Sergei Shandarin. A model for describing the development of the large-scale structure of the universe. *Soviet Physics Doklady*, 30:921, 10 1985.

[24] Oliver Hahn, Raul E. Angulo, and Tom Abel. The properties of cosmic velocity fields. *Monthly Notices of the Royal Astronomical Society*, 454(4):3920–3937, 10 2015.

[25] Oliver Hahn, Cornelius Rampf, and Cora Uhlemann. Higher-order initial conditions for mixed baryon-CDM simulations. 8 2020.

[26] A. J. S. Hamilton. Formulae for growth factors in expanding universes containing matter and a cosmological constant. *Monthly Notices of the Royal Astronomical Society*, 322(2):419–425, 04 2001.

[27] H. Helmholtz. Über integrale der hydrodynamischen gleichungen, welche den wirbelbewegungen entsprechen. *Journal für die reine und angewandte Mathematik*, 1858(55):25 – 55, 01 Jan. 1858.

[28] Richard P. Feynman A. R. Hibbs. *Quantum Mechanics and Path Integrals*. First edition edition, 1965.

[29] Jian Hu and Yu-Qing Lou. Collisional interaction limits between dark matter particles and baryons in 'cooling flow' clusters. *Monthly Notices of the Royal Astronomical Society*, 384(2):814–820, 01 2008.

[30] Lam Hui, Austin Joyce, Michael Landry, and Xinyu Li. Vortices and waves in light dark matter. *preprint*, 04 2020.

[31] Lam Hui, Jeremiah P. Ostriker, Scott Tremaine, and Edward Witten. Ultralight scalars as cosmological dark matter. *Phys. Rev. D*, 95:043541, Feb 2017.

[32] K. Husimi. Some formal properties of the density matrix. *Proceedings of the Physico-Mathematical Society of Japan. 3rd Series*, 22(4):264–314, 1940.

[33] Dragan Huterer and Daniel L Shafer. Dark energy two decades after: observables, probes, consistency tests. *Reports on Progress in Physics*, 81(1):016901, dec 2017.

[34] Lars Hörmander. *The Analysis of Linear Partial Differential Operators I: Distribution Theory and Fourier Analysis*. Grundlehren der mathematischen Wissenschaften 256. Springer Berlin Heidelberg, 1983.

[35] Shi Jin and Zhouping Xin. The relaxation schemes for systems of conservation laws in arbitrary space dimensions. *Communications on Pure and Applied Mathematics*, 48(3):235–276, 1995.

[36] Ben Kain and Hong Y. Ling. Vortices in bose-einstein condensate dark matter. *Phys. Rev. D*, 82:064042, Sep 2010.

[37] Michael Kopp, Kyriakos Vattis, and Constantinos Skordis. Solving the Vlasov equation in two spatial dimensions with the Schrödinger method. *Phys. Rev. D*, 96(12):123532, 2017.

[38] S. Stringari L. Pitaevskii. *Bose-Einstein condensation*. The International Series of Monographs on Physics. Oxford University Press, USA, 2003.

[39] Ofer Lahav, Per B. Lilje, Joel R. Primack, and Martin J. Rees. Dynamical effects of the cosmological constant. *Monthly Notices of the Royal Astronomical Society*, 251:128–136, July 1991.

[40] S. LeBohec. Quantum mechanical approaches to the virial. 2015.

[41] Xinyu Li, Lam Hui, and Greg L. Bryan. Numerical and perturbative computations of the fuzzy dark matter model. *Phys. Rev. D*, 99:063509, Mar 2019.

[42] Thomson W. Lord Kelvin. On vortex motion. *Trans. Roy. Soc. Edin.*, 1869.

[43] E. Madelung. Quantentheorie in hydrodynamischer Form. *Zeitschrift für Physik*, 40(3):322–326, 03 1927.

[44] Alireza Maleki, Shant Baghram, and Sohrab Rahvar. Constraint on the mass of fuzzy dark matter from the rotation curve of the Milky Way. *Phys. Rev. D*, 101(10):103504, 2020.

[45] Peter A. Markovich, Paola Pietra, and Carsten Pohl. Numerical approximation of quadratic observables of schrödinger-type equations in the semi-classical limit. *Numerische Mathematik*, 81(4):595–630, 1999.

[46] Peter A. Markowich, Paola Pietra, Carsten Pohl, and Hans Peter Stimming. A wigner-measure analysis of the dufort-frankel scheme for the schrödinger equation. *SIAM Journal on Numerical Analysis*, 40(4):1281–1310, 2003.

[47] S. Matarrese and R. Mohayaee. The growth of structure in the intergalactic medium. *Mon. Not. R. Astron. Soc*, 329:37–60, 2002.

[48] Patrick McDonald, Jordi Miralda-Escude, Michael Rauch, Wallace L. W. Sargent, Tom A. Barlow, and Renyue Cen. A measurement of the temperature-density relation in the intergalactic medium using a new ly$\alpha$ absorption-line fitting method. *The Astrophysical Journal*, 562(1):52–75, nov 2001.

[49] Mattia Mina, David F. Mota, and Hans A. Winther. Solitons in the dark: non-linear structure formation with fuzzy dark matter, 2020.

[50] Houjun Mo, Frank C. van den Bosch, and Simon White. *Galaxy Formation and Evolution*. 2010.

[51] Philip Mocz, Lachlan Lancaster, Anastasia Fialkov, Fernando Becerra, and Pierre-Henri Chavanis. Schrödinger-Poisson–Vlasov-Poisson correspondence. *Phys. Rev. D*, 97(8):083519, 2018.

[52] Julio F. Navarro, Carlos S. Frenk, and Simon D. M. White. The Structure of Cold Dark Matter Halos. *astrophysical journal*, 462:563, May 1996.

[53] U. Niederer. The maximal kinematical invariance group of the free Schrodinger equation. *Helv. Phys. Acta*, 45:802–810, 1972.

[54] A. Nusser. Analytic solutions for coupled linear perturbations. *Mon. Not. R. Astron. Soc*, 317:902–906, 2000.

[55] L. Onsager. Statistical hydrodynamics. *Il Nuovo Cimento*, 6(2):279–287, March 1949.

[56] P. J. E. Peebles. *The large-scale structure of the universe*. 1980.

[57] Oliver F. Piattella, Davi C. Rodrigues, Júlio C. Fabris, and José A. de Freitas Pacheco. Evolution of the phase-space density and the jeans scale for dark matter derivedfrom the vlasov-einstein equation. *JCAP*, 11:002, 2013.

[58] Natalia Porqueres, Oliver Hahn, Jens Jasche, and Guilhem Lavaux. A hierarchical field-level inference approach to reconstruction from sparse Lyman-$\alpha$ forest data. 5 2020.

[59] Cornelius Rampf, Cora Uhlemann, and Oliver Hahn. Cosmological perturbations for two cold fluids in ΛCDM. 8 2020.

[60] Mario Trigiante (auth.) Riccardo D'Auria. *From Special Relativity to Feynman Diagrams: A Course of Theoretical Particle Physics for Beginners*. UNITEXT. Springer-Verlag Mailand, 1 edition, 2012.

[61] Tanja Rindler-Daller and Paul R. Shapiro. Angular momentum and vortex formation in Bose–Einstein-condensed cold dark matter haloes. *Monthly Notices of the Royal Astronomical Society*, 422(1):135–161, 04 2012.

[62] Hans-Walter Rix and Jo Bovy. The Milky Way‘s stellar disk. *Astron. Astrophys. Rev.*, 21:61, 2013.

[63] Arthur Yu. Savchenko and Boris Ya. Zel'dovich. Speckle beams with nonzero vorticity and poincaré–cartan invariant. *J. Opt. Soc. Am. A*, 16(7):1665–1671, Jul 1999.

[64] Aurel Schneider. *Dark matter structures and the free streaming scale*. PhD thesis, University of Zurich, August 2012.

[65] A. E. Schulz, Walter Dehnen, Gerard Jungman, and Scott Tremaine. Gravitational collapse in one dimension. *Monthly Notices of the Royal Astronomical Society*, 431(1):49–62, 03 2013.

[66] Bodo Schwabe. *Simulating Structure Formation with Ultra-light Bosonic Dark Matter*. PhD thesis, Gottingen U., 1 2019.

[67] C J Short and P Coles. Gravitational instability via the schrödinger equation. *Journal of Cosmology and Astroparticle Physics*, 2006(12):012–012, dec 2006.

[68] C J Short and P Coles. Wave mechanics and the adhesion approximation. *Journal of Cosmology and Astroparticle Physics*, 2006(12):016–016, dec 2006.

[69] M. Silverman and Ronald Mallett. Dark matter as a cosmic bose-einstein condensate and possible superfluid. *General Relativity and Gravitation*, 34:633–649, 05 2002.

[70] V. Springel, Simon White, A. Jenkins, C. Frenk, N. Yoshida, Liang Gao, J. Navarro, R. Thacker, D. Croton, J. Helly, Joe Peacock, and Shaun Cole. Simulating the joint evolution of quasars, galaxies and their large-scale distribution supplementary information. *Nature*, 435, 01 2005.

[71] Gilbert Strang. On the construction and comparison of difference schemes. *SIAM Journal on Numerical Analysis*, 5(3):506–517, 1968.

[72] Cora Uhlemann, Michael Kopp, and Thomas Haugg. Schrödinger method as $n$-body double and uv completion of dust. *Phys. Rev. D*, 90:023517, Jul 2014.

[73] Cora Uhlemann, Cornelius Rampf, Mateja Gosenca, and Oliver Hahn. Semiclassical path to cosmic large-scale structure. *Phys. Rev. D*, 99:083524, Apr 2019.

[74] M. Viel, S. Matarrese, H. J. Mo, Tom Theuns, and M. G. Haehnelt. Modelling the IGM and the Ly$\alpha$ forest at high redshift from the dark matter distribution. *Monthly Notices of the Royal Astronomical Society*, 336(2):685–698, 10 2002.

[75] Eleonora Villa and Cornelius Rampf. Relativistic perturbations in ΛCDM: Eulerian \& Lagrangian approaches. *JCAP*, 01:030, 2016. [Erratum: JCAP 05, E01 (2018)].

[76] Elias Wegert. *Visual complex functions: An introduction with phase portraits*. 01 2012.

[77] Lawrence M. Widrow and Nick Kaiser. Using the Schroedinger Equation to Simulate Collisionless Matter. *apjl*, 416:L71, October 1993.

[78] E. Wigner. On the quantum correction for thermodynamic equilibrium. *Phys. Rev.*, 40:749–759, Jun 1932.

[79] Y. B. Zel'Dovich. Gravitational instability: an approximate theory for large density perturbations. *Astron.Astrophys.*, 500:13–18, March 1970.

[80] Tim Zimmermann, Massimo Pietroni, Javier Madroñero, Luca Amendola, and Sandro Wimberger. A Quantum Model for the Dynamics of Cold Dark Matter. *Condens. Mat.*, 4(4):89, 2019.

[81] Nikolaj Zinner. Vortex structures in a rotating bec dark matter component. *Physics Research International*, 2011, 08 2011.